Report No. NAWCADWAR-95033-4.3 (Vol. II)
Contract No. N62269-85-C-0256

RESIDUAL STRESS CHANGES IN FATIGUE

VOLUME II — A CONTINUUM SURFACE LAYER EFFECT IN POLYCRYSTALLINE AGGREGATES

M.P. Laurent**
Engineering Science and Mechanics Department
VIRGINIA POLYTECHNIC INSTITUTE AND STATE UNIVERSITY
Blacksburg, VA 24061-0219

*Currently at Zimmer, Inc., Warsaw, IN

15 JANUARY 1994

FINAL REPORT
Period Covering October 1985 to October 1990

Approved for Public Release; Distribution is Unlimited.

Prepared for
Air Vehicle Department — Structures Division (Code 4.3.3.R)
NAVAL AIR WARFARE CENTER
AIRCRAFT DIVISION WARMINSTER
P.O. Box 5152
Warminster, PA 18974-0591

NOTICES

REPORT NUMBERING SYSTEM - The numbering of technical project reports issued by the Naval Air Warfare Center, Aircraft Division, Warminster is arranged for specific identification purposes. Each number consists of the Center acronym, the calendar year in which the number was assigned, the sequence number of the report within the specific calendar year, and the official 2-digit correspondence code of the Functional Department responsible for the report. For example: Report No. NAWCADWAR-95010-4.6 indicates the tenth Center report for the year 1995 and prepared by the Crew Systems Engineering Department. The numerical codes are as follows.

Code	Department
4.1	Systems Engineering Department
4.2	Cost Analysis Department
4.3	Air Vehicle Department
4.4	Propulsion and Power Department
4.5	Avionics Department
4.6	Crew Systems Engineering Department
4.10	Conc. Analy., Eval. and Plan (CAEP) Department

PRODUCT ENDORSEMENT - The discussion or instructions concerning commercial products herein do not constitute an endorsement by the Government nor do they convey or imply the license or right to use such products.

Reviewed By: Annette Crocker **Date:** OCT 4, 1995
Author/COTR

Reviewed By: [signature] **Date:** 10/10/95
LEVEL III Manager

REPORT DOCUMENTATION PAGE

Form Approved
OMB No. 0704-0188

1. AGENCY USE ONLY *(Leave blank)*	2. REPORT DATE	3. REPORT TYPE AND DATES COVERED
	15 Jan 94	Final: Oct. 85 to Oct 90

4. TITLE AND SUBTITLE
Residual Stress Changes in Fatigue
Vol.II: A Continuum Surface Layer Effect in Polycrystalline Aggregates

5. FUNDING NUMBERS
N62269-85-C-0256

6. AUTHOR(S)
N. E. Dowling, D. O. Dunn, and M. P. Laurent
Vol. II: M. P. Laurent

7. PERFORMING ORGANIZATION NAME(S) AND ADDRESS(ES)
Virginia Polytechnic Institute and State University
Blacksburg, VA 24061-0219

8. PERFORMING ORGANIZATION REPORT NUMBER

9. SPONSORING / MONITORING AGENCY NAME(S) AND ADDRESS(ES)
Naval Air Systems Command
4.3.T
1421 Jefferson Davis Hwy
Arlington VA 22243

Naval Air Warfare Center
Aircraft Division
Air Vehicle Department 4.3.3.R
Warminster PA 18974

10. SPONSORING / MONITORING AGENCY REPORT NUMBER
NAWCADWAR-95033
(Vol. II)

11. SUPPLEMENTARY NOTES

12a. DISTRIBUTION / AVAILABILITY STATEMENT
Approved for Public Release
Distribution is Unlimited

12b. DISTRIBUTION CODE

13. ABSTRACT *(Maximum 200 words)*

Vol. II: A Continuum Surface Layer Effect in Polycrystalline Aggregates

Uniaxial tension tests on uniform cross section specimens of Ti-6Al-4V and aluminum 7475-T651 show that the stress in the direction of load application determined by x-ray diffraction and the nominal applied stress display the expected linear correspondence up to a maximum stress somewhat below the bulk yield point. Above this stress, the x-ray stress is noticeably less than expected. Upon unloading, there is a substantial acquired compressive residual stress. Because the x-ray diffraction measurements provided average stress values in a surface layer of only a few grain diameters, these results suggest that the surface layer of the metal is yielding at a lower stress than the bulk. This anomalous behavior is duplicated qualitatively with a continuum model of an aggregate of soft and hard square grains obeying the Von Mises yield criterion. The effect is purely mechanical. No material effects, such as lower yield point or dislocation density for the surface grains, are invoked. The continuum effect decreases rapidly with depth, becoming negligible for depths exceeding 2-3 grain or domain diameters.

14. SUBJECT TERMS
Airframes; Fatigue (Mechanics); Fatigue Life; Predictions; Failure (Mechanics); Spectra; Computerized Simulation; Residual Stress; X-Ray Diffraction

15. NUMBER OF PAGES
223

16. PRICE CODE

17. SECURITY CLASSIFICATION OF REPORT	18. SECURITY CLASSIFICATION OF THIS PAGE	19. SECURITY CLASSIFICATION OF ABSTRACT	20. LIMITATION OF ABSTRACT
UNCLASSIFIED	UNCLASSIFIED	UNCLASSIFIED	

FOREWORD

The work described in this report was performed by the Virginia Polytechnic Institute and State University, Engineering Science and Mechanics Department, for the Naval Air Development Center under contract number N62269-85-C-0256. The principal investigator was Professor Norman E. Dowling. The program manager for NADC was L. W. Gause; the project engineer was R. E. Vining. The x-ray experimental work presented in Volume II was performed jointly by D. O. Dunn and M. P. Laurent.

TABLE OF CONTENTS

LIST OF FIGURES

LIST OF FIGURES
(Continued)

LIST OF FIGURES
(Continued)

LIST OF FIGURES
(Continued)

LIST OF FIGURES
(Continued)

LIST OF FIGURES
(Continued)

LIST OF FIGURES
(Continued)

LIST OF FIGURES
(Continued)

LIST OF FIGURES
(Continued)

LIST OF FIGURES
(Continued)

LIST OF FIGURES
(Continued)

LIST OF FIGURES
(Continued)

LIST OF FIGURES
(Continued)

LIST OF TABLES

LIST OF TABLES
(Continued)

LIST OF TABLES
(Continued)

LIST OF TABLES
(Continued)

1.0 INTRODUCTION

1.1 OBSERVATION OF A SURFACE LAYER EFFECT IN OUR LABORATORY

In the course of validating the determination of stress by x-ray diffraction in a Ti-6Al-4V alloy, Dowling and Dunn in 1989 [1] obtained anomalous results. Testing a uniform cross-section specimen under uniaxial tension, they found that the axial stress determined from the x-ray diffraction data is in good agreement with the nominal applied stress S only up to a certain value; above this value, associated approximately with the proportional limit of the material, the value of the x-ray stress is less than the applied stress (Figure 1-1). Based on the shallow penetration depth of the x-ray radiation (about 10 μm) and because the x-ray diffraction method monitors only the elastic strain, Dowling and Dunn concluded that the stress in a thin surface layer actually decreases. In other words, a thin surface layer appears to have a lower global yield point than the interior parts of the material. This behavior is not expected for a homogeneous isotropic or anisotropic material. A uniform cross section specimen of homogeneous material subjected to a uniform tensile load must have a uniform stress throughout its cross section. The state of stress arbitrarily near the surface is thus identical to that in the interior of the material. Because the test specimens were carefully prepared so that surface material would be representative of the bulk, the anomalous x-ray data was initially perplexing [2]. Noting that, in general, a piece of metal is not a homogeneous continuum but a polycrystalline aggregate, and that a free surface can have a significant effect on the stress field arising from an inclusion in a uniform matrix (Reference [3], Section 15), a surface layer effect in a metal may actually be inevitable on purely mechanical grounds.

1.2 PREVIOUS OBSERVATIONS

One of the earliest reports of a surface layer effect appears to be that of Bollenrath, Hauk, and Osswald in 1939 [4]. From X-ray diffraction measurements, they inferred the presence of a compressive macroscopic stress in the surface layer of mild steel bars that had been plastically extended. The effect they reported was considerable: the sum of the normal compressive stresses in the surface was comparable to the yield point of the steel (40

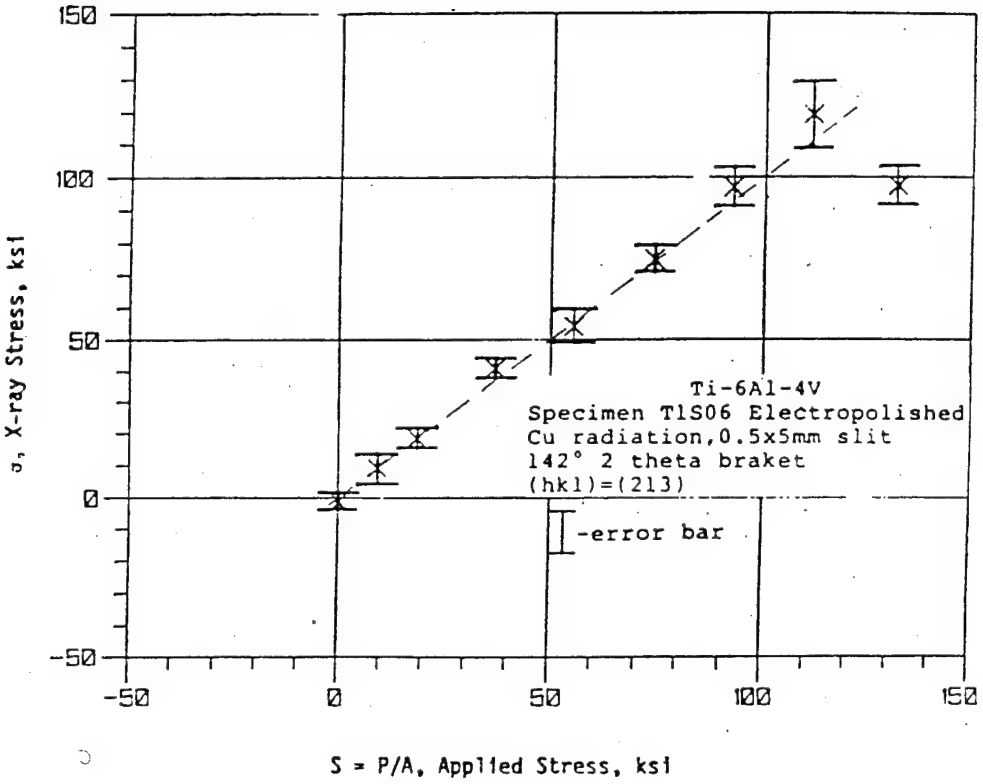

Figure 1-1. Stresses measured by x-ray diffraction during monotonic loading of a uniform cross section electropolished Ti-6Al-4V specimen. The dashed line corresponds to perfect agreement with the applied stress (Dowling and Dunn, 1989 [1]).

ksi) and the surface layer extended to a depth of approximately 0.04 inch. Subsequent work by other investigators did not confirm these results [5]. In particular, Smith and Wood [6] concluded that the residual lattice strains they observed in plastically extended mild steel rod could not be due to a macrostress because these strains did not change appreciably with depth. They proposed these residual strains are microstrains arising from a differential deformation of the grain interior and its boundary layers. Greenough [7] further refined this concept of microstrains with less speculative assumptions. He developed a model based on the plastic anisotropy of the individual crystals of the aggregate. As the aggregate is deformed, grains in favorable orientations for plastic slip yield first and become more plastically strained than neighboring grains. Upon release of the external load, the "soft" parts are driven into compression by the hard parts. To test this hypothesis, Greenough performed residual lattice strain measurements by x-ray diffraction on plastically extended samples of commercially pure aluminum, copper, and nickel. The results for these f.c.c. polycrystalline aggregates were in satisfactory agreement with his semi-quantitative model, except for a small component of the strain, consistent with a macroscopic compressive stress superimposed on the calculated intergranular microstresses.

Greenough [8] subsequently demonstrated by x-ray diffraction the existence of significant macroscopic residual surface stresses in plastically extended Armco iron. Specimens were elongated plastically 11% with an applied tensile stress of 44 ksi. From residual lattice strains determined by x-ray diffraction in the unloaded specimens, Greenough infers the existence of macroscopic stresses superimposed on the Heyn [9] intergranular stresses. Whereas the latter extend throughout the specimen, the macroscopic stresses are confined to a surface layer about 2 to 3 grains in depth (0.008 in), as determined from etching experiments. The macroscopic stress is biaxial with both components compressive: the transverse stress, i.e., perpendicular to the elongation direction, and the longitudinal stress, i.e., in the direction of elongation, are almost equal (5.7 and 6.3 ksi, respectively). Greenough [8] also inferred the presence of a residual macroscopic stress system in the surface layer of mild steel (0.10 C) specimens plastically extended 6% by an applied tensile stress of 43 ksi. The transverse stress found is 6.3 ksi, close to the value for Armco iron. The longitudinal stress and stressed layer depth could not be determined because the etching process introduced compressive stresses in the steel. In fact, Greenough [8] suggests that a reason for the disagreement of his results with those of Bollenrath et al.

[4], who observed much larger effects, and those of Smith and Wood [6], who found no macroscopic surface stresses, is that these earlier workers used an unsuitable etching technique. He attributes the development of a macroscopic compressive surface stress in the direction of plastic elongation to the yield stress of grains with a free surface being lower than that of grains of the same orientation in the interior of the aggregate, where they are completely surrounded by other grains [5], [8]. He offers no explanation for the transverse compressive surface stress.

In 1955, Nakanishi [10], also observed a surface layer effect in mild steel, concluding that the surface layer yields at a stress 0.778 times the yield stress of the bulk material and that the inherent strength of the surface layer, which experiences only half of the mutual crystal interference of the inner parts, is only half of the bulk inherent strength or yield point. He estimates the thickness of this surface layer to be about 5 mean grain diameters [11]. Kolb and Macherauch [12] studied by x-ray diffraction the flow stress in the surface layer of polycrystalline pure nickel (99.8%) specimens subjected to uniaxial tension deformed plastically to strains of up to 27%. They found that after passing the yield point the surface layer has a stress which is less than the average stress in the sample, the difference increasing with increasing plastic deformation. Upon unloading, a residual compressive macrostress is observed in the surface layer, which increases with the plastic deformation to which the specimens was subjected during tensile loading.

They explain these results by noting that the surface crystallites and those near the surface are less hindered relative to their slip processes than the crystallites in the interior. They hypothesize that, as a consequence, work hardening of the surface grains is less than that of the inner grains. This inhomogeneity of work hardening leads to an inhomogeneous stress distribution over the cross-section. The surface layer being less work hardened can yield first and is thus driven into a macroscopic compressive stress upon unloading. In summary, they propose that a difference in the work hardening of the grains in the surface layer and the interior of the specimen account for the experimental observation. As further proof of this mechanism, they note that the distribution of etched dislocations in the surface of a 16% deformed nickel sample is markedly lower that the density in the same specimen after removing a thin layer (0.3 mm) by electropolishing. Similar results were obtained previously with two other f.c.c. metals, aluminum and copper [12]. These results appear to be supported by tensile data reported by Fleischer and

Hosford in 1961 [13]for coarse grained aluminum polycrystals (99.99 Al), containing 2 to 13 crystals per cross-section. The stress required for a given plastic strain (0.5 to 4%) increases with the average number of grains in the cross section both at 295°K and 4.2°K. In addition, the specimens with 1.9 to 4.2 grains in the cross section exhibit a region of increasing slope in the stress versus strain curve at 4.2°K, attributed to easy glide occurring across part of the samples. The authors conclude that the "grain size" effect is probably a result of the surface crystals hardening less rapidly than the interior grains. Thus, the surface crystals have an effective yield point which is lower than the interior crystals. Based on the dependence of stress required for a given plastic strain (1%), they concluded that dislocation pileups at grain boundaries are not a significant effect for their coarse specimens. Such pileups become important only when the crystals are small enough that the separation of grain boundaries become comparable with that of barriers within the grain.

More recently, Sasaki and Sato [14] also deduced a surface layer effect in a mild steel (1022) based on the load-strain curves of thin-walled hollow cylinders under compression, bending, or torsion and rectangular beams under bending. The load-strain curves thus obtained deviate from the elastic line before reaching the lower yield point. The stress at which departure from linearity is detectable is about 0.75 of the yield under uniform stress. Thus, they conclude that the surface layer has a yield stress 0.75 times that of the bulk material under uniform stress. The effect is also more pronounced for the large grain material (24 μm) than for the smaller grained steel (16 μm).

Although workers have recognized the surface layer effect as being connected with the lesser spacial constraint of the surface crystals, which have a free surface, compared with the inner crystals, their explanation of the surface layer effect when offered in more detail involves a material effect, e.g., a difference in dislocation density arising at the surface versus the interior, or lower yield point of surface grains resulting from easier slip as a result of being less confined. Other explanations consider the surface layer effect an artifact rather than a real effect, arising from the nature of x-ray diffraction measurements. These include a lattice parameter change in going from the annealed to the cold worked metal (after plastic deformation), which gives the impression of a macroscopic residual stress after plastic deformation. Another suggestion is the "indicator grain" model whereby the apparent position of diffraction peak is mostly determined

by the grain and subgrain that have been deformed least during plastic flow, while the work-hardened, highly deformed grains produce broad, diffuse reflections which contribute little to peak position (Reference [15], pp. 333-335, Reference [16], pp. 483-484).

The possibility that a surface layer effect can be expected from purely continuum mechanical considerations does not appear to have been considered by earlier workers. Although the surface layer effect, when it exists, probably arises from a combination of causes, this report focuses on the contribution of continuum effects. Work presented here suggests that even if the interior and surface grains of the polycrystalline aggregate are identical, a continuum analysis predicts a surface layer effect. This makes a surface layer effect an inherent property of an aggregate of anisotropic crystals. This approach may be viewed as an extension of the Heyn intergranular stresses to include the effect of a free surface.

1.3 INCLUSIONS IN A HALF SPACE

The simplest idealized case demonstrating the continuum effect of a free surface on the deformation of a crystal might be an isotropic inclusion with a plastic strain imbedded in an elastic half-space. Lin and Tung [17] obtained a closed-form analytical solution for cuboidal inclusion with uniform plastic slip embedded at the free surface of a semi-infinite elastic solid. Comparing their results with the corresponding ones for an infinite solid, they conclude that there is a significant surface effect. In particular, they find that for the crystals to have the same relief of resolved shear stress, the surface grains has to undergo a larger plastic strain, i.e. elongate more. Chiu [18] provides an analytical solution for the stress field in a half space containing an embedded cuboidal zone at an arbitrary distance from the surface and which has a uniform arbitrary eigenstrain. He does not provide numerical results for a case corresponding to plastic deformation. However, his results for the case of an initial strain in a direction parallel to the free surface show that the resistance of the elastic matrix (half-space) to the inelastic strain decreases as the grain is brought closer to the free surface, demonstrating a surface layer effect. The surface effect decreases rapidly with depth. For a cubic inclusion, it vanishes when the depth exceeds 3 times the inclusion width. Seo and Mura's [19] solution for the elastic field in a half space due to ellipsoidal inclusions with uniform dilatational

eigenstrains shows that the shape of the inclusion is important in determining the stress field in the inclusion and the matrix.

1.4 APPROACH

The contribution of purely mechanical considerations to a surface layer effect in a metallic polycrystalline aggregate was investigated. Because of the complexity of the problem, the finite element method (FEM) was used rather than an analytical approach. The FEM has the advantage of offering considerable flexibility in the formulation of the problem, including grain size, shape, and distribution, constitutive models, specimen shape (e.g. rectangular versus cylindrical), and dimensionality (2-D and 3-D problems). An advantage of an analytical solution is that point-accurate values of stress can be obtained. However, because the macrostress system in the surface layer is an average stress effect, accurate values of stress at specialized zones, such as the grain boundaries and corners, are not essential, so long as their overall contribution to the surface layer effect is small.

2.0 EXPERIMENTAL

2.1 MATERIALS

The materials for which results are presented in this report are the titanium alloy Ti-6Al-4V and the aluminum alloy 7475-T651. Identification and mechanical properties for the materials used are given in Table 2.1-1. Both were obtained as plate from which the specimens were machined. The microstructure in three mutually perpendicular planes, one of which is normal to the plate rolling direction, was examined by metallography. The titanium alloy exhibits an oblate structure, with slight flattening of the grains in the plane of the plate (Figure 2.1-1). It consists of alpha phase (hexagonal closed-packed) grains with intergranular beta phase (body-centered cubic), as determined by reference to published micrographs [20, 21]. The aluminum alloy plate, on the other hand, has the "pancake" microstructure typical of rolling with extreme flattening of the grains in the plane of plate. The grains form a matrix in which are embedded small precipitate particles (Figure 2.1-2). Grain size in the direction normal to the irradiated surface is approximately 10-30 μm for the titanium alloy and of similar dimension through the thickness of the aluminum alloy, but 100-200 μm in the rolling direction. For the latter, grain boundaries are poorly defined and grain sizes vary over a wide range.

2.2 SPECIMENS

Uniform cross section tensile specimens were machined from plate such that the specimen long axis is parallel to the rolling direction, and the specimen center plane coincides with that of the plate. The gauge section of the straight specimen is one inch long with a cross section of 0.22 in by 0.50 in (Figure 2.2-1). The gauge area of all the specimens was electropolished 0.002 to 0.003 in, thereby removing the worked surface layer and the attendant residual stresses. The electropolishing was performed by Lambda Research, Cincinnati, Ohio, with a proprietary process.

2.3 X-RAY STRESS DETERMINATIONS

The determination of stress by x-ray diffraction was made by the well-known "d" versus $\sin^2 \psi$ method. A detailed description of this method is

Table 2.1-1. Materials identification and properties.

	T_i-6Al-4V	7475-T651-Al
Identification	Ingot 9902110200	Serial No. 511348-1
Source	RMI, Niles, OH	Alcoa Labs, Alcoa Center, PA
Form	3/8 inch plate	3/4 inch plate
Condition	mill-annealed 1450°F, 15 minutes	solution-treated and aged
Ultimate (ksi)	142	---
Yield (ksi) 0.2% 0.02%	 133 124	 78.5 72.3
Proportional limit (ksi)	115	54
Elongation	14	---

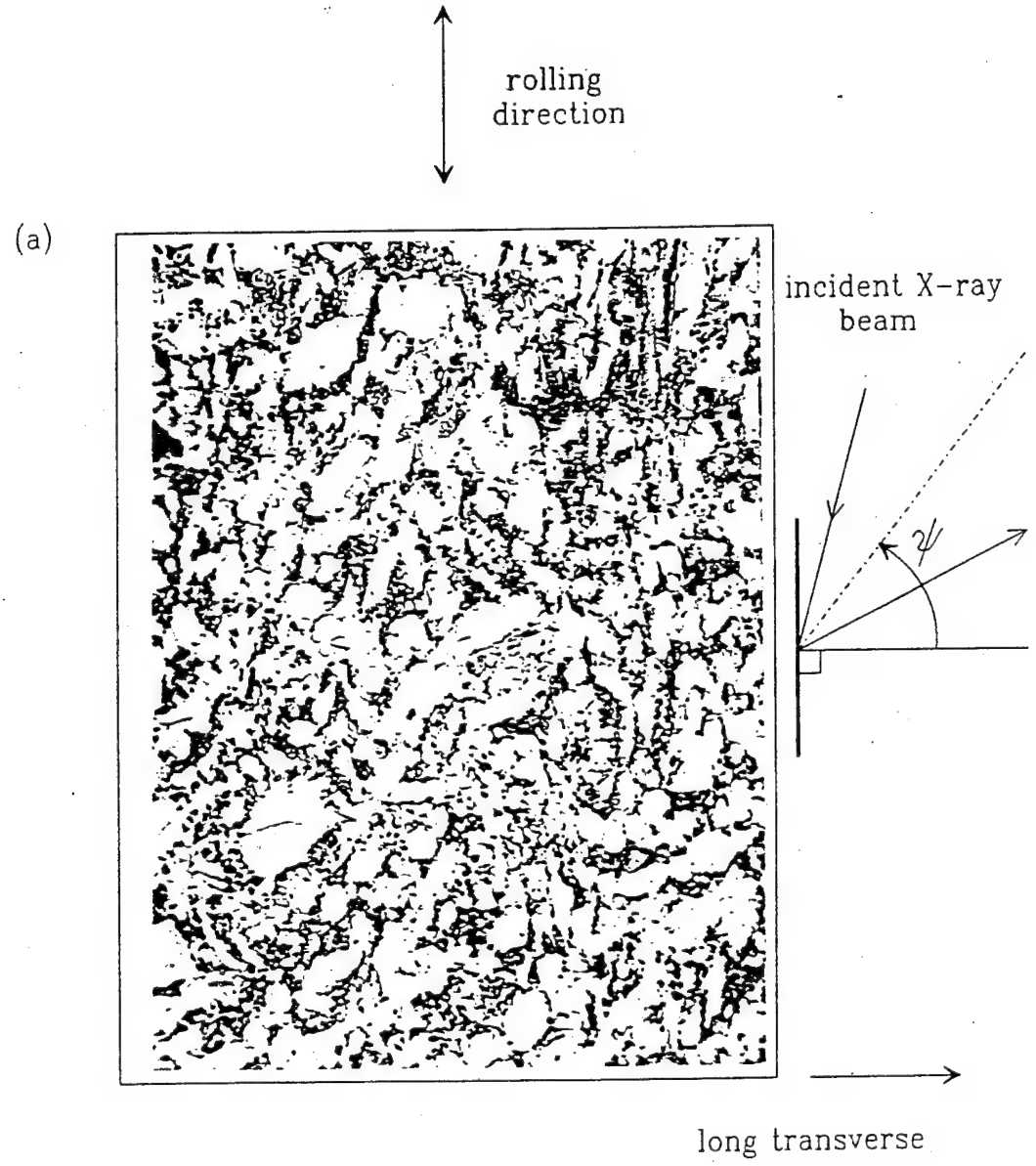

Figure 2.1-1. Microstructure of the Ti-6Al-4V alloy. (a) Plane parallel to the rolling direction and the long transverse. The incidence of the x-ray beam relative to this surface is shown. (500X)

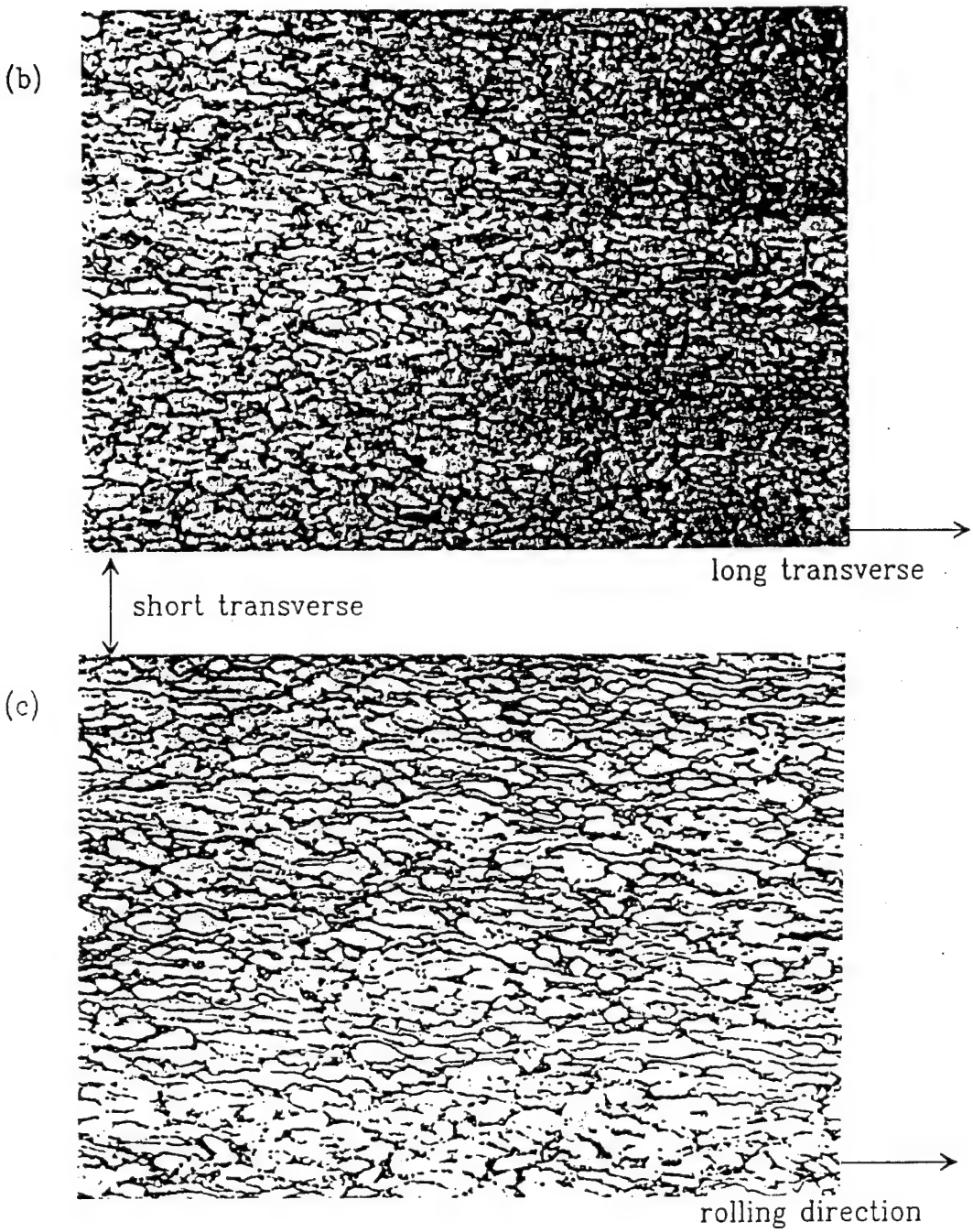

Figure 2.1-1 (continued). Microstructure of the Ti-6Al-4V alloy. (b) Plane normal to the rolling direction. (c) Plane containing the rolling direction and the short transverse. This plane is parallel to the irradiated surface. (500X)

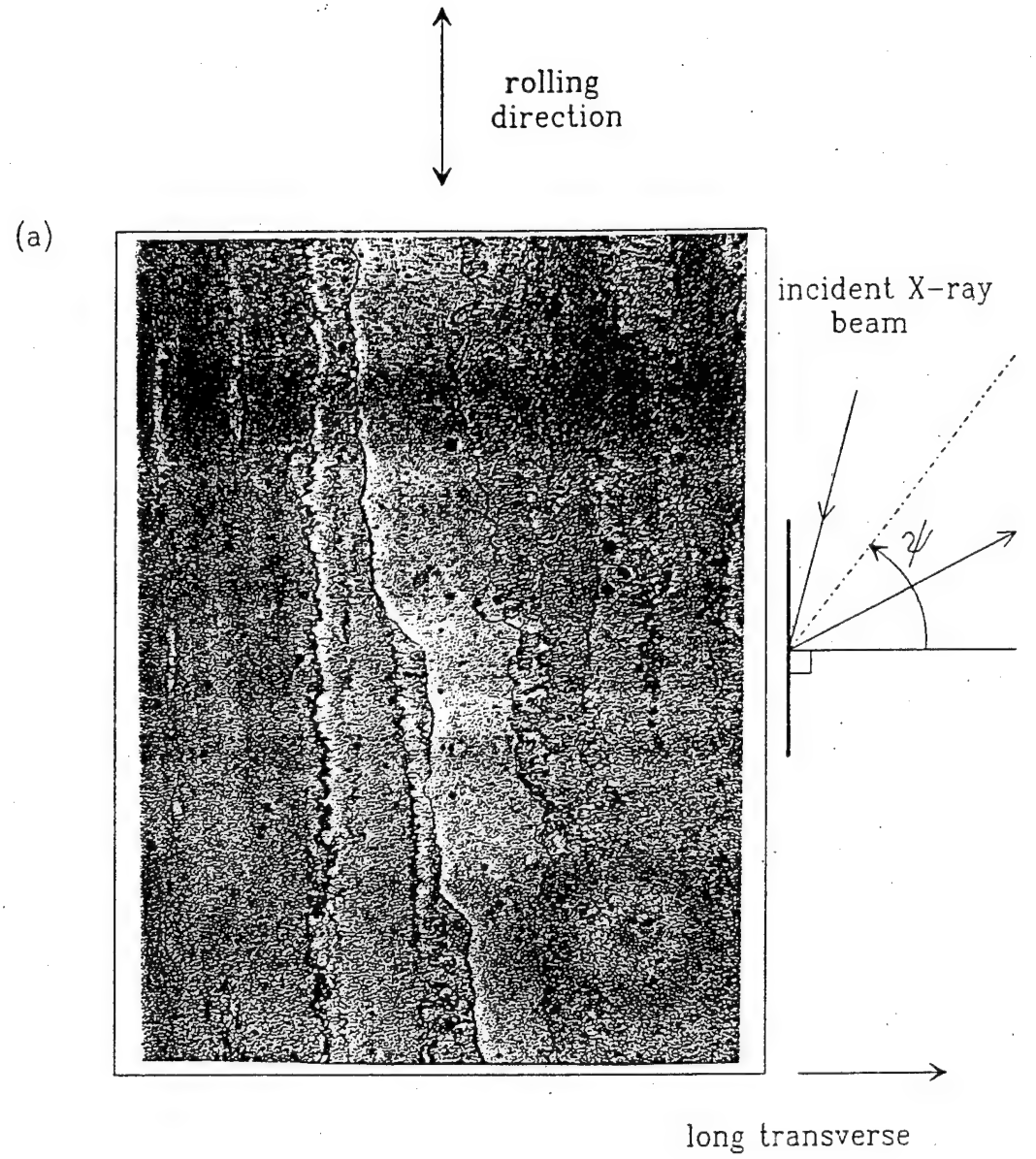

Figure 2.1-2. Microstructure of the 7475-T651 alloy. (a) Plane parallel to the rolling direction and the long transverse. The incidence of the x-ray beam relative to this surface is shown. (125X)

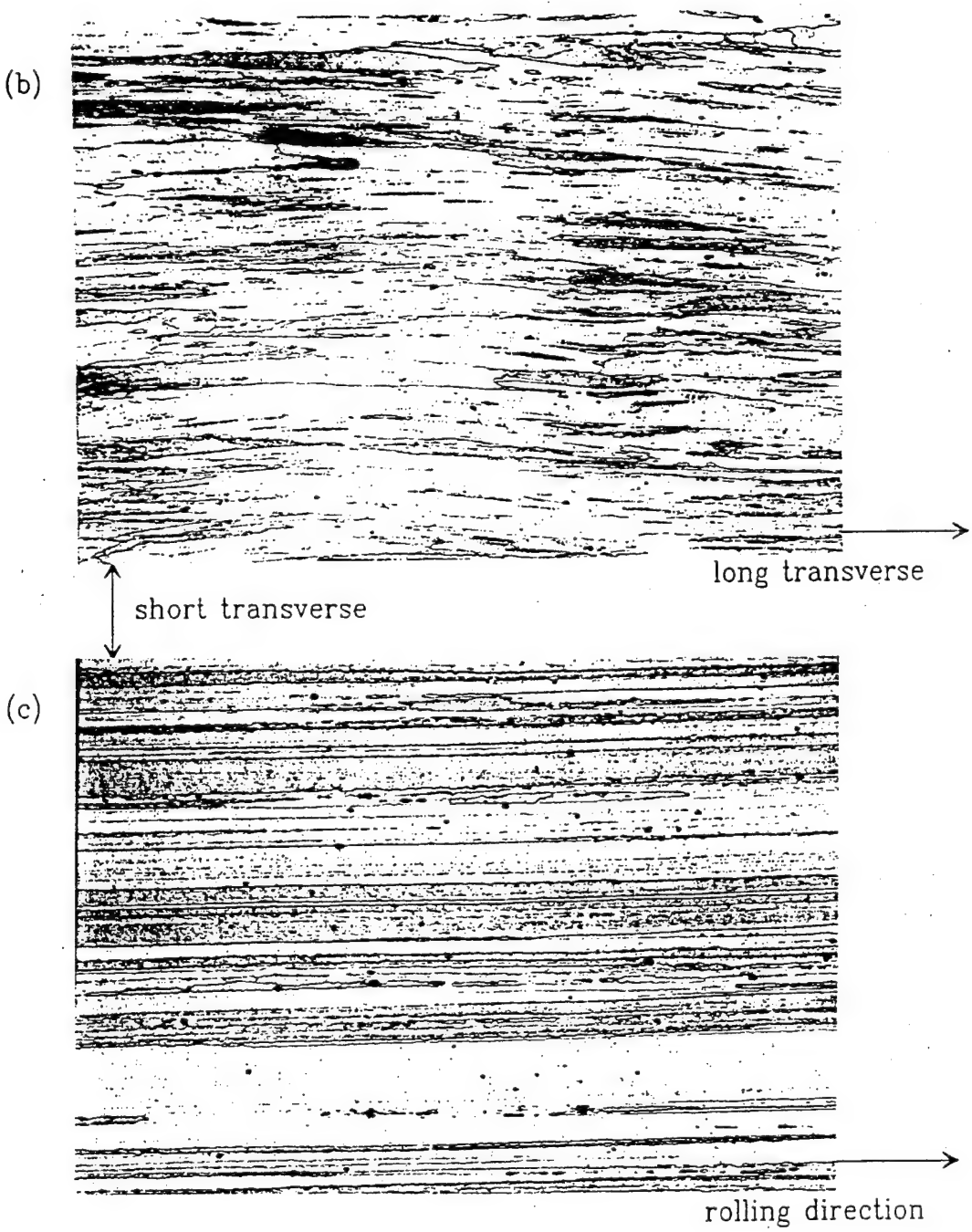

Figure 2.1-2. Microstructure of the 7475-T651 alloy. (a) Plane parallel to the rolling direction and the long transverse. The incidence of the x-ray beam relative to this surface is shown. (125X)

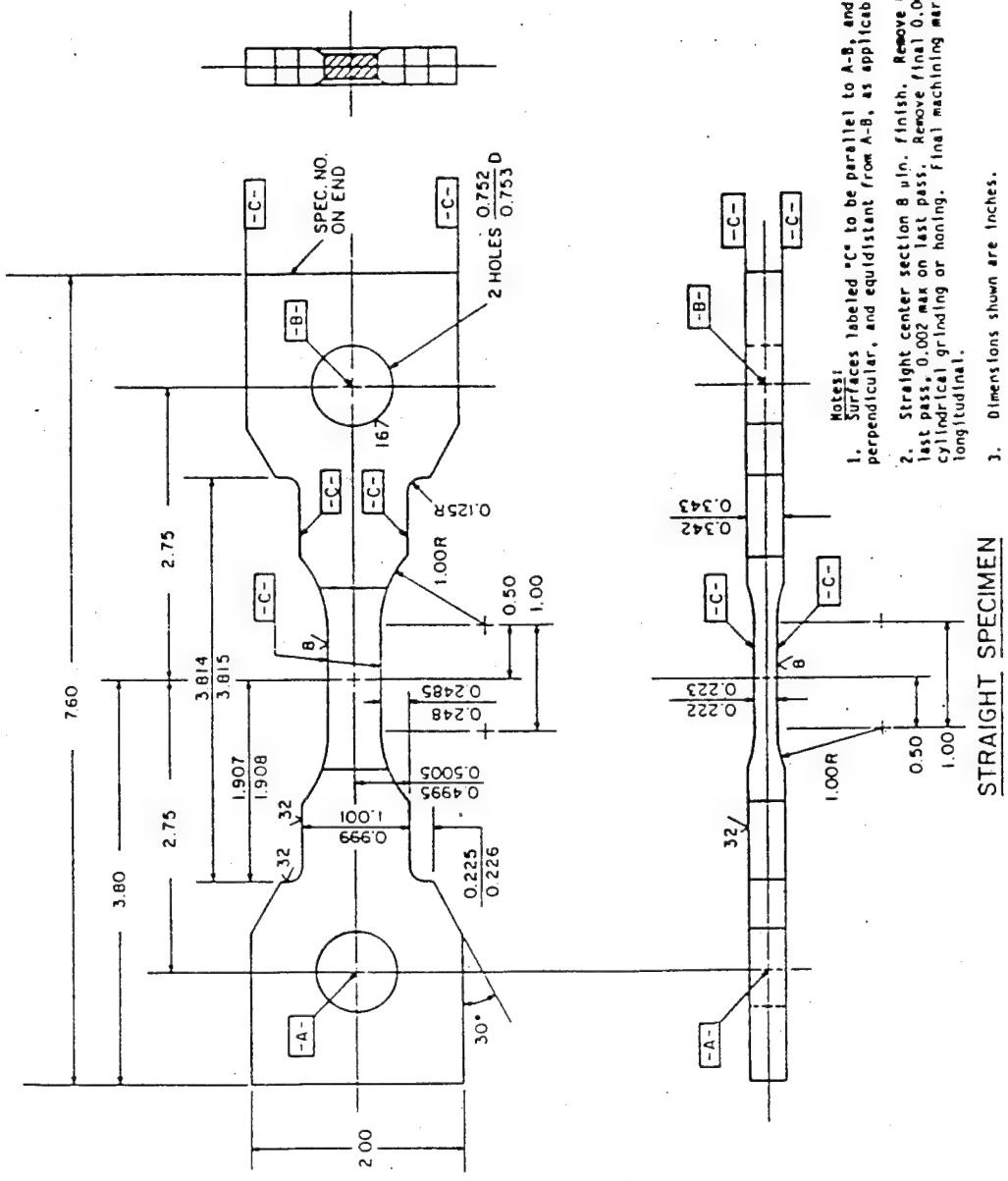

Figure 2.2-1. Drawing of the uniform cross section specimen used in the experiments to determine stress by x-ray diffraction.

given by Noyan and Cohen [22]. For a biaxial state of stress, the lattice spacing is related to the stress by

$$\frac{d - d_0}{d_0} = \frac{1 + \nu}{E} \sigma_\phi \sin^2\psi \qquad (1)$$

where Figure 2.3-1 is employed and

ψ is the angle of the diffracting planes with respect to the specimen surface plane.

ϕ is the angle which the plane containing the incident and diffracted x-ray beams make with the sample coordinate system as defined in Figure 2.3-1.

d_0 is the lattice spacing of the diffracting planes in the unstrained specimen.

d is the corresponding lattice spacing in the strained specimen determined at angles ϕ, ψ.

σ_ϕ is the normal stress in direction ϕ.

E and υ are the diffraction elastic constants, corresponding to Young's modulus and Poisson's ratio, respectively, for the chosen crystallographic planes.

This equation is based on the assumption that the polycrystalline material behavior is isotropic on a macroscopic scale. This assumption is justified when the number of grains in the diffracting volume is large and the grain orientations within it are sufficiently disordered (random, ideally). The stress σ_ϕ is typically obtained from the slope of the line fitted to a plot of d versus $\sin^2\psi$. If there is a shear stress component in the plane perpendicular to the sample surface, the stresses are no longer biaxial, and equation 2.3.1 acquires an additional term which depends on $\sin(2\psi)$. This term leads to a readily observable split in the d versus $\sin^2\psi$ graph.

The x-ray stress determinations were made with a TEC Model 1610 Mobile X-Ray Stress Analysis System [23]. The specimen remains stationary while a prescribed set of ψ angles are achieved in succession by automated motion of the x-ray source and detector. The system is compact enough that measurements

can be made on a specimen under load in a mechanical testing machine. Details of the system have been given previously by Dowling, Hendricks [24]. The position-sensitive proportional counter (PSPC) in tandem with computerized data acquisition and reduction results in measurement times of 5-20 minutes per ψ angle.

Setup parameters for the x-ray diffraction measurements are given in Table 2.3-1 for both Ti-6Al-4V and 7475-T651 aluminum. Copper K_α radiation, 1.54178 angstroms, was used in all cases. The small grain size and low degree of texture in the titanium alloy [1] made the stress determinations in this material fairly straightforward. The aluminum alloy exhibits a marked degree of preferred grain orientation [1]. However, it was possible to find a set of ψ angles for which good linear d versus $\sin^2\psi$ plots and excellent linearity between applied load and the x-ray determined stress resulted, until reaching the anomalous region which is the topic of this study. A 3° ψ-angle oscillation was used in all cases because such oscillation has been shown to reduce the effects of preferred orientation [25]. Typical d versus $\sin^2\psi$ plots are shown in Figures 2.3-2 and 2.3-3.

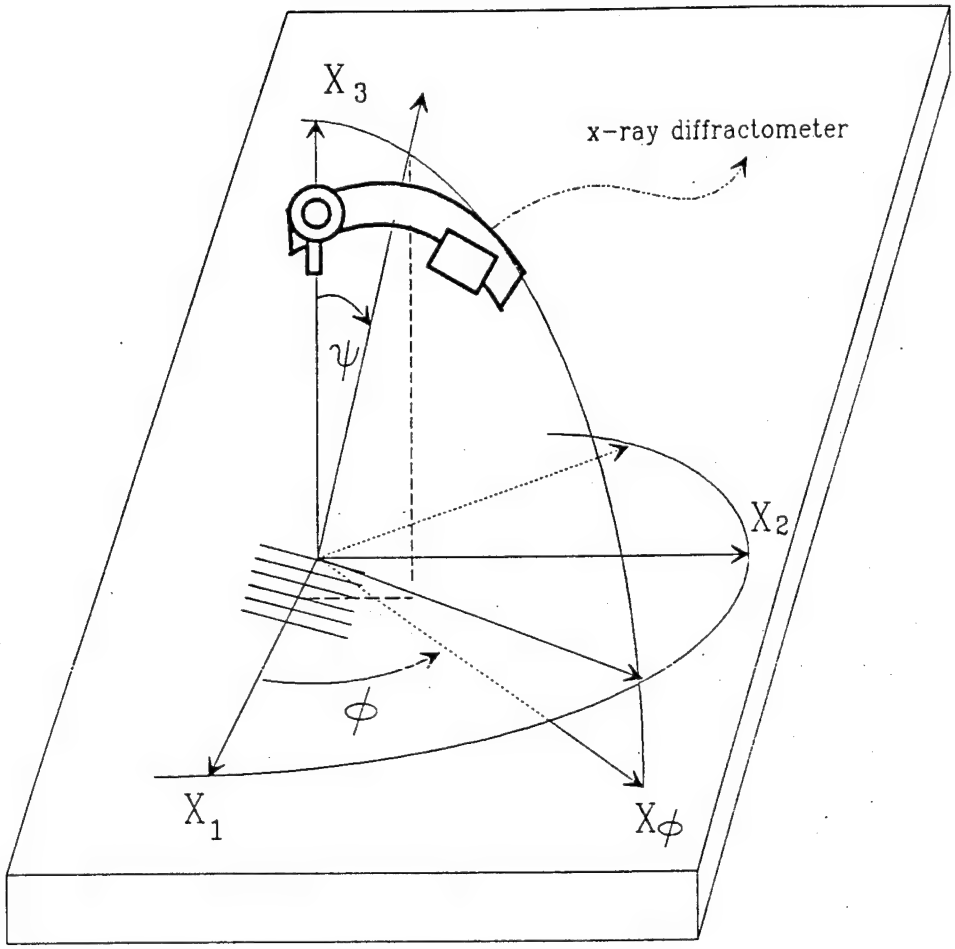

Figure 2.3-1. Definition of the sample coordinate system and the angles ψ and ϕ for the x-ray diffraction measurements.

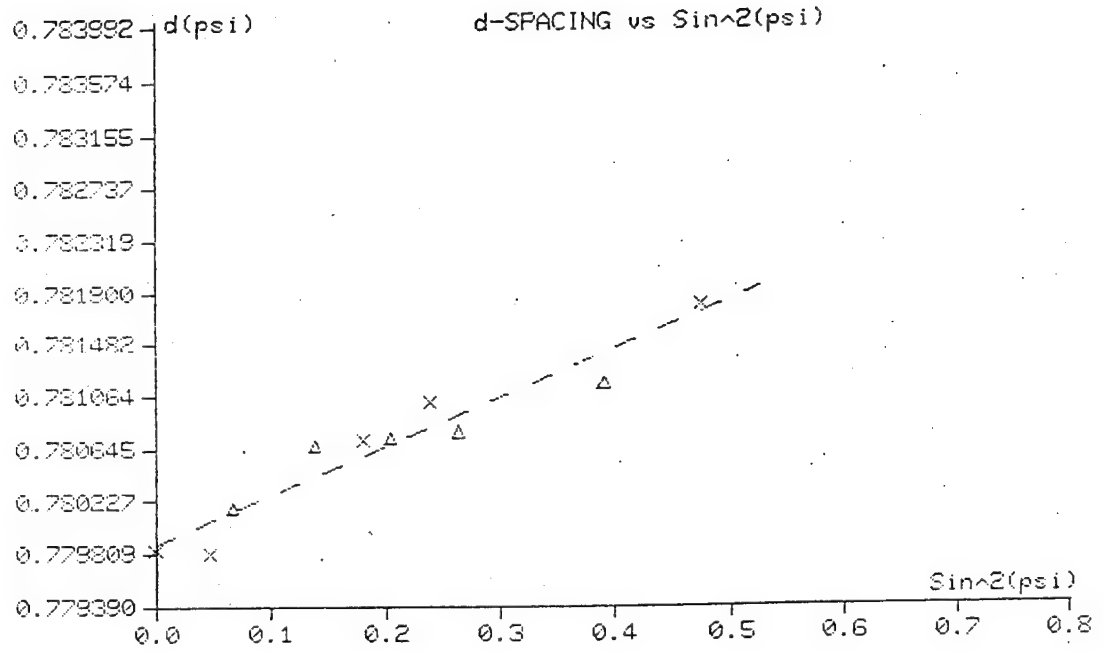

Figure 2.3-2. Typical d versus $\sin^2\psi$ plot for the 7475-T651 aluminum alloy.

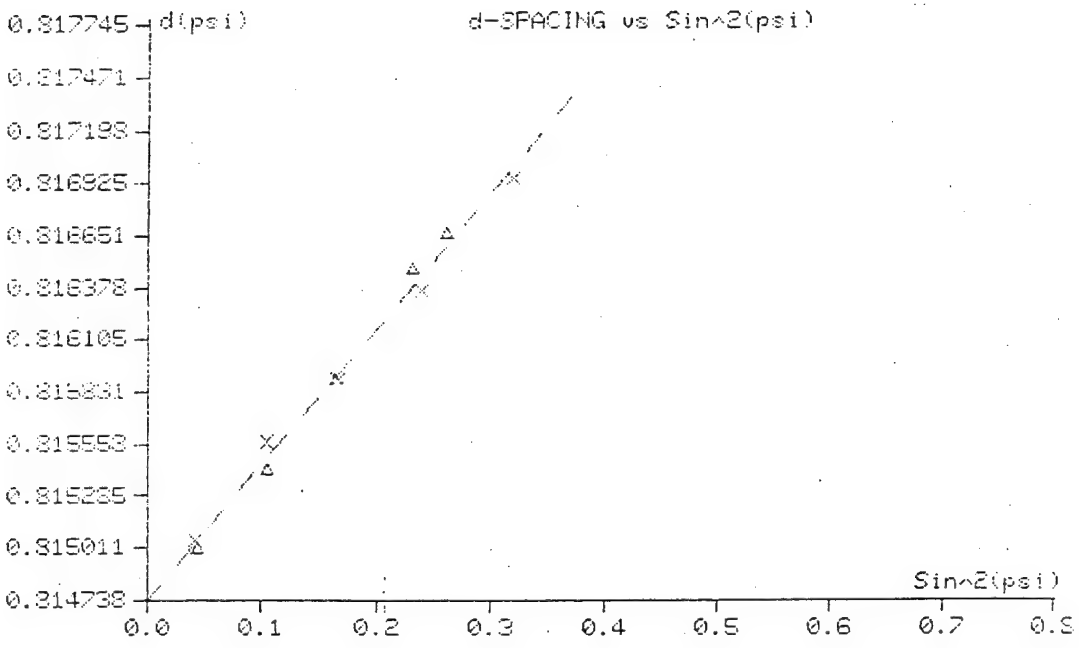

Figure 2.3-3. Typical d versus $\sin^2\psi$ plot for the Ti-6Al-4V alloy.

3.0 FINITE ELEMENT CALCULATIONS

3.1 MODELING

The "specimens" modeled are slabs consisting of lower yield point ("soft") and higher yield point ("hard") isotropic grains. In general, the hard grains formed a matrix in which the soft grains are embedded. Up to the yield point, all grains have identical isotropic linear elastic properties. The plastic anisotropy is thus modeled by the lower yield point of some grains, representing crystals in favorable orientations for yielding. For most calculations the soft grains are elastic-perfectly plastic, whereas the hard grains exhibit some work hardening to represent work hardening in the specimen. This also allowed the finite element calculations to be performed in load control, for which convergence was faster than in displacement control. To be general, calculations in which both types of grains work harden or neither type work hardens were also performed.

Because of the relatively small number of grains in the model and because only two states are considered, "soft" and "hard", a given random array of grains will, in general be less representative of average behavior than an ordered array of the same size, i.e. the ordering is itself an averaging process. For example, in a random array of 200 grains, 20 by 10 across, with 25% soft grains, it is likely that the soft grains will form a path of weakness such that the specimen will yield at a stress approximately equal to that of the yield point of the soft grains. In the limiting case of an infinitely wide array, the yield point will be approximately equal to the average yield point because the proportion of the cross section contributed by the hard grains equals their volume fraction.

The use of only two types of grains is also an averaging approximation, because in a random polycrystalline array containing an arbitrarily large number of grains, the number of grain orientations in a arbitrarily small angular interval is arbitrarily large. If low angle boundaries between grains are favored, soft and hard domains embedded in a matrix of intermediate hardness will tend to result. Thus, the grains in our model may in some cases be more properly visualized as "domains" consisting of several grains, rather than single grains.

Three concentrations (volume-fractions) of soft grains were considered: 33%, 25%, and 17%. The corresponding grain patterns for soft square grains are shown in Figures 3.1-1 (a), 3.1-2 (a), and 3.1-3 (a). The pattern for rectangular soft grains at 33% concentration is shown in Figure 3.1-4. Use of symmetry considerably reduces the number of grains required to model the specimen. First, by assigning a longitudinal and a traverse plane of symmetry to the aggregate or slab, the number of grains is reduced by a factor of four. This is deemed reasonable based on Saint-Venant's principle, from which one expects the contribution to the stress field at a given point from grains sufficiently far away to depend only on the average material properties. Analytical results for a cubic inclusion indicate that the local effect of the inclusion on the stress field becomes negligible at distances of 2 to 3 times the width of the inclusion [26]. Thus, if the specimen halfwidth exceeds 2 to 3 times the surface layer thickness, the two free surfaces, one each side, do not interfere with each other. This was verified by calculation. Halfwidths as small as 2.5 grains were found to give meaningful results for the 33% soft array.

Next, a further reduction in model size is achieved by using the symmetry planes of the ordered grain arrays, as shown in Figures 3.1-1, 3.1-2, and 3.1-3. In particular, it is desirable for the arrays to extend to infinity in the longitudinal direction, as this leads to the best longitudinal plane-averaged stresses and representation of the load boundaries in the actual specimen. If the specimen extends to infinity, then every traverse plane passing through the middle of a row of soft grains in a plane of symmetry. The minimum "cell" required for the calculations is that enclosed by the symmetry planes and the free surface (Figures 3.1-1 (b), 3.1-2 (b), and 3.1-3 (b)). The surface-free array is modeled with an infinite 2-D space, which has additionally an infinite number of symmetry planes in the longitudinal direction. The minimal cell is therefore even smaller, reducing to only 1.5, 3, and 4.5 grains for 33%, 25%, and 17% soft grain arrays, respectively (Figures 3.1-1 (c), 3.1-2 (c), and 3.1-3 (c)). The surface-free model is useful to determine the bulk mechanical properties of the array and as a control to evaluate the effect of the free surface.

From these symmetry considerations, it is clear that a non-ordered array requires a much larger minimal cell for calculation that the corresponding ordered array. Because of this, calculations for only three disordered arrays were performed. Each array is 10.5 grains wide and 20 grains long, and

repeats itself to infinity in the longitudinal direction and is symmetric with respect to its longitudinal midplane.. The soft grains concentrations were 24% (Figure 3.1-5), 25% (Figure 3.1-6), and 29% (Figure 3.1-7).

The meshes and elements used are rectangular. The meshes are defined in an x-y Cartesian coordinate system such that the y axis coincides with the free surface, and the x-axis defines the bottom plane of symmetry, which is fixed. The y-axis is thus in the longitudinal or vertical direction of the specimen, and the x-axis is normal to the free surface, the depth below this surface being equal to x. The load is applied in the y-direction. A grain was typically modeled with 8 x 8 bilinear elements, based on mesh refinement runs, although in some cases acceptable results could be obtained with as few as 4 x 4 elements. Element aspect ratios were typically one, and never exceeded 2. Mesh refinement in the surface layer region was not found to be necessary, although it was used in some runs to obtain more detail in that region, or for large problems which required minimizing the number of elements, such as for the disordered arrays (Figure 3.1-8). A mesh of uniform square elements gave the best convergence characteristics. Bilinear elements were found to be more economical than biquadratic elements for comparable accuracy, even with reduced integration.

The boundary conditions for the specimens with a free surface are as follows, given that w is the mesh width (i.e., the specimen halfwidth), h is the mesh height, u_x is the nodal displacement in the x-direction, and u_y is the nodal displacement in the y-direction:

(1) $u_x = 0$ for x = w, defining the vertical plane of symmetry, which is fixed;

(2) $u_y = 0$ for y = 0, defining the bottom plane of symmetry, which is fixed;

(3) u_y is equal for all the nodes at y = h, defining the top plane of symmetry, which can move in the y-direction in reaction to the applied load.

The load was applied to an arbitrary node on the top plane, typically the node at x = w, y = h, i.e., in the upper right hand corner of the mesh.

The modeled specimen was loaded uniaxially in the y-direction, with the ends moving rigidly in this direction, as required by symmetry. The load was applied in steps until the bulk yield point was exceeded and longitudinal strains on the order of 3-5% were achieved. Typically, the specimen was unloaded after every load increase to obtain the residual stresses as a function of applied load and the bulk longitudinal plastic strain. Specific loading histories are given in the Results section.

The nonlinear nature of these calculations requires the careful selection of the loading steps to ensure convergence and to obtain the desired bulk deformation. Although displacement loading has the advantage of affording specimen deformation control, it was determined that convergence is difficult or impossible at strains above 0.001 for meshes with more than a few hundred elements. By contrast, load control exhibited excellent convergence characteristics up to strains exceeding 0.05 for all mesh sizes tries. Two schemes proved feasible: mixed applied up to 0.001 strain, followed by load control. Appropriate loads and displacements were calculated by a preprocessing program from the stress-strain curve of a test run or a similar final run. The infinite space calculations, being modest, were useful to estimate the stress-strain curve. Values of stress at desired plastic strains were interpolated from cubic spline fits during postprocessing.

Grain plasticity was modelled with an inviscid incremental plasticity theory using a Mises-Hill yield surface and an associative flow rule, i.e., the plastic strain rate is in the direction of the normal to the yield surface. A detailed treatment of plasticity with finite elements is given by Hinton and Owen [27] and, more recently, by Chen and Han [28]. Isotropic hardening was assumed in view of the modest degree of work hardening assigned to the grains (typically zero for the soft grains). In trial runs, kinematic and isotropic hardening (Figure 3.1-9) lead to almost identical results. Linear geometry was assumed, unless otherwise stated.

3.2 IMPLEMENTATION AND PROCESSING

The finite element calculations were performed with ABAQUS, Versions 4.8, 4.9, and 5.2 (Hibbitt, Karlsson, and Sorensen, Inc.) Preprocessing and postprocessing were accomplished with in-house FORTRAN and REXX programs and CAEDS version 3, Release 1, of the International Business Machines Corporation. CAEDS V3 is equivalent to I-DEAS Level 4 of the Structural

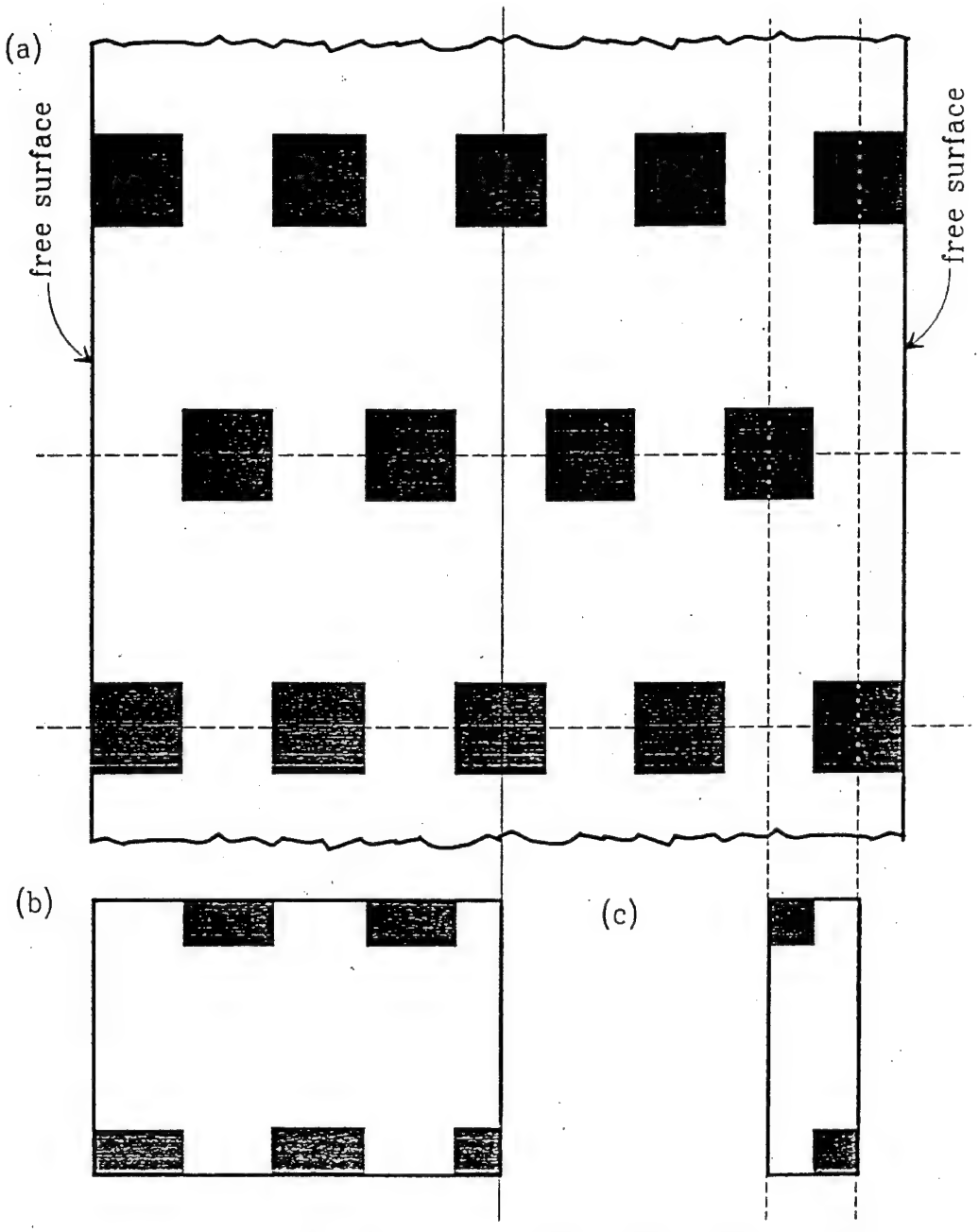

Figure 3.1-1 Ordered array with 17% soft grains (shaded). (a) The infinite strip with two free surfaces, shown here with a width of 9 grains. It is symmetrical about the center line. (b) The minimum cell required to represent the array in (a). (c) The minimum cell to represent the infinite, surface-free version of (a). The horizontal dashed lines denote representative planes of symmetry in the strip and infinite space, and the vertical dashed lines denote additional symmetry planes in the infinite space.

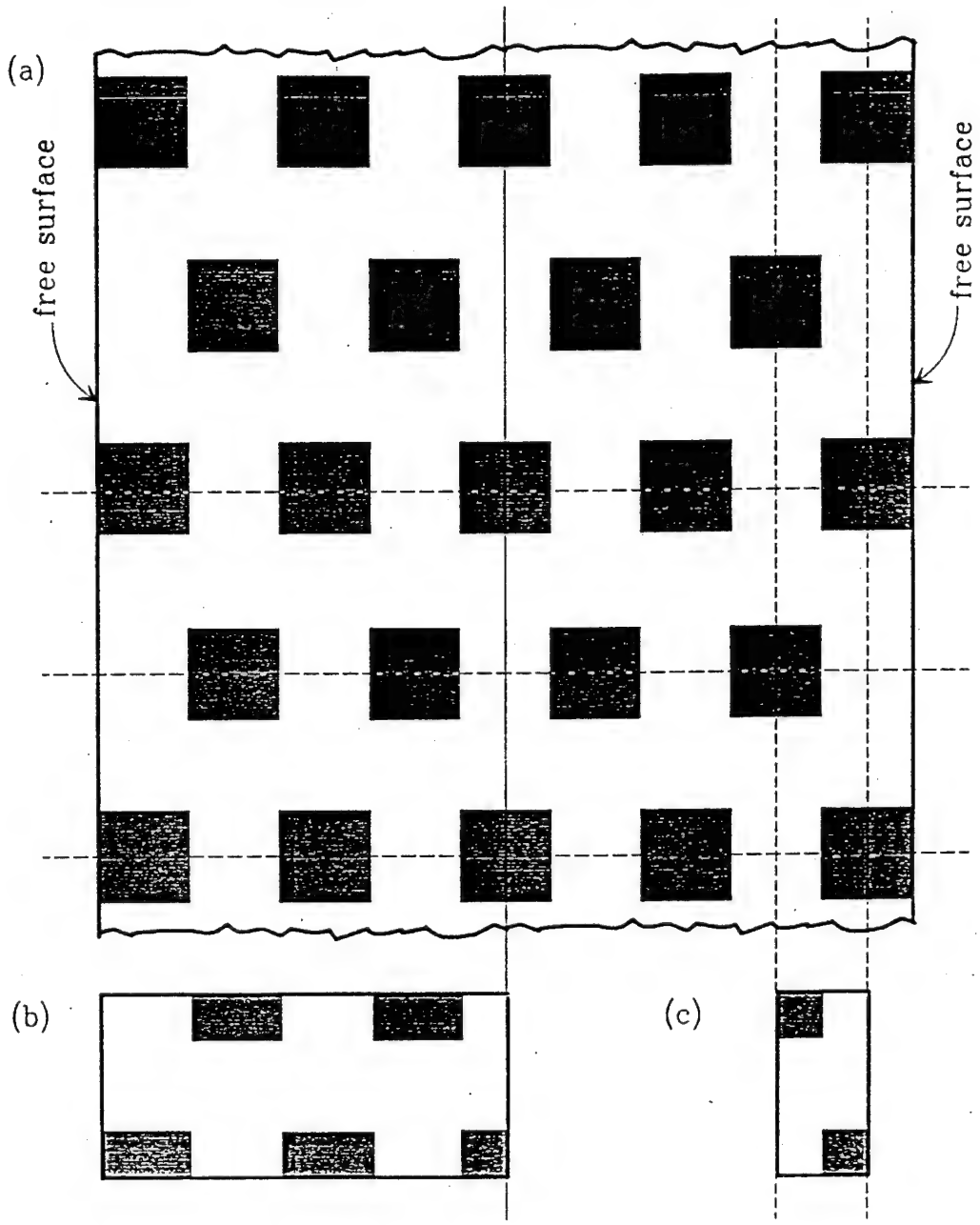

Figure 3.1-2 Ordered array with 25% soft grains (shaded). (a) The infinite strip with two free surfaces, shown here with a width of 9 grains. It is symmetrical about the center line. (b) The minimum cell required to represent the array in (a). (c) The minimum cell to represent the infinite, surface-free version of (a). The horizontal dashed lines denote representative planes of symmetry in the strip and infinite space, and the vertical dashed lines denote additional symmetry planes in the infinite space.

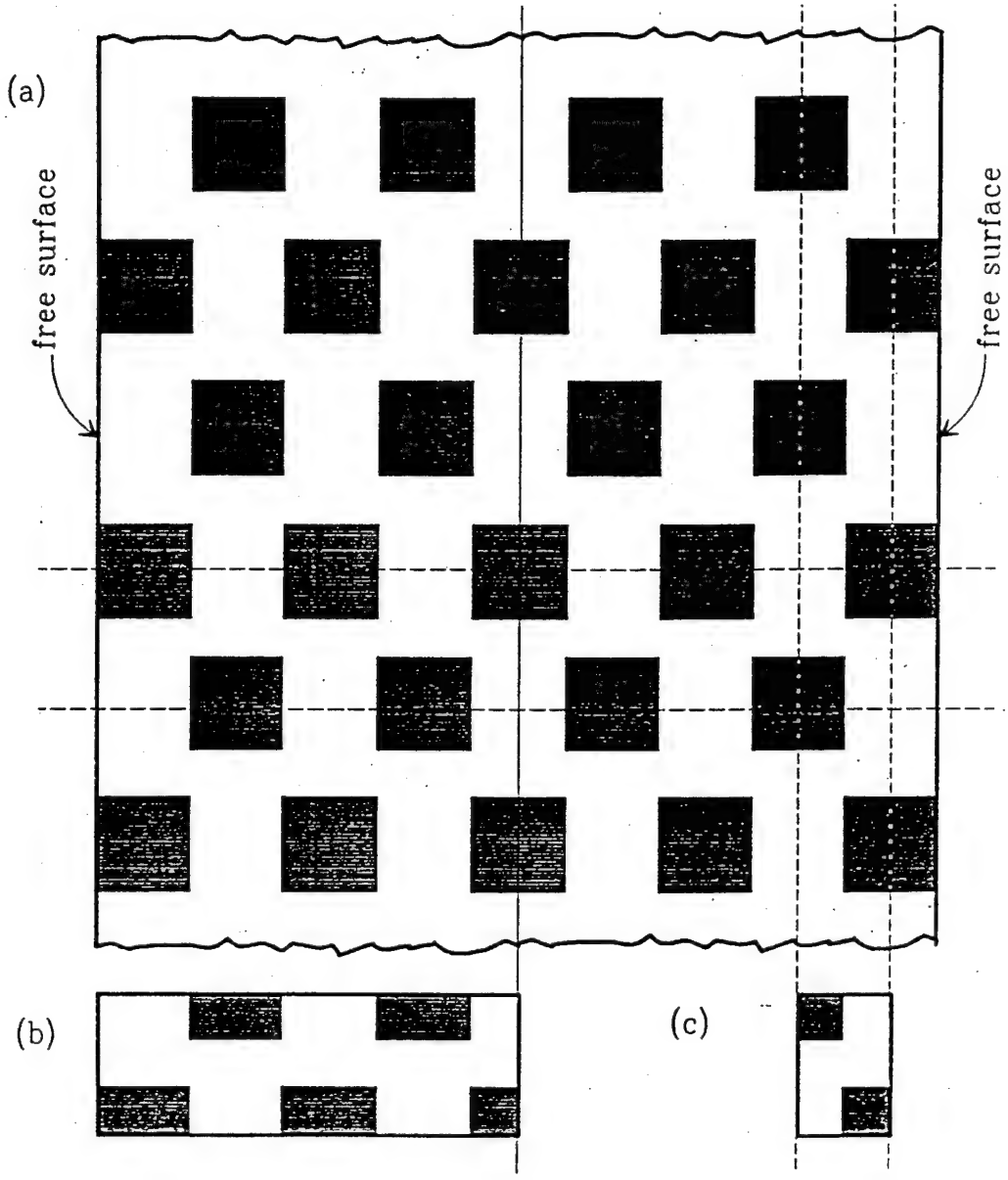

Figure 3.1-3 Ordered array with 33% soft grains (shaded). (a) The infinite strip with two free surfaces, shown here with a width of 9 grains. It is symmetrical about the center line. (b) The minimum cell required to represent the array in (a). (c) The minimum cell to represent the infinite, surface-free version of (a). The horizontal dashed lines denote representative planes of symmetry in the strip and infinite space, and the vertical dashed lines denote additional symmetry planes in the infinite space.

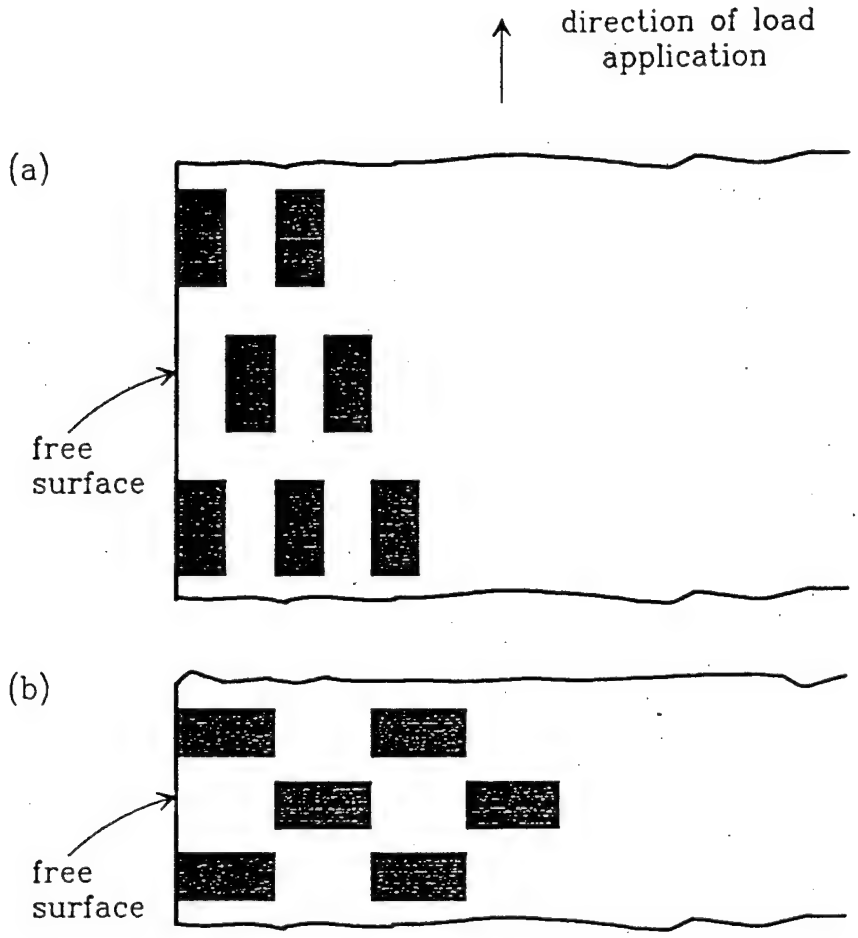

Figure 3.1-4. Ordered arrays with rectangular grains, shown here with an aspect ratio of two and a soft grain concentration of 33% (shaded areas). (a) Elongated grains (GAR = 2). (b) Wide grains (GAR = 0.5).

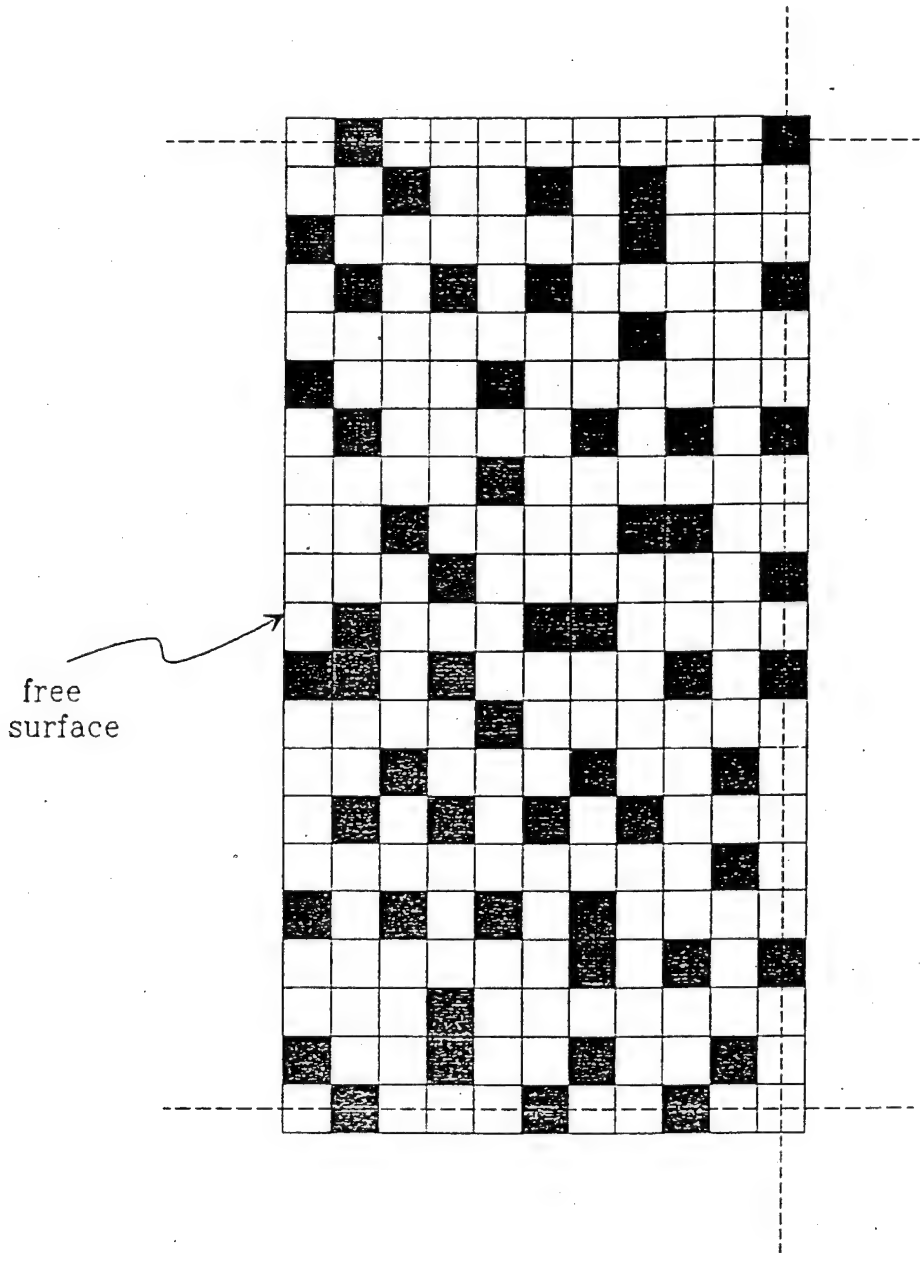

Figure 3.1-5 Disordered array, 24% soft grains (shaded). Dashed lines denote the planes of symmetry used in the finite element calculations.

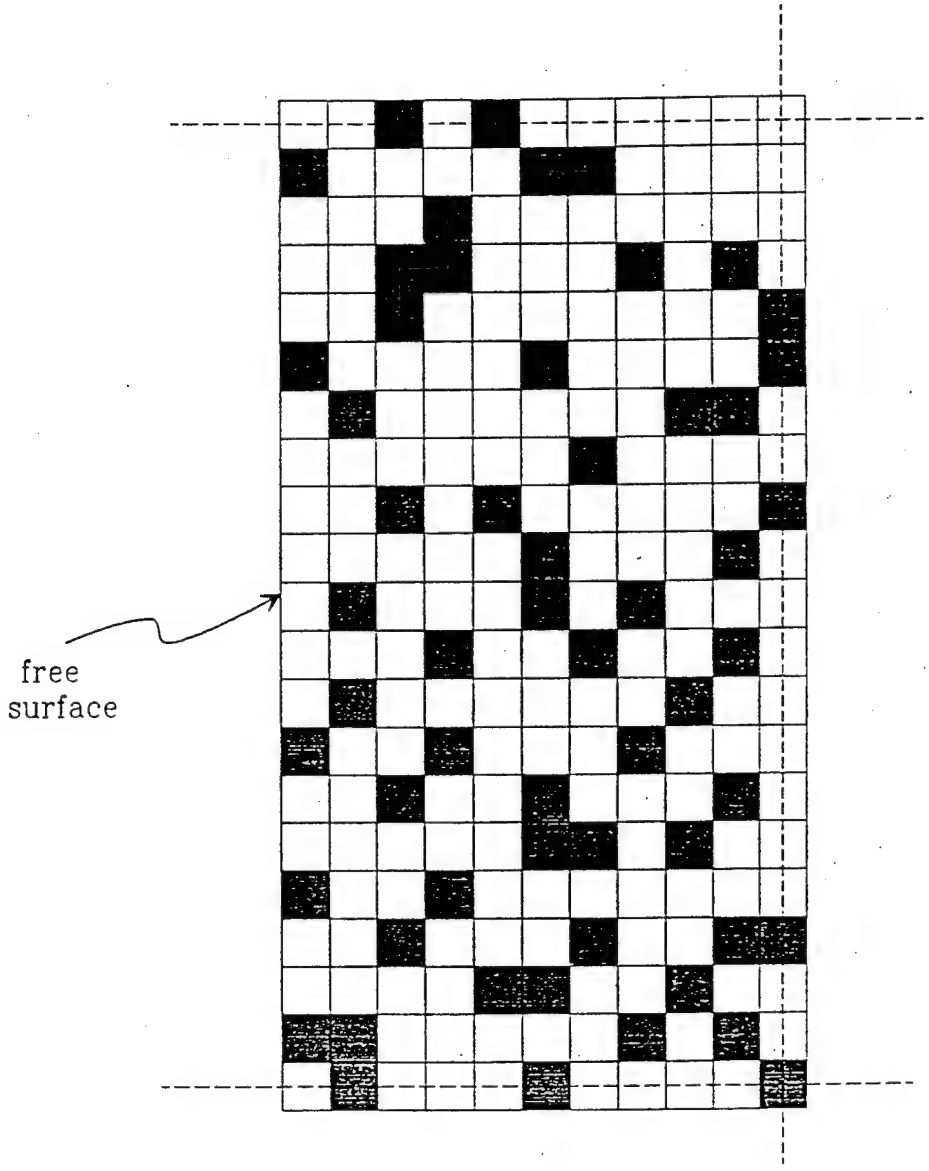

Figure 3.1-6 Disordered array, 25% soft grains (shaded). Dashed lines denote the planes of symmetry used in the finite element calculations.

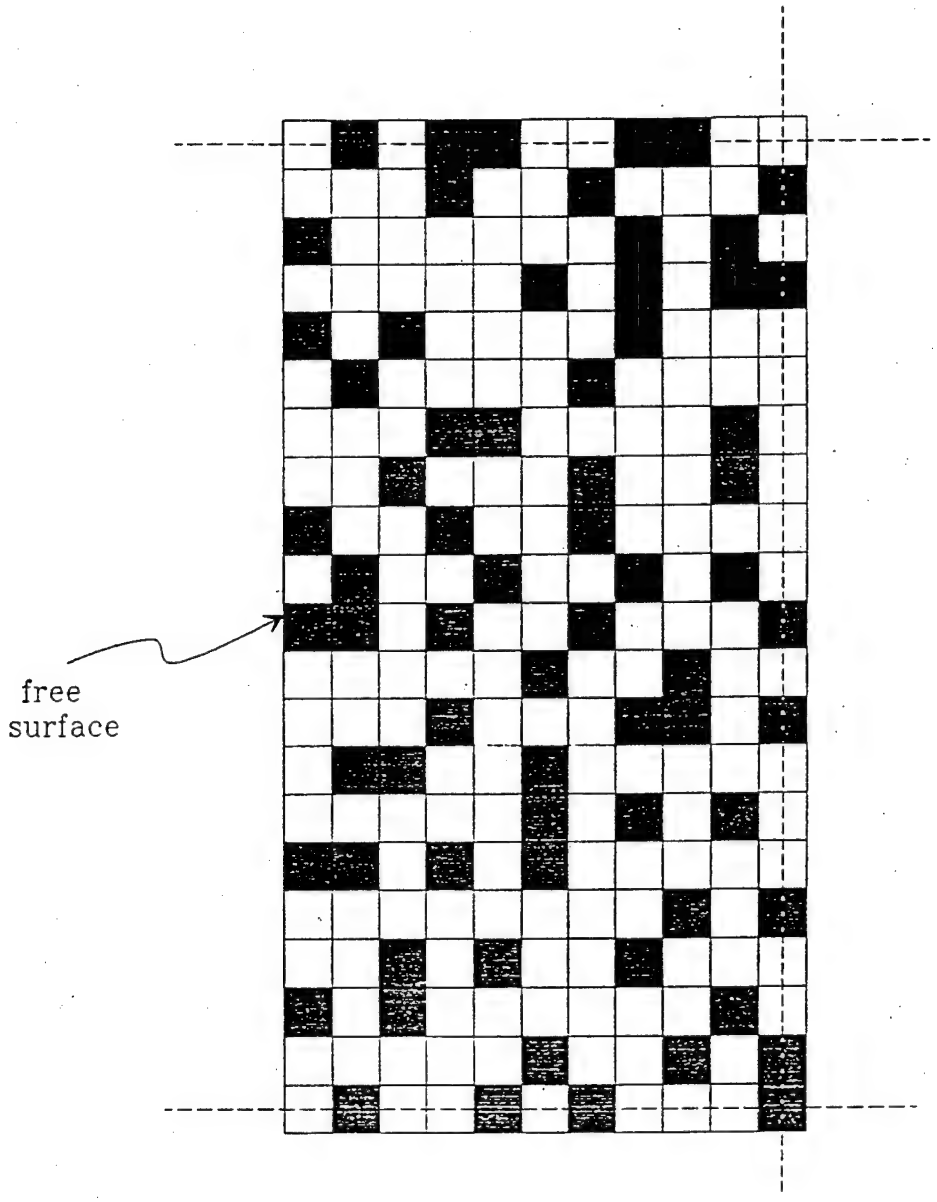

Figure 3.1-7 Disordered array, 29% soft grains (shaded). Dashed lines denote the planes of symmetry used in the finite element calculations.

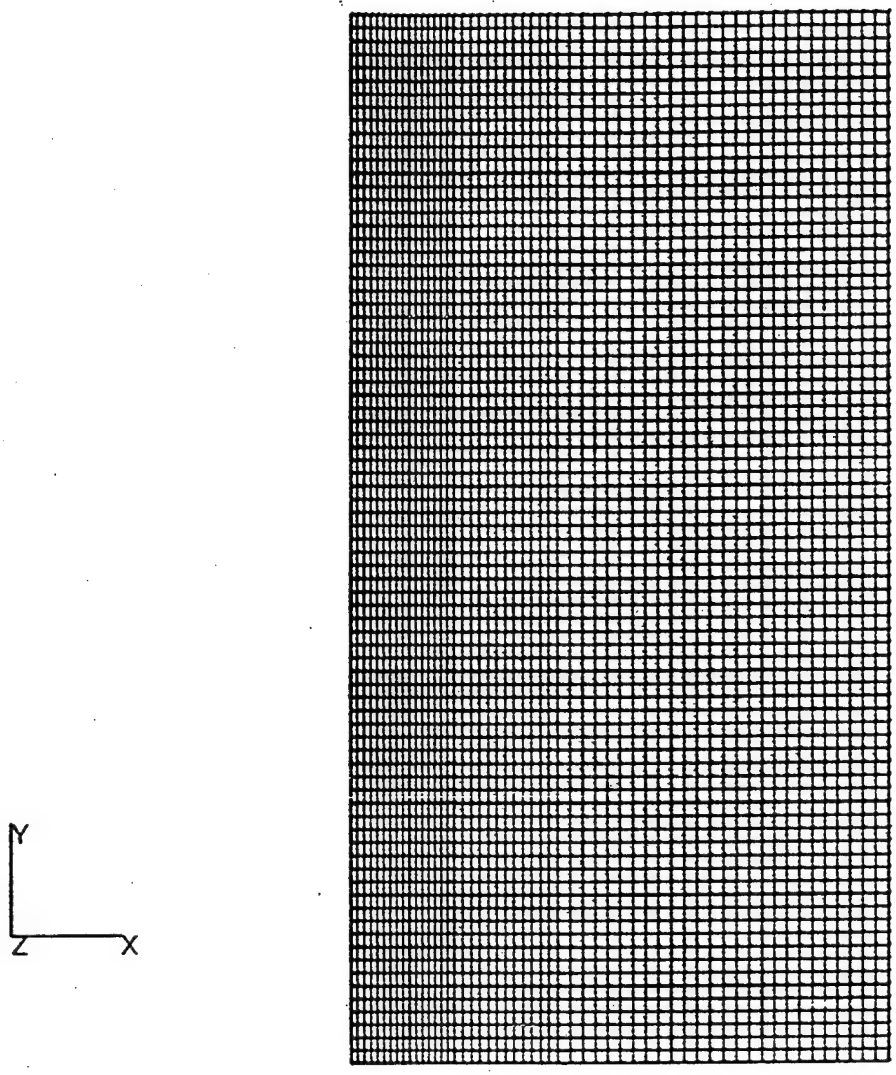

Figure 3.1-8. Mesh for the disordered grain arrays. It contains 10.5 grains in the horizontal direction and 20 grains in the vertical direction. Starting from the free surface (left), the number of elements per grain in each region is 8 X 8, 6 X 4, and 4 X 4. The load is applied uniaxially in the y-direction.

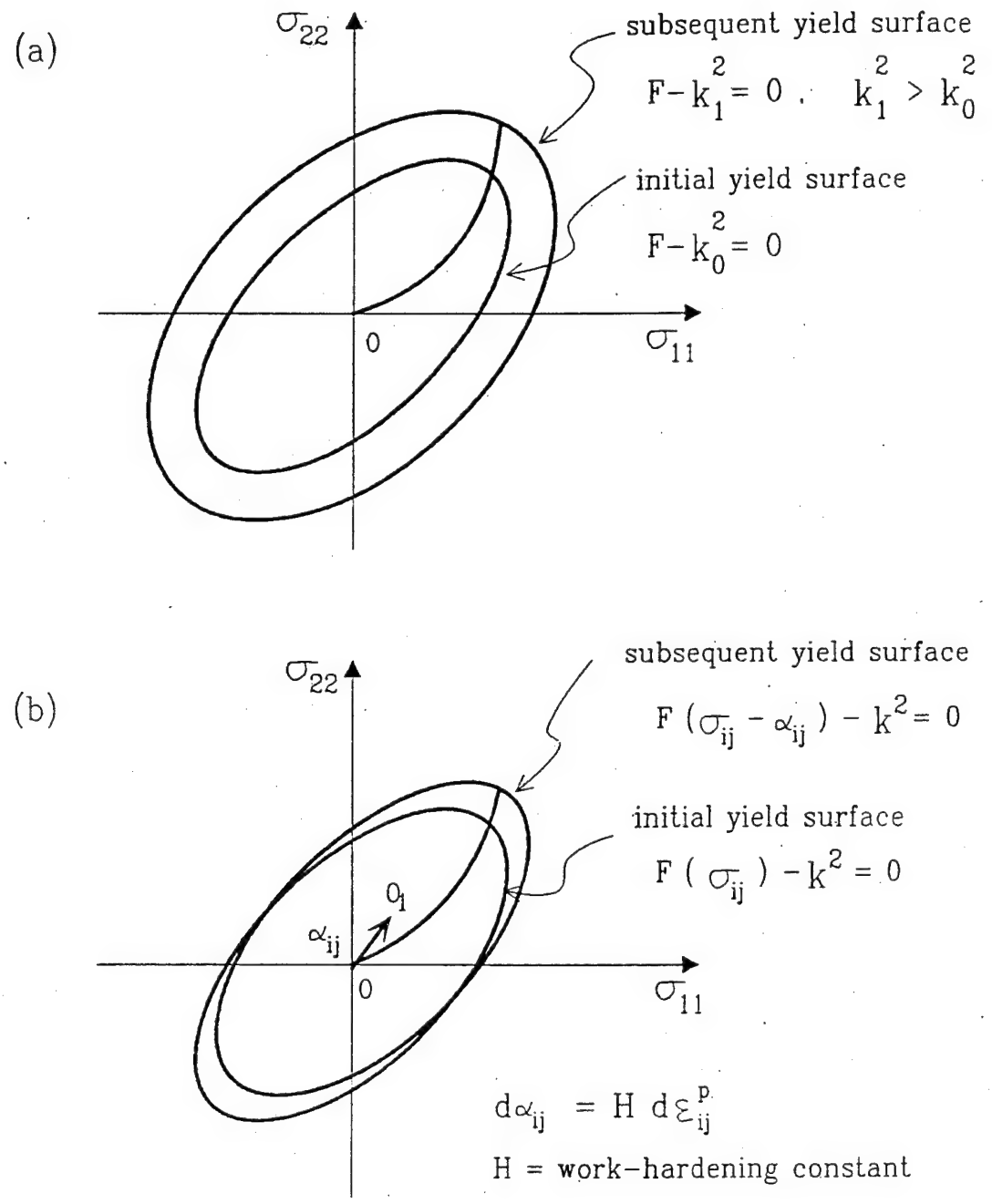

Figure 3.1-9 Hardening rules. (a) Isotropic. (b) Kinematic, with Prager's hardening rule and the associated flow rule. The center of the yield surface is translated by vector $d\alpha_{ij}$ which is in the direction of the normal n_i of the current yield surface in stress space.

Dynamics Research Corporation, Milford, Ohio 45150. ABAQUS was run on an IBM 3090 processor complex with Vector Facility, whereas CAEDS was implemented on an IBM 3084 computer and run interactively. CAEDS was used to provide visualization of the results, in particular mesh deformation. Stress and strain fields were examined with contour maps. In addition, PATRAN (PDA Engineering, PATRAN Division, Costa Mesa, California 92626) was used on an APOLLO (Apollo Computer Co., Chelmsford, Massachusetts 01824) work station to obtain printed output.

The main steps in preprocessing were:

- Creation of the mesh module. It defines the finite element mesh, specifying the node coordinates, node connectivity, and element type.

- Assignment of the grain and corresponding element material properties. This was accomplished with the FORTRAN program SRAP (Surface layer effect - Random Assignment of grain Properties), which can assign the properties using a random number generator or an external data file. SRAP generates the element property assignment module which is incorporated directly into the ABAQUS program dec.

- Specifying the type (force or displacement) and magnitude of loading.

- The creation of the ABAQUS input deck by combining the following modules: (1) title and program description (optional); (2) mesh; (3) element material properties assignment; (4) material properties definition, and (5) loading. The REXX program ABQINP (ABAqus INPut code assembler) accomplished this task, computing loads and writing ABAQUS code as required by the specific problem.

This preprocessing scheme is outlined in Figure 3.2-1.

The ABAQUS finite element run resulted in two main output files: the ASCII text file PRINT and the binary file. The latter can be read by commercial postprocessors and was the input to CAEDS and PATRAN. Although FILE can also be used for one's own postprocessing programs, it was found unsuitable because it was prohibitively large, because it is less selective than PRINT in the choice of output variables, e.g., in order to obtain selected values of nodal displacements, all nodal displacements must be

output. The required data was extracted from the PRINT file with a series of REXX programs. Computation of the plane-averaged stresses and x-ray stresses was performed by the FORTRAN program SLAS (Surface Layer effect - Average Stresses). The postprocessing train is outlined in Figure 3.2-2.

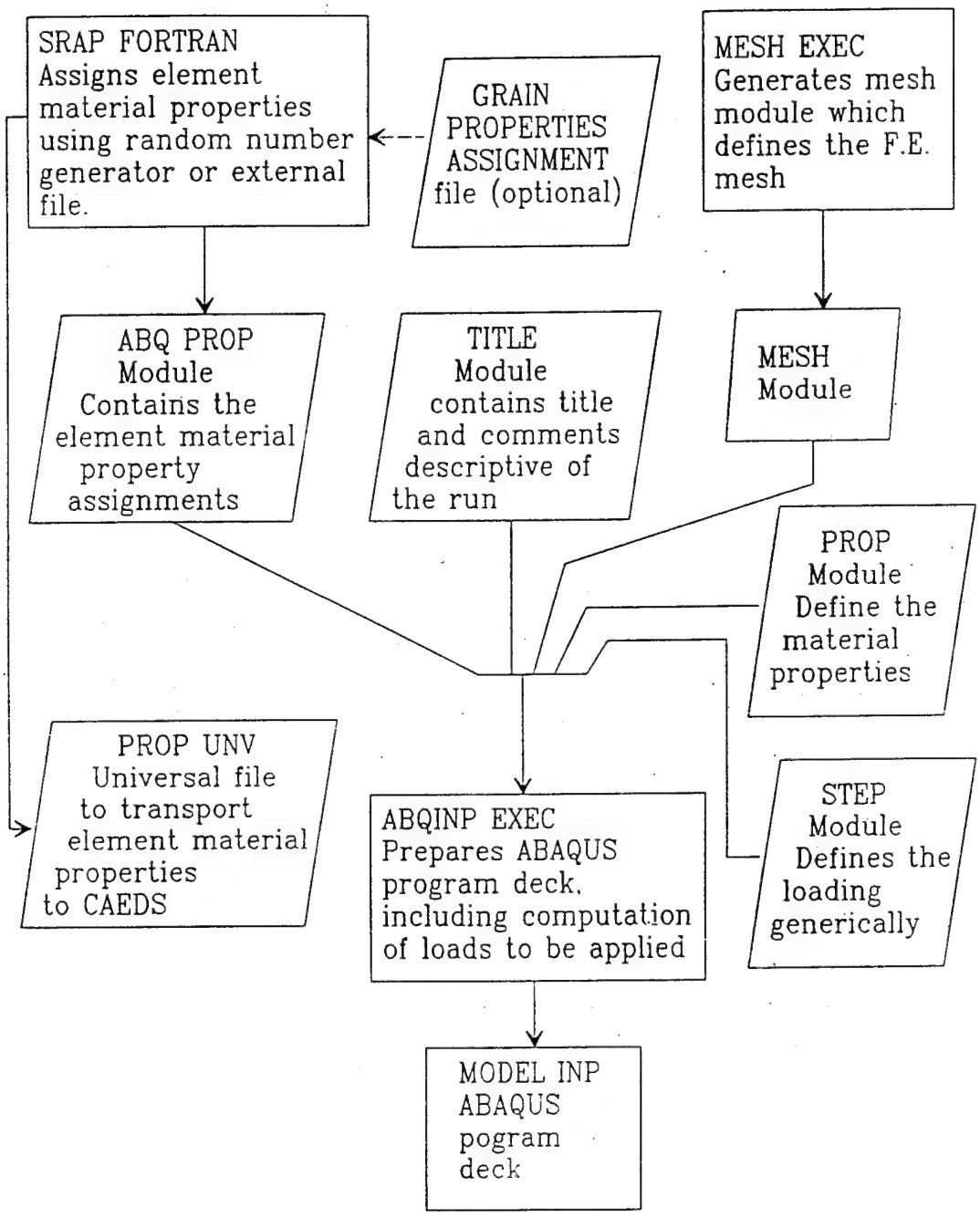

Figure 3.2-1 Flow chart for the preparation of the ABAQUS input deck to be submitted to ABAQUS for the finite element calculation. EXEC programs are written in REXX (IBM Restructured Extended Executor Language).

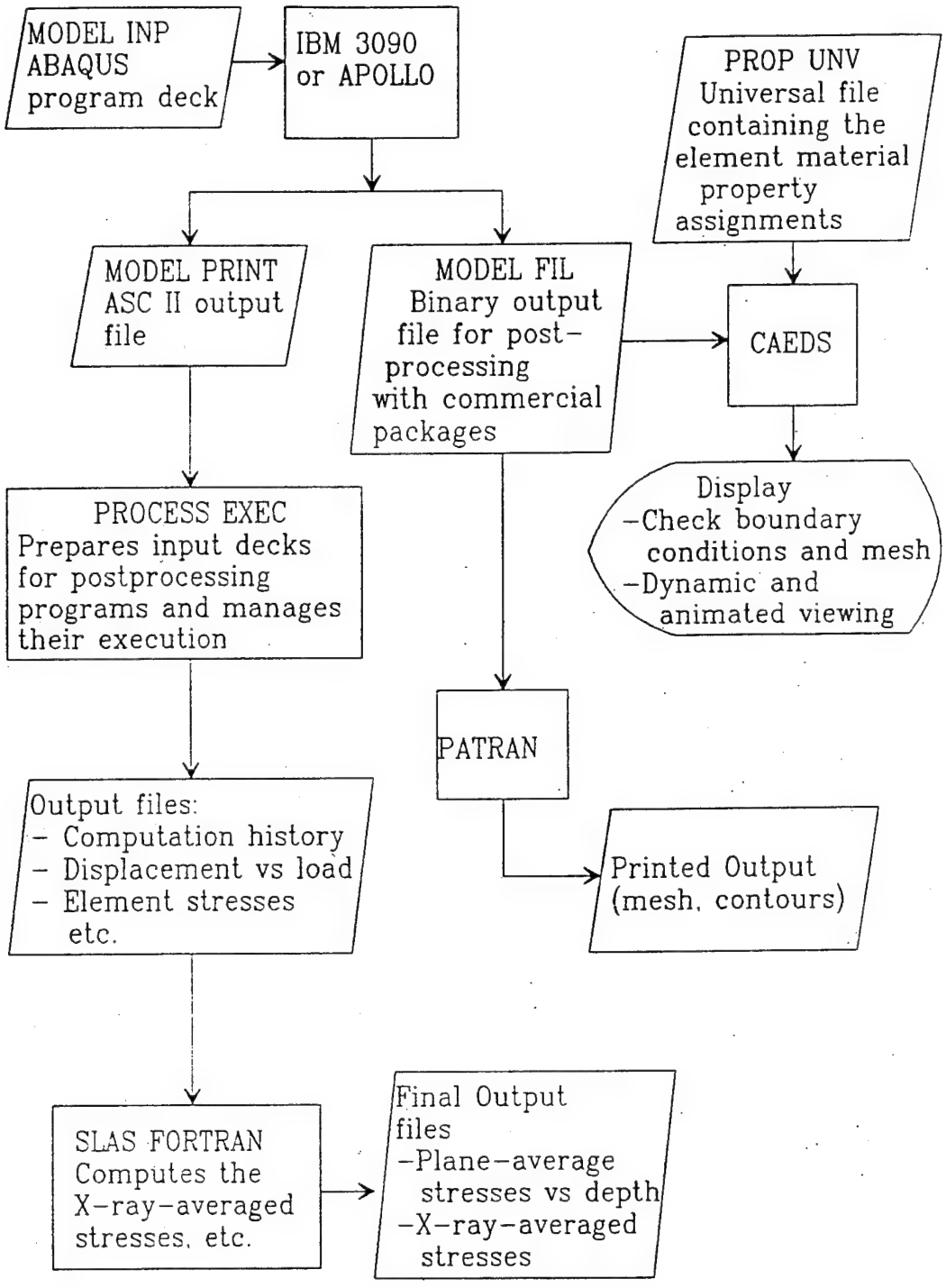

Figure 3.2-2 Postprocessing flow chart. EXEC Programs are written in REXX.

4.0 RESULTS AND DISCUSSION

4.1 EXPERIMENTAL RESULTS

When uniform cross section specimens of Ti-6Al-4V and Al 7475-T651 are loaded in tension, there is the expected linear correspondence between the x-ray stress and the applied nominal stress up to a stress below the bulk yield point. Above this stress, the x-ray stress levels off or is noticeably less than the nominal applied stress. Upon unloading, there is a significant acquired compressive residual x-ray stress. X-ray stress versus applied stress curves are shown in Figure 4.1-1 for Ti-6Al-4V and in Figure 4.1-2 for Al 7475-T651. For Ti-6Al-4V, which has a fairly well defined proportional limit, the applied stress at which the deviation becomes significant is close to that limit. The maximum acquired residual stress was -15.1 ksi for Al 7475-T651 and -45.8 ksi for Ti-6Al-4V. Its value increases with plastic strain. The results are summarized in Table 4.1-1. Similar results have been obtained for a notched Ti-6Al-4V specimen [1]. With a notch radius of 0.25 inch, the residual stress measured by x-ray diffraction was -78 ksi, instead of the expected -37 ksi (Figure 4.1-3).

Because the x-ray diffraction measurements detect only the elastic component of strain, such a leveling off of the x-ray determined stress versus applied stress is not expected. The effective penetration depth (99% of the total diffracted intensity) of the copper radiation used in these measurements is 23 μm for the titanium alloy and 173 μm for the aluminum alloy at $\psi = 0°$. It will be less at other ψ angles. For both metals, this corresponds to sampling a surface layer of only about one grain in thickness, suggesting that a thin surface layer in the metal has a lower yield point than the bulk of the metal. Upon unloading, this yielded layer is driven into compression by the elastic unloading of the bulk material.

A complication for Ti-6Al-4V is that this alloy is biphasic, consisting of an α phase (hexagonal) and a β phase (bcc). For the heat treatment used here (annealed at 1450 °F for 15 minutes, air cooled) the α phase is dominant, forming the bulk of the grains observed in the microstructure (Figure 2.1-1). The β phase appears to be essentially intergranular. The x-ray diffraction measurements performed here sample the α phase. Accounting for the anomalous

x-ray results by hypothesizing that the α phase yields first appears unreasonable given the microstructure which indicates that the α phase accounts for the greater bulk of the material and that the β phase is too fragmented to support substantial elastic tensile loads on its own. In other words, when the α phase crystals yield globally, bulk yielding should ensue.

4.2 FINITE ELEMENT RESULTS

The specimens modeled are 2-D slabs consisting of lower yield point ("soft") and higher yield point ("hard") isotropic grains, such that the hard grains form a matrix in which the soft grains are embedded. Up to the yield point, all grains have identical isotropic linear elastic properties. The plastic anisotropy is thus modeled by the lower yield point of some grains, representing crystals or groups of crystals ("domains") in favorable orientations for yielding. In most runs, the soft grains are elastic-perfectly plastic, whereas the hard grains undergo some work hardening. It has been shown experimentally for aluminum and iron that crystals in a favorable direction for yielding work-harden less than those in unfavorable orientations [29]. The effect of work hardening is explored further on. The meshes and other aspect of the finite element calculations are described in the previous section, "Finite Element Calculations".

It was sought by finite element modeling to determine if and under what conditions a polycrystalline aggregate, modeled by isotropic hard and soft grains, develops a surface layer wherein the average stresses differ significantly from the bulk averages. To this end, a basic model or "specimen" consisting of a regular array of soft square grains (yield point of 15 ksi, volume fraction of 0.33) in a matrix of hard grains (yield point of 20 ksi) (Figure 3.1-3) under plane stress loading was used as the benchmark. This model conforms well qualitatively to the experimental data, and, as will be seen later, the values used for the yield points are reasonable when related to typical metal crystal properties. In addition, the influence of the following factors on the surface layer effect is examined:

- bulk elastic constants;
- soft grain concentration;
- array disorder;
- yield point spread between hard and soft grains;
- hard grain hardening rate;

Table 4.1-1. Deviation stresses and residual stresses determined in uniaxial tension for the Ti-6Al-4V and Al 7475-T651 specimens of this study.

Specimen ID	σ_{dev}	σ_{rx}	ϵ_p
Ti-6Al-4V (σ_{pl} = 115 ksi, σ_y = 132.5 ksi)			
T1S06	111-132	---	---
T1S04	109-120	-45.8 ± 5.3	0.01 to 0.02
TISI3	112-120	-20.4 ± 4.5	0.004
Al 7475-T651 (σ_{pl} = 54 ksi, σ_y = 78.5)			
AS00	69-73	-11.4 ± 2.7	0.003
AS22	[59-64]*	-7.0 ± 3.0	0.003
		-15.1 ± 5.6	0.0083

σ_{dev} is the stress or stress range for which the x-ray stress starts to deviate appreciably from the nominal applied stress.

σr_x is the net residual x-ray stress.

* Tentative values; not well defined.

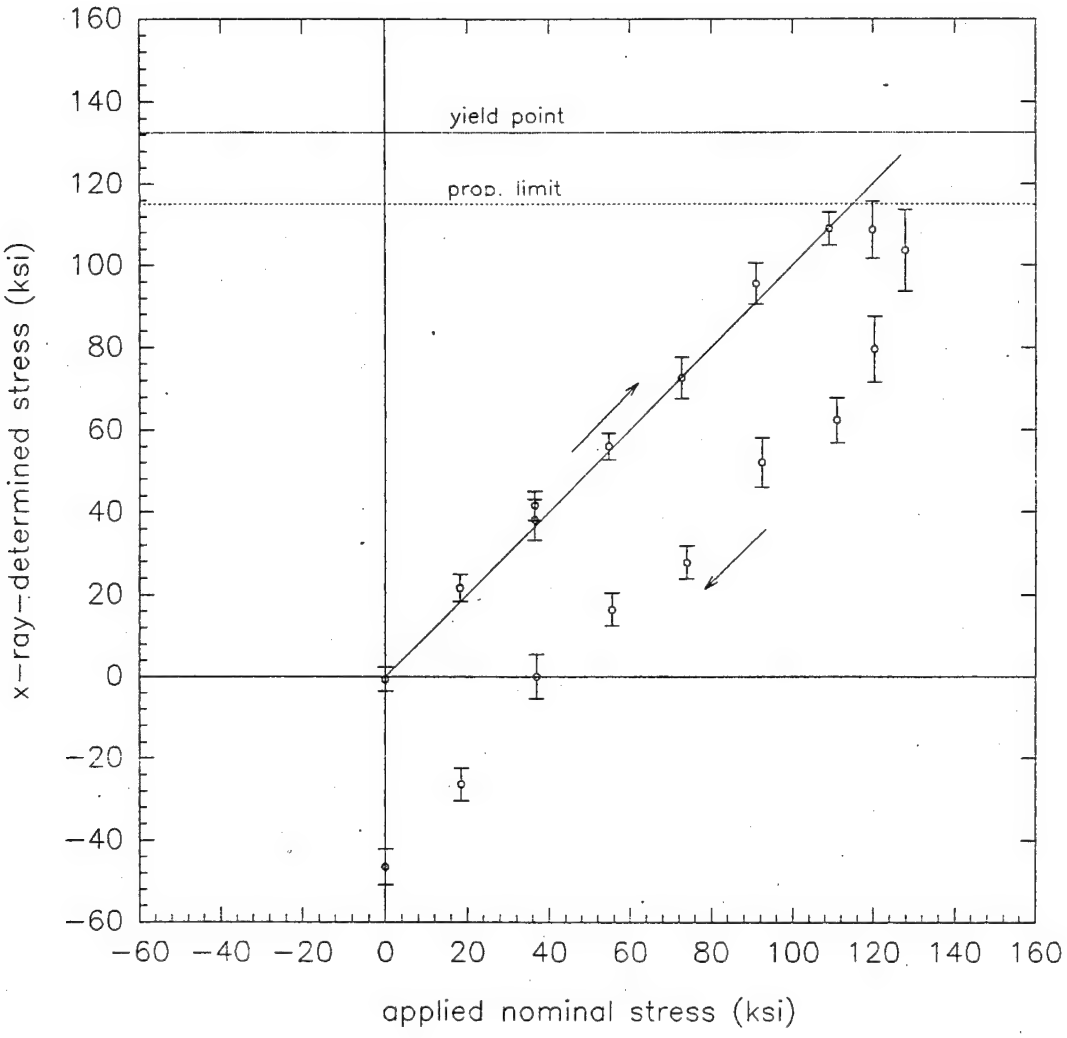

Figure 4.1-1. X-ray-determined stress versus the applied nominal stress for two uniform cross section Ti-6Al-4V specimens. (a) First specimen and (b) second specimen (next page). The setup parameters for the x-ray measurements are given in Table 2.3-1. The dark line is the expected response, assuming no initial residual stress. The arrows indicate the direction of loading.

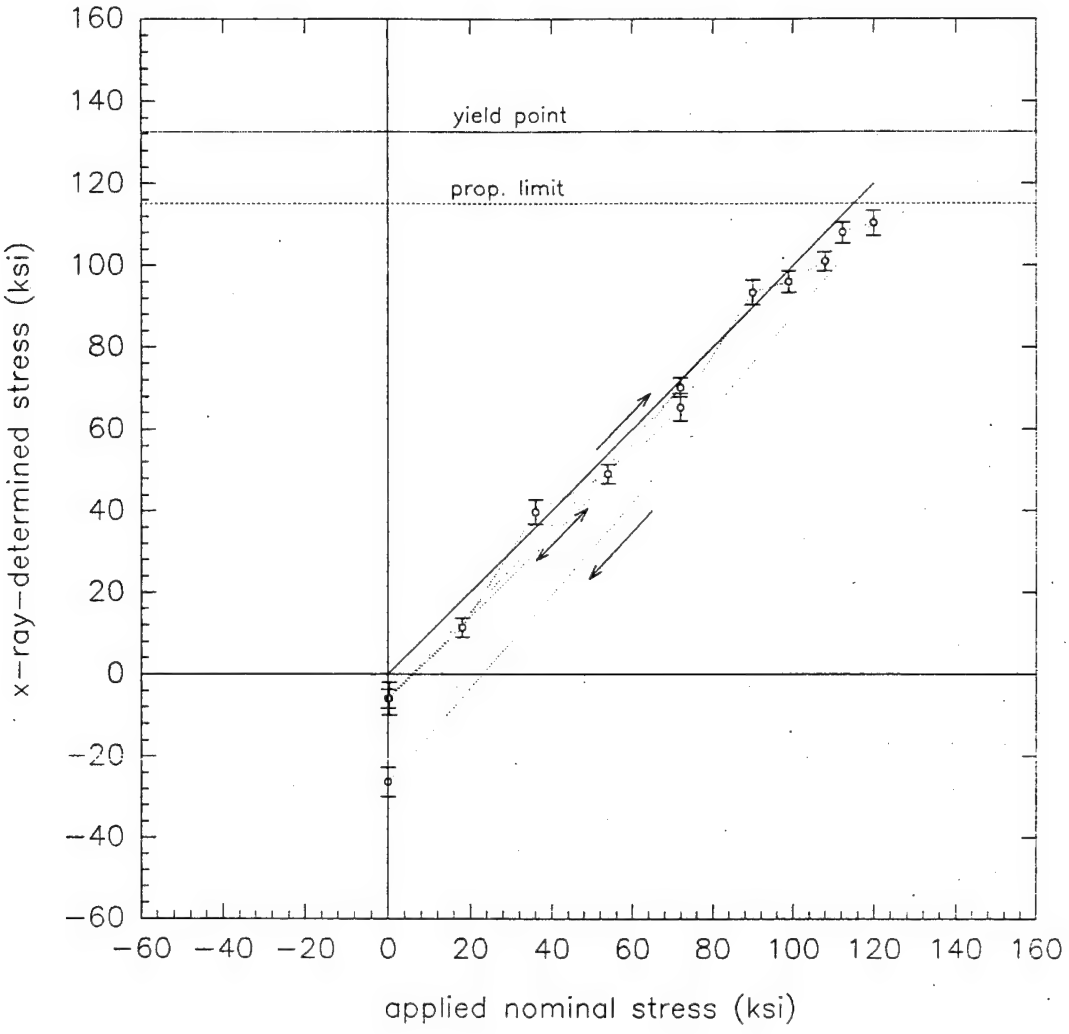

Figure 4.1-1 (continued). (b) Second Ti-6Al-4V specimen.

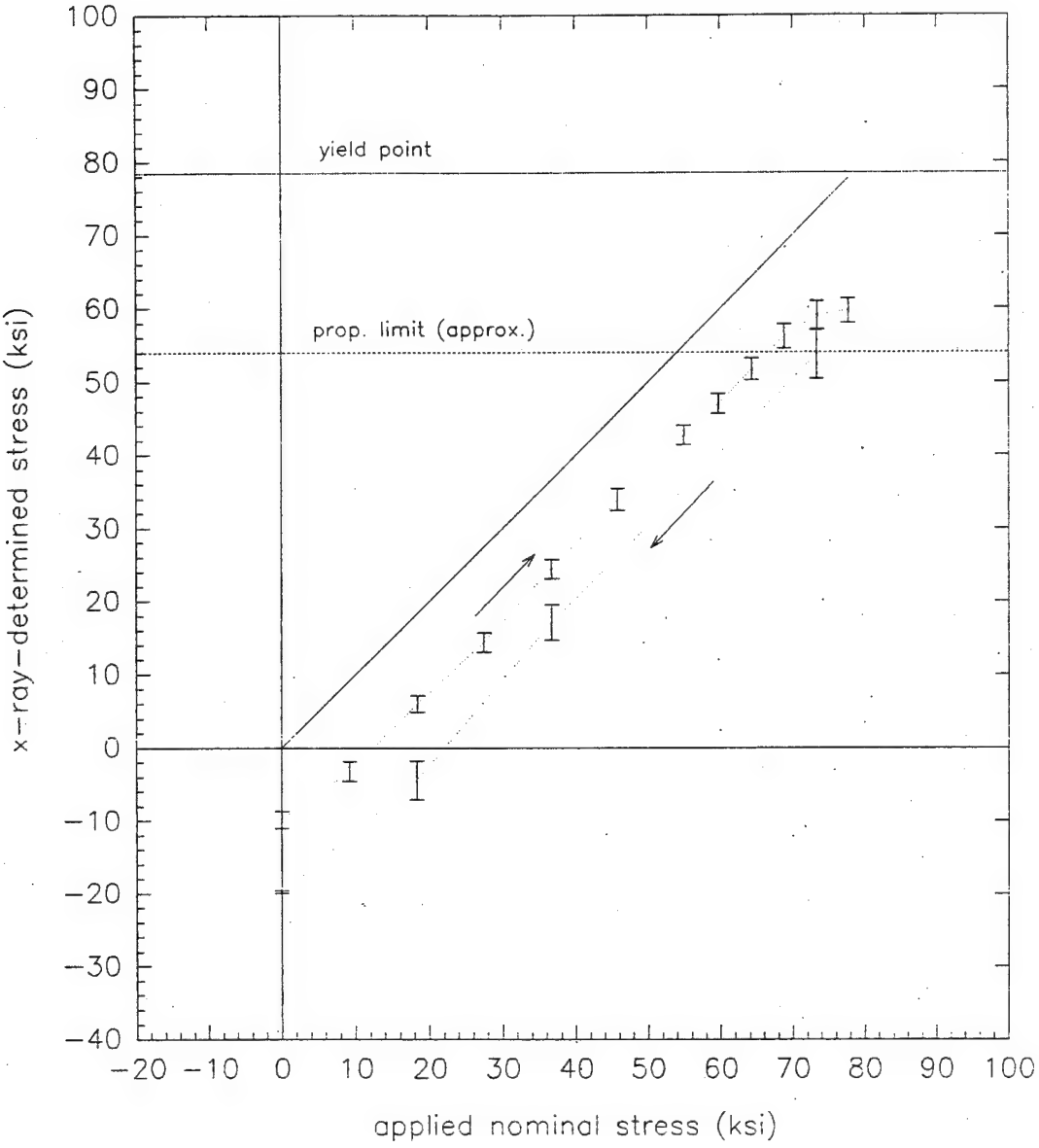

Figure 4.1-2. X-ray-determined stress versus the applied nominal stress for two uniform cross section Al 7475-T651 specimens. (a) First specimen and (b) second specimen (next page). The dark line (slope 1) is the expected response, given no initial residual stress. The arrows indicate the direction of loading. The setup parameters for the x-ray measurements are given in Table 2.3-1.

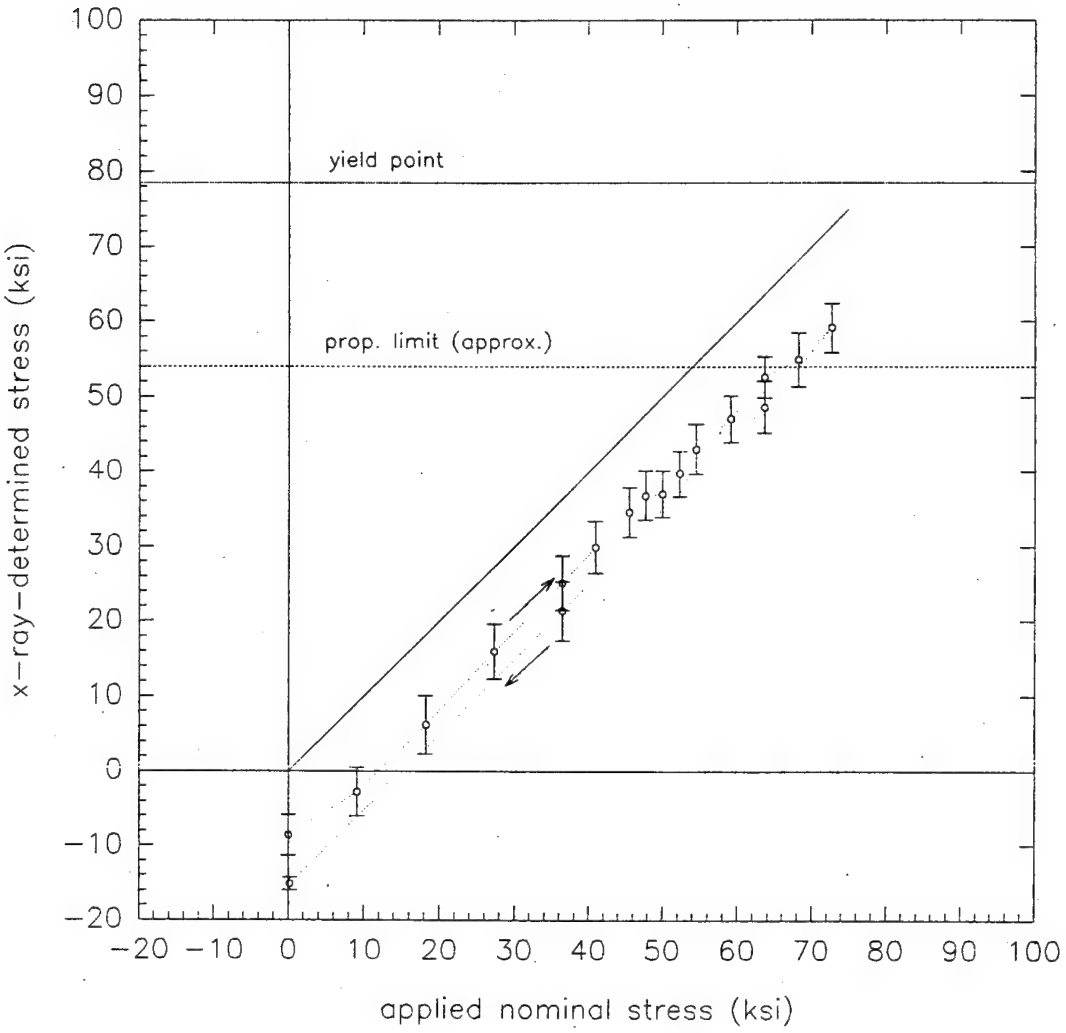

Figure 4.1-2 (continued). (b) Second Al 7475-T651 specimen.

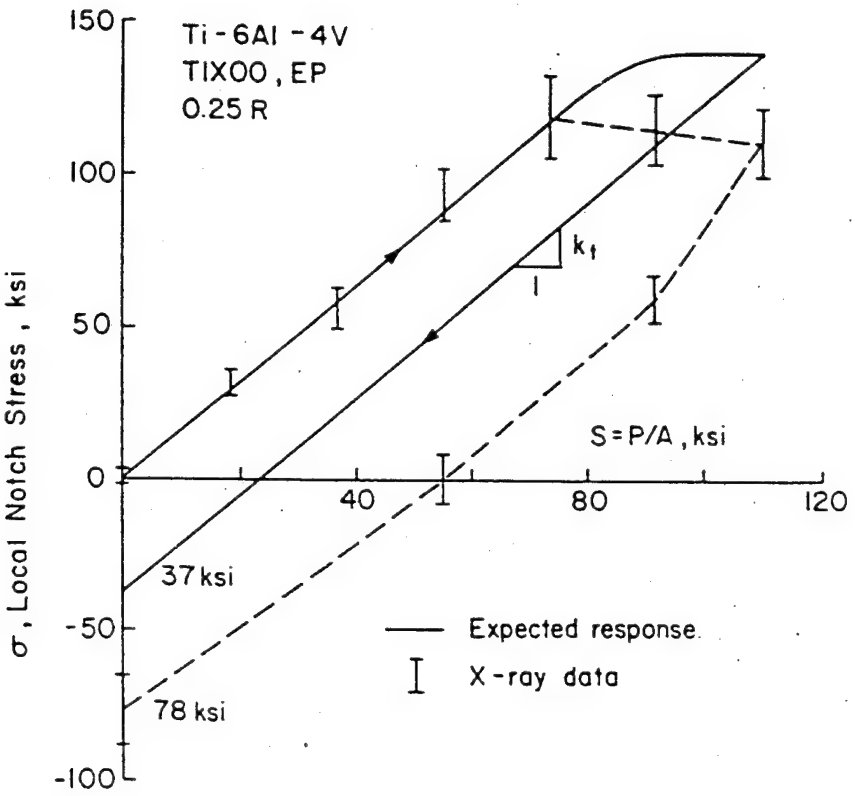

Figure 4.1-3. X-ray-determined stress versus the applied nominal stress for a notched Ti-6Al-4V specimen. Notch radius is 0.25 inch. For comparison, the estimated notch stress is also shown (Dowling and Dunn [1]).

- soft grain hardening rate;
- value of the yield points relative to the elasticity modulus E;
- grain aspect ratio;
- constraint (plane stress, plane strain, generalized plane strain).

The loading is uniaxial in all cases, in the longitudinal direction of the specimen. This direction is also referred to as the y-direction or the vertical direction. The transverse direction normal to the free surface plane is x, whereas the transverse direction parallel to this plane is z (Figure 3.1-3). In indicial tensor notation, the Cartesian axes x, y, and z correspond to indices 1, 2, and 3, respectively.

In relating the calculations to the x-ray stress measurements and the mechanical test data, the basic values of interest are the average stresses in vertical layers of material parallel to the surface. Non-zero averages lead to macrostresses. The macrostresses arising from the differential deformation of grains are the average of microstresses taken over a statistically representative number of grains. In plane stress we need only concern ourselves with the average longitudinal stress σ_{yy}. The other stress components are either zero by definition or their average must be zero. Thus, the average shear stress σ_{xy} in any vertical layer must be exactly zero by symmetry in the ordered arrays; it must also tend to zero in a disordered array given a sufficiently large sampling volume because in such an array every transverse plane is a plane of quasi-symmetry, i.e., the average properties and stresses of the material above and below are the same. That the layer-averaged transverse stress σ_{xx} is also zero can be deduced from the equation relating the average stress to the body and surface forces:

$$\int_V \sigma_{ij}\,dV = \int_S \sigma_{ik} x_j n_k\,dS - \int_V \sigma_{ik,k} x_j\,dV \qquad (2)$$

where σ_{ij} are the stress tensor components, V is the volume of the body, S is its boundary surface, x_i are the Cartesian coordinates (i = 1, 2, 3 for x, y, z, respectively), n_i are the components of the vector normal to the boundary surface element, and f_i are the body force components.
Here, the body forces are zero, so the second integral on the right vanishes. For σ_{11}, this equation reduces to

$$\int_V \sigma_{11}\, dV = \int_S (\sigma_{11} n_1 + \sigma_{12} n_2)\, x_1\, dS \qquad (3)$$

taking into account that the out-of-plane shear stress σ_{13} is zero by definition. Referring to Figure 4.2-1, consider the slab of material ABB'A' enclosed by the free surface (AA'), the top plane (A'B'), the bottom plane (AB), and the vertical plane (BB') parallel to the free surface. Integrating over S, the terms in the integral are as follows:

S-component	AA'	A'B'	BB'	AB
	free surf.	top	right	bottom
n_1	-1	0	1	0
σ_{11}	0	$\neq 0$	$\neq 0$	$\neq 0$
n_2	0	1	0	-1
σ_{12}	0	0	$\neq 0$	0

Thus only the $\sigma_{11} n_1 x_1$ on BB' is non-zero, so that

$$\int_V \sigma_{11}\, dV = \int_{BB'} \sigma_{11} x_1\, dS = x_{BB'} \int_{BB'} \sigma_{11}\, dS \qquad (4)$$

The last integral is simply proportional to the total normal force on BB'. It must be zero by force equilibrium because the stress component in the 1-direction is zero on the other faces of the slab ABB'A' (σ_{11} = 0 on the free surface, σ_{12} = 0 on the top and bottom surfaces). By the same reasoning, the average transverse stress in the adjacent slab (BCC'B' in Fig 4.2-1) must be also zero, and so forth for successive slabs. It is readily shown that the volume-average of the other transverse stress, σ_{33}, parallel to the free surface, can be non-zero even though no external load is applied in this direction. This situation can arise in 2-D for generalized plane strain and axisymmetry, and in 3-D.

Unless otherwise stated, the Lagrange linear strain tensor is used in the calculations presented in this work and the stresses are based on the original rather than the deformed geometry.

4.2.1 Results for The Basic Model.

The calculations were performed in two modes for comparison: using the linear and nonlinear geometry assumptions. Results for each will be

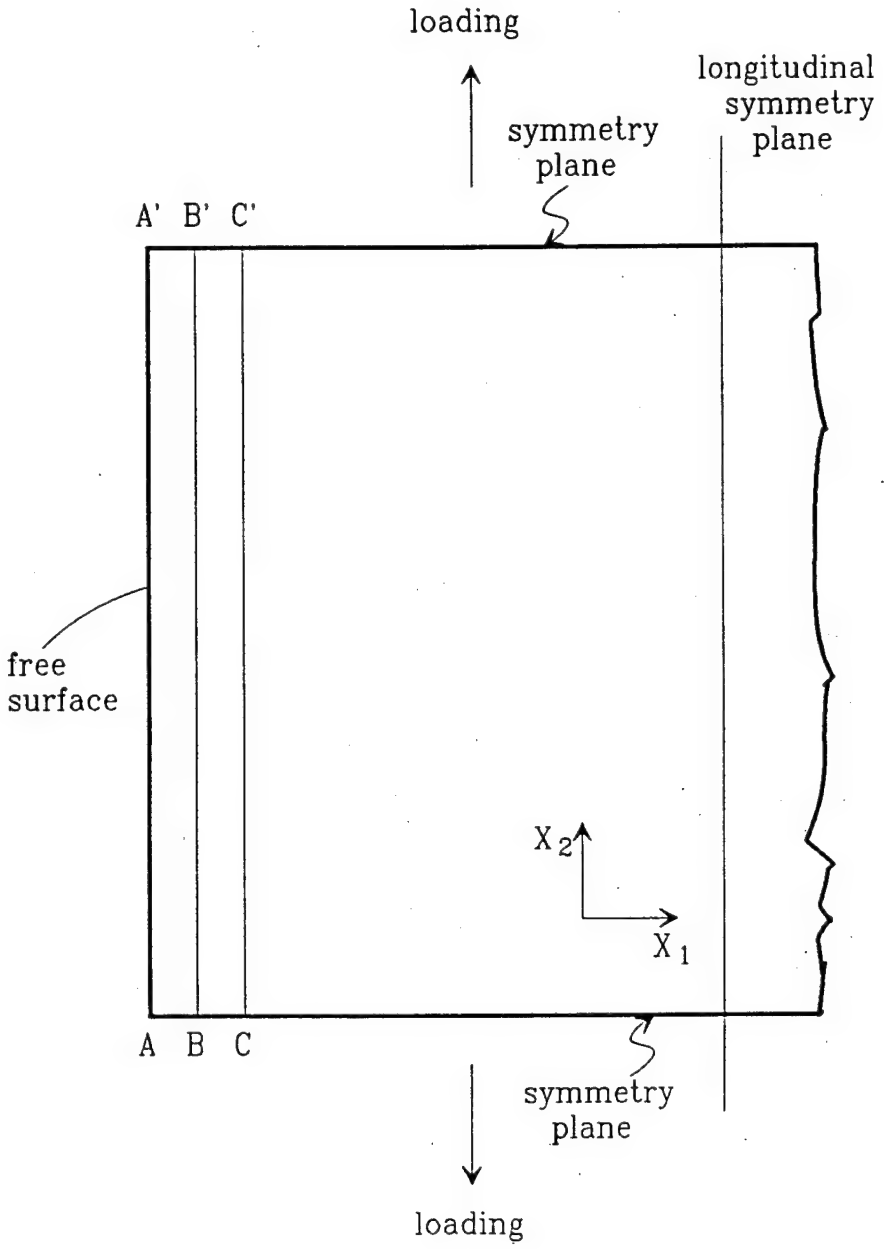

Figure 4.2-1 Longitudinal layers of material, ABB'A', BCC'B', etc., over which the stresses are averaged in the model.

denoted (L) and (NL), respectively. Results which apply to both will have no marking. The models for the two modes were otherwise identical, with 10 X 10 elements per grain and a mesh width of 6.5 grains (which by symmetry is the specimen half-width - see Section 3.2).

The specimen was loaded incrementally up to a plastic strain of approximately 5%. The loading histories are given in Tables 4.2.1-1 (L) and 4.2.1-2 (NL). These Tables also list x-ray-averaged stresses which are defined further on. The resulting stress-strain curves are shown in Figure 4.2.1-1. The curves are linear up to the yield point of the soft grains, followed by a rapid deviation from linearity until the onset of bulk plasticity, when the slope decreases dramatically, to a hardening rate of 39 (L), 15 (NL) ksi per unit strain. The 0.002 offset yield points are 17.90 ksi (L), 17.84 ksi (NL). For comparison, the yield points of the corresponding infinite space array (i.e. surface-free) are 18.10 ksi (L), 18.06 ksi (NL), and the predicted yield point from the rule of mixtures is 18.33 ksi. Because the corners of the soft square grains are zones of stress concentration [30], the yield point of the infinite array is expected to be below that calculated by the rule of mixtures. The lower yield point of the specimen compared to the infinite space array is in turn due to the surface layer effect.

The plane-averaged longitudinal stresses decrease markedly as the free surface is approached, the effect becoming more pronounced as the plastic strain is increased. This is illustrated in Figs. 4.2.1-2 and 4.2.1-3, in which the average stress is plotted versus depth (distance from the free surface) for plastic strains of 0.002 and 0.05, respectively. The surface layer spans about 3 grains, with the stress being significantly reduced for the first 2 grains. In the first grain layer the average stress drops approximately linearly until close to the surface, whereupon there is a steep drop of the stress over a thickness of about 0.1 grains. Calculations with more elements close to the surface to obtain more resolution, indicate this drop is real rather than a numerical artifact (Figure 4.2.1-4). It is the result of a hinge-type effect on the surface hard grains, which are in tension at the interface with the next layer of grains, but are driven into compression near the free surface where the soft grains are at the yield point (stress contour plots are presented further on). Away from the surface layer zone, the average stress has the repetitive pattern found in the surface-free specimen. The peaks match the location of the vertical grain boundaries, which are zones of stress concentration. The sum over all the planes of the

plane-averaged stress multiplied by the plane cross-section equals the applied load, indicating proper force balance (Table 4.2.1-3).

Another indication of a surface layer effect is the substantial compressive residual stresses in the surface layer after unloading, balanced by tensile stresses in the bulk of the material (Figures 4.2.1-2,3). For a plastic elongation of 5%, the average compressive longitudinal stress in the surface grain layer is -1.5 ksi (L), -1.9 ksi (NL) or 8% (L), 11% (NL) of the bulk yield point (Tables 4.2.1-1 and 4.2.1-1). The greater plastic deformation of the soft grains in the surface region compared to those further in is evident in the deformed mesh, shown in Figure 4.2.1-5 for 5% plastic elongation. The deformation is greatest in the soft grain at the interface with the hard grain and near the free surface. This is consistent with the steep drop of the plane averaged longitudinal stress $\langle\sigma_{yy}\rangle_{pl}$ as the free surface is approached.

It is of particular interest to relate these results to the x-ray measurements. The x-ray beam diffracted from the specimen to determine the strains and thereby the stresses, decays exponentially in the material of the specimen. The x-ray measurement therefore provide a weighed average of the actual stresses in a surface layer of the specimen. More specifically, the x-ray averaged stress is related to the longitudinal stress in the specimen by

$$\sigma_{x\text{-}ray} = \frac{\int_{x=o}^{\infty} \sigma(x)\, dI}{\int_{x=o}^{\infty} dI} \qquad (5)$$

where:

x	is the depth below the surface.
$\sigma_{x\text{-}ray}$	is the x-ray-averaged stress component.
$\sigma(x)$	is the plane-averaged stress component, which is a function of the depth x.
dI	is the intensity diffracted from an infinitesimally thin layer at depth x below the surface.

The intensity dI is given by

$$dI = \frac{I_o f_c f_D}{\sin(\theta+\psi)} e^{-\mu x\left[\frac{1}{\sin(\theta+\psi)} + \frac{1}{\sin(\theta-\psi)}\right]} dx \qquad (6)$$

(Reference 20, p. 110), where:

- I_o is the intensity of the incident beam.
- f_c is the volume fraction of grains that can diffract at the given diffraction angle θ.
- f_D is the fraction of incident energy diffracted per unit volume.
- θ is the diffraction angle.
- ψ is the angle of the diffracting planes (cf. Figure 2.3.1).
- μ is the linear absorption coefficient.

In the present application, it is desirable to express dI in terms of an effective penetration depth, defined as the sample thickness which contributes a given fraction of the diffracted intensity, taken here to be 99 percent. It can be shown that:

$$dI = \frac{I_o f_c f_D}{\sin(\theta+\psi)} (1-G_p)^{x/x_p} dx \qquad (7)$$

where

- x_p is the effective penetration depth.
- G_p is the fraction of the total intensity diffracted by the surface layer of thickness x_p.

Substituting this expression for dI, Equation (5)of Section 4.2.1 becomes

$$\sigma_{x\text{-}ray} = \frac{\int_o^\infty \sigma(x)(1-G_p)^{x/x_p} dx}{\int_o^\infty (1-G_p)^{x/x_p} dx} \qquad (8)$$

Because of the finite dimensions of our model specimens, the integrals were carried out to a finite length rather than infinity. At least 99% of the intensity was accounted for. In addition, the original goemetry of the specimen was used to perform the integration over depth, i.e., the Poisson contraction of the grains in the elongated specimens was not taken into account because the correction is very small, on the order of $\epsilon_p/2$.

To simulate the experimental measurements, the expected x-ray averaged stress for penetration depths ranging from 0.5 grains to the halfwidth of the

specimen were calculated as a function of the applied stress (Tables 4.2.1-1 (L) and 4.2.1-2(NL)). Plots of the calculated x-ray stress versus the applied stress for a penetration depth of one grain are shown in Figure 4.2.1-6. The plots follow a pattern which is qualitatively similar to that observed experimentally for Ti-6Al-4V and 7475-T651 aluminum specimens (Figures 4.1-1 and 4.1-2): the x-ray stress equals the applied stress until the yield point of the softer grains is reached; beyond this point, it becomes significantly less than the applied stress, leveling off; upon unloading, it follows the applied stress linearly, but offset by a residual compressive stress. The residual x-ray stress is of the same order of magnitude relative to the bulk yield point as that observed in the actual specimens. Its magnitude increases when the plastic elongation of the specimen is increased, as observed by Kobb and Macherauch [12]. The x-ray residual stress is substantial even for much larger effective penetration depths (G_p = 0.99) than one grain because of the greater weight given to the stress values near the surface by the exponential decay of the x-ray intensity with depth. Thus, for the current model, the x-ray residual stress is -1.2 ksi for a penetration depth of 5 grains and plastic strain of 0.05, which is almost a third of the corresponding value for a penetration depth of one grain.

In comparing the linear and the nonlinear geometry calculations, it is found that the x-ray-averaged stresses are not significantly different up to plastic strains of about 1%. Above this value, the magnitudes of the residual stresses become larger for the nonlinear geometry calculation (Figure 4.2.1-7). The major effect of ignoring the geometric nonlinearity in tension is to underestimate the surface area reduction due to Poisson contraction, and thus underestimate the stress in the loading direction. Because this effect is less pronounced in regions which have reached the plastic limit (stress independent of elongation) than in regions which can still deform elastically, the residual stresses upon unloading are underestimated more than is expected from the permanent reduction in cross-sectional area, which is on the order of ϵ_p. Despite the lower accuracy above 1% plastic strain, the linear assumption is deemed adequate and is used in all the calculations because the proposed model is rudimentary and the results are meant to be only representative and comparative. Computation times are substantially longer and convergence less likely for the nonlinear than for the linear geometry models.

The required mesh refinement was determined with a series of calculations for the basic model using 4 X 4 to 20 X 20 el/gr. The values of

σ_{xx1} and σ_{xx1} at ϵ_p = 0.0001, 0.002, 0.045 were used as the benchmark. The residual stress values stabilize at 12 X 12 el/gr, as long as the surface nodal stresses σ_{surf} are included in the calculation of σ_{xx1}. Without this inclusion, stabilization of σ_{xx1} occurs at 20 X 20 el/gr (Figure 4.2.1-8). The surface nodal stresses help take into account the large stress drop near the free surface (Figure 4.2.1-4). However, it is found that 8 X 8 el/gr gives sufficiently accurate results for the present purpose, and that for comparative purposes even 4 X 4 el/gr is adequate. Unless otherwise noted, the finite element calculations for all the models with square grains were performed using 8 X 8 or 10 X 10 el/gr.

4.2.2 Effect of Various Parameters

The following three criteria, with emphasis on the first, are used to quantify the surface layer effect:

(1) the magnitude of the residual compressive stress in the surface layer;

(2) the initial deviation of the x-ray stress from the applied stress;

(3) the depth of the surface layer.

Criterion (1) is defined in two ways: (i) as the magnitude of the x-ray-averaged residual stress for a penetration depth of one grain; (ii) as the average residual stress in the surface-grain layer. These two variants of the criterion will be used interchangeably. The x-ray-averaged value has the advantage of relating directly to the experimental data, but the surface-grain-averaged value is more physically meaningful because it is an unweighted average.

Criterion (2) is defined as the ratio of the change in the x-ray stress to the applied stress when the proportional limit has just being exceeded. This ratio is denoted by Ω and is given by

$$\Omega = \frac{\sigma_{x\text{-}ray} - \sigma_{pl}}{\sigma_{applied} - \sigma_{pl}} \qquad (9)$$

where the x-ray stress corresponds to a penetration depth of one grain (0.99 diffraction intensity). The values of Ω which follow have been calculated for $\epsilon_p \approx 0.0001$.

Table 4.2.1-1. Loading history, surface-grain-averaged stresses (σ_{rgl}), and x-ray-averaged stresses for a specimen with a soft grain concentration of 33%. Linear geometry, 100 el/g used in the finite element calculations. All stresses are longitudinal, i.e., in the direction of load application. Mechanical constants: σ_{ys} = 15 ksi, σ_{yh} = 20 ksi, H_s = 0, H_h = 100 ksi.

Step No.	Applied Stress (ksi)	Plastic Strain	σ_{rgl} (ksi)	X-Ray-Averaged Stress (ksi) Penetration Depth (grains)			
				0.500	1.000	2.000	5.000
1	15.000	0.0000E+00	15.00	15.00	15.00	15.00	15.00
2	15.835	0.4906E-04	15.53	15.19	15.25	15.39	15.60
3	0.000	0.4907E-04	-0.31	-0.64	-0.59	-0.45	-0.23
4	15.835	0.4906E-04	15.53	15.19	15.25	15.39	15.60
5	16.670	0.1011E-03	16.04	15.36	15.47	15.76	16.20
6	0.000	0.1012E-03	-0.63	-1.31	-1.20	-0.91	-0.47
7	16.670	0.1011E-03	16.04	15.36	15.47	15.76	16.20
8	17.411	0.1748E-03	16.49	15.47	15.66	16.09	16.73
9	0.000	0.1748E-03	-0.92	-1.94	-1.75	-1.32	-0.68
10	17.411	0.1748E-03	16.49	15.47	15.66	16.09	16.73
11	17.645	0.2290E-03	16.65	15.47	15.72	16.21	16.91
12	0.000	0.2290E-03	-1.00	-2.17	-1.93	-1.43	-0.74
13	17.645	0.2290E-03	16.65	15.47	15.72	16.21	16.91
14	17.762	0.3844E-03	16.80	15.32	15.68	16.29	17.04
15	0.000	0.3844E-03	-0.96	-2.44	-2.08	-1.47	-0.72
16	17.762	0.3844E-03	16.80	15.32	15.68	16.29	17.04
17	17.847	0.1193E-02	16.93	14.70	15.43	16.28	17.13
18	0.000	0.1193E-02	-0.91	-3.15	-2.42	-1.57	-0.71
19	17.847	0.1193E-02	16.93	14.70	15.43	16.28	17.13
20	17.923	0.2525E-02	17.03	14.21	15.28	16.30	17.21
21	0.000	0.2525E-02	-0.89	-3.71	-2.64	-1.62	-0.71
22	17.923	0.2525E-02	17.03	14.21	15.28	16.30	17.21
23	18.032	0.4812E-02	17.15	13.94	15.28	16.39	17.32
24	0.000	0.4812E-02	-0.88	-4.09	-2.75	-1.64	-0.72
25	18.032	0.4812E-02	17.15	13.94	15.28	16.39	17.32
26	18.229	0.9350E-02	17.30	13.69	15.30	16.50	17.47
27	0.000	0.9349E-02	-0.89	-4.16	-2.72	-1.62	-0.72
28	18.229	0.9370E-02	17.30	13.95	15.42	16.55	17.48
29	18.622	0.1892E-01	17.52	13.30	15.21	16.59	17.71
30	0.000	0.1891E-01	-1.00	-4.33	-2.84	-1.74	-0.80
31	18.622	0.1898E-01	17.52	13.95	15.52	16.72	17.75
32	19.211	0.3396E-01	17.81	12.81	15.06	16.68	18.06
33	0.000	0.3397E-01	-1.24	-4.83	-3.26	-2.06	-0.97
34	19.211	0.3406E-01	17.82	13.81	15.52	16.88	18.12
35	19.801	0.4971E-01	18.10	12.37	14.89	16.76	18.41
36	0.000	0.4970E-01	-1.50	-5.46	-3.79	-2.45	-1.17

Table 4.2.1-2. Loading history, surface-grain-averaged stresses (σ_{rgl}), and x-ray-averaged stresses for a specimen with a soft grain concentration of 33%. Nonlinear strain tensor and 100 el/g used in the finite element calculations. All stresses are longitudinal, i.e., in the direction of load application. Mechanical constants: σ_{ys} = 15 ksi, σ_{yh} = 20 ksi, H_s = 0, H_h = 100 ksi.

Step No.	Applied Stress (ksi)	Plastic Strain	σ_{rgl} (ksi)	X-Ray-Averaged Stress (ksi) Penetration Depth (grains)			
				0.500	1.000	2.000	5.000
1	15.00	0.000E+00	15.00	15.00	15.00	15.00	15.00
2	15.84	0.499E-04	15.53	15.19	15.24	15.38	15.61
3	0.00	0.495E-04	-0.31	-0.65	-0.60	-0.46	-0.24
4	15.84	0.499E-04	15.53	15.19	15.24	15.38	15.61
5	16.68	0.102E-03	16.05	15.35	15.45	15.75	16.20
6	0.00	0.101E-03	-0.63	-1.33	-1.23	-0.93	-0.48
7	16.68	0.102E-03	16.05	15.35	15.45	15.75	16.20
8	17.46	0.183E-03	16.52	15.46	15.65	16.10	16.76
9	0.00	0.183E-03	-0.94	-2.01	-1.81	-1.36	-0.70
10	17.46	0.183E-03	16.52	15.46	15.65	16.10	16.76
11	17.66	0.237E-03	16.66	15.44	15.69	16.20	16.91
12	0.00	0.237E-03	-1.00	-2.22	-1.97	-1.46	-0.75
13	17.66	0.237E-03	16.66	15.44	15.69	16.20	16.91
14	17.75	0.342E-03	16.77	15.33	15.67	16.26	17.01
15	0.00	0.341E-03	-0.97	-2.41	-2.08	-1.49	-0.74
16	17.75	0.342E-03	16.77	15.33	15.67	16.26	17.01
17	17.81	0.790E-03	16.88	14.91	15.48	16.25	17.08
18	0.00	0.790E-03	-0.94	-2.90	-2.33	-1.56	-0.73
19	17.81	0.790E-03	16.88	14.91	15.48	16.25	17.08
20	17.89	0.204E-02	16.96	14.20	15.20	16.21	17.15
21	0.00	0.204E-02	-0.93	-3.68	-2.69	-1.68	-0.74
22	17.89	0.204E-02	16.96	14.20	15.20	16.21	17.15
23	17.97	0.382E-02	17.04	13.80	15.10	16.23	17.22
24	0.00	0.382E-02	-0.94	-4.17	-2.88	-1.74	-0.76
25	17.97	0.382E-02	17.04	13.80	15.10	16.23	17.22
26	18.13	0.748E-02	17.13	13.42	15.01	16.27	17.32
27	0.00	0.748E-02	-0.97	-4.45	-2.97	-1.78	-0.78
28	18.13	0.748E-02	17.13	13.61	15.10	16.31	17.33
29	18.46	0.159E-01	17.23	12.68	14.70	16.20	17.46
30	0.00	0.159E-01	-1.13	-4.82	-3.22	-1.97	-0.89
31	18.46	0.159E-01	17.23	13.38	15.04	16.35	17.50
32	19.01	0.308E-01	17.32	11.48	14.07	16.01	17.67
33	0.00	0.308E-01	-1.50	-5.74	-3.92	-2.47	-1.13
34	19.01	0.310E-01	17.32	12.53	14.55	16.20	17.73
35	19.68	0.520E-01	17.38	9.91	13.16	15.68	17.91
36	0.00	0.520E-01	-1.99	-7.15	-5.01	-3.19	-1.46

Table 4.2.1-3. Verification of load equilibrium for the basic model calculations (linear geometry). $S_{xy}(P)$ is the calculated stress in the primitive or minimum array cell (Figure 3.1-3 (c)), whereas $S_{xy}(D)$ is the corresponding stress in the double primitive array cell, which completely reflects the symmetry of the shear stresses.

Step No.	Applied Stress (ksi)	Calculated Stress by Summing over all Planes (ksi)			
		S_{xx}	S_{yy}	$S_{xy}(P)$	$S_{xy}(D)$
1	15.000	0.000	15.000	0.000	0.000
2	15.835	0.000	15.835	0.023	0.000
3	0.000	0.000	0.000	0.023	0.000
4	15.835	0.000	15.835	0.023	0.000
5	16.670	0.000	16.670	0.046	0.000
6	0.000	0.000	0.000	0.046	0.000
7	16.670	0.000	16.670	0.046	0.000
8	17.411	0.000	17.411	0.071	0.000
9	0.000	0.000	0.000	0.071	0.000
10	17.411	0.000	17.411	0.071	0.000
11	17.645	0.000	17.645	0.083	0.000
12	0.000	0.000	0.000	0.083	0.000
13	17.645	0.000	17.645	0.083	0.000
14	17.762	0.000	17.762	0.090	0.000
15	0.000	0.000	0.000	0.089	0.000
16	17.762	0.000	17.762	0.089	0.000
17	17.847	0.000	17.847	0.093	0.000
18	0.000	0.000	0.000	0.093	0.000
19	17.847	0.000	17.847	0.093	0.000
20	17.923	0.000	17.923	0.094	0.000
21	0.000	0.000	0.000	0.094	0.000
22	17.923	0.000	17.923	0.094	0.000
23	18.032	0.000	18.032	0.094	0.000
24	0.000	0.000	0.000	0.095	0.000
25	18.032	0.000	18.032	0.095	0.000
26	18.229	0.000	18.229	0.099	0.000
27	0.000	0.000	0.000	0.099	0.000
28	18.229	0.000	18.229	0.100	0.000
29	18.622	0.000	18.622	0.114	0.000
30	0.000	0.000	0.000	0.114	0.000
31	18.622	0.000	18.622	0.114	0.000
32	19.211	0.000	19.211	0.133	0.000
33	0.000	0.000	0.000	0.133	0.000
34	19.211	0.000	19.211	0.134	0.000
35	19.801	0.000	19.801	0.152	0.000
36	0.000	0.000	0.000	0.152	0.000

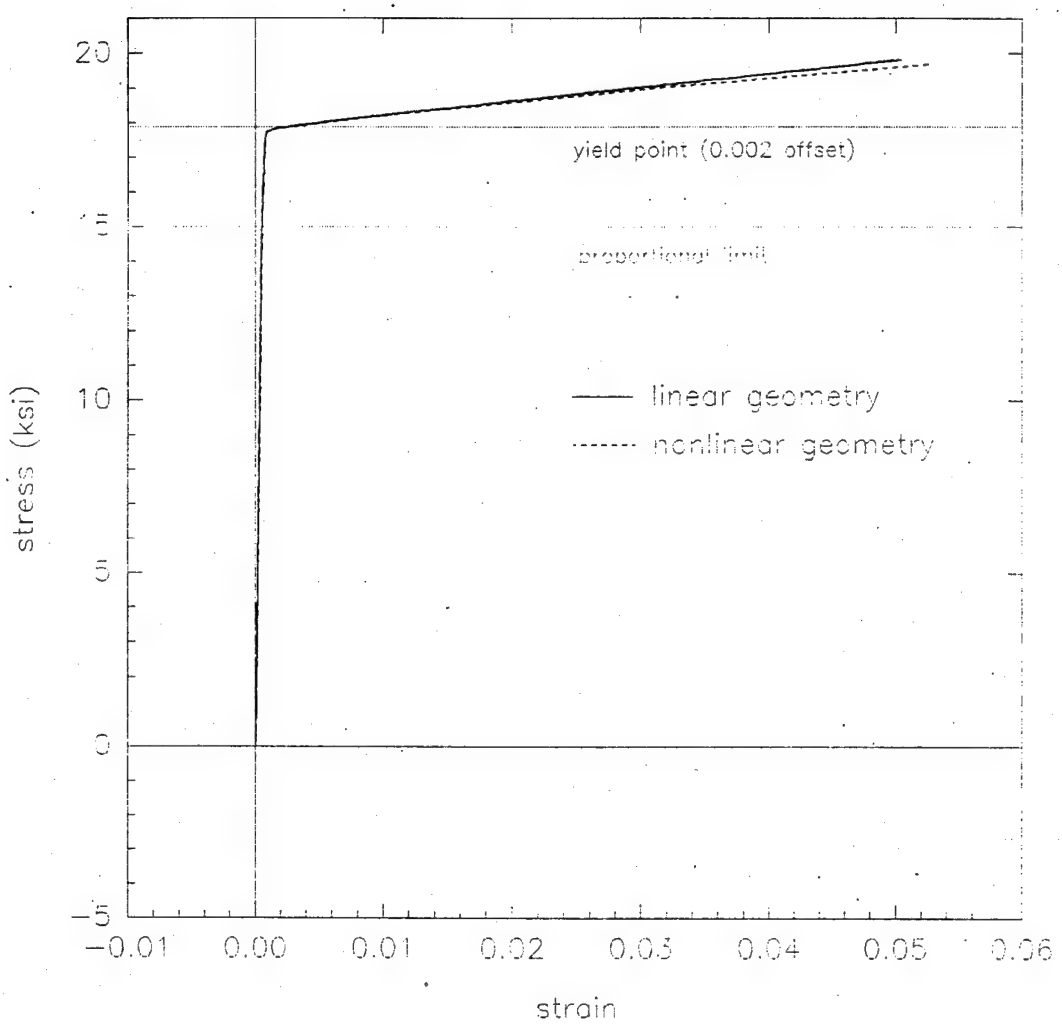

Figure 4.2.1-1. Stress-strain curve for the basic model under plane stress using linear geometry and nonlinear geometry. Model description: $f_s = 0.33$, $E = 30{,}000$ ksi, $\upsilon = 0.29$, $\sigma_{ys} = 15$ ksi, $\sigma_{yh} = 20$ ksi, $H_s = 0$, $H_h = 100$ ksi

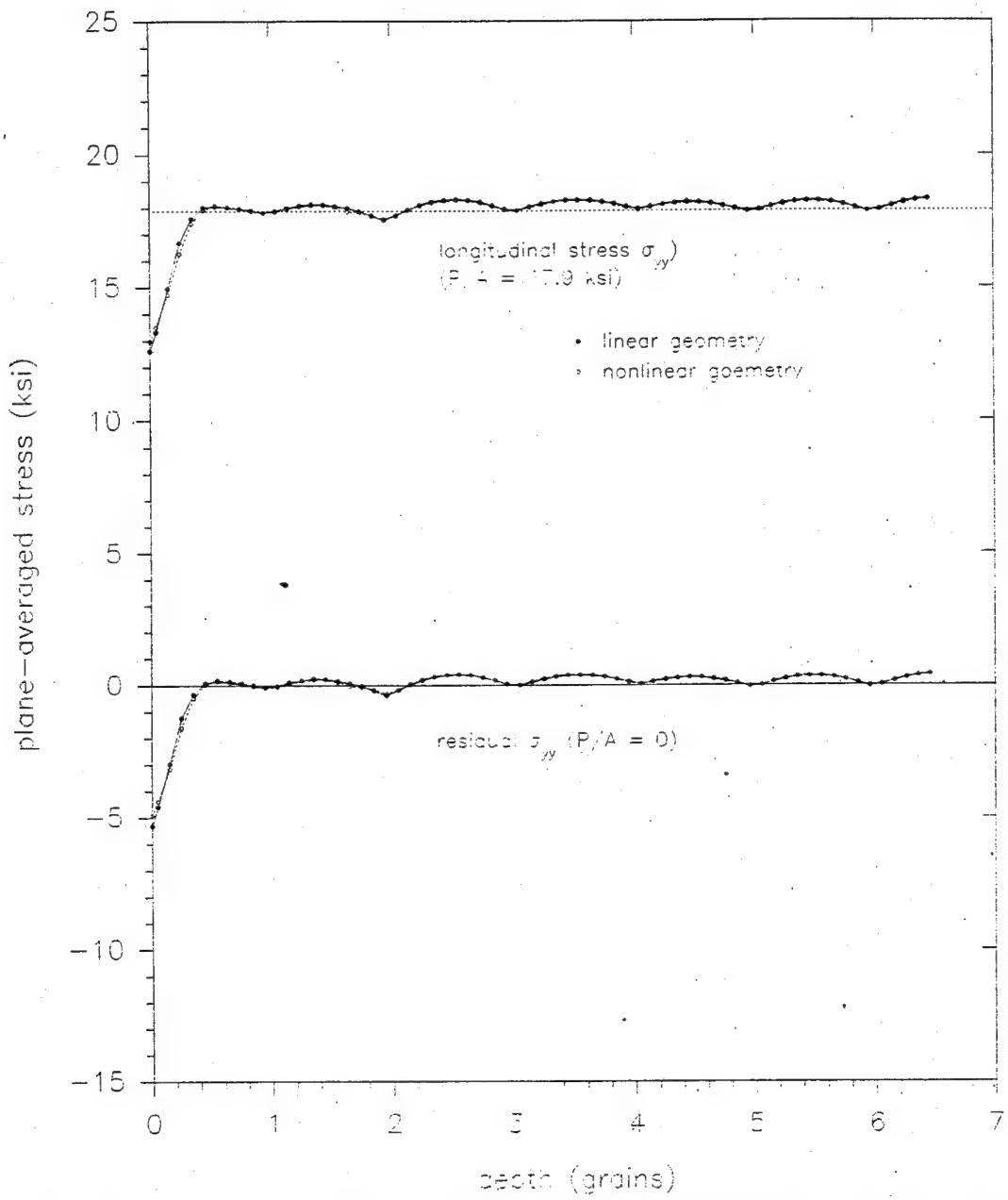

Figure 4.2.1-2. Plane-averaged longitudinal stress versus depth in the basic model for a plastic strain of 0.002, before and after removal of the load. The linear and nonlinear geometry calculations almost coincide. (f_s = 0.33, σ_{ys} = 15 ksi, σ_{yh} = 20 ksi, H_s = 0, H_h = 100 ksi.)

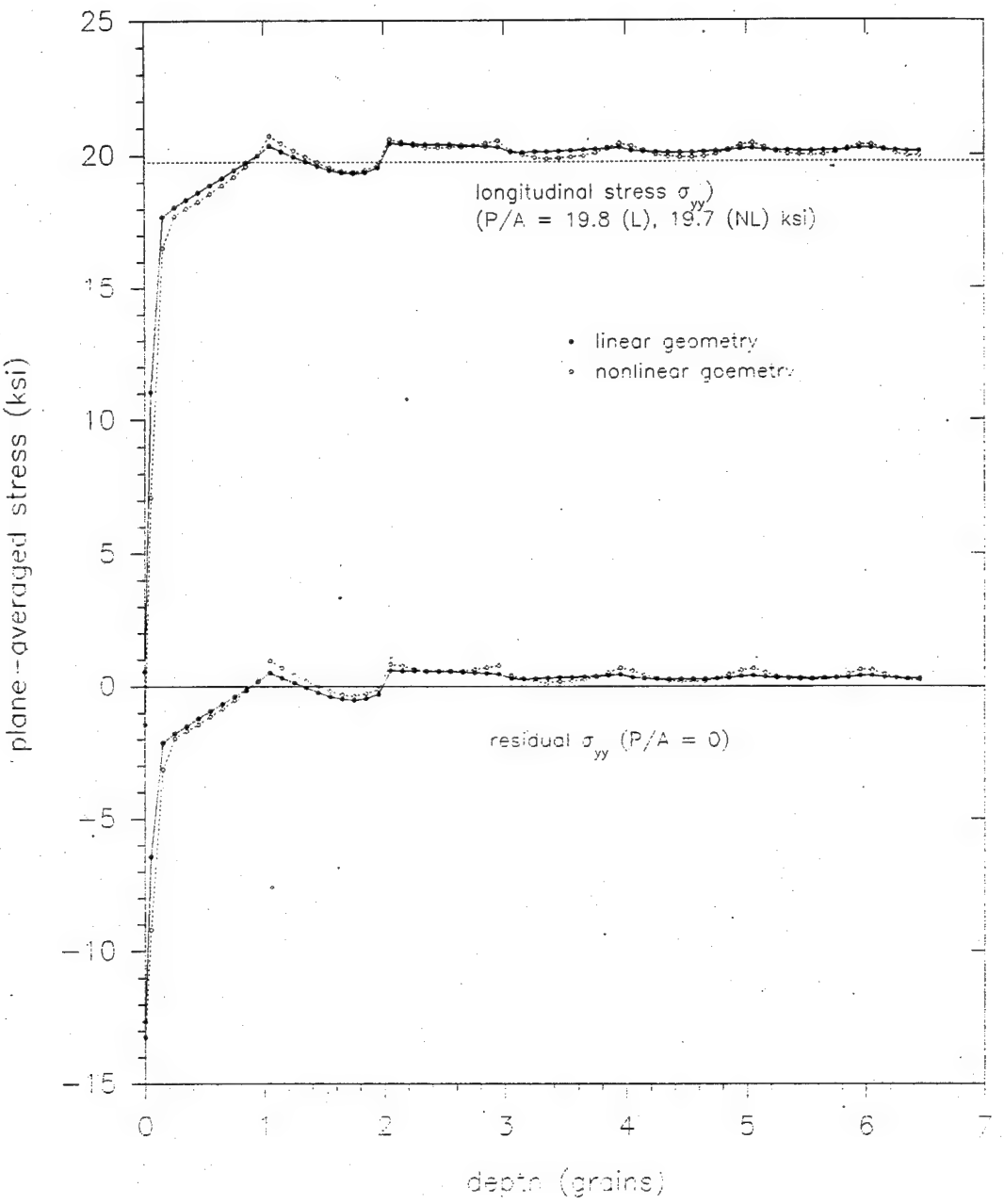

Figure 4.2.1-3. Plane-averaged longitudinal stress versus depth in the basic model for a plastic strain of 0.05, before and after removal of the load. The stress peaks at the grain interface planes are more pronounced for the nonlinear than for the linear geometry calculations. (f_s = 0.33, σ_{ys} = 15 ksi, σ_{yh} = 20 ksi, H_s = 0, H_h = 100 ksi.)

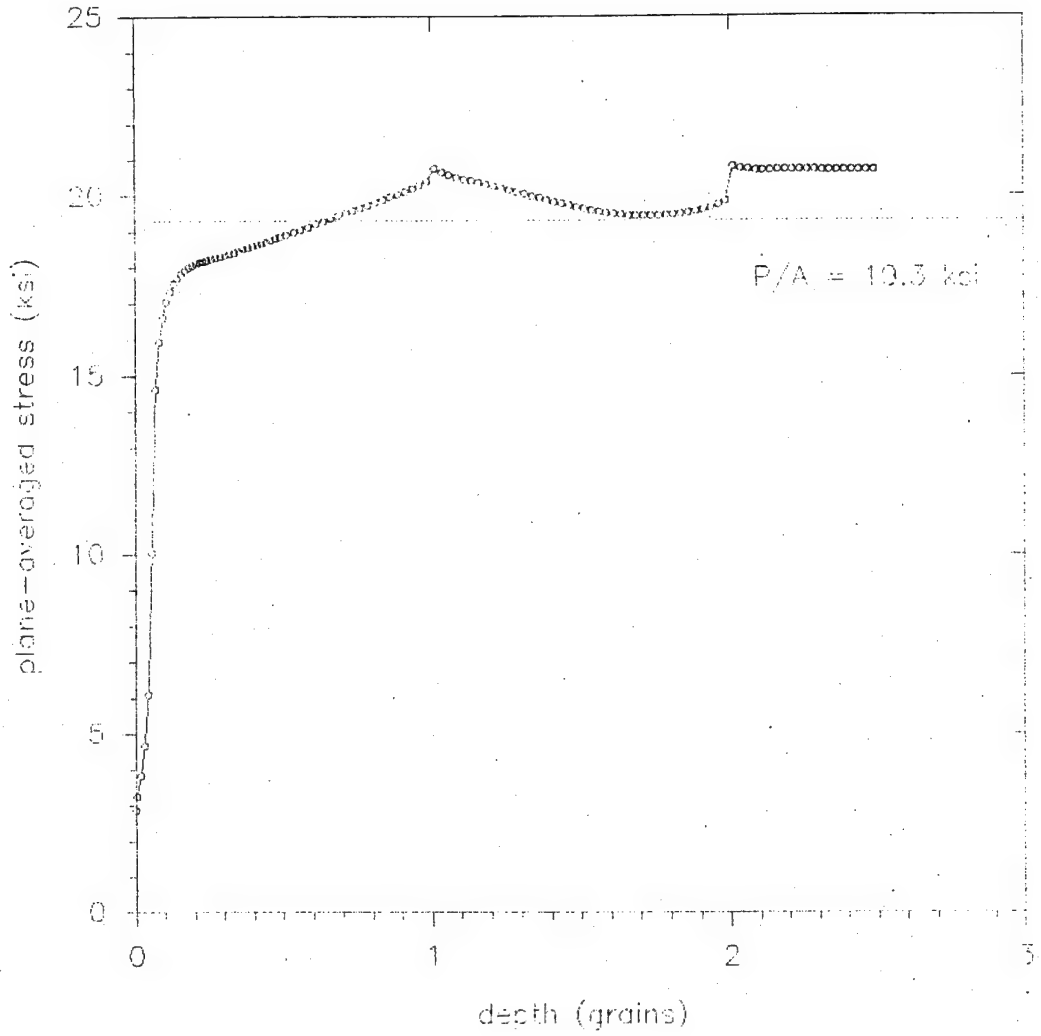

Figure 4.2.1-4. Close-up view of the plane-averaged longitudinal stress versus depth in the surface layer region for a plastic strain of 0.055, under load. 3200 el/g in the surface region, 80 el/g in the horizontal direction. (f_s = 0.33, σ_{ys} = 15 ksi, σ_{yh} = 20 ksi, H_s = 0, H_h = 100 ksi.)

Figure 4.2.1-5. Deformed geometry of the basic model at 5% plastic strain after unloading. The darkened regions correspond to the soft grains. (f_s = 0.33, E = 30,000 ksi, υ = 0.29, σ_{ys} = 15 ksi, σ_{yh} = 20 ksi, H_s = 0, H_h = 100 ksi.)

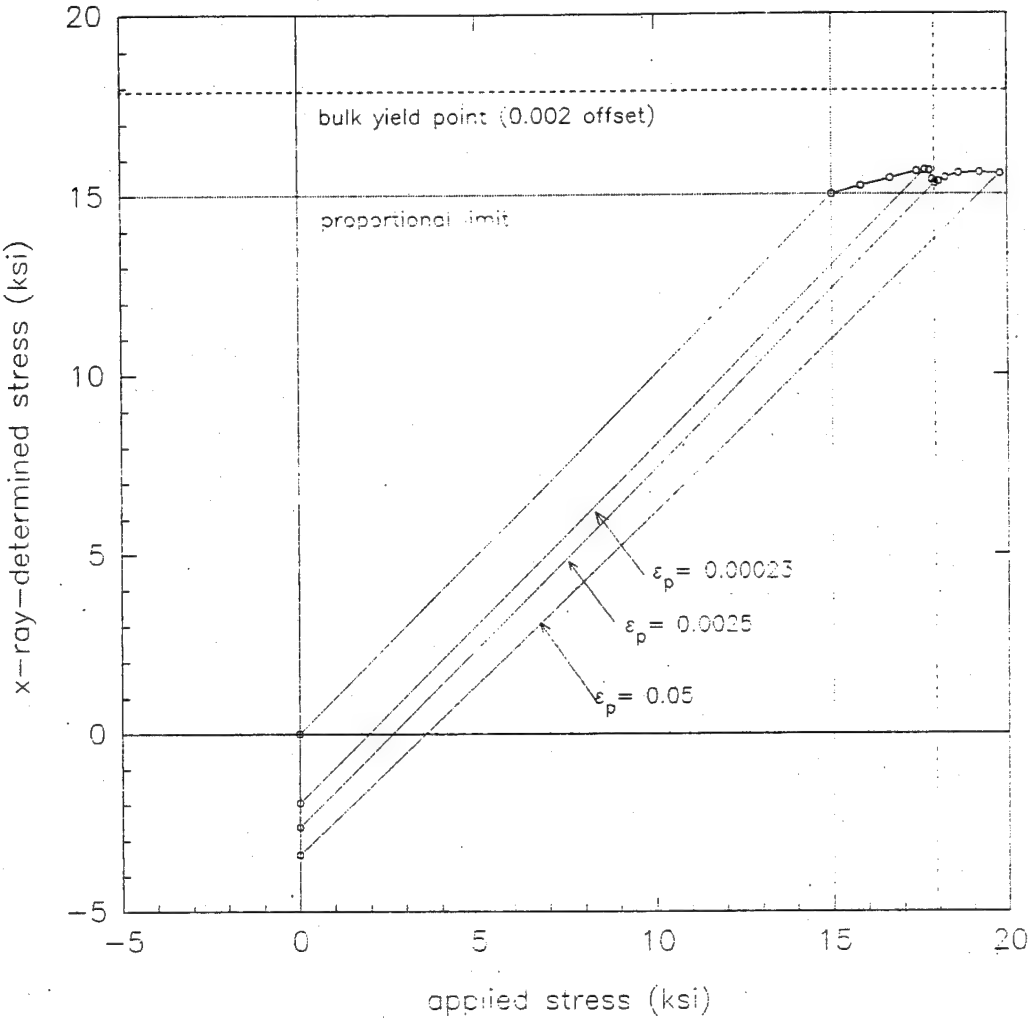

Figure 4.2.1-6. X-ray-determined stress versus the applied nominal stress for the basic model for an effective penetration depth of one grain. (a) Linear geometry. (Continued.)

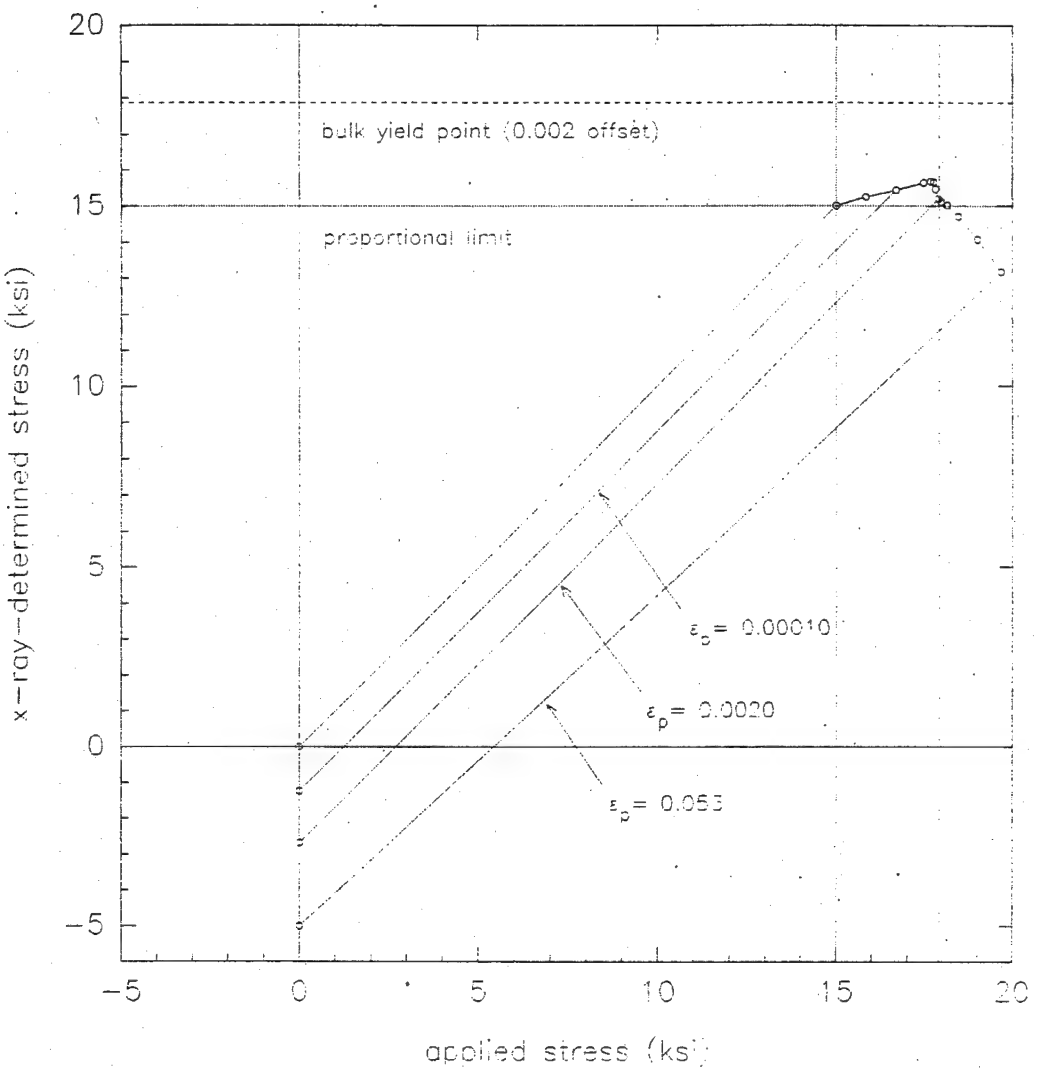

Figure 4.2.1-6 (Continued). X-ray-determined stress versus the applied nominal stress for the basic model for an effective penetration depth of one grain. (b) Nonlinear geometry. (f_s = 0.33, σ_{ys} = 15 ksi, σ_{yh} = 20 ksi, H_s = 0, H_h = 100 ksi.)

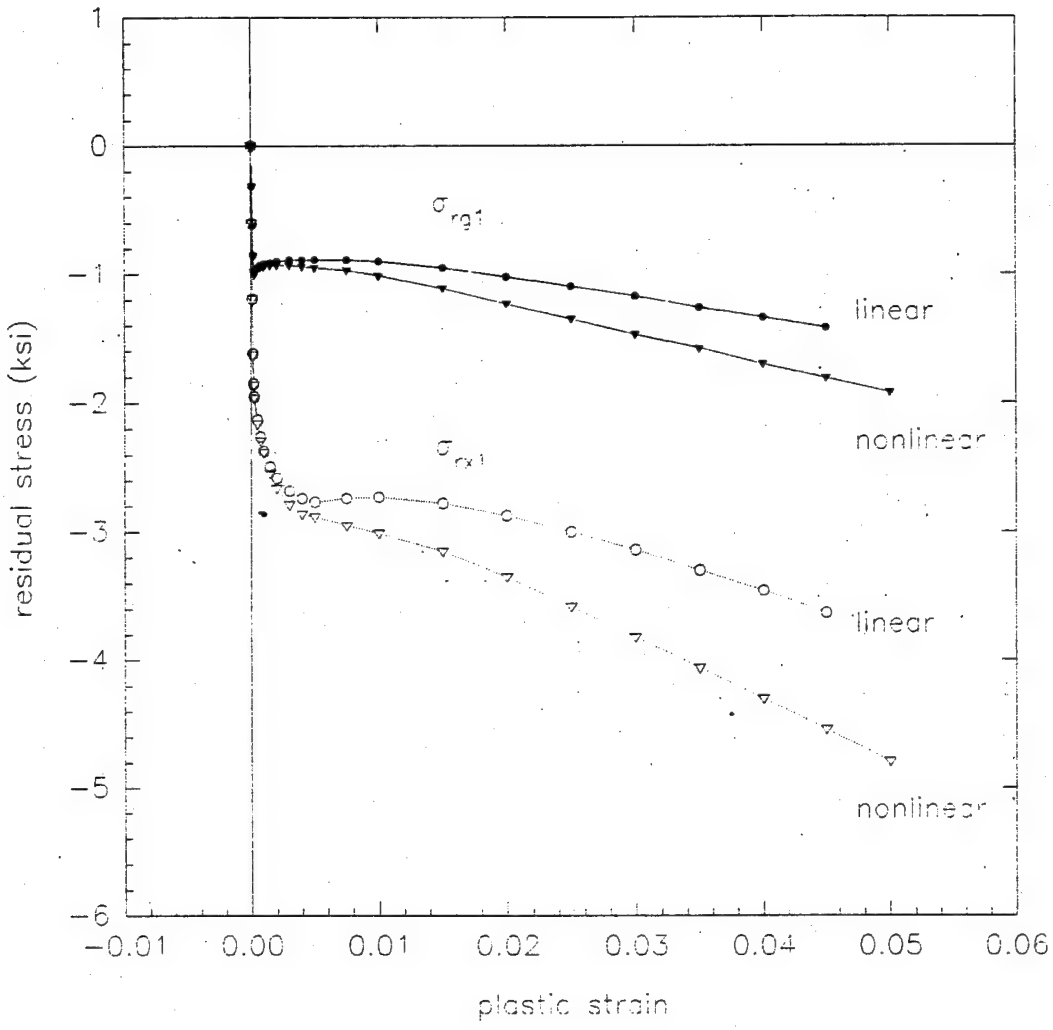

Figure 4.2.1-7. Surface-grain-averaged residual stresses (σ_{rg1}) and x-ray-averaged residual stresses (σ_{rx1}) versus plastic strain for the basic model. Results for the linear and nonlinear geometry calculations are shown. (f_s = 0.33, σ_{ys} = 15 ksi, σ_{yh} = 20 ksi, H_s = 0, H_h = 100 ksi.)

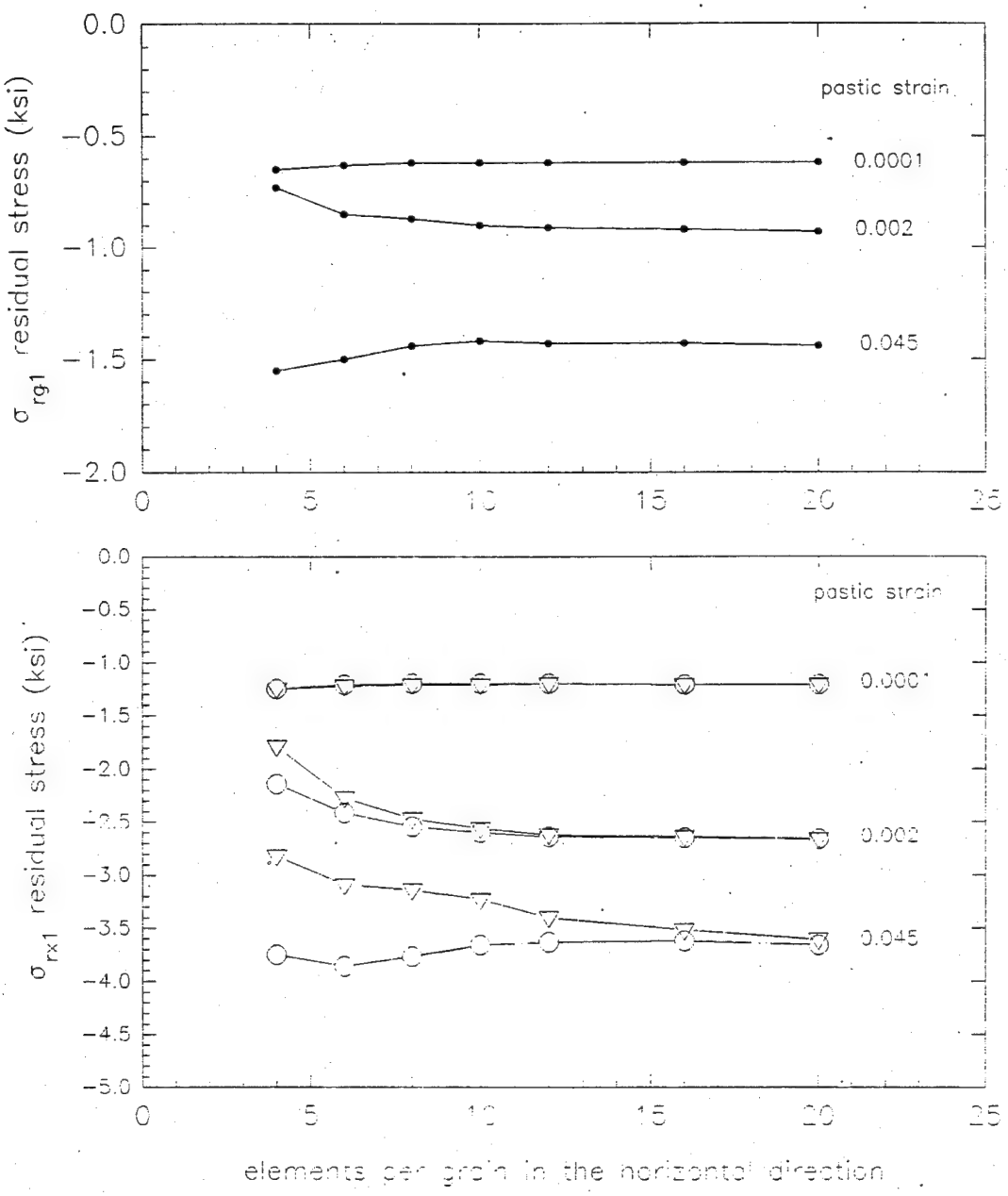

Figure 4.2.1- 8 . Results of a mesh refinement check for the basic model: surface-grain-averaged residual stresses (σ_{rg1}) and x-ray-averaged residual stresses (σ_{rx1}) for ϵ_p = 0.0001, 0.002, and 0.045 versus the number of elements per grain side. (f_s = 0.33, σ_{ys} = 15 ksi, σ_{yh} = 20 ksi, H_s = 0, H_h = 100 ksi.)

The depth of the surface layer or the surface layer thickness is denoted by τ and is defined as the thickness of the surface layer over which the plane-averaged longitudinal stress appears lower overall than that in the bulk, as determined by inspection of a stress versus depth plot. It is therefore only an approximate value. The total depth over which the stress pattern is noticeably disturbed relative to that in the bulk may be significantly greater than τ.

4.2.2.1 Effect of the Bulk Elastic Constants. The bulk elastic constants E and υ are fundamental mechanical properties of the specimen. It is therefore of special interest to determine their effect on the surface layer effect. The effect of E was studied for specimens for which σ_{ys} = 15 ksi, σ_{yh} = 22.5 ksi, H_s = 0, H_h = 100 ksi, for values of E = 10, 20, 30, and 40 thousand ksi in plane stress. The surface layer effect is proportional to E for very small plastic strains (< 0.0002), but it is only slightly affected for plastic strains above 0.01 (Table 4.2.2.1). The general pattern is readily explained if the specimens are viewed as having a surface layer elastically identical to the bulk material, but having a lower yield point, and such that the hardening rate of the bulk material just above the proportional limit is linear and proportional to E. Below the bulk yield point, the residual stress in the surface layer is approximately proportional to E, whereas above the bulk yield point, the residual compressive stresses depend only on the difference between the effective yield points of bulk and surface materials upon unloading. This is shown schematically in Fig.4.2.2.1. The residual stresses become somewhat smaller at large plastic strains (≥ 0.03) as E increases, as might be expected from the corresponding increase in the constraint of the hard grains on the soft grains.

The effect of the value of the Poisson ratio was studied on specimens for which σ_{ys} = 15 ksi, σ_{yh} = 20 ksi, H_s = 0, H_h = 100 ksi, for υ = 0.21, 0.29, and 0.40. The surface layer effect is found to be insensitive to υ. The stress deviation ratios and residual stresses are virtually identical for the three Poisson ratios (Table 4.2.2.2). The elastic value of υ has little effect because the elastic strains are much smaller than the plastic strains after the onset of yielding, and the Poisson ratio for plastic deformation is the same for all the grains, namely 0.5.

In conclusion, the bulk elastic constants E and υ have little effect on the magnitude of the surface layer effect, except for E at very small plastic

strains. In the latter case, the residual compressive stress is approximately proportional to E. Similar results are obtained in generalized plane strain.

4.2.2.2 Effect of Soft Grain Concentration. In modelling the effect of the plastic anisotropy of individual grains in a polycrystalline aggregate with soft and hard grains, there is a choice in the soft grain concentration. A low concentration will localize the "softness", whereas a high concentration will spread it out. A detailed statistical analysis which is beyond the scope of this initial study is required to determine the most appropriate soft grain concentration for a particular distribution of crystal yield point versus orientation with respect to the load. Lacking this analysis, we will examine the effect of the soft grain concentration to gauge the sensitivity of the model to this parameter.

Models having soft grain concentrations of 17%, 25%, and 33% were used to study the effect of soft grain concentration on the surface layer effect. The corresponding grain patterns are shown in Figs. 3.1-1, 3.1-2, and 3.1-3, respectively. The grain material properties are identical for the three models and are those for the basic model (E = 30,000 psi, υ = 0.29, σ_{ys} = 15 ksi, σ_{yh} = 20 ksi, H_s = 0, H_h = 100 ksi). It is found that the plane-averaged longitudinal stress versus depth profiles for a plastic strain of 0.05 change consistently with soft grain concentration. For f_s = 0.17% (Figure 4.2.2.2-1), the surface layer is clearly defined, has a depth of one grain, and the stress profile is fairly flat, i.e., the average stress is fairly constant throughout the surface grain layer. For f_s = 0.25% (Figure 4.2.2.2-2), the surface layer is still one grain in depth (although the total depth of the perturbed layer is 3 to 4 grains), but the stress slowly drops through most of the surface grain layer and then more steeply near (≈ 0.1 gr) the free surface. As already described in Section 4.2.1, for f_s = 0.33%, the surface layer depth increases to two grains; the slope of the drop in stress is greater than for f_s = 0.25%, and the drop near the surface is much more pronounced (Figure 4.2.1-3). Thus, not only does the depth of the surface layer increase in going from a soft grain concentration of 0.17% to 0.33%, but the stress profile changes from approximately constant stress to linear decrease with steep drop near the surface.

The loading histories, surface grain-averaged and x-ray-averaged stresses are given in Tables 4.2.2.2-1 (17%), -2 (25%), and 4.2.1-1 (33%), and the corresponding plots of x-ray stress versus applied stress are shown in

Table 4.2.2.1-1. Comparison of specimens having elastic moduli E of 10, 20, 30, and 40 million psi in plane stress. For all the specimens the soft grain concentration is 33%, υ = 0.29, σ_{ys} = 15 ksi, σ_{yh} = 22.5 ksi, H_s = 0, H_h = 100 ksi

Model		SDF41GL	SDF42GL	SDH43HM	SDF44GL
E (ksi)		10,000	20,000	30,000	40,000
Ω		0.32	0.30	0.29	0.27
τ (gr)		2	2	2	2
Average residual stress in surface grain layer, σ_{rgl}					
ϵ_p	0.00005	-0.20	-0.40	-0.60	-0.80
	0.0001	-0.40	-0.80	-1.20	-1.61
	0.0002	-0.79	-1.59	-2.27	-2.67
	0.002	-3.3	-3.7	-3.9	-4.2
	0.01	-4.3	-4.4	-4.4	-4.4
	0.02	-4.7	-4.6	-4.4	-4.4
	0.05	-5.5	-5.2	-5.2	-5.2
X-ray-averaged residual stress, σ_{rxl}					
ϵ_p	0.00005	-0.10	-0.21	-0.31	-0.42
	0.0001	-0.21	-0.42	-0.63	-0.84
	0.0002	-0.42	-0.83	-1.19	-1.40
	0.002	-1.45	-1.44	-1.42	-1.42
	0.01	-1.5	-1.4	1.4	-1.4
	0.02	-1.6	-1.5	-1.4	-1.4
	0.05	-2.0	-1.9	-1.9	-1.9

Table 4.2.2.1-2. Comparison of specimens having Poisson constants of 0.21, 0.29, and 0.40 in plane stress. For all the specimens the soft grain concentration is 33%, E = 30,000 ksi, σ_{ys} = 15 ksi, σ_{yh} = 20 ksi, H_s = 0, H_h = 100 ksi.

Model		SASV1GC	SAS01GC	SASW1GL
υ		0.21	0.29	0.40
Ω		0.28	0.28	0.28
τ (gr)		2	2	2
X-ray-averaged residual stress, σ_{rx1}				
ϵ_p	0.00005	-0.60	-0.60	-0.60
	0.0001	-1.19	-1.19	-1.19
	0.0002	-1.86	-1.85	-1.85
	0.002	-2.58	-2.58	-2.58
	0.01	-2.72	-2.73	-2.72
	0.02	-2.87	-2.87	-2.88
	0.05	-3.79	-3.79	-3.81
Surface-grain-averaged stress, σ_{rg1}				
ϵ_p	0.00005	-0.31	-0.31	-0.31
	0.0001	-0.62	-0.62	-0.62
	0.0002	-0.97	-0.97	-0.97
	0.002	-0.90	-0.90	-0.90
	0.01	-0.90	-0.90	-0.90
	0.02	-1.02	-1.02	-1.02
	0.05	-1.51	-1.50	-1.51

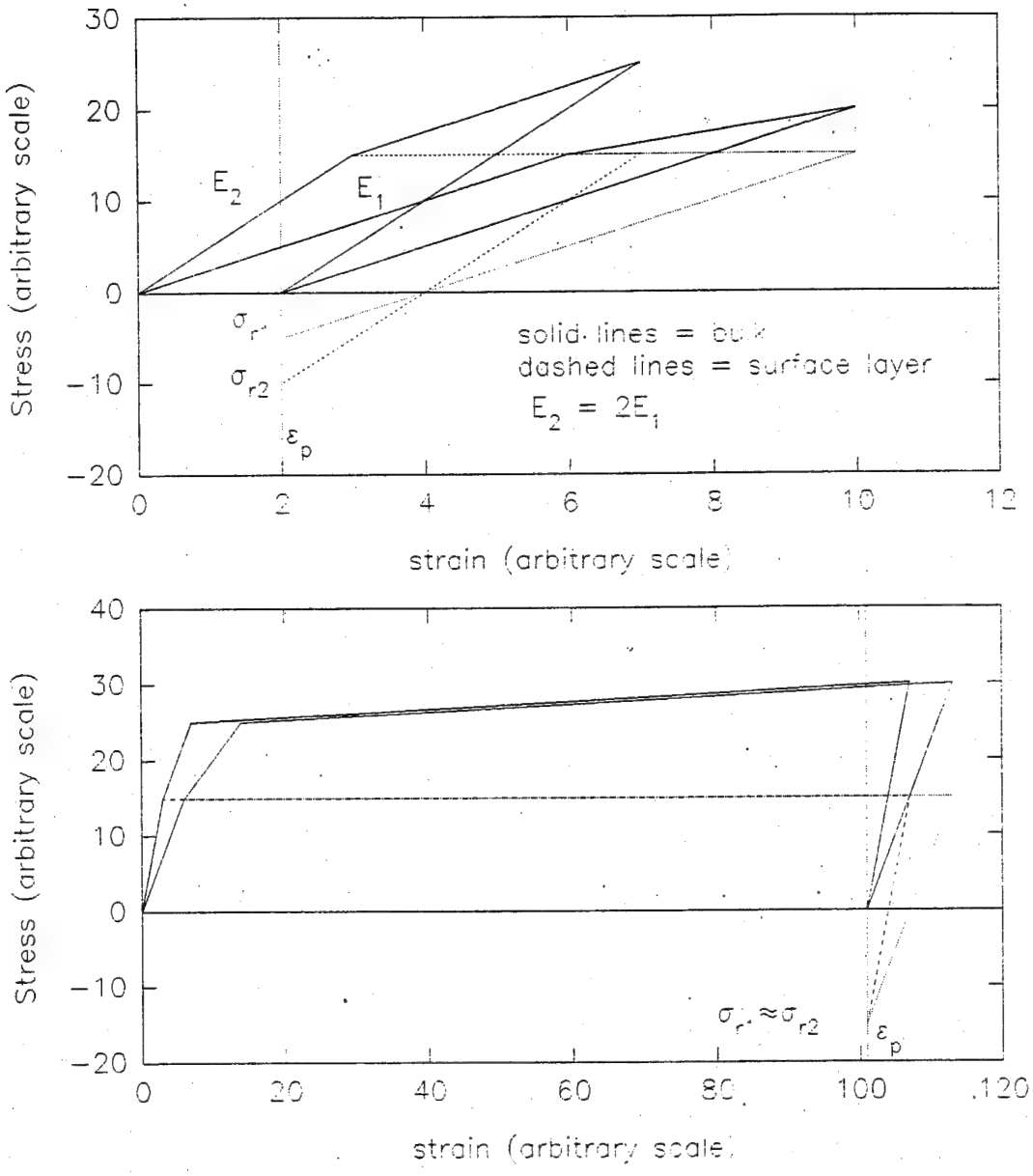

Figure 4.2.2.1-1. Soft surface-layer model to depict the effect of E on the surface layer effect. Specimens 1 and 2 are compared, with $E_2 = 2E_1$, $H_{a2} = 2H_{a1}$ (initial work hardening), $H_{b2} = H_{b1}$ (subsequent work hardening), and the same proportional limit. The surface layer is elastic-perfectly plastic. In this simplified model, the residual stress in the surface layer is proportional to E when the strains are well below the bulk yield point (top graph), but are approximately independent of E at large plastic strains (bottom graph).

Figures 4.2.2.2-3, -4, and 4.2.1-8, respectively. The combined results (Ω, τ, σ_{rxl}, σ_{rgl}) are summarized in Table 4.2.2.2-3. As the soft grain concentration increases, the stress deviation ratio Ω decreases, consistent with an increase in the surface layer effect. Referring to the σ_{rxl} versus P/A plots, it is also seen that there is a jump in the x-ray stress when the specimen undergoes bulk yielding (ϵ_p = 0.002) which is more pronounced as the soft grain concentration decreases. For f_s = 17%, this jump is accompanied by a *decrease* in the residual stress, so that residual stress at ϵ_p = 0.0001 is greater than that at ϵ_p = 0.002 (Table 4.2.2.2-3). At the onset of bulk yielding, the hard grains at the surface are suddenly forced to follow the bulk plastic deformation, leading to less concentration of the plastic deformation in the soft grains, and a concomitant decrease in the compressive residual stresses in the surface layer upon unloading.

At low plastic strains ($\leq$ 0.0001), the residual stresses, both x-ray and grain-averaged, *decrease* with increasing soft grain concentration (Table 4.2.2.2-3). This surprising result may be partly explained as follows. At low plastic strains, almost all of the plastic deformation in the surface grains is confined to the soft grains. For a given plastic strain, the fewer the number of grains, the greater the plastic strain in each grain, and the greater the residual stress in the grain upon unloading. Above the bulk yield point, the x-ray compressive residual stresses increase with soft grain concentration. This is illustrated in Figure 4.2.2.2-5 with plots of σ_{rxl} versus ϵ_p for each value of f_s.

When the bulk plastic strain becomes large enough, plastic deformation spreads to all the grains, and the residual stresses tend to increase with grain concentration, as expected. Different results are obtained with x-ray and grain-averaged residual compressive stresses, reflecting the greater weight given by the x-ray-averaged stresses to the stresses near the free surface. The x-ray stresses σ_{rxl} increase monotonically with f_s; the effect is approximately additive, the residual stress being roughly proportional to the soft grain concentration for ϵ_p = 0.05. The grain-average residual stress σ_{rgl} increases markedly as expected in going from 17% to 25% soft grain concentration, but decreases in going to 33% soft grain concentration (Figure 4.2.2.2-6). In other words, the average compressive residual stress in the surface grains is less in the 33% than the 25% soft grain array. However, as noted before, the surface layer depth is approximately two grains in the 33%

soft array, versus one grain in the 25% soft array. Thus the compressive stresses are more spread out in the higher concentration array.

In conclusion, soft grain concentration affects significantly the depth and profile of the surface layer effect, the magnitude of the residual stresses and the shape of the x-ray stress versus applied stress curve. Surprisingly, some aspects of the surface layer effect increase with a decrease in soft grain concentration. Thus, at the onset of plastic deformation, the residual stresses decrease with an increase in f_s. On the other hand, as f_s increases, the stress deviation ratio Ω decreases, the x-ray stress versus applied stress curve exhibits less stress leveling, and the compressive residual stresses for large plastic strains increase, as expected. The surface layer depth τ increases from one to two grains upon increasing f_s from 25% to 33% ($\epsilon_p \approx 0.05$). However, the compressive stresses are more spread out in the 33% model than the 25% model, explaining why the surface-grain-averaged compressive residual stress σ_{rsl} is greater for the lower concentration model ($\epsilon_p \approx 0.05$). Which value of f_s is chosen to model a polycrystalline aggregate can be based on statistical considerations or on experimental data. As shown in Section 4.2.3, "Comparison of the Model with Experimental Data," the 33% soft model leads to surprisingly good semi-quantitative agreement with the experimental data.

4.2.2.3 Effect of Grain Disorder. Because polycrystalline aggregates in actual metals are not ordered, but tend to be disordered or random in crystal orientation, it is of interest to consider a disordered array. For this purpose, models containing 24%, 25%, and 29% soft grains in disordered arrays were constructed. Grain properties were initially assigned with a random number generator, followed by some reassignments to eliminate lines of weakness in the specimen. Practical limits on mesh size (i.e. the number of elements) precluded higher soft grain concentrations than about 30%, because the higher the soft grain concentration, the greater the number grains must be in order to avoid arrangements of soft grains which form lines of weakness through the specimen.

The arrays used in the calculations are shown in Figures 3.1-5 (24%), 3.1-6 (25%), and 3.1-7 (29%). The loading histories, surface grain-averaged and x-ray-averaged stresses are given in Tables 4.2.2.3-1 (24%), -2 (25%), and -3 (29%), and the corresponding plots of x-ray stress versus applied stress

Table 4.2.2.2-1. Loading history, surface-grain-averaged stresses, and x-ray-averaged stresses for a specimen with a soft grain concentration of 17%. Mesh width 6.5 grains, 100 el/gr, E = 30,000 ksi, υ = 0.29, σ_{ys} = 15 ksi, σ_{yh} = 20 ksi, H_s = 0, H_h = 100 ksi.

Step No.	Applied Stress (ksi)	Plastic Strain	σ_{rg1} (ksi)	X-Ray-Averaged Stress (ksi) Penetration Depth (grains) 0.500	1.000	2.000	5.000
1	15.000	0.0000E+00	15.00	15.00	15.00	15.00	15.00
2	17.778	0.5770E-04	16.97	16.72	16.74	16.91	17.29
3	0.000	0.5771E-04	-0.81	-1.06	-1.03	-0.87	-0.49
4	17.778	0.5770E-04	16.97	16.72	16.74	16.91	17.29
5	18.378	0.1686E-03	17.65	17.50	17.49	17.60	17.89
6	0.000	0.1686E-03	-0.73	-0.87	-0.89	-0.78	-0.49
7	18.378	0.1686E-03	17.65	17.50	17.49	17.60	17.89
8	18.473	0.2378E-03	17.88	17.82	17.79	17.84	18.06
9	0.000	0.2378E-03	-0.60	-0.65	-0.69	-0.63	-0.42
10	18.473	0.2378E-03	17.88	17.82	17.79	17.84	18.06
11	18.565	0.3721E-03	18.13	18.20	18.15	18.13	18.24
12	0.000	0.3721E-03	-0.43	-0.37	-0.42	-0.43	-0.32
13	18.565	0.3721E-03	18.13	18.20	18.15	18.13	18.24
14	18.672	0.7957E-03	18.39	18.46	18.44	18.40	18.43
15	0.000	0.7957E-03	-0.28	-0.21	-0.23	-0.27	-0.25
16	18.672	0.7957E-03	18.39	18.46	18.44	18.40	18.43
17	18.770	0.1697E-02	18.55	18.56	18.56	18.54	18.56
18	0.000	0.1697E-02	-0.22	-0.21	-0.21	-0.23	-0.21
19	18.770	0.1697E-02	18.55	18.56	18.56	18.54	18.56
20	18.867	0.2856E-02	18.63	18.58	18.60	18.60	18.65
21	0.000	0.2856E-02	-0.23	-0.29	-0.27	-0.26	-0.22
22	18.867	0.2856E-02	18.63	18.58	18.60	18.60	18.65
23	19.068	0.5497E-02	18.76	18.60	18.67	18.72	18.82
24	0.000	0.5496E-02	-0.31	-0.47	-0.40	-0.35	-0.24
25	19.068	0.5497E-02	18.76	18.60	18.67	18.72	18.82
26	19.404	0.1020E-01	18.98	18.76	18.85	18.94	19.11
27	0.000	0.1020E-01	-0.43	-0.64	-0.56	-0.46	-0.29
28	19.404	0.1020E-01	18.98	18.76	18.85	18.94	19.11
29	20.075	0.2011E-01	19.43	19.30	19.35	19.45	19.70
30	0.000	0.2011E-01	-0.65	-0.77	-0.73	-0.62	-0.37
31	20.075	0.2011E-01	19.43	19.30	19.35	19.45	19.70
32	21.081	0.3560E-01	20.11	20.11	20.10	20.21	20.56
33	0.000	0.3560E-01	-0.97	-0.98	-0.98	-0.87	-0.52
34	21.081	0.3560E-01	20.11	20.11	20.10	20.21	20.56
35	22.155	0.5246E-01	20.82	20.78	20.78	20.94	21.45
36	0.000	0.5247E-01	-1.33	-1.38	-1.38	-1.21	-0.70

Table 4.2.2.2-2. Loading history, surface-grain-averaged stresses, and x-ray-averaged stresses for a specimen with a soft grain concentration of 25%. Mesh width 6.5 grains, 100 el/gr, E = 30,000 ksi , υ = 0.29, σ_{ys} = 15 ksi, σ_{yh} = 20 ksi, H_s = 0, H_h = 100 ksi.

Step No.	Applied Stress (ksi)	Plastic Strain	σ_{rg1} (ksi)	X-Ray-Averaged Stress (ksi) Penetration Depth (grains) 0.500	1.000	2.000	5.000
1	15.000	0.0000E+00	15.00	15.00	15.00	15.00	15.00
2	16.640	0.5317E-04	16.06	15.67	15.73	15.92	16.26
3	0.000	0.5317E-04	-0.58	-0.97	-0.91	-0.72	-0.38
4	16.640	0.5317E-04	16.06	15.67	15.73	15.92	16.26
5	17.895	0.1274E-03	16.82	16.07	16.21	16.57	17.18
6	0.000	0.1274E-03	-1.08	-1.83	-1.69	-1.32	-0.71
7	17.895	0.1274E-03	16.82	16.07	16.21	16.57	17.18
8	18.057	0.2285E-03	16.96	16.00	16.21	16.65	17.34
9	0.000	0.2284E-03	-1.09	-2.06	-1.85	-1.41	-0.72
10	18.057	0.2285E-03	16.96	16.00	16.21	16.65	17.34
11	18.164	0.5667E-03	17.09	15.71	16.09	16.68	17.44
12	0.000	0.5666E-03	-1.07	-2.46	-2.07	-1.48	-0.72
13	18.164	0.5667E-03	17.09	15.71	16.09	16.68	17.44
14	18.270	0.1307E-02	17.26	15.38	16.05	16.78	17.58
15	0.000	0.1307E-02	-1.01	-2.89	-2.22	-1.49	-0.69
16	18.270	0.1307E-02	17.26	15.38	16.05	16.78	17.58
17	18.362	0.2243E-02	17.42	15.25	16.13	16.92	17.70
18	0.000	0.2243E-02	-0.94	-3.11	-2.23	-1.44	-0.66
19	18.362	0.2243E-02	17.42	15.25	16.13	16.92	17.70
20	18.450	0.3291E-02	17.55	15.25	16.24	17.05	17.81
21	0.000	0.3291E-02	-0.90	-3.20	-2.21	-1.40	-0.64
22	18.450	0.3291E-02	17.55	15.25	16.24	17.05	17.81
23	18.625	0.5682E-02	17.74	15.42	16.49	17.28	18.00
24	0.000	0.5682E-02	-0.88	-3.20	-2.14	-1.35	-0.62
25	18.625	0.5682E-02	17.74	15.42	16.49	17.28	18.00
26	18.916	0.1022E-01	18.01	16.07	16.98	17.65	18.30
27	0.000	0.1022E-01	-0.90	-2.85	-1.93	-1.26	-0.62
28	18.916	0.1022E-01	18.01	16.07	16.98	17.65	18.30
29	19.498	0.2034E-01	18.42	17.52	17.94	18.33	18.85
30	0.000	0.2034E-01	-1.07	-1.98	-1.55	-1.18	-0.65
31	19.498	0.2034E-01	18.42	17.52	17.94	18.33	18.85
32	20.371	0.3636E-01	18.86	18.21	18.48	18.83	19.50
33	0.000	0.3636E-01	-1.51	-2.17	-1.89	-1.53	-0.87
34	20.371	0.3636E-01	18.86	18.20	18.48	18.83	19.50
35	21.302	0.5399E-01	19.28	18.39	18.73	19.22	20.14
36	0.000	0.5400E-01	-2.02	-2.91	-2.57	-2.08	-1.16

Table 4.2.2.2-3. Comparison of specimens having 17%, 25%, and 33% soft grain concentrations. Mesh width 6.5 grains, 100 el/gr. In all cases E = 30,000 ksi , υ = 0.29, σ_{ys} = 15 ksi, σ_{yh} = 20 ksi, H_s = 0, H_h = 100 ksi.

f_s		0.167	0.250	0.333
σ_{ymix} (ksi)		19.16	18.75	18.33
σ_{yB} (ksi)		18.80	18.34	17.90
σ_{ys}/σ_{yB}		0.80	0.82	0.84
Ω		0.68	0.42	0.28
τ (grain)		1	1	2
Surface-grain-averaged stress, σ_{rgl}				
ϵ_p	0.00005	-1.01	-0.86	-0.60
	0.0001	-1.01	-1.51	-1.19
	0.0005	-0.32	-2.04	-2.13
	0.002	-0.22	-2.24	-2.58
	0.01	-0.55	-1.94	-2.73
	0.03	-0.89	-1.67	-3.14
	0.05	-1.31	-2.39	-3.79
X-ray-averaged residual stress, σ_{rxl}				
ϵ_p	0.00005	-0.79	-0.55	-0.31
	0.0001	-0.81	-0.98	-0.62
	0.0005	-0.36	-1.08	-0.95
	0.002	-0.22	-0.96	-0.90
	0.01	-0.42	-0.90	-0.90
	0.03	-0.85	-1.33	-1.17
	0.05	-1.28	-1.90	-1.5

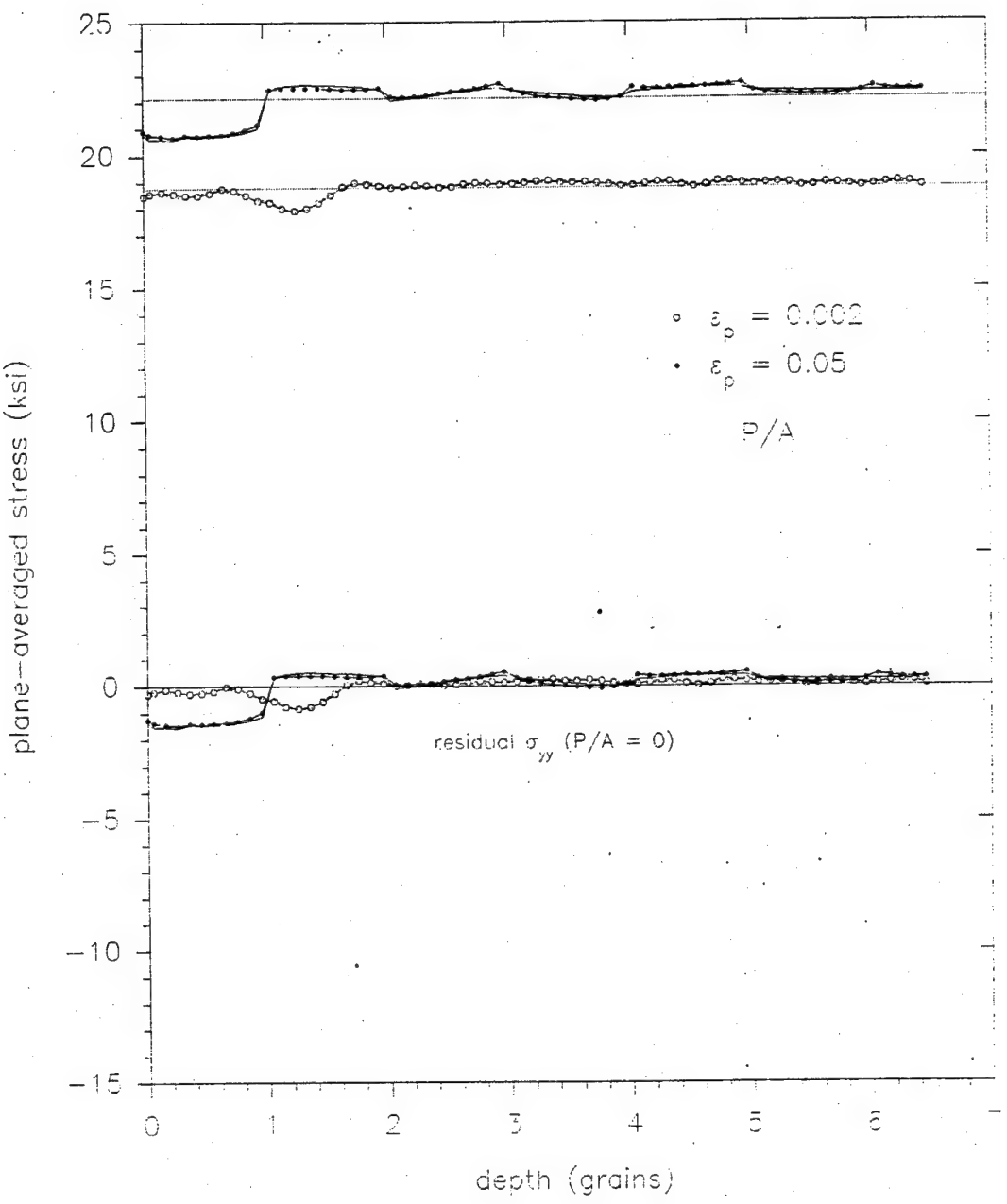

Figure 4.2.2.2-1. Plane-averaged longitudinal stress versus depth in a specimen with 17% soft grain concentration for plastic strains of 0.002 and 0.051, before and after removal of the load. (f_s = 0.17, E = 30,000 ksi, υ = 0.29, σ_{ys} = 15 ksi, σ_{yh} = 20 ksi, H_s = 0, H_h = 100 ksi.)

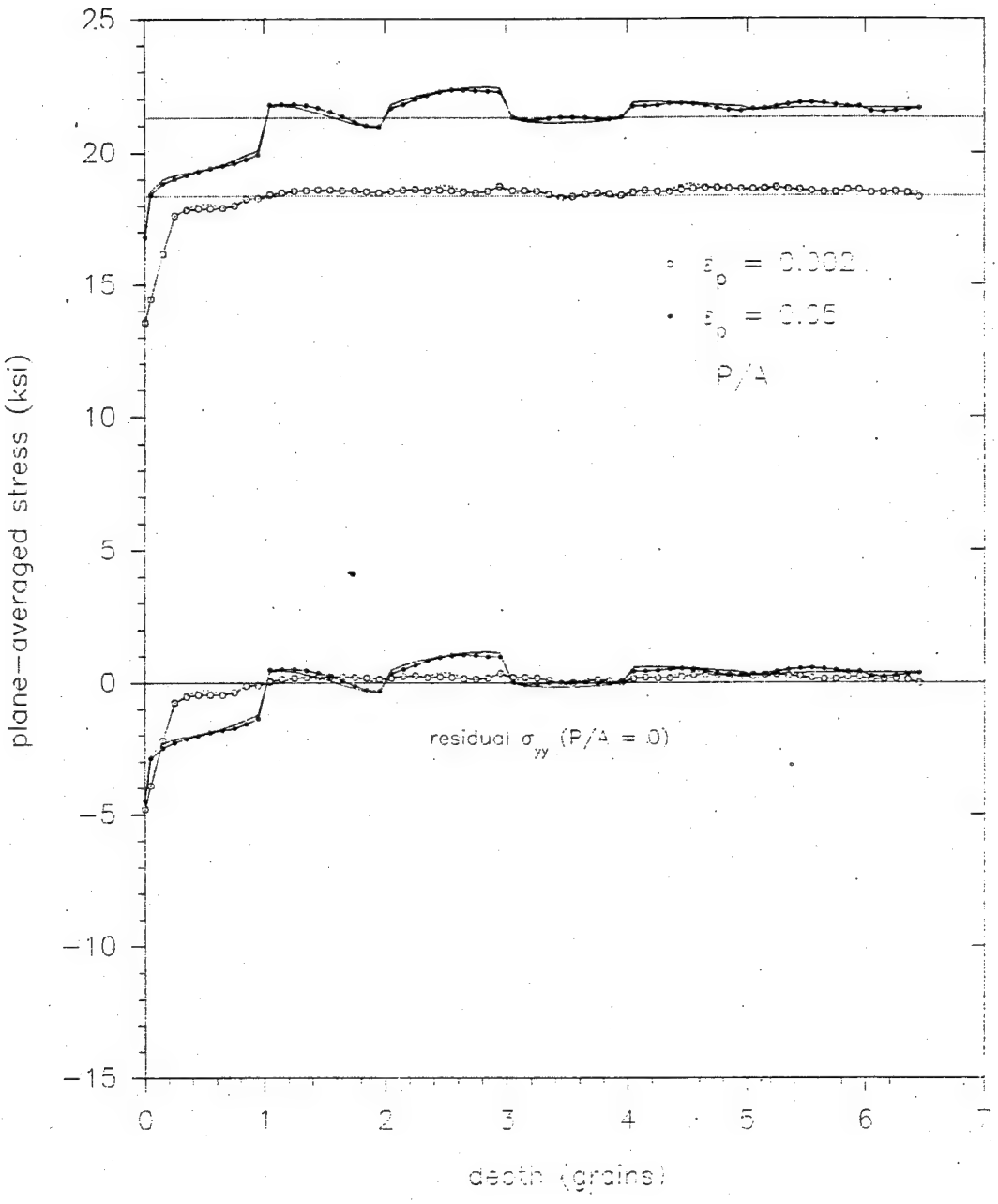

Figure 4.2.2.2-2. Plane-averaged longitudinal stress versus depth in a specimen with 25% soft grain concentration for plastic strains of 0.002 and 0.052, before and after removal of the load. (f_s = 0.25, E = 30,000 ksi, υ = 0.29, σ_{ys} = 15 ksi, σ_{yh} = 20 ksi, H_s = 0, H_h = 100 ksi.)

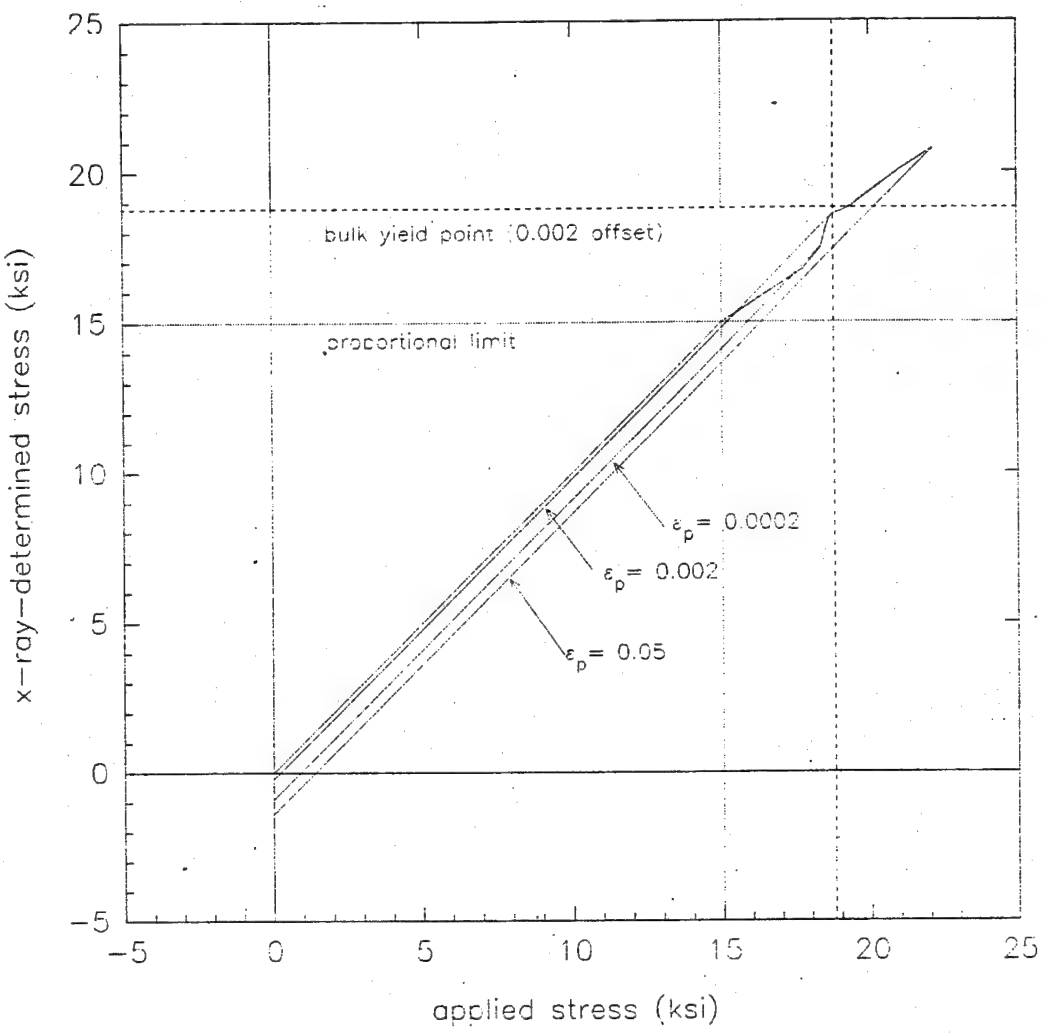

Figure 4.2.2.2-3. X-ray-determined stress versus the nominal applied stress for a model with 17% soft grain concentration. The x-ray effective penetration depth is one grain. (f_s = 0.17, E = 30,000 ksi, υ = 0.29, σ_{ys} = 15 ksi, σ_{yh} = 20 ksi, H_s = 0, H_h = 100 ksi.)

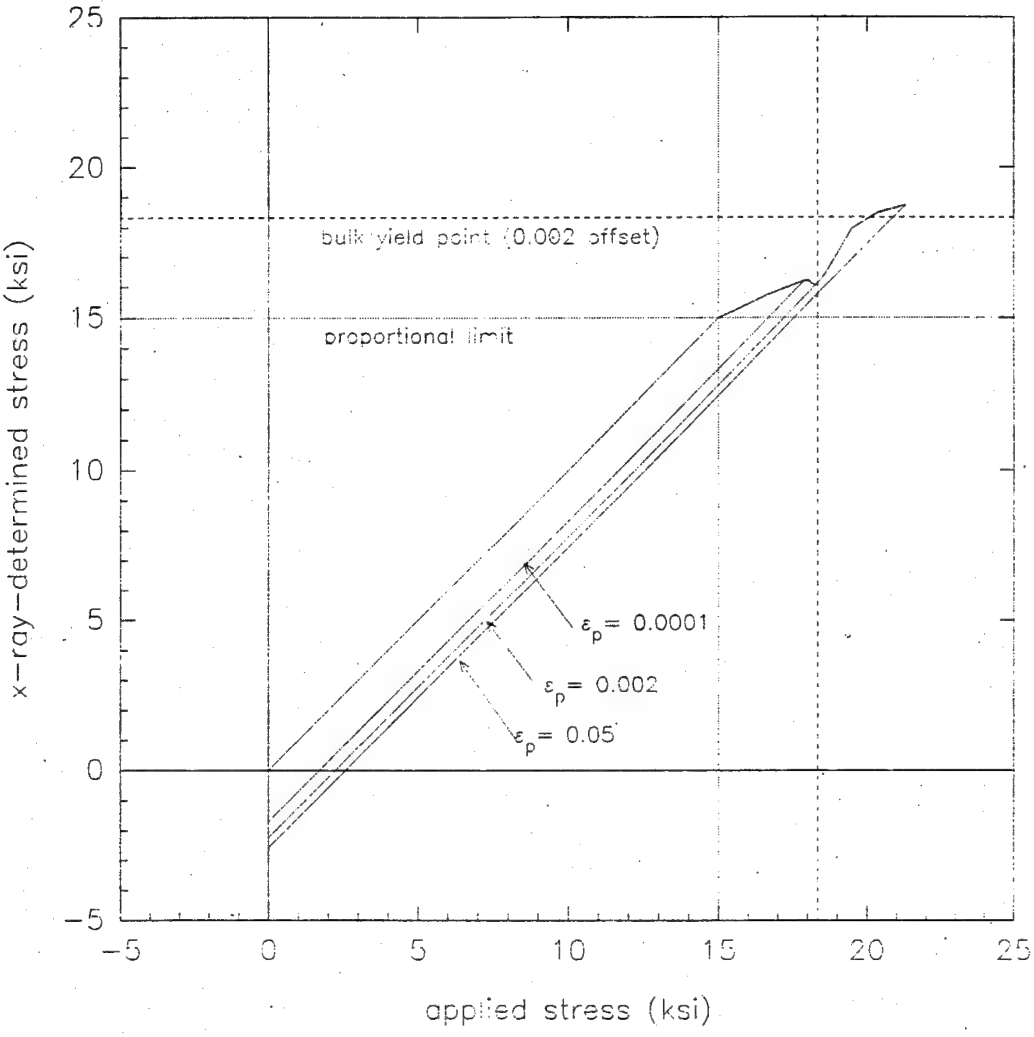

Figure 4.2.2.2-4. X-ray-determined stress versus the nominal applied stress for a model with 25% soft grain concentration. The x-ray effective penetration depth is one grain. (f_s = 0.25, E = 30,000 ksi, υ = 0.29, σ_{ys} = 15 ksi, σ_{yh} = 20 ksi, H_s = 0, H_h = 100 ksi.)

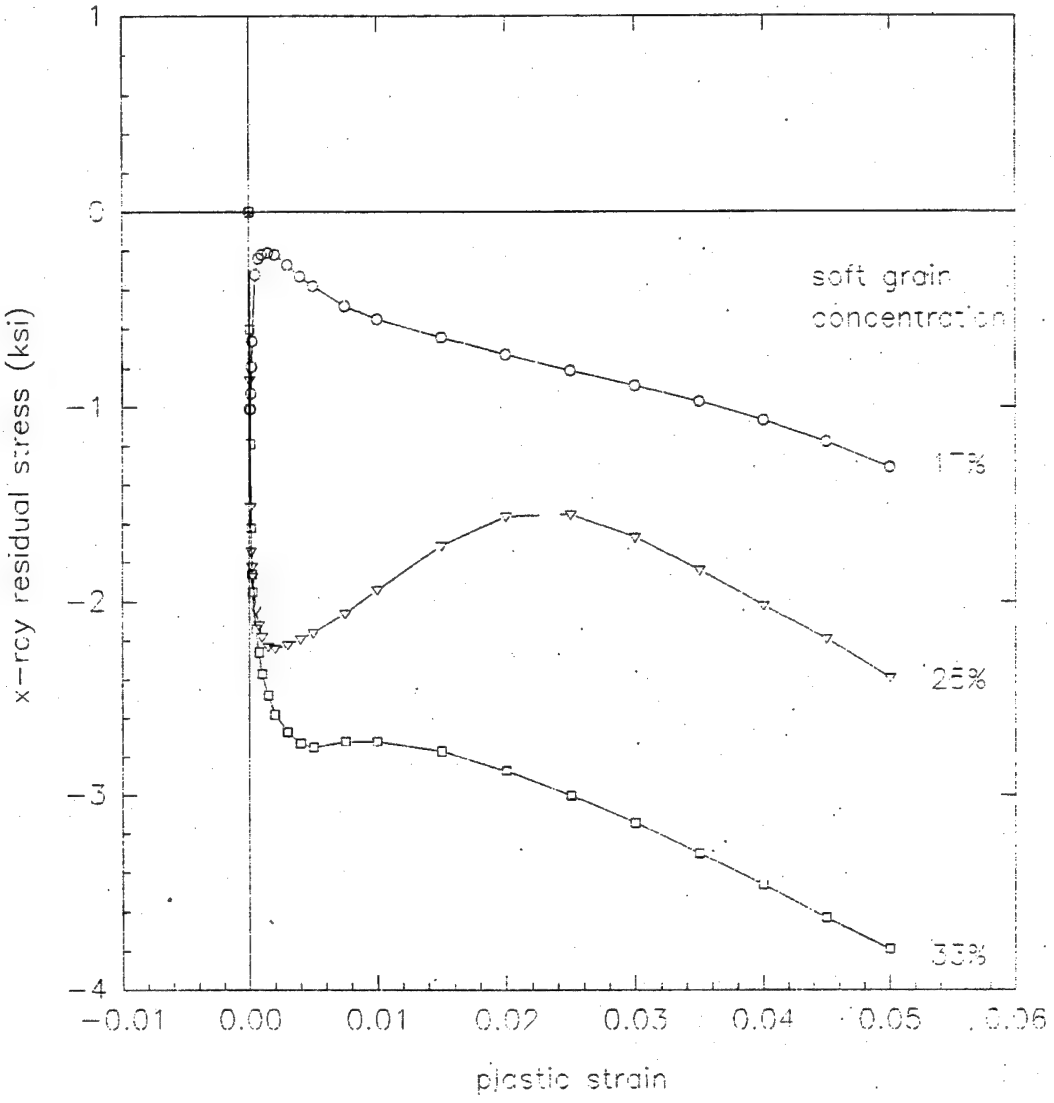

Figure 4.2.2.2-5. X-ray-averaged residual stress (σ_{rxi}) versus plastic strain for soft grain concentrations of 17%, 25%, and 33%. (E = 30,000 ksi, υ = 0.29, σ_{ys} = 15 ksi, σ_{yh} = 20 ksi, H_s = 0, H_h = 100 ksi.)

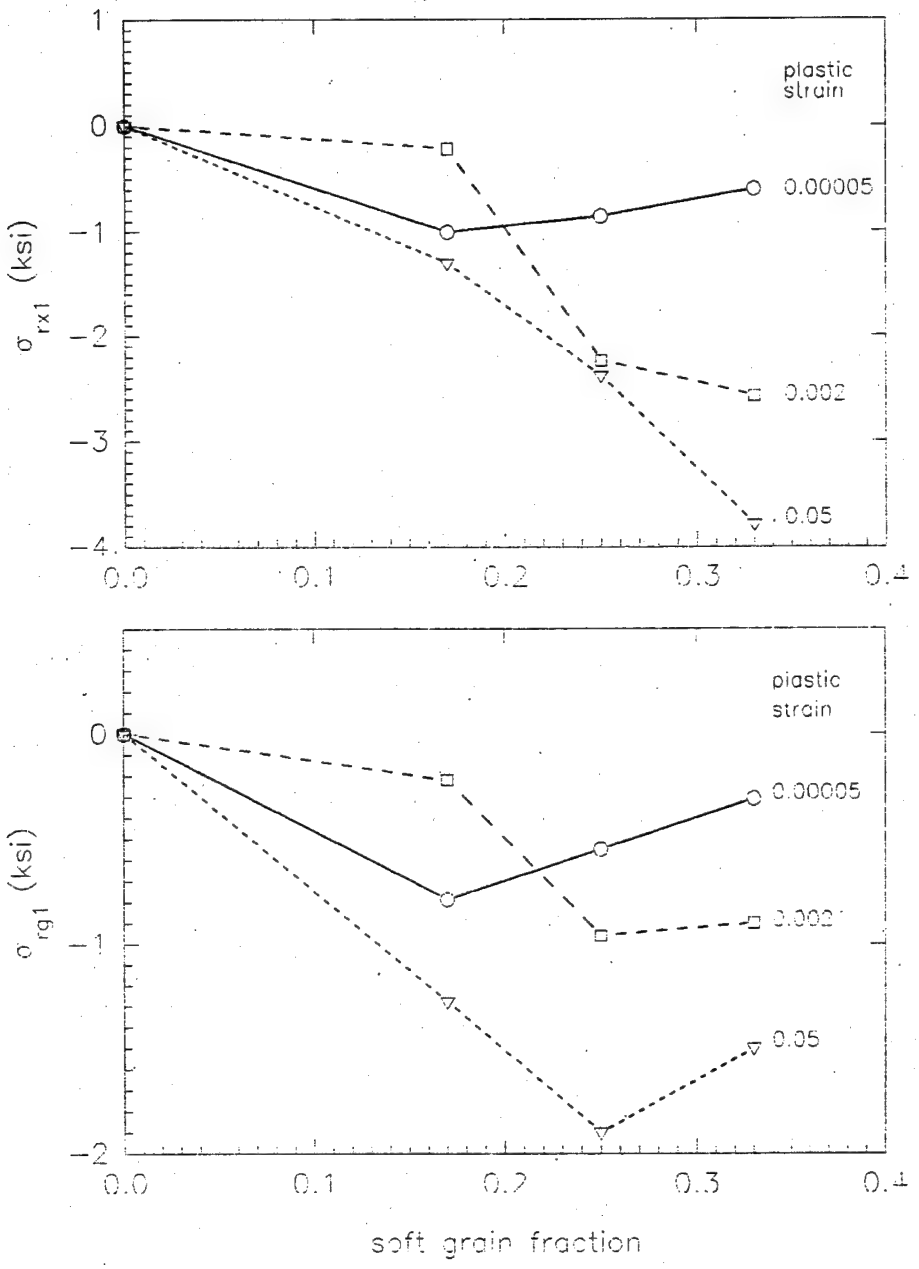

Figure 4.2.2.2-6. X-ray-averaged residual stress (σ_{rx1}) and surface-grain-averaged stress (σ_{rg1}) versus soft grain fraction. (E = 30,000 ksi, υ = 0.29, σ_{ys} = 15 ksi, σ_{yh} = 20 ksi, H_s = 0, H_h = 100 ksi.)

are shown in Figures 4.2.2.3-1, -2, and -3, respectively. The results for these models are summarized in Table 4.2.2.3-4, with the results for the ordered 25% and 33% models included for comparison. The x-ray stress versus applied stress curves for the disordered arrays exhibit the typical leveling of the x-ray stress above the proportional limit and a compressive x-ray residual stresses upon unloading. The curves are actually smoother than the corresponding curve for the 25%, ordered array, i.e., the sudden jump in the x-ray stress at the onset of the bulk yield ($\epsilon_p \approx 0.002$) is less prominent. The curve for the 29%, disordered array (Figure 4.2.2.3-3) is almost smooth in this region, emulating the 33%, ordered array (Figure 4.2.1-8). The compressive residual stresses in the 24% and 25% disordered arrays are comparable but not identical to those for the corresponding 25% ordered array. They are less for plastic strains below 0.5 to 1% and more for plastic strains above that in the disordered arrays (Figure 4.2.2.3-4). At 5% plastic strain, the x-ray compressive residual stress is 3.0 ksi for the 24% and 25% disordered arrays, whereas it is only 2.3 ksi for the 25% ordered array.

The plane-averaged longitudinal stress ($<\sigma_{yy}>_{pl}$) varies considerably more as a function of depth in the disordered arrays (Figures 4.2.2.3-5 (24%), -6 (25%), and -7 (29%)) than in the ordered arrays (Figures 4.2.2.2-4 (25%) and 4.2.1-8 (33%)). These large oscillations are induced by the nonuniform grain distribution and would presumably die out as the model size increased and approached a truly random array. As pointed out in Section 3.1, there is implicit averaging of grain distribution in the ordered arrays. The surface layer depth is about one grain for the 25% disordered array and two grains in the 24% and 29% disordered array. These values compare with the values of one and two grains for the ordered 25% and 33% soft arrays, respectively. However, because of the large stress oscillations, there is some probability that the surface layer depth and stress profile in the disordered arrays may be significantly different from the corresponding parent population averages. This is likely the cause of the unusually large value for the 24% disordered array. The otherwise good agreement between the 24% and 25% disordered arrays suggest the overall results are general. The plane-averaged stress in the three disordered arrays drops sharply near the free surface, as observed in the 25% and 33% ordered arrays and at a rate intermediate between the two.

In conclusion, the surface layer effect is comparable in the ordered and disordered arrays. It may be larger in the disordered arrays for plastic strains greater than 0.01.

Table 4.2.2.3-1. Loading history and x-ray-averaged stresses for the disordered array model shown in Figure 3.1-5, with a soft grain concentration of 24%. Surface nodal stresses not included. (E = 30,000 ksi , υ = 0.29, σ_{ys} = 15 ksi, σ_{yh} = 20 ksi, H_s = 0, H_h = 100 ksi.)

Step No.	Applied Stress (ksi)	Plastic Strain	X-Ray-Averaged Stress (ksi) Penetration Depth (grains) 0.500	1.000	2.000	5.000	10.500
1	15.000	0.0000E+00	15.00	15.00	15.00	15.00	15.00
2	16.735	0.6010E-04	15.65	15.66	15.77	16.06	16.32
3	0.000	0.6011E-04	-1.08	-1.07	-0.97	-0.67	-0.39
4	16.735	0.6015E-04	15.65	15.66	15.77	16.06	16.32
5	17.750	0.2479E-03	16.39	16.41	16.55	16.93	17.28
6	0.000	0.2479E-03	-1.35	-1.34	-1.20	-0.82	-0.47
7	17.750	0.2480E-03	16.40	16.41	16.55	16.93	17.28
8	17.904	0.4553E-03	16.73	16.77	16.90	17.21	17.50
9	0.000	0.4553E-03	-1.17	-1.14	-1.01	-0.69	-0.40
10	17.904	0.4554E-03	16.73	16.77	16.90	17.21	17.50
11	18.029	0.9640E-03	16.88	16.97	17.13	17.42	17.67
12	0.000	0.9639E-03	-1.15	-1.06	-0.90	-0.61	-0.36
13	18.029	0.9640E-03	16.88	16.97	17.13	17.42	17.67
14	18.163	0.2141E-02	17.05	17.17	17.33	17.59	17.82
15	0.000	0.2141E-02	-1.11	-0.99	-0.83	-0.57	-0.34
16	18.163	0.2141E-02	17.05	17.17	17.33	17.59	17.82
17	18.284	0.3708E-02	17.14	17.28	17.44	17.70	17.93
18	0.000	0.3708E-02	-1.15	-1.01	-0.84	-0.58	-0.36
19	18.284	0.3708E-02	17.14	17.28	17.44	17.70	17.93
20	18.400	0.5441E-02	17.15	17.31	17.49	17.78	18.02
21	0.000	0.5440E-02	-1.25	-1.09	-0.90	-0.62	-0.38
22	18.400	0.5441E-02	17.15	17.31	17.49	17.77	18.02
23	18.570	0.8211E-02	17.08	17.29	17.52	17.86	18.15
24	0.000	0.8210E-02	-1.49	-1.28	-1.05	-0.71	-0.42
25	18.570	0.8211E-02	17.08	17.29	17.52	17.86	18.15
26	18.854	0.1317E-01	16.99	17.28	17.58	18.01	18.35
27	0.000	0.1316E-01	-1.86	-1.57	-1.27	-0.85	-0.50
28	18.854	0.1317E-01	16.99	17.28	17.58	18.01	18.35
29	19.421	0.2372E-01	16.98	17.38	17.76	18.32	18.78
30	0.000	0.2372E-01	-2.43	-2.04	-1.65	-1.10	-0.64
31	19.421	0.2372E-01	16.99	17.38	17.77	18.32	18.78
32	20.271	0.4042E-01	17.14	17.60	18.06	18.78	19.41
33	0.000	0.4042E-01	-3.07	-2.63	-2.19	-1.48	-0.86
34	20.271	0.4042E-01	17.19	17.63	18.07	18.79	19.41
35	21.122	0.5860E-01	17.20	17.73	18.28	19.20	20.00
36	0.000	0.5860E-01	-3.77	-3.29	-2.79	-1.90	-1.11

Table 4.2.2.3-2. Loading history and x-ray-averaged stresses for the disordered array model shown in Figure 3.1-6, with a soft grain concentration of 25%. Surface nodal stresses not included. (E = 30,000 ksi, υ = 0.29, σ_{ys} = 15 ksi, σ_{yh} = 20 ksi, H_s = 0, H_h = 100 ksi.)

Step No.	Applied Stress (ksi)	Plastic Strain	X-Ray-Averaged Stress (ksi) Penetration Depth (grains) 0.500	1.000	2.000	5.000	10.500
1	15.000	0.0000E+00	15.00	15.00	15.00	15.00	15.00
2	16.443	0.6029E-04	15.71	15.70	15.81	16.12	16.31
3	0.000	0.6030E-04	-0.73	-0.74	-0.63	-0.33	-0.13
4	16.443	0.6034E-04	15.71	15.70	15.81	16.12	16.31
5	17.432	0.2700E-03	16.45	16.38	16.54	16.96	17.23
6	0.000	0.2701E-03	-0.98	-1.05	-0.89	-0.47	-0.20
7	17.432	0.2701E-03	16.45	16.39	16.54	16.96	17.23
8	17.614	0.5604E-03	16.60	16.57	16.76	17.18	17.43
9	0.000	0.5604E-03	-1.01	-1.04	-0.86	-0.43	-0.18
10	17.614	0.5604E-03	16.60	16.57	16.76	17.18	17.43
11	17.752	0.1306E-02	16.54	16.58	16.83	17.32	17.58
12	0.000	0.1306E-02	-1.21	-1.18	-0.92	-0.43	-0.17
13	17.752	0.1307E-02	16.54	16.58	16.83	17.32	17.58
14	17.897	0.2736E-02	16.35	16.49	16.85	17.42	17.71
15	0.000	0.2736E-02	-1.55	-1.41	-1.05	-0.48	-0.18
16	17.897	0.2736E-02	16.35	16.49	16.85	17.42	17.72
17	18.026	0.4469E-02	16.10	16.35	16.82	17.48	17.81
18	0.000	0.4471E-02	-1.93	-1.67	-1.21	-0.55	-0.21
19	18.026	0.4469E-02	16.10	16.35	16.82	17.48	17.81
20	18.151	0.6435E-02	15.89	16.26	16.82	17.54	17.91
21	0.000	0.6435E-02	-2.26	-1.89	-1.33	-0.61	-0.24
22	18.151	0.6435E-02	15.89	16.26	16.82	17.54	17.91
23	18.309	0.9155E-02	15.71	16.22	16.87	17.65	18.04
24	0.000	0.9155E-02	-2.60	-2.09	-1.44	-0.66	-0.26
25	18.309	0.9155E-02	15.71	16.22	16.87	17.65	18.04
26	18.571	0.1401E-01	15.59	16.26	17.00	17.85	18.28
27	0.000	0.1400E-01	-2.98	-2.32	-1.57	-0.72	-0.29
28	18.571	0.1401E-01	15.59	16.26	17.00	17.85	18.28
29	19.096	0.2461E-01	15.75	16.50	17.31	18.27	18.76
30	0.000	0.2461E-01	-3.22	-2.52	-1.74	-0.81	-0.33
31	19.096	0.2461E-01	15.86	16.56	17.34	18.28	18.76
32	19.884	0.4266E-01	15.99	16.79	17.69	18.85	19.46
33	0.000	0.4266E-01	-3.46	-2.82	-2.04	-0.98	-0.39
34	19.884	0.4266E-01	16.34	16.99	17.79	18.88	19.47
35	20.671	0.6741E-01	15.77	16.77	17.90	19.39	20.17
36	0.000	0.6740E-01	-3.94	-3.30	-2.43	-1.15	-0.44

Table 4.2.2.3-3. Loading history and x-ray-averaged stresses for the disordered array model shown in Figure 3.1-7, with a soft grain concentration of 29%. (E = 30,000 ksi, υ = 0.29, σ_{ys} = 15 ksi, σ_{yh} = 20 ksi, H_s = 0, H_h = 100 ksi.)

Step No.	Applied Stress (ksi)	Plastic Strain	σ_{rg1} (ksi)	X-Ray-Averaged Stress (ksi) Penetration Depth (grains) 0.500	1.000	2.000	5.000
1	15.000	0.0000E+00	15.00	15.00	15.00	15.00	15.00
2	16.087	0.4986E-04	15.51	15.44	15.42	15.48	15.69
3	0.000	0.4985E-04	-0.57	-0.65	-0.67	-0.61	-0.40
4	16.087	0.4986E-04	15.51	15.44	15.42	15.48	15.69
5	16.929	0.1174E-03	15.90	15.74	15.71	15.84	16.23
6	0.000	0.1174E-03	-1.03	-1.19	-1.22	-1.09	-0.70
7	16.929	0.1174E-03	15.90	15.74	15.71	15.84	16.23
8	17.130	0.1662E-03	16.02	15.81	15.78	15.94	16.39
9	0.000	0.1662E-03	-1.11	-1.32	-1.35	-1.19	-0.73
10	17.130	0.1662E-03	16.02	15.81	15.78	15.94	16.39
11	17.277	0.2447E-03	16.12	15.86	15.83	16.02	16.54
12	0.000	0.2447E-03	-1.16	-1.42	-1.44	-1.25	-0.74
13	17.277	0.2447E-03	16.12	15.86	15.83	16.02	16.54
14	17.428	0.4743E-03	16.27	15.85	15.87	16.12	16.70
15	0.000	0.4743E-03	-1.16	-1.57	-1.56	-1.31	-0.73
16	17.428	0.4743E-03	16.27	15.85	15.87	16.12	16.70
17	17.560	0.1020E-02	16.44	15.77	15.89	16.22	16.84
18	0.000	0.1020E-02	-1.12	-1.78	-1.66	-1.33	-0.72
19	17.560	0.1020E-02	16.44	15.78	15.89	16.22	16.84
20	17.689	0.1947E-02	16.58	15.62	15.88	16.30	16.95
21	0.000	0.1947E-02	-1.10	-1.95	-1.74	-1.35	-0.72
22	17.689	0.1953E-02	16.58	15.71	15.93	16.32	16.96
23	17.833	0.3466E-02	16.70	15.51	15.90	16.39	17.06
24	0.000	0.3466E-02	-1.11	-2.16	-1.83	-1.39	-0.75
25	17.833	0.3467E-02	16.71	15.64	15.97	16.42	17.07
26	18.072	0.7257E-02	16.89	15.46	16.01	16.56	17.26
27	0.000	0.7255E-02	-1.13	-2.20	-1.82	-1.38	-0.76
28	18.072	0.7262E-02	16.90	15.78	16.17	16.63	17.28
29	18.551	0.1697E-01	17.16	15.50	16.16	16.79	17.58
30	0.000	0.1696E-01	-1.31	-2.44	-2.02	-1.56	-0.89
31	18.551	0.1700E-01	17.18	15.94	16.38	16.89	17.61
32	19.270	0.3330E-01	17.46	15.40	16.22	17.00	17.99
33	0.000	0.3330E-01	-1.72	-3.17	-2.63	-2.05	-1.19
34	19.270	0.3331E-01	17.47	15.91	16.49	17.12	18.02
35	20.036	0.5168E-01	17.70	15.23	16.21	17.14	18.37
36	0.000	0.5170E-01	-2.24	-4.00	-3.35	-2.64	-1.57

Table 4.2.2.3-4. Comparison of disordered array specimens with ordered array specimens. In all cases E = 30,000 ksi , υ = 0.29, σ_{ys} = 15 ksi, σ_{yh} = 20 ksi, H_s = 0, H_h = 100 ksi

	DISORDERED			ORDERED	
Soft grain concentration (%)	24	25	29	25	33
σ_{ymix}	18.76	18.76	18.53	18.75	18.33
σ_{yB}	18.15	17.83	17.68	18.53	17.98
σ_{ys}/σ_{yB}	0.83	0.84	0.85	0.81	0.83
Ω	0.38	0.49	0.36	0.43	0.28
τ	2	1	2	1	2
σ_{rx1}, ϵ_p: 0.00005	-1.00	-0.69	-0.68	-0.89	-0.65
0.002	-1.00	-1.29	-1.75	-1.86	-2.50
0.01	-1.4	-2.1	-1.8	-1.4	-2.6
0.05	-3.0	-3.0	-3.1	-2.4	-3.4

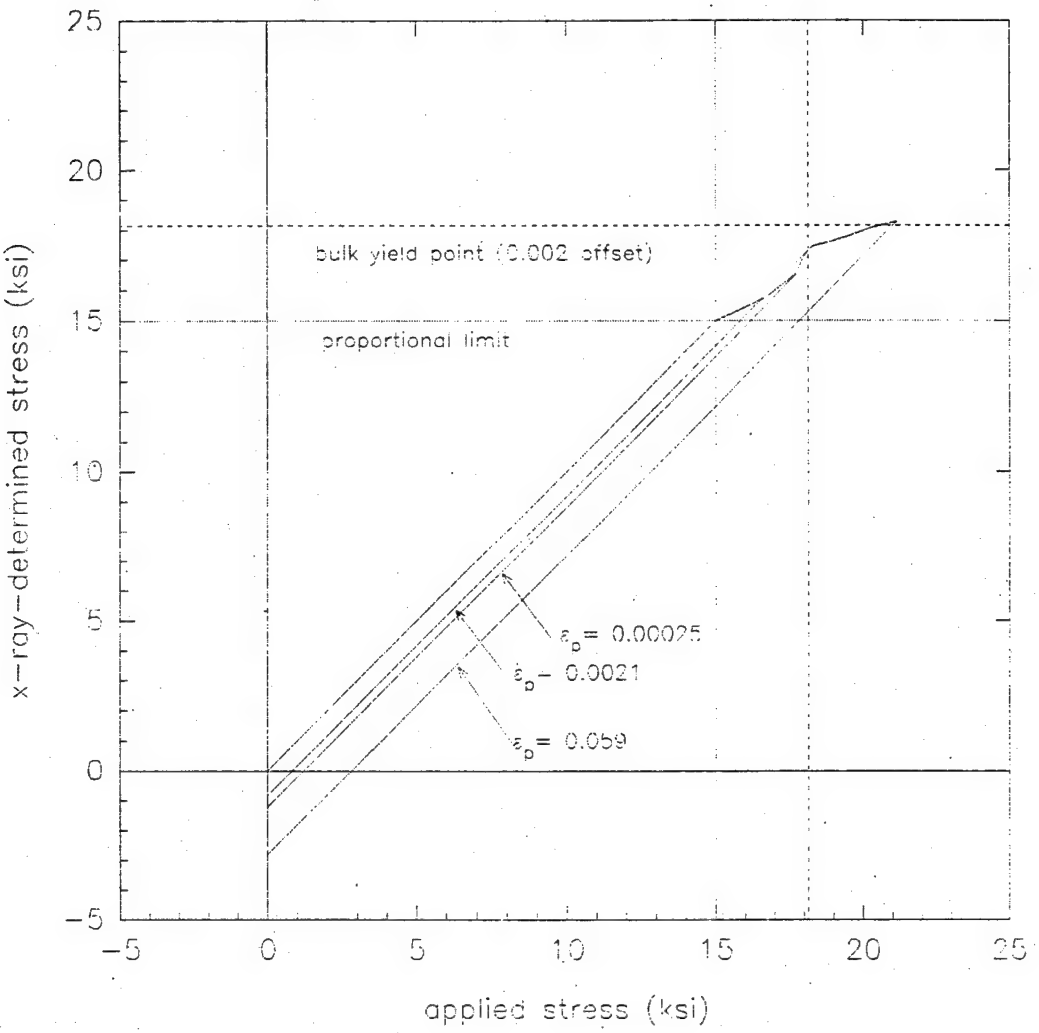

Figure 4.2.2.3-1. X-ray-determined stress versus the nominal applied stress for a disordered array model with 24% soft grain concentration. The array is shown in Figure 3.1-5. The x-ray effective penetration depth is one grain. (E = 30,000 ksi, υ = 0.29, σ_{ys} = 15 ksi, σ_{yh} = 20 ksi, H_s = 0, H_h = 100 ksi.)

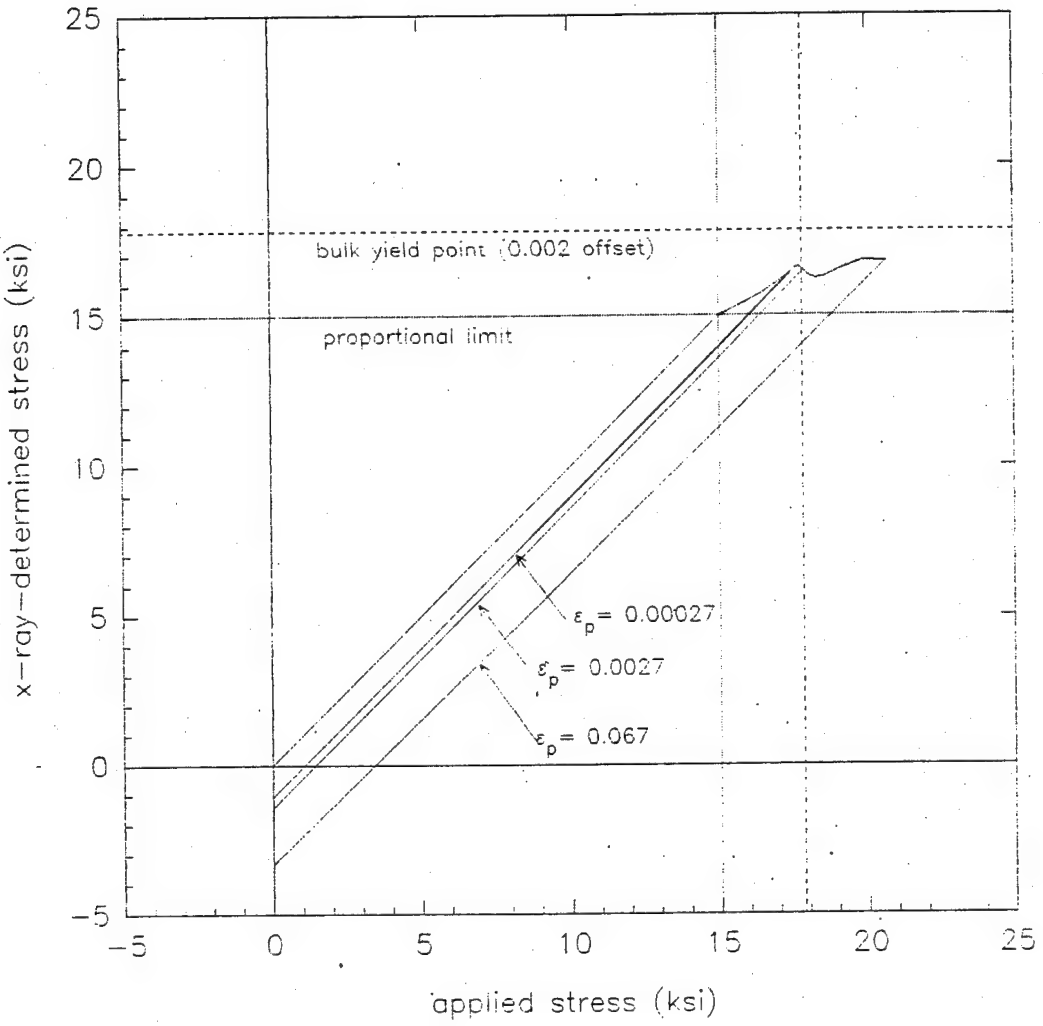

Figure 4.2.2.3-2. X-ray-determined stress versus the nominal applied stress for a disordered array model with 25% soft grain concentration. The array is shown in Figure 3.1-6. The x-ray effective penetration depth is one grain. (E = 30,000 ksi, υ = 0.29, σ_{ys} = 15 ksi, σ_{yh} = 20 ksi, H_s = 0, H_h = 100 ksi.)

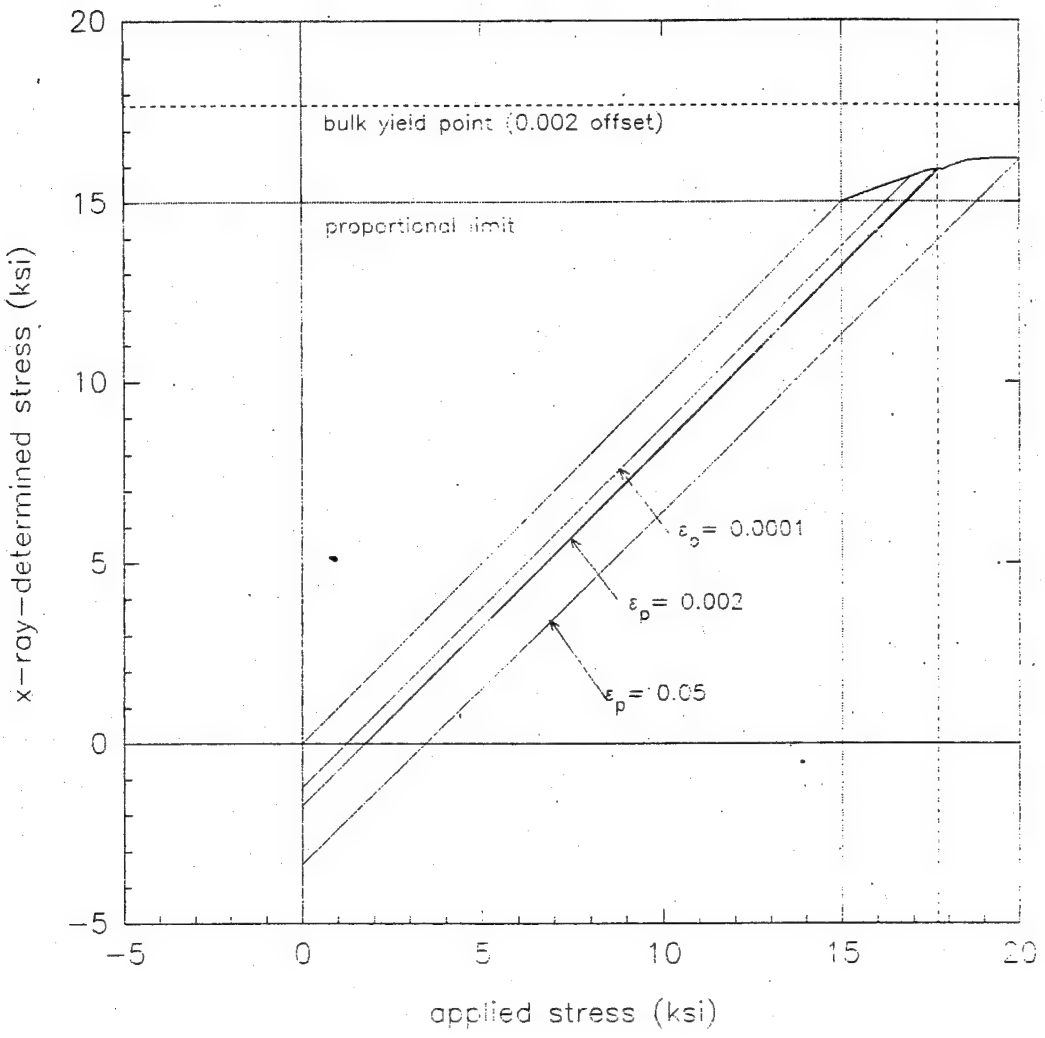

Figure 4.2.2.3-3. X-ray-determined stress versus the nominal applied stress for a disordered array model with 29% soft grain concentration. The array is shown in Figure 3.1-7. The x-ray effective penetration depth is one grain. (E = 30,000 ksi, υ = 0.29, σ_{ys} = 15 ksi, σ_{yh} = 20 ksi, H_s = 0, H_h = 100 ksi.)

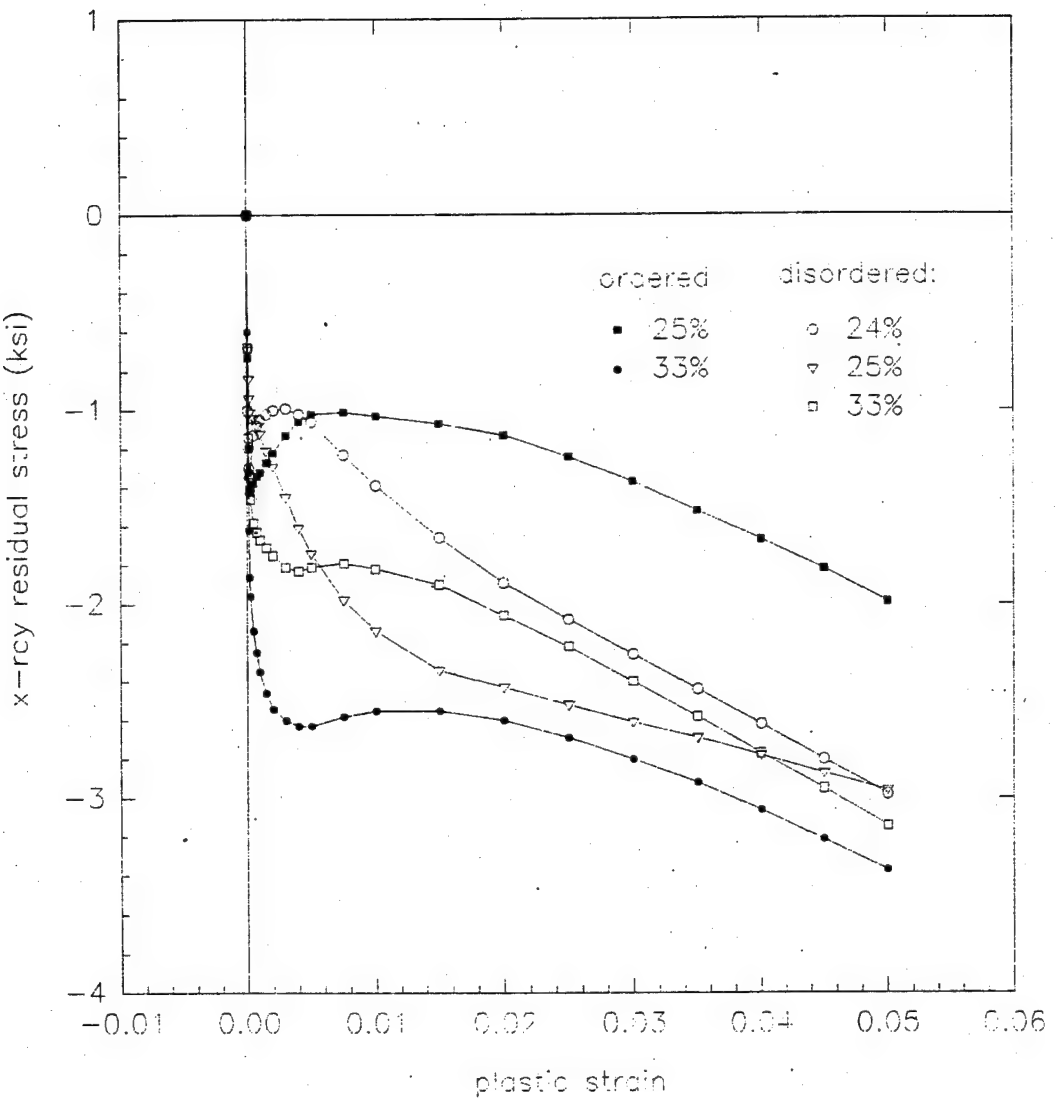

Figure 4.2.2.3-4. The x-ray-averaged residual stress (σ_{rxl}) versus plastic strain for the disordered arrays with 24%, 25%, and 29% soft grain concentration and the ordered arrays with 25% and 33% soft grain concentration. (E = 30,000 ksi, υ = 0.29, σ_{ys} = 15 ksi, σ_{yh} = 20 ksi, H_s = 0, H_h = 100 ksi.)

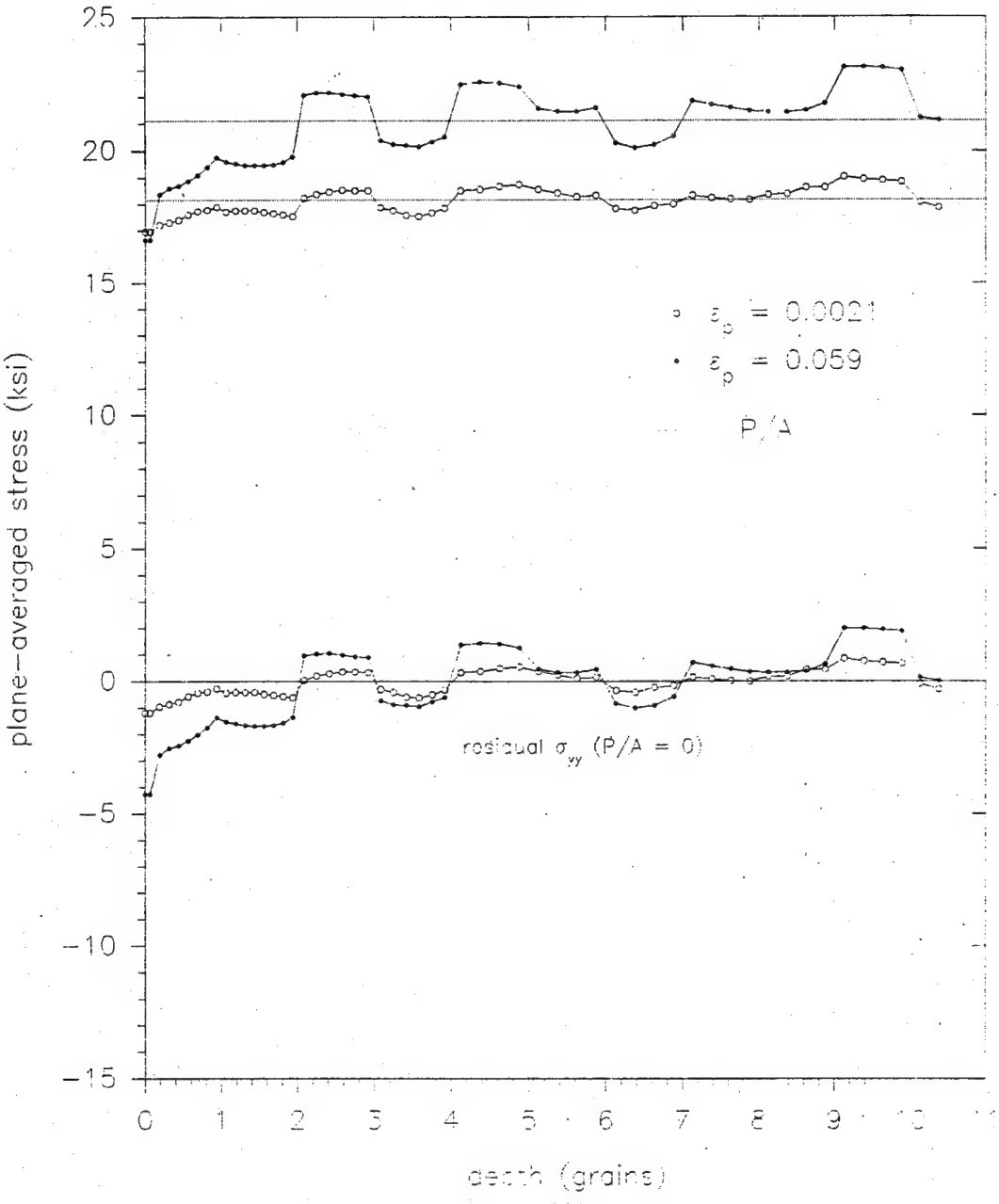

Figure 4.2.2.3-5. Plane-averaged longitudinal stress versus depth in a disordered array with 24% soft grain concentration for plastic strains of 0.0021 and 0.059, before and after removal of the load. The array is shown in Figure 3.1-5. (E = 30,000 ksi, υ = 0.29, σ_{ys} = 15 ksi, σ_{yh} = 20 ksi, H_s = 0, H_h = 100 ksi.)

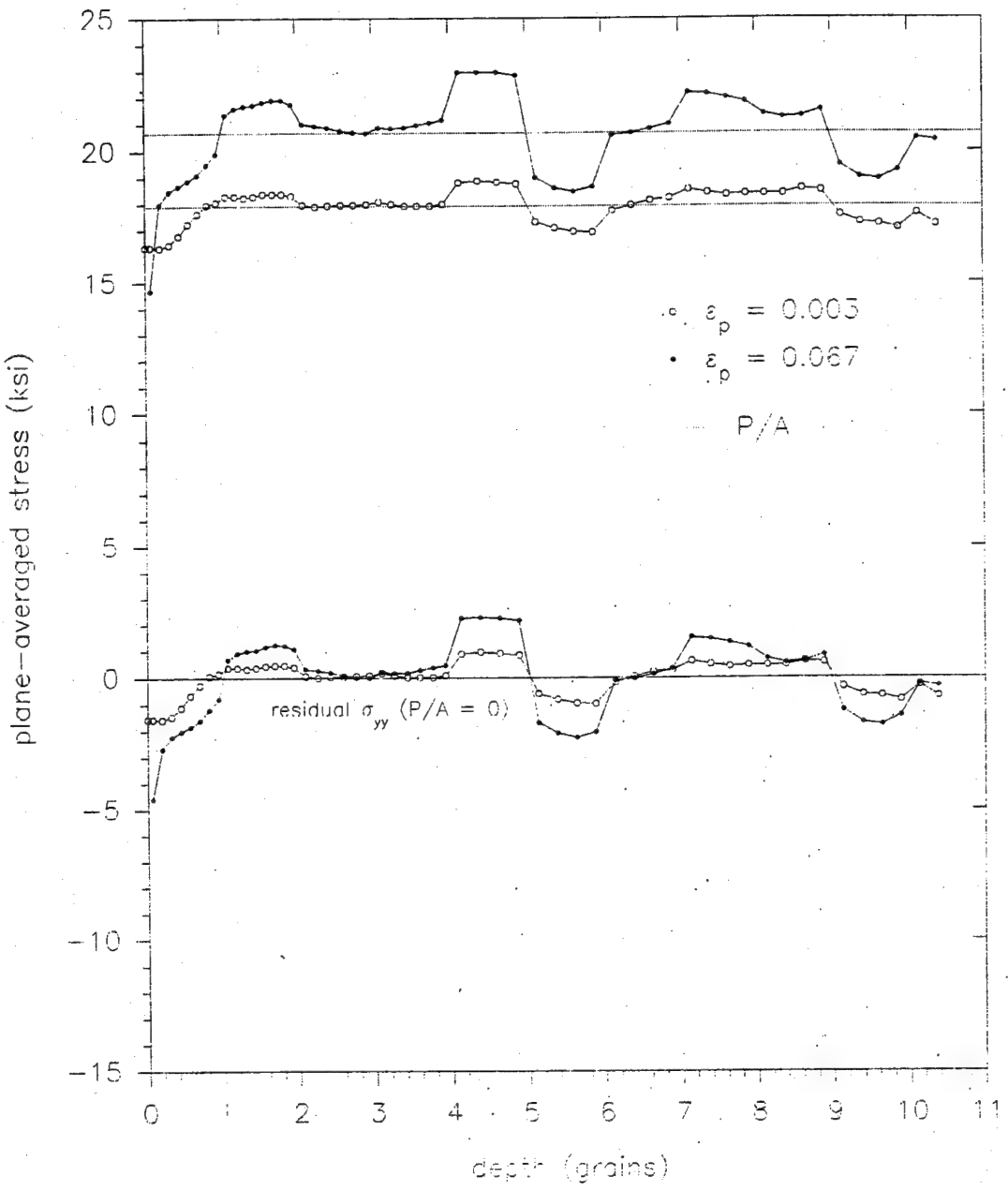

Figure 4.2.2.3-6. Plane-averaged longitudinal stress versus depth in a disordered array with 25% soft grain concentration for plastic strains of 0.0027 and 0.067, before and after removal of the load. The array is shown in Figure 3.1-6. (E = 30,000 ksi, υ = 0.29, σ_{ys} = 15 ksi, σ_{yh} = 20 ksi, H_s = 0, H_h = 100 ksi.)

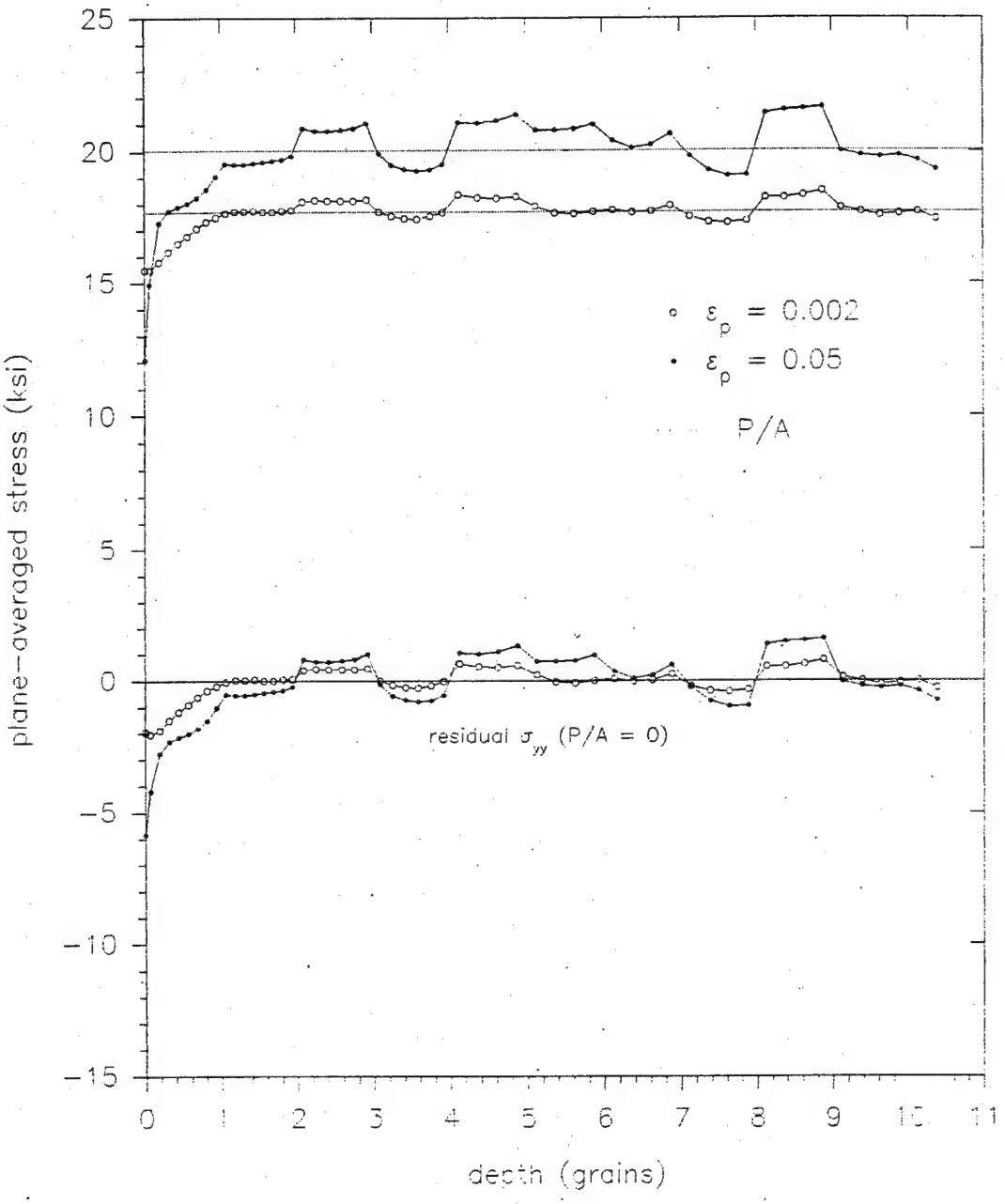

Figure 4.2.2.3-7. Plane-averaged longitudinal stress versus depth in a disordered array with 29% soft grain concentration for plastic strains of 0.002 and 0.052, before and after removal of the load. The array is shown in Figure 3.1-7. (E = 30,000 ksi, υ = 0.29, σ_{ys} = 15 ksi, σ_{yh} = 20 ksi, H_s = 0, H_h = 100 ksi.)

4.2.2.4 Effect of Yield Point Spread. The yield point spread (YPS) between the soft and hard grains is clearly an important factor in determining the magnitude of the surface layer effect. In the limit of no difference in the yield points of the soft and hard grains, the solid becomes homogeneous and there is no surface layer effect. In effect, the yield point spread models the grain yield point distribution in the polycrystalline aggregate arising from the plastic anisotropy of the crystals and their orientation with respect to the applied stress. As such, the yield point spread is one of the key parameters for modeling the aggregate.

Calculations were performed for specimens with yield point spreads of 7.5 and 15 ksi, but otherwise constructed the same as the basic model, which has a yield point spread of 5 ksi. The stress-strain curves for the three models are similar, except, of course, that the yield point increases with YPS (Figure 4.2.2.4-1). In particular, the models have nearly equal bulk tangent hardening rates, H_B, in the range of 37 to 39 ksi. These results, as well as the values of Ω, τ, and the residual stresses are summarized in Table 4.2.2.4.1.

At very low plastic strains, ≤ 0.00015, the residual stresses are comparable in the three specimens, as is expected because there is little hard grain plasticity. Consistent with this, the stress deviation ratio is independent of the yield spread. At higher plastic strains, however, the residual stresses increase with yield point spread, becoming roughly proportional to yield spread for a plastic elongation of 5% (Figure 4.2.2.4-2). The greater the yield point of the hard grains, the greater the elastic extension of these grains and the compressive forces they exert on the soft grains upon unloading. The surface layer thickness is unaffected by the yield point spread, being approximately two grains at ϵ_p = 5 - 6% for the three models (Figure 4.2.2.4-3). The levelling- off of the x-ray stress becomes more pronounced as the yield point spread increases, the x-ray stress σ_{xl} actually dropping 6 ksi below the proportional limit for YPS = 15 ksi at $\epsilon_p = 0.062$. Plots of σ_{xl} versus the applies stress are shown in Figure 4.2.1-8(a) for YPS = 5 ksi, Figure 4.2.2.4-4 for YPS = 7.5 ksi, and Figure 4.2.2.4-5 for YPS = 15 ksi.

In relation to the polycrystalline aggregate it is sought to model, these results suggest that (1) the surface layer effect at the onset of plastic deformation and (2) the depth and stress profile-form of the surface

layer at high plastic strains ($\epsilon_p \approx 0.05$) are insensitive to the grain yield point distribution within rather wide limits. They also suggest that soon after the onset of plasticity ($\epsilon_p \geq 0.0005$) the residual stresses increase roughly proportionally to the yield point difference between the soft and hard grain groups in the aggregate.

4.2.2.5 Effect of Hard Grain Hardening Rate. The hardening rate of the hard grains (H_h) in the basic model is 100 ksi per unit strain, leading to a specimen secant hardening rate of 39 ksi per unit strain for ϵ_p = 0.005 to 0.05. In order to determine the sensitivity of the results to the value of the hard grain hardening rate, models with H_h equal to 0, 50, 100, and 200 ksi were compared. The results for these models are summarized in Table 4.2.2.5-1. It is found that the hardening rate has little effect on the value of the residual stresses for plastic strains below 0.005; above this strain, the greater the hardening rate the greater the residual stresses (Figure 4.2.2.5-1).

In the absence of grain hardening, the residual stresses effectively stop increasing for plastic elongations greater than 0.005, stabilizing at σ_{xl} = -3.0 ksi and σ_{zl} = -0.8 ksi (Figure 4.2.2.5-1). At ϵp = 5%, the added residual stress observed with hard grain hardening is roughly proportional to H_h (Figure 4.2.2.5-2). For σ_{xl}, this linear relationship starts at H_h = 50 ksi rather than at 0 because the x-ray stress is sensitive to the stress profile near the surface. For sufficiently low plastic strains, hard grain plastic deformation is small and hardening is not important, thereby explaining the observed behavior. At high bulk plastic strains the hard grains can undergo significant hardening. The greater H_h the greater resulting increase in the magnitude of the tensile stresses in the hard matrix, which upon unloading leads to a correspondingly greater compression of the plastically extended soft grains. The effect is similar to that of increasing the yield point spread between the hard and soft grains.

The surface layer depth is ≈ 2 grains and the stress drops sharply near the surface (< 0.1 gr) for all the models, but away from the surface the stress profile changes from flat to triangular as H_h is increased (Figure 4.2.2.5-3).

Table 4.2.2.4-1. Comparison of specimens with yield point spreads between hard and soft grains of 5, 7.5, and 15 ksi. (f_s = 0.33, E = 30,000 ksi, υ = 0.29, σ_{ys} = 15 ksi, H_s = 0, H_h = 100 ksi.)

Model		SAS01GE	SAS03GL	SAS02GL
Yield point spread (ksi)		5.00	7.50	15.00
σ_{ymix} (ksi)		18.35	20.02	25.05
σ_{yB} (ksi)		17.90	19.08	21.83
H_B (ksi)		39	37	37
σ_{ys}/σ_{yB}		0.84	0.79	0.69
Ω		0.27	0.27	0.27
τ (grain)		2	2	2
Surface-grain-averaged stress, σ_{rg1} (ksi)				
ϵ_p:	0.00005	-0.31	-0.31	-0.31
	0.0001	-0.62	-0.63	-0.63
	0.002	-0.90	-1.43	-2.78
	0.01	-0.90	-1.4	-2.8
	0.05	-1.5	-1.9	-2.9
X-ray-averaged stress, σ_{rx1} (ksi)				
ϵ_p:	0.00005	-0.60	-0.60	-0.60
	0.0001	-1.19	-1.20	-1.20
	0.002	-2.58	-4.0	-6.7
	0.01	-2.7	-4.3	-8.7
	0.05	-3.8	-5.2	-8.8

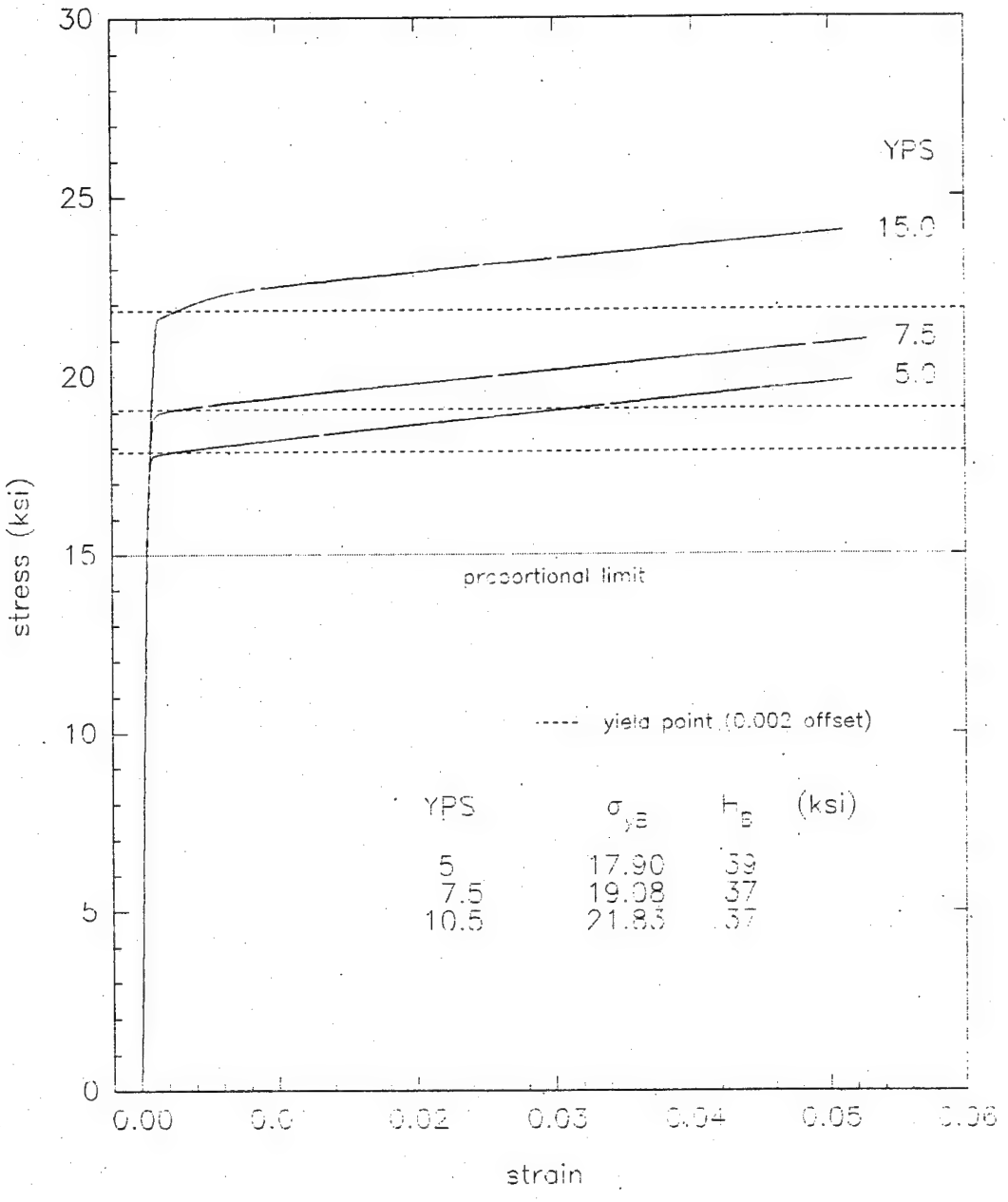

Figure 4.2.2.4-1. The stress-strain curves for models with yield point spreads of 5, 7.5, and 15 ksi. σ_{yB} is the yield point at 0.002 strain offset, and H_B is the tangent hardening rate from 0.01 to 0.045 plastic strain. (f_s = 0.33, E = 30,000 ksi, υ = 0.29, σ_{ys} = 15 ksi, H_s = 0, H_h = 100 ksi.)

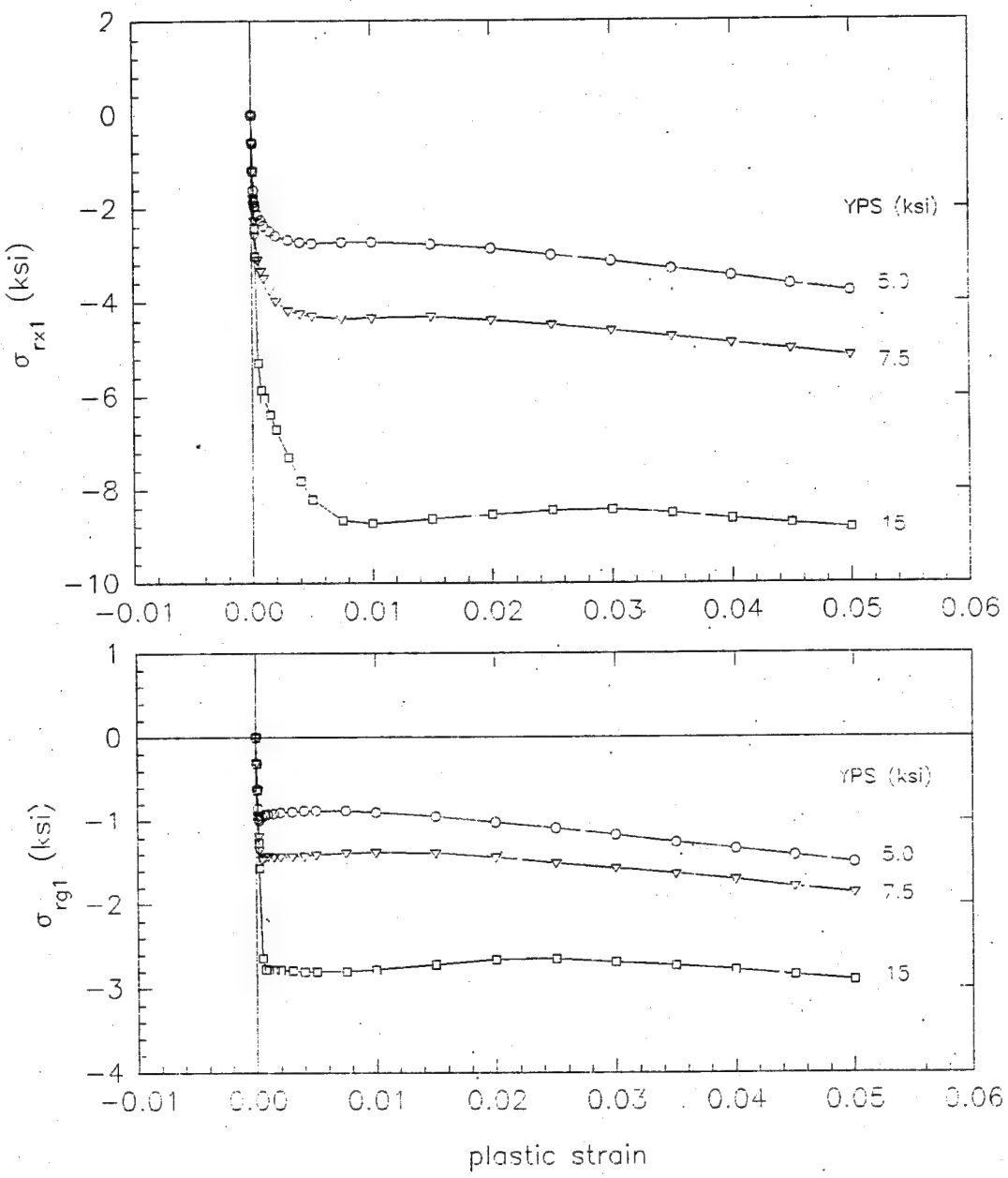

Figure 4.2.2.4-2. The x-ray-averaged residual stress (σ_{rx1}) and the surface-grain-averaged residual stress (σ_{rg1}) versus plastic strain for models with yield point spreads of 5, 7.5, and 15 ksi. (f_s = 0.33, E = 30,000 ksi, υ = 0.29, σ_{ys} = 15 ksi, H_s = 0, H_h = 100 ksi.)

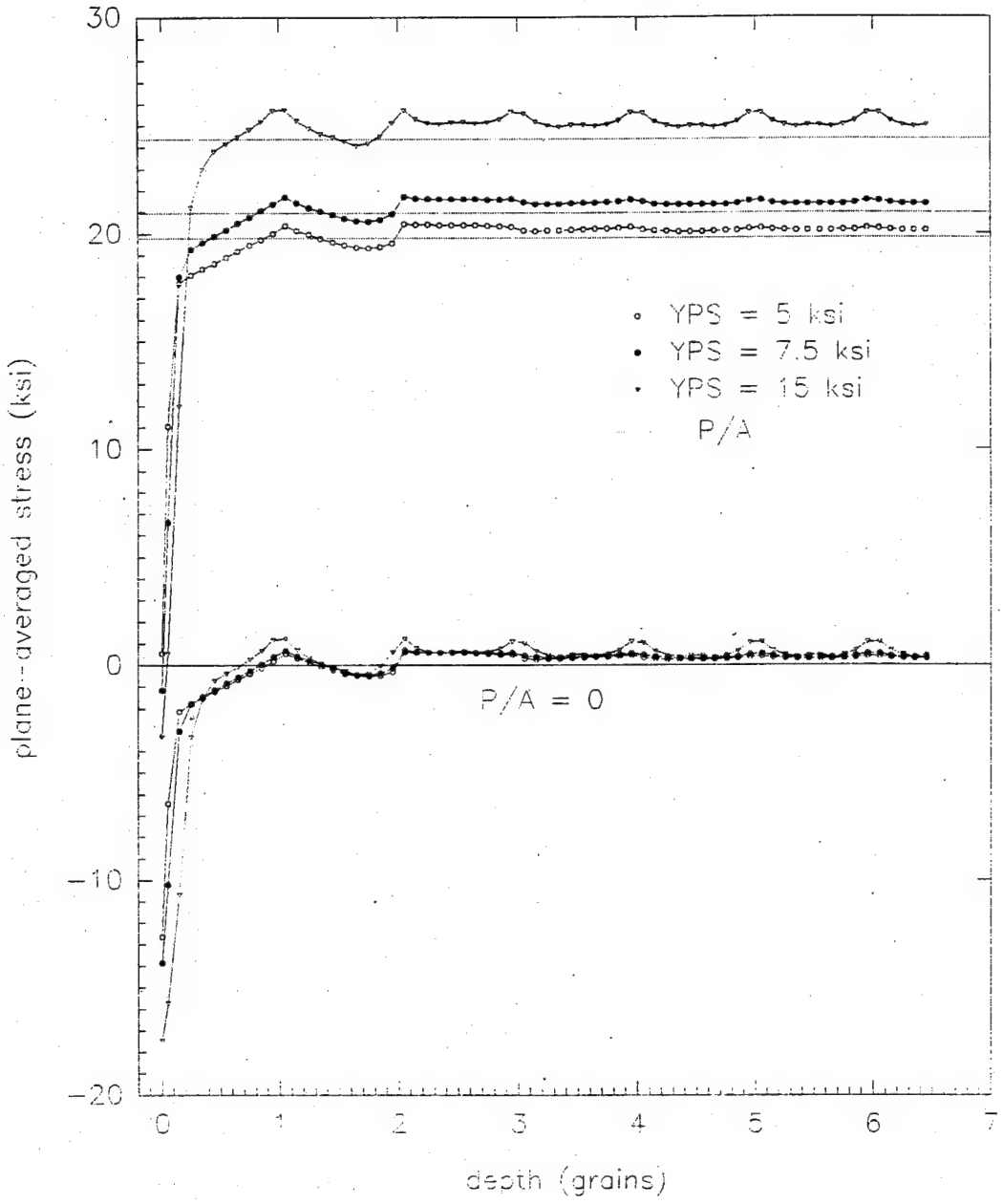

Figure 4.2.2.4-3. Plane-averaged longitudinal stress versus depth in specimens with yield point spreads of 5, 7.5, and 15 ksi for a plastic strain in the vicinity of 5% (5.0%, 5.2%, and 6.2%, respectively), before and after removal of the load. (f_s = 0.33, E = 30,000 ksi, υ = 0.29, σ_{ys} = 15 ksi, H_s = 0, H_h = 100 ksi.)

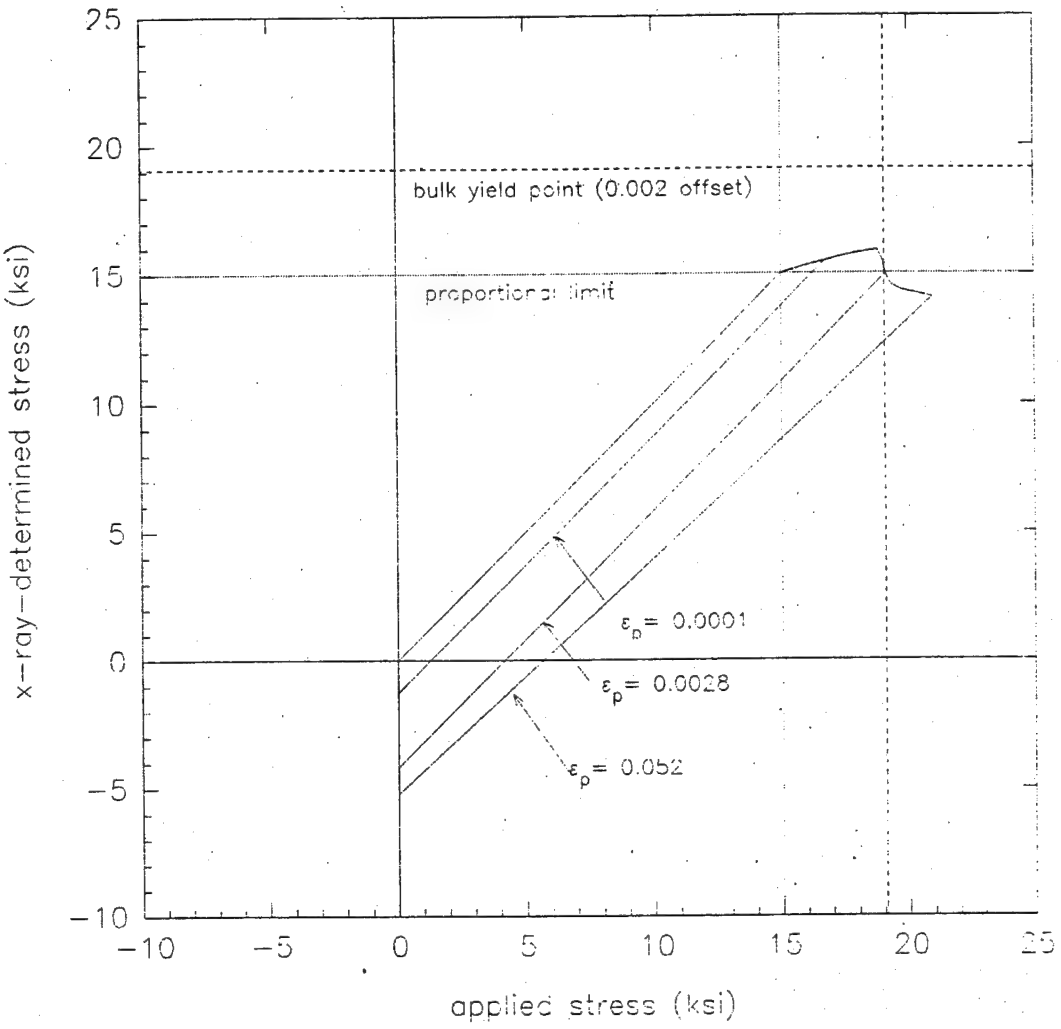

Figure 4.2.2.4-4. X-ray-determined stress versus the nominal applied stress for a model with a yield point spread of 7.5 ksi. The x-ray effective penetration depth is one grain. (f_s = 0.33, E = 30,000 ksi, υ = 0.29, σ_{ys} = 15 ksi, σ_{yh} = 22.5 ksi, H_s = 0, H_h = 100 ksi.)

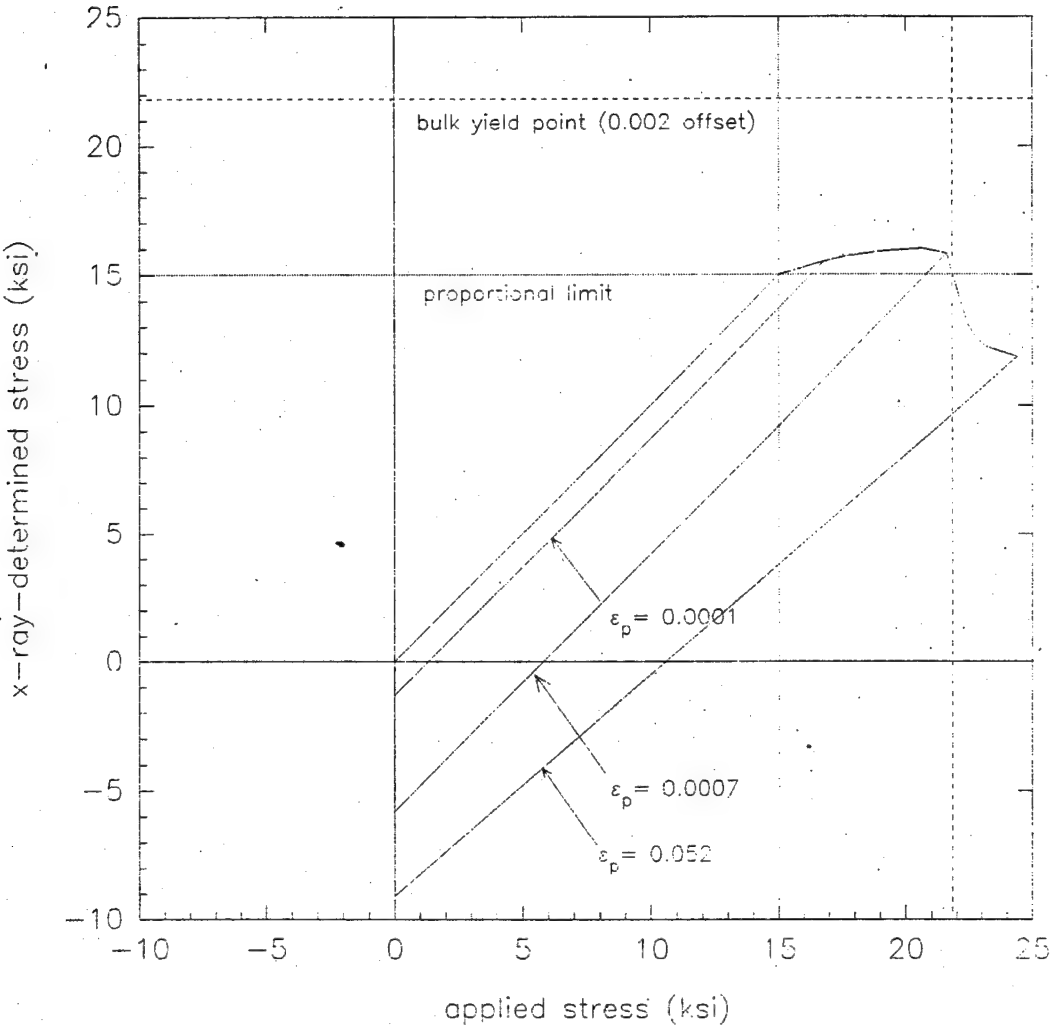

Figure 4.2.2.4-5. X-ray-determined stress versus the nominal applied stress for a model with a yield point spread of 15 ksi. The x-ray effective penetration depth is one grain. (f_s = 0.33, E = 30,000 ksi, υ = 0.29, σ_{ys} = 15 ksi, σ_{yh} = 30 ksi, H_s = 0, H_h = 100 ksi.)

It is concluded that hard grain hardening in the range of 0 - 200 ksi has little effect below 0.005 plastic strain. This limit may decrease for larger H_h. Above this strain, the residual stresses increase with H_h, remaining essentially constant if $H_h = 0$, and increasing approximately linearly with H_h at 0.05 plastic strain. The surface layer depth remains about the same (≈ 2 grains), but the stress profile flattens as H_h is decreased.

4.2.2.6 Effect of Soft Grain Hardening Rate. Because the surface layer effect depends in part on the differential elastic extension between hard and soft grains, soft grain hardening must have a significant effect. Calculations were performed for the basic model using soft grain hardening rates of 0, 10, 20, 40, and 100 ksi for YPS = 5 ksi, and 0, 10 ksi for YPS = 15 ksi. The results are summarized in Table 4.2.2.6-1.

Referring to the results for YPS = 5 ksi, it is found that the effect of soft grain hardening is small up to the yield point, $\epsilon p = 0.002$, but that even a modest hardening rate has a marked effect at greater plastic strains. Thus, even at the lowest hardening rate investigated, 10 ksi, the residual stress stops increasing significantly above the yield point. As the soft grain hardening rate is increased, the residual stress above the yield point is increasingly inhibited, becoming essentially zero at 100 ksi hardening rate (Figure 4.2.2.6-1). The effect of H_s on the residual compressive stresses is shown in Figure 4.2.2.6-2 in plots of σ_{x1} and σ_{z1} for $\epsilon_p = 0.00005$ (no effect), $\epsilon_p = 0.002$ (minor inhibition), and $\epsilon_p = 0.05$ (major inhibition). The surface layer stress profile flattens as H_s increases, becoming completely flat (i.e., no surface layer effect) for $H_s = 100$ ksi. The surface layer thickness remains ≈ 2 grains up to $H_s = 40$ ksi (Figure 4.2.2.6-3). As expected, the effect of soft grain hardening is much less pronounced for a large yield spread. It is almost negligible for yield spread of 15 ksi and soft and hard grain hardening rates of 10 ksi and 100 ksi, respectively (Table 4.2.2.6-1).

In conclusion, soft grain hardening has a negligible to small effect on the surface layer effect below the yield point, but considerably decreases the effect at high plastic strains, the decrease being greater as the yield point spread is smaller. Because the hardening rate of the soft and hard grains is not common knowledge for most metals, this is an uncertainty in applying this

Table 4.2.2.5-1. Comparison of the surface layer effect in specimens with hard grain hardening rates of 0, 50, 100, and 200 ksi. (f_s = 0.33, E = 30,000 ksi , υ = 0.29, σ_{ys} = 15 ksi, σ_{yh} = 20 ksi, H_s = 0 ksi.)

Model		SASZAHG	SAS05HL	SDE01HK	SAS07HL
Hard grain hardening rate (ksi)		0	50	100	200
Ω		0.28	0.27	0.27	0.27
τ (gr)		2	2	2	2
Average residual stress in surface grain layer, σ_{rg1}					
ϵ_p	0.00005	-0.31	-0.31	-0.31	-0.31
	0.0005	-0.94	-0.95	-0.95	-0.95
	0.002	-0.91	-0.91	-0.90	-0.90
	0.01	-0.88	-0.84	-0.90	-1.08
	0.05	-0.81	-1.07	-1.50	-2.18
X-ray-averaged residual stress, σ_{rx1}					
ϵ_p	0.00005	-0.60	-0.61	-0.60	-0.61
	0.0005	-2.15	-2.18	-2.14	-2.17
	0.002	-2.66	-2.65	-2.58	-2.55
	0.01	-3.1	-2.76	-2.72	-3.0
	0.05	-3.0	-3.0	-3.63	-5.3

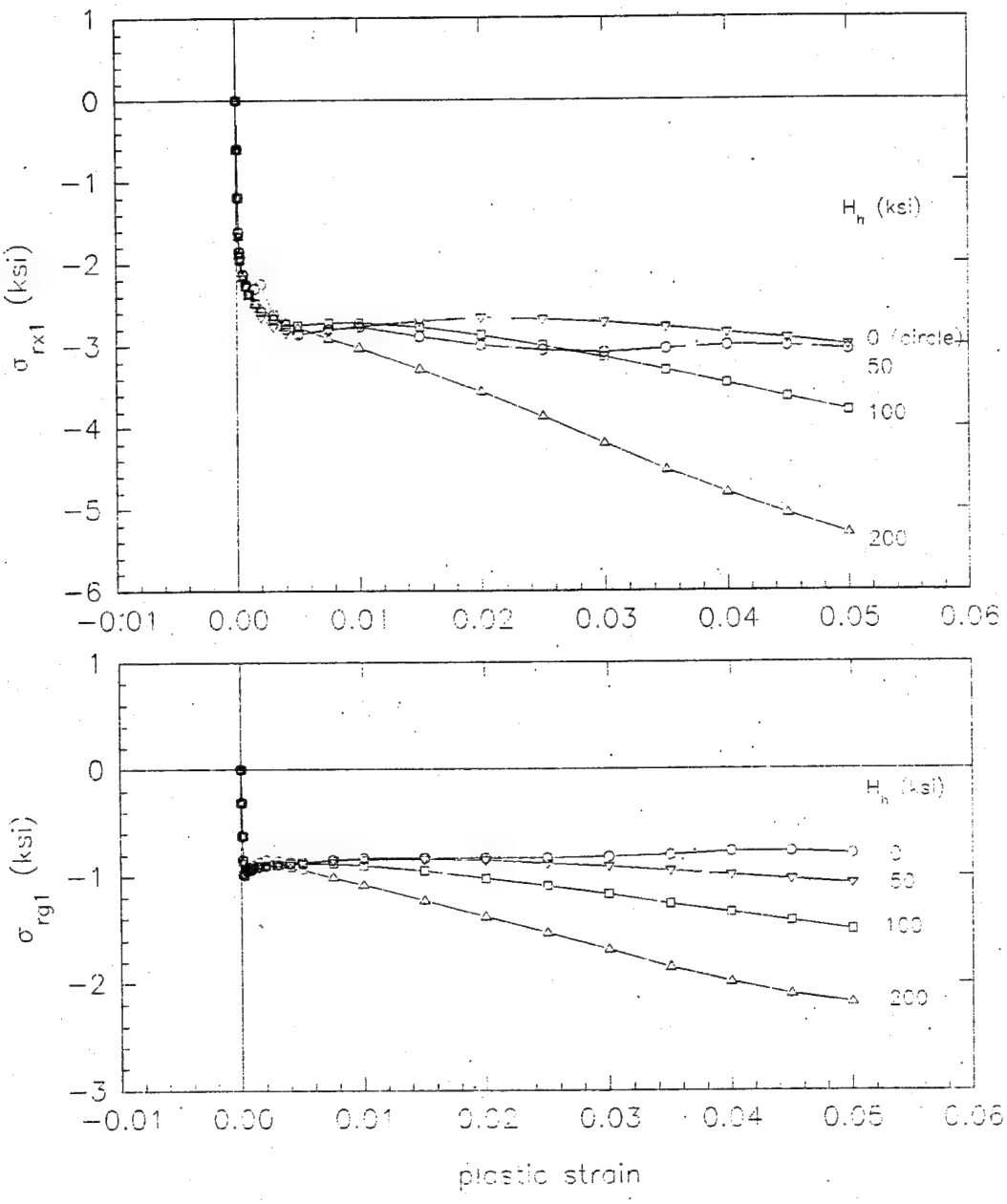

Figure 4.2.2.5-1. The x-ray-averaged residual stress (σ_{rx1}) and the surface-grain-averaged residual stress (σ_{rg1}) versus plastic strain for models with hard grain hardening rates of 0, 50, 100, and 200 ksi. (f_s = 0.33, E = 30,000 ksi, υ = 0.29, σ_{ys} = 15 ksi, H_s = 0 ksi.)

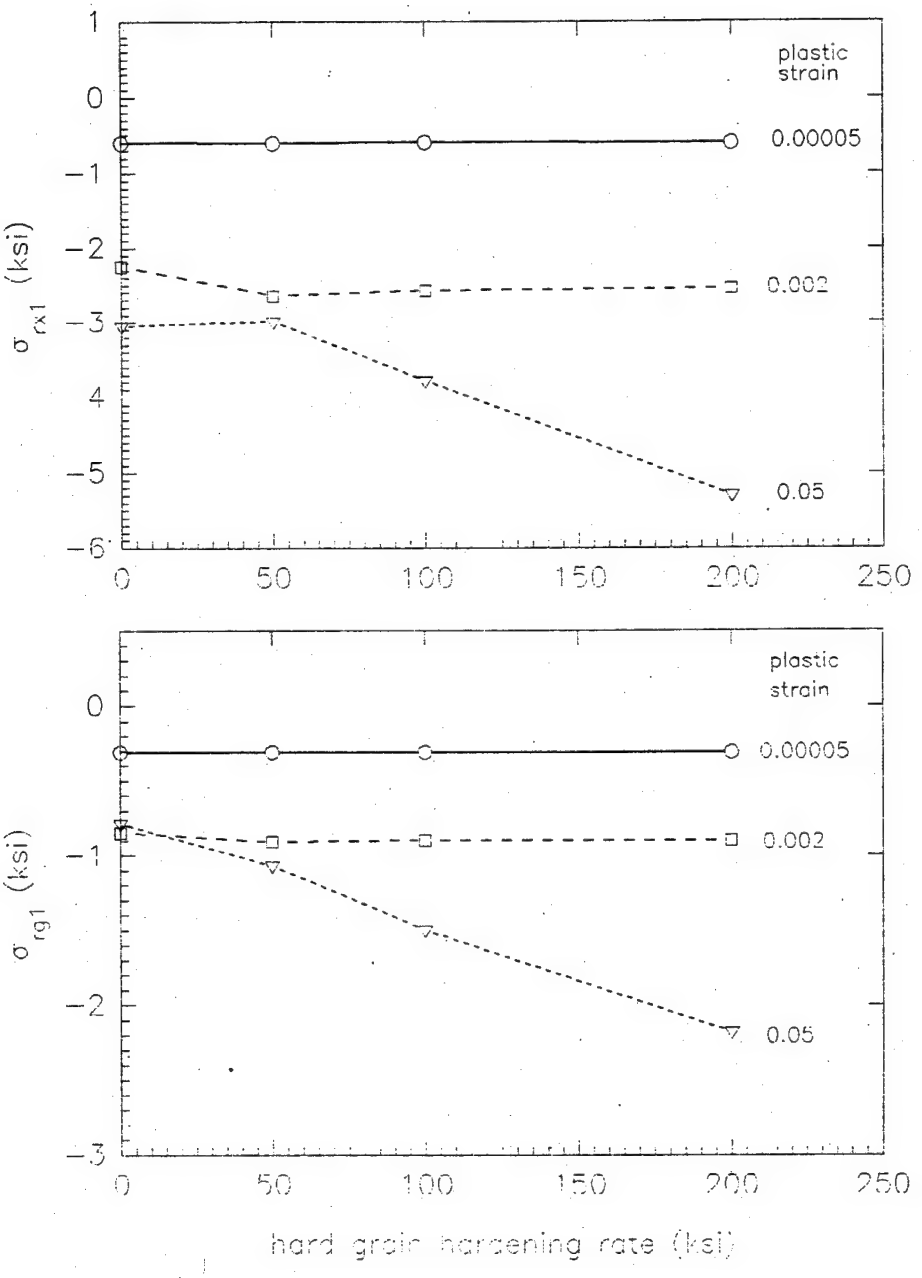

Figure 4.2.2.5-2. The x-ray-averaged residual stress (σ_{rx1}) and the surface-grain-averaged residual stress (σ_{rg1}) versus hard grain hardening rate for plastic strains of 0.00005, 0.002, and 0.05. (f_s = 0.33, E = 30,000 ksi, υ = 0.29, σ_{ys} = 15 ksi, H_s = 0 ksi.)

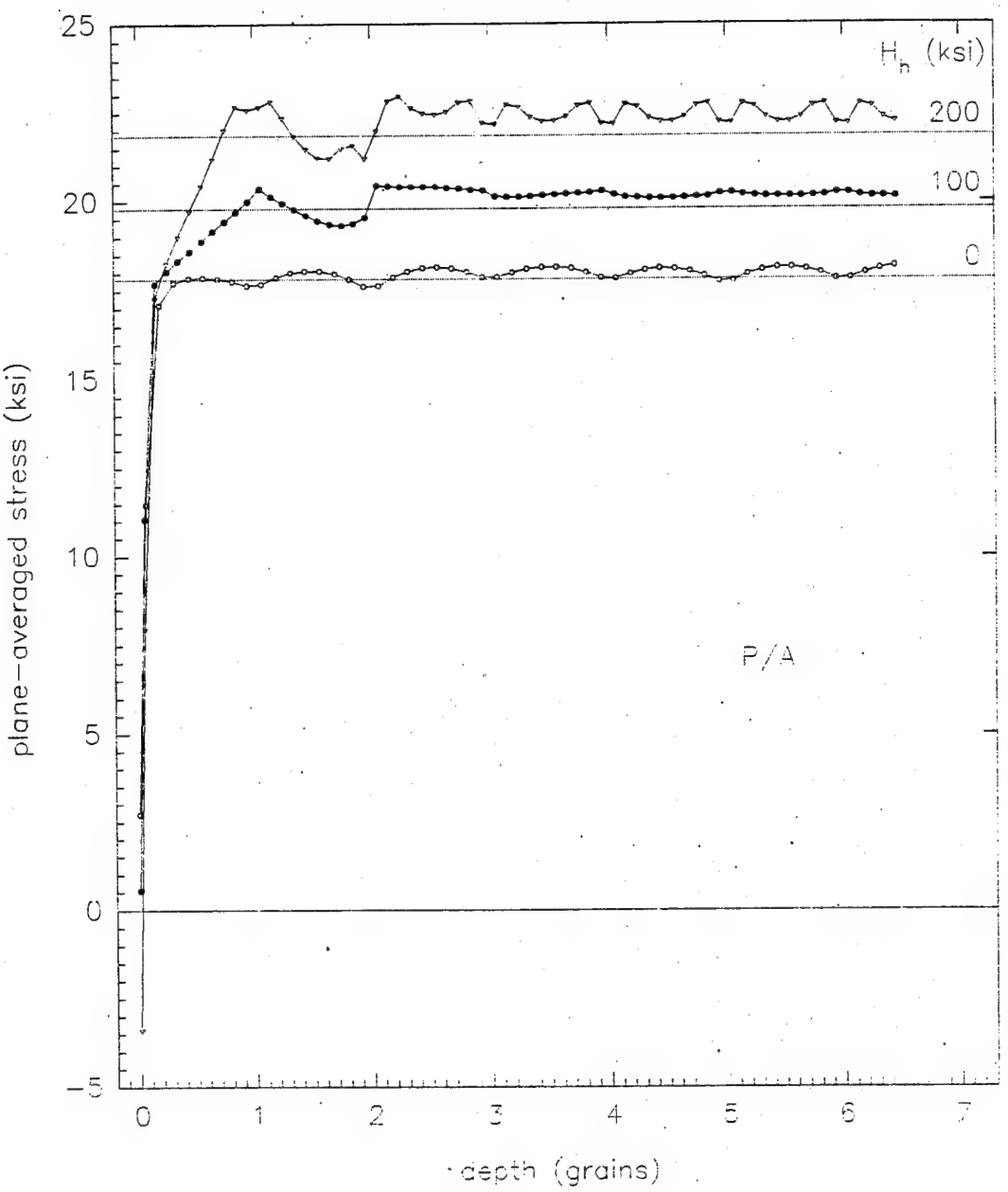

Figure 4.2.2.5-3. Plane-averaged longitudinal stress versus depth in specimens with hard grain hardening rates of 0, 100, and 200 ksi for a plastic strain in the vicinity of 5% (5.0%, 5.0%, and 6.1%, respectively), under load. (f_s = 0.33, E = 30,000 ksi, υ = 0.29, σ_{ys} = 15 ksi, H_s = 0 ksi.

model, unless the yield spread is large and/or the hardening rate of the metal is close to zero.

4.2.2.7 Effect of the Magnitude of the yield points. Metal families, such as steels, can have similar microstructure, composition and elastic constants, but widely differing yield points. The dependence of the surface layer effect on the magnitude of the bulk yield point is therefore of interest. The effect of two types of yield point changes will be considered: translational and proportional. For the translational change, the yield points of the soft and hard grains are each changed or shifted by the same amount, preserving the yield point spread between the grains. For the proportional change, the soft and hard grain yield points are changed in the same proportion. The proportional change is the more meaningful in describing metals because the crystal yield surface is scaled relative to the basic properties of the crystal which define its plasticity, e.g., the critical stress Γ_α for slip along the dominating slip system. Thus, in a collection of crystals which are identical in properties and have a given distribution of orientation with respect to the applied load, an increase of the slip system critical stress will lead to a corresponding proportional increase of the crystal yield surface because this surface is scaled with respect to Γ_α. This in turn leads to a proportional increase of the minimum yield point of the grain ("soft" configuration) and maximum yield of the crystal ("hard" configuration). These concepts are developed in detail in Section 4.2.3.1, The Onset of the Surface Layer Effect.

First consider the effect of a constant shift in the grain yield points. Calculations were performed for models for which the yield points are in the range of 8 to 58 ksi, but are otherwise identical to the basic model. The results are compared in Table 4.2.2.7-1. The residual stresses are almost equal to those for the basic model up to the bulk yield point (0.002 plastic strain). Above the yield point, the residual stresses become markedly less in the higher yield models, decreasing to about half the values of the basic model for plastic strains of several percent (Figure 4.2.2.7-1). Plots of the residual stresses versus the yield point for ϵ_p = 0.00005, 0.002, 0.05 are shown in Figure 4.2.2.7-2. The initial behavior is expected on the basis of the soft surface layer model (Section 4.2.2.1). The subsequent decrease when the initial yielding is 25 ksi or greater, is, however, not easy to explain physically. The surface hard grains appear to follow the bulk deformation more closely when their yield point is greater, allowing for less plastic

Table 4.2.2.6-1. Comparison of specimens having soft grain hardening rates of 0, 10, 20, 40, and 100 ksi, for yield point spreads (YPS) of 5 and 15 ksi. For all the specimens f_s = 0.33, E = 30,000 ksi, υ = 0.29, σ_{ys} = 15 ksi, σ_{ys} = 15 ksi, H_h = 100 ksi.

YPS (ksi)		5					15	
H_s (ksi)		0	10	20	40	100	0	10
Ω		0.27	0.27	0.27	0.28	0.29	0.28	0.28
τ (gr)		2	2	2	2	0	2	2
Average residual stress in surface grain layer, σ_{rg1}								
ϵ_p	0.00005	-0.31	-0.31	-0.31	-0.31	-0.31	-0.31	-0.31
	0.0005	-0.95	-0.95	-0.94	-0.92	-0.89	-2.64	-2.60
	0.002	-0.90	-0.87	-0.84	-0.79	-0.64	-2.78	-2.79
	0.01	-0.90	-0.79	-0.69	-0.50	-0.04	-2.78	-2.72
	0.05	-1.50	-1.14	-0.80	-0.33	0.04	-2.90	
X-ray-averaged residual stress, σ_{rx1}								
ϵ_p	0.00005	-0.60	-0.60	-0.60	-0.60	-0.59	-0.60	-0.60
	0.0005	-2.14	-2.13	-2.10	-2.10	-2.03	-5.28	-5.22
	0.002	-2.58	-2.52	-2.46	-2.34	-1.98	-6.70	-6.87
	0.01	-2.72	-2.45	-2.19	-1.69	-0.28	-8.73	-8.56
	0.05	-3.79	-2.77	-1.73	-0.55	0.05	-8.83	

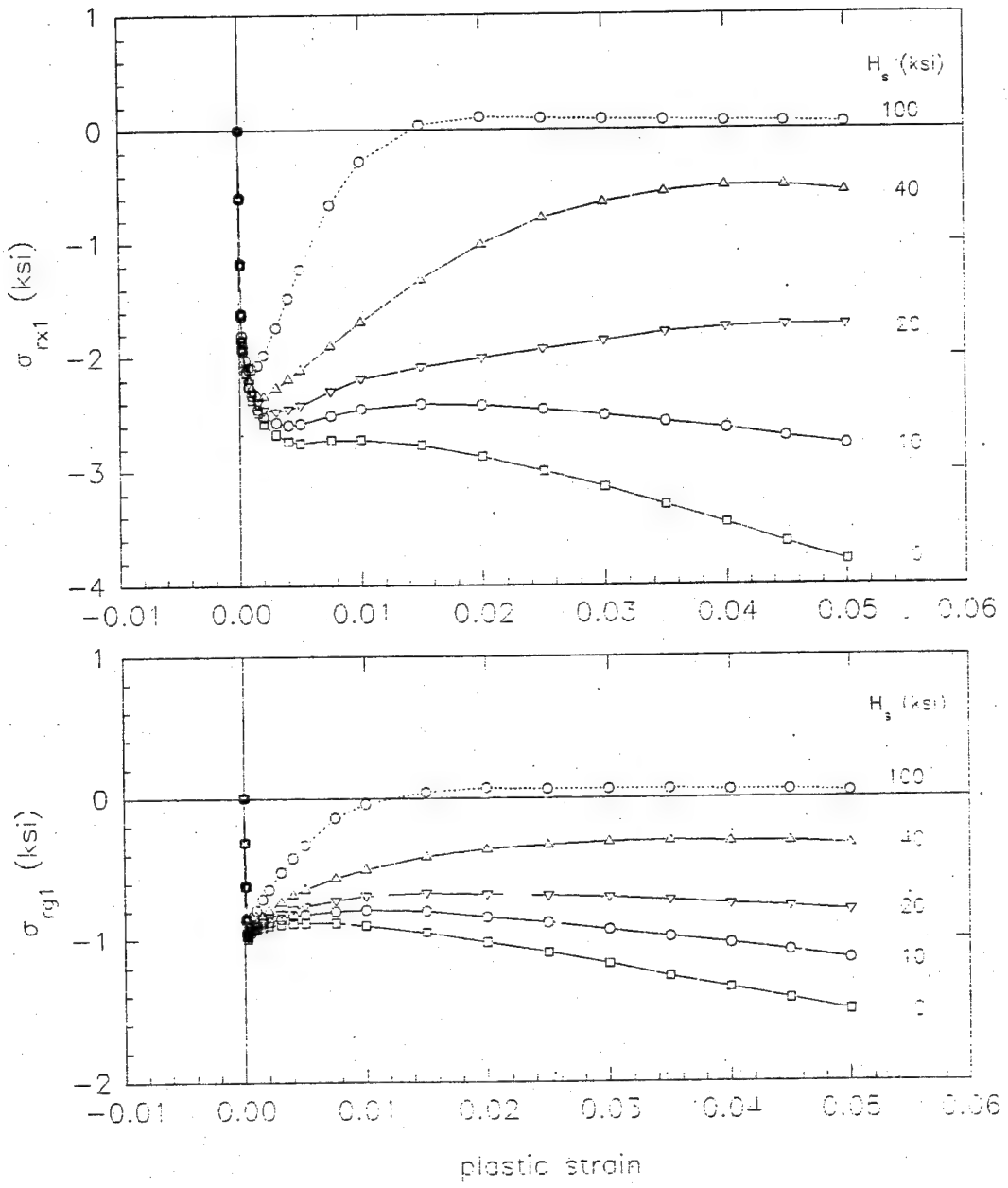

Figure 4.2.2.6-1. The x-ray-averaged residual stress (σ_{rx1}) and the surface-grain-averaged residual stress (σ_{rg1}) versus plastic strain for models with soft grain hardening rates of 0, 10, 20, 40, and 100 ksi. (f_s = 0.33, E = 30,000 ksi, υ = 0.29, σ_{ys} = 15 ksi, H_h = 100 ksi.)

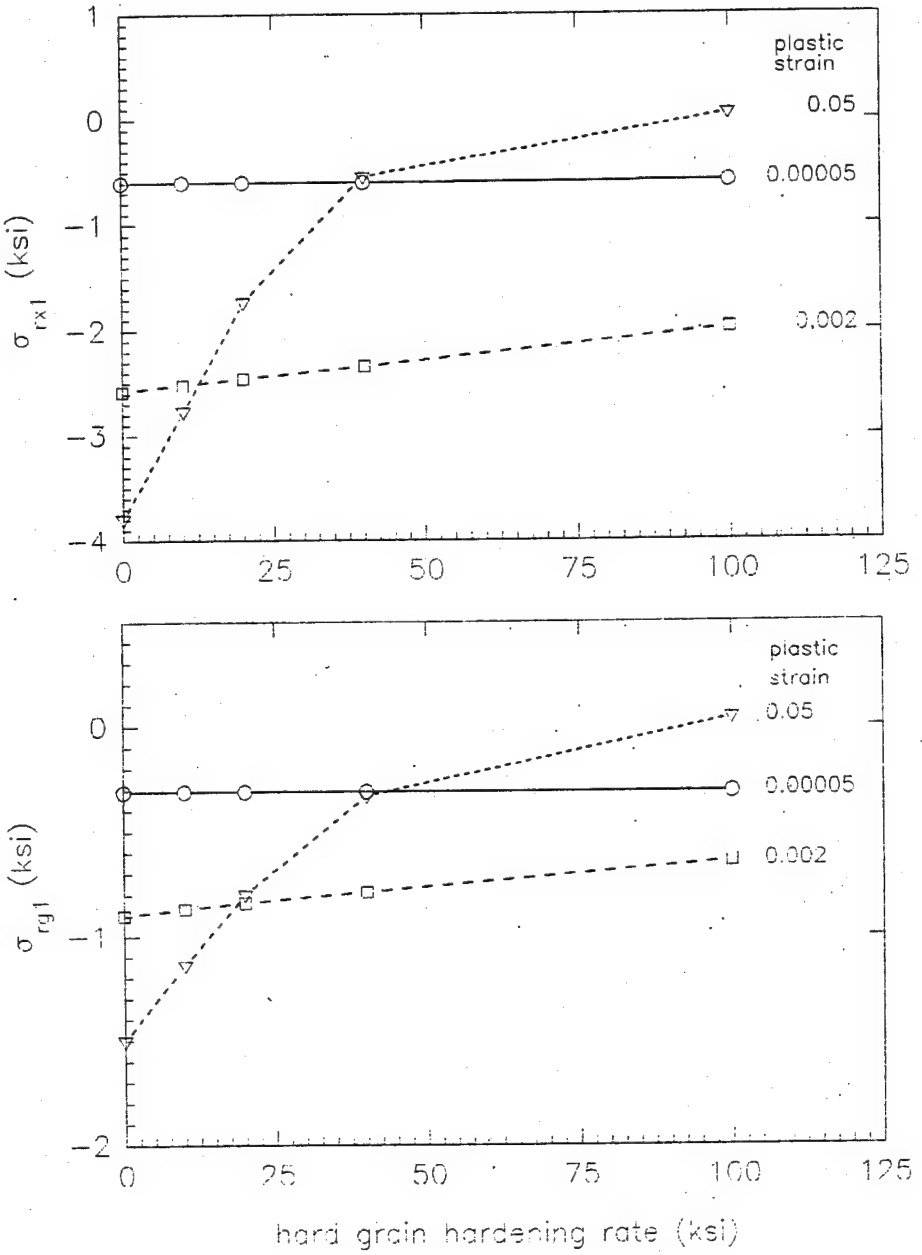

Figure 4.2.2.6-2. The x-ray-averaged residual stress (σ_{rx1}) and the surface-grain-averaged residual stress (σ_{rg1}) versus soft grain hardening rate for plastic strains of 0.00005, 0.002, and 0.05. (f_s = 0.33, E = 30,000 ksi, υ = 0.29, σ_{ys} = 15 ksi, H_h = 100 ksi.)

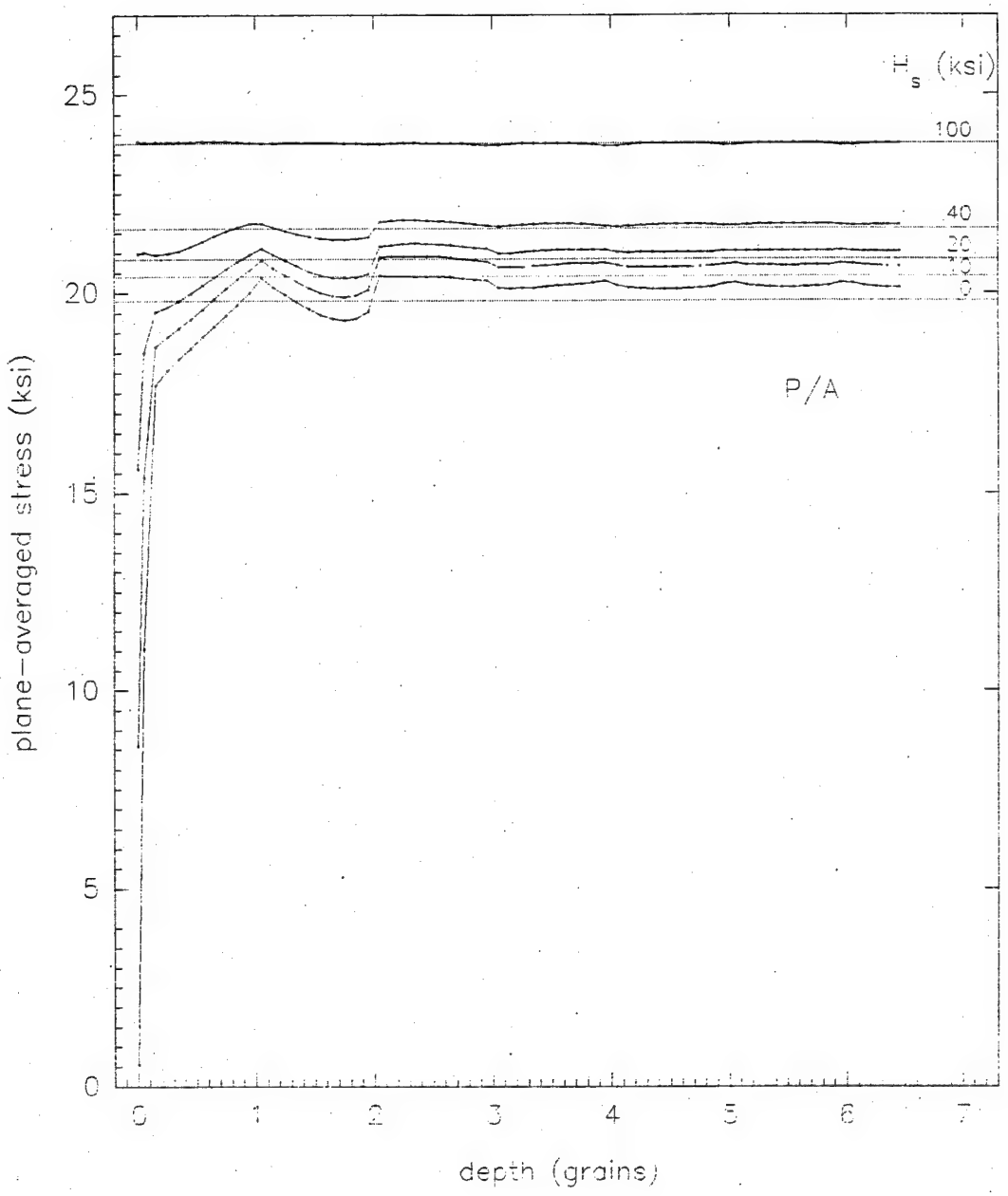

Figure 4.2.2.6-3. Plane-averaged longitudinal stress versus depth in specimens with soft grain hardening rates of 0, 10, 20, 40, and 100 ksi for a plastic strain in the vicinity of 5% (5.0%, 5.2%, 5.1%, 5.1%, and 5.5%, respectively), under load. (f_s = 0.33, E = 30,000 ksi, υ = 0.29, σ_{ys} = 15 ksi, H_h = 100 ksi.)

deformation of the soft grains. Despite this considerable inhibition of the residual stresses, the surface layer thickness remains two grains up to the highest yield point (proportional limit) considered, 58 ksi (55 ksi). The surface layer stress profile also remain similar, except near the free surface, where the steep drop observed at the lowest yield point gradually disappears as the yield point is increased (Figure 4.2.2.7-3).

Now consider a proportional change in the soft and hard grain yield points. Calculations were performed for three models for which $\sigma_s/\sigma_h = 0.62 \pm 0.01$ and σ_{yB} = 31, 42, and 50 ksi. They model iron or mild steel (see Section 4.2.3.2). The results are summarized in Table 4.2.2.7-2. The initial stress deviation and the residual stresses for very small plastic strains ($\epsilon_p \leq 0.0005$) are again almost independent of the yield point. Thus Ω is in the range of 0.76-0.78 and σ_{rl} ($\epsilon_p = 0.0005$) for the three models. However, very different results from those for the translational yield point change are obtained at higher plastic strains. The compressive residual stresses (σ_{rl} and σ_{rgl}) *increase* approximately linearly with the bulk yield point for plastic strains of 0.01 or greater, instead of *decreasing* with bulk yield point. This dependence of the residual stresses versus plastic strain as a function of yield point is illustrated in Figure 4.2.2.7-4 (σ_{rl} and σ_{rgl} versus ϵ_p) and Figure 4.2.2.7-5 (σ_{rl} and σ_{rgl} versus yield point for ϵ_p = 0.00005, 0.002, 0.05). This increase of the compressive residual stresses is expected from scaling considerations and from the soft layer model (see Section 4.2.2.1). On the other hand, the surface layer depth is insensitive to the yield point, remaining approximately two grains for all the models, with the stress profile becoming smoother as the bulk yield point is increased (Figure 4.2.2.7-6).

In conclusion, the surface layer effect in metals, as measured from the residual compressive stresses, is expected to be insensitive to the bulk yield point for small plastic strains, but become proportional to the yield point for plastic strains of ≈ 0.01 or greater. The initial stress deviation ratio and surface layer depth are insensitive to the yield point.

4.2.2.8 Effect of Grain Aspect Ratio. Grain shapes other than equiaxed are common in metals. Inclusion shape is known to have a significant effect on the stress fields in the inclusion and in the matrix. Grain shape can therefore be expected to influence the surface layer effect. To obtain an

Table 4.2.2.7-1. Comparison of specimens having proportional limits of 10, 15, 25, 35, and 55 ksi, but with an equal yield point spread of 5 ksi. (f_s = 0.33, E = 30,000 ksi , υ = 0.29, H_s = 0, H_h = 100 ksi.)

σ_{ys} (ksi)		10	15	25	35	55
σ_{yh} (ksi)		15	20	30	40	60
σ_{ymix} (ksi)		13.33	18.33	28.33	38.33	58.33
σ_{yB} (ksi)		12.75	17.90	28.03	38.10	58.18
σ_{ys}/σ_{Yb}		0.78	0.84	0.89	0.92	0.95
Ω		0.24	0.28	0.29	0.30	0.31
τ (grain)		2	2	2	2	2
Average residual stress in surface grain layer, σ_{rgl}						
ϵ_p	0.00005	-0.31	-0.31	-0.31	-0.31	-0.31
	0.0005	-0.96	-0.95	-0.94	-0.90	-0.87
	0.002	-0.95	-0.90	-0.79	-0.72	-0.61
	0.01	-0.94	-0.90	-0.73	-0.59	-0.41
	0.05	-1.47	-1.50	-1.48	-1.29	-1.03
X-ray-averaged residual stress, σ_{rxl}						
ϵ_p	0.00005	-0.61	-0.60	-0.61	-0.60	-0.60
	0.0005	-2.24	-2.14	-2.07	-2.02	-1.96
	0.002	-2.83	-2.58	-2.28	-2.07	-1.79
	0.01	-2.93	-2.72	-2.08	-1.49	-0.86
	0.05	-3.89	3.79	-3.27	-2.18	-1.37

Table 4.2.2.7-2. Comparison of specimens having bulk yield points of 31, 42, and 50 ksi and a proportional yield point spread between the soft and hard grains. (f_s = 0.33, E = 30,000 ksi, υ = 0.29, H_s = 0, H_h = 100 ksi.)

σ_{yB} (ksi)		31.4	41.8	50.1
σ_{ymix} (ksi)		34.0	44.7	55.0
σ_{ys} (ksi)		24	32	39
σ_{yh} (ksi)		39	51	63
σ_{ys}/σ_{yB}		0.76	0.77	0.78
Ω		0.30	0.31	0.31
τ (grain)		2	2	2
Average residual stress in surface grain layer, σ_{rg1}				
ϵ_p	0.00005	-0.31	-0.31	-0.31
	0.0005	-2.69	-2.96	-3.12
	0.002	-2.82	-3.64	-4.30
	0.01	-2.85	-3.61	-4.61
	0.045	-2.98	-3.62	-4.59
X-ray-averaged residual stress, σ_{rx1}				
ϵ_p	0.00005	-0.60	-0.60	-0.60
	0.0005	-5.18	-5.95	-5.99
	0.002	-6.91	-8.28	-9.55
	0.01	-9.0	-11.1	-13.8
	0.045	-9.1	-11.1	-14.2

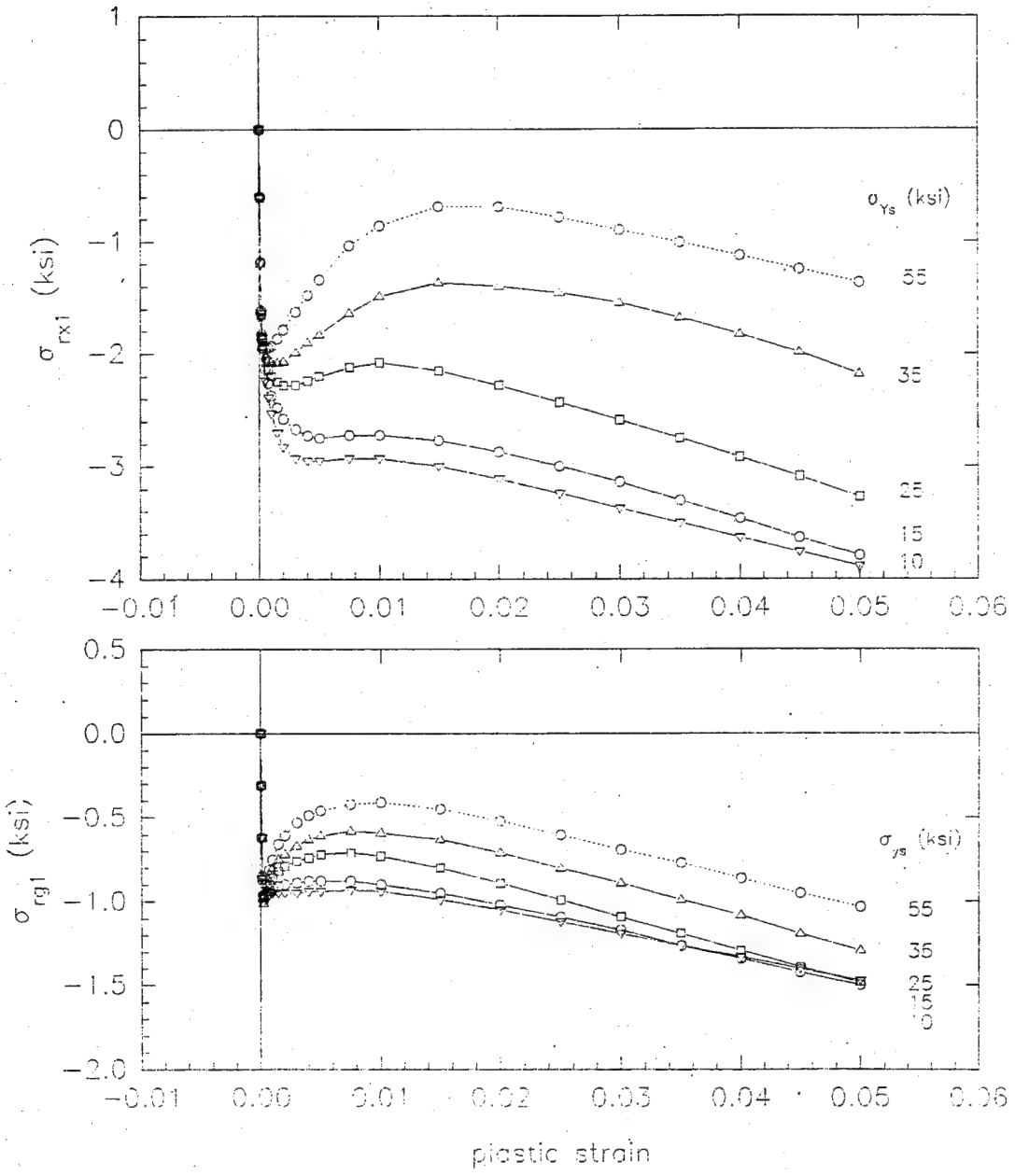

Figure 4.2.2.7-1. The x-ray-averaged residual stress (σ_{rx1}) and the surface-grain-averaged residual stress (σ_{rg1}) versus plastic strain for models with soft grain yield points of 10, 15, 25, 35, and 55 ksi and a yield point spread of 5 ksi. (f_s = 0.33, E = 30,000 ksi , υ = 0.29, $\sigma_{yh} - \sigma_{ys}$ = 5 ksi, H_s = 0, H_h = 100 ksi.)

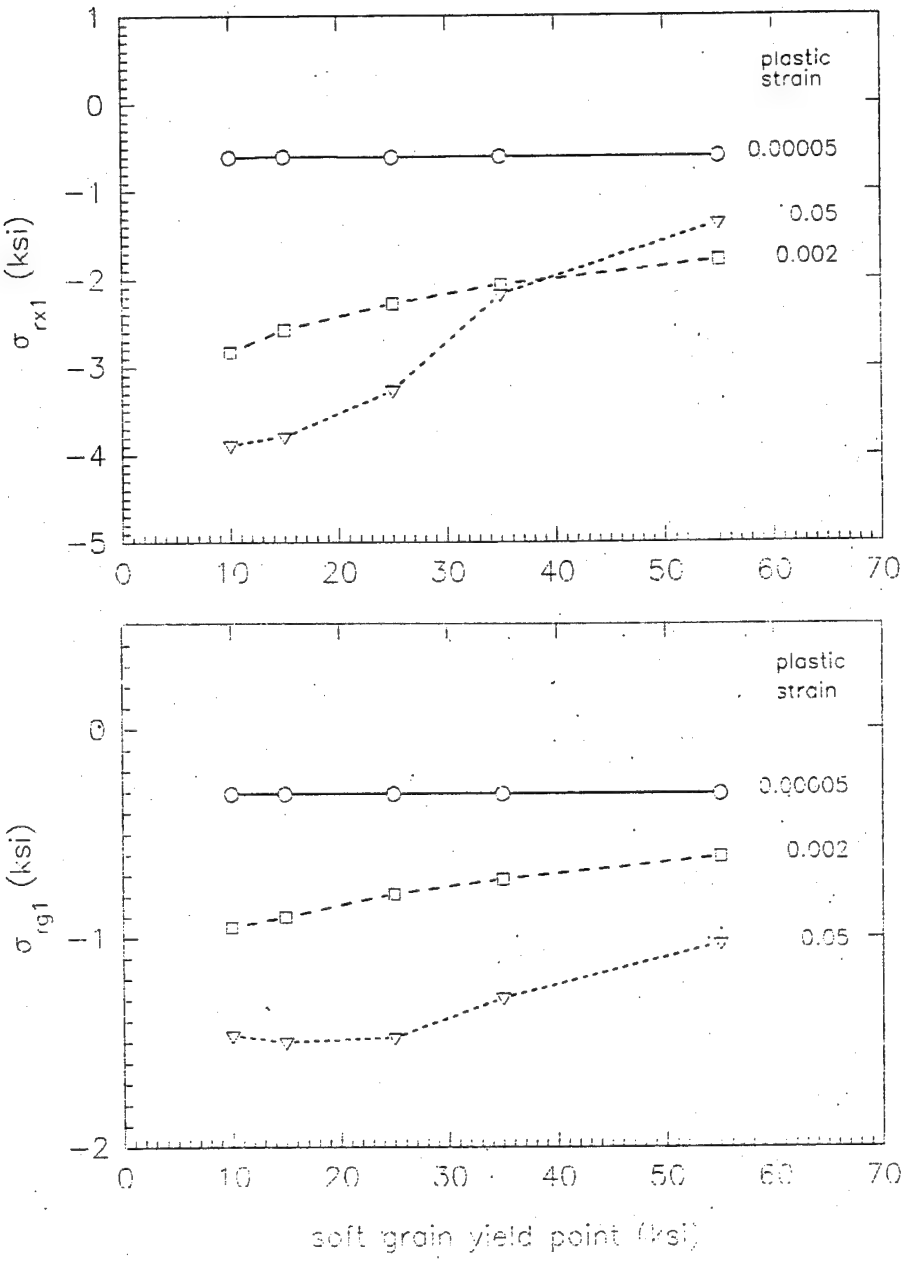

Figure 4.2.2.7-2. The x-ray-averaged residual stress (σ_{rx1}) and the surface-grain-averaged residual stress (σ_{rg1}) versus soft grain yield point for plastic strains of 0.00005, 0.002, and 0.05. (f_s = 0.33, E = 30,000 ksi , υ = 0.29, $\sigma_{yh} - \sigma_{ys}$ = 5 ksi, H_s = 0, H_h = 100 ksi.)

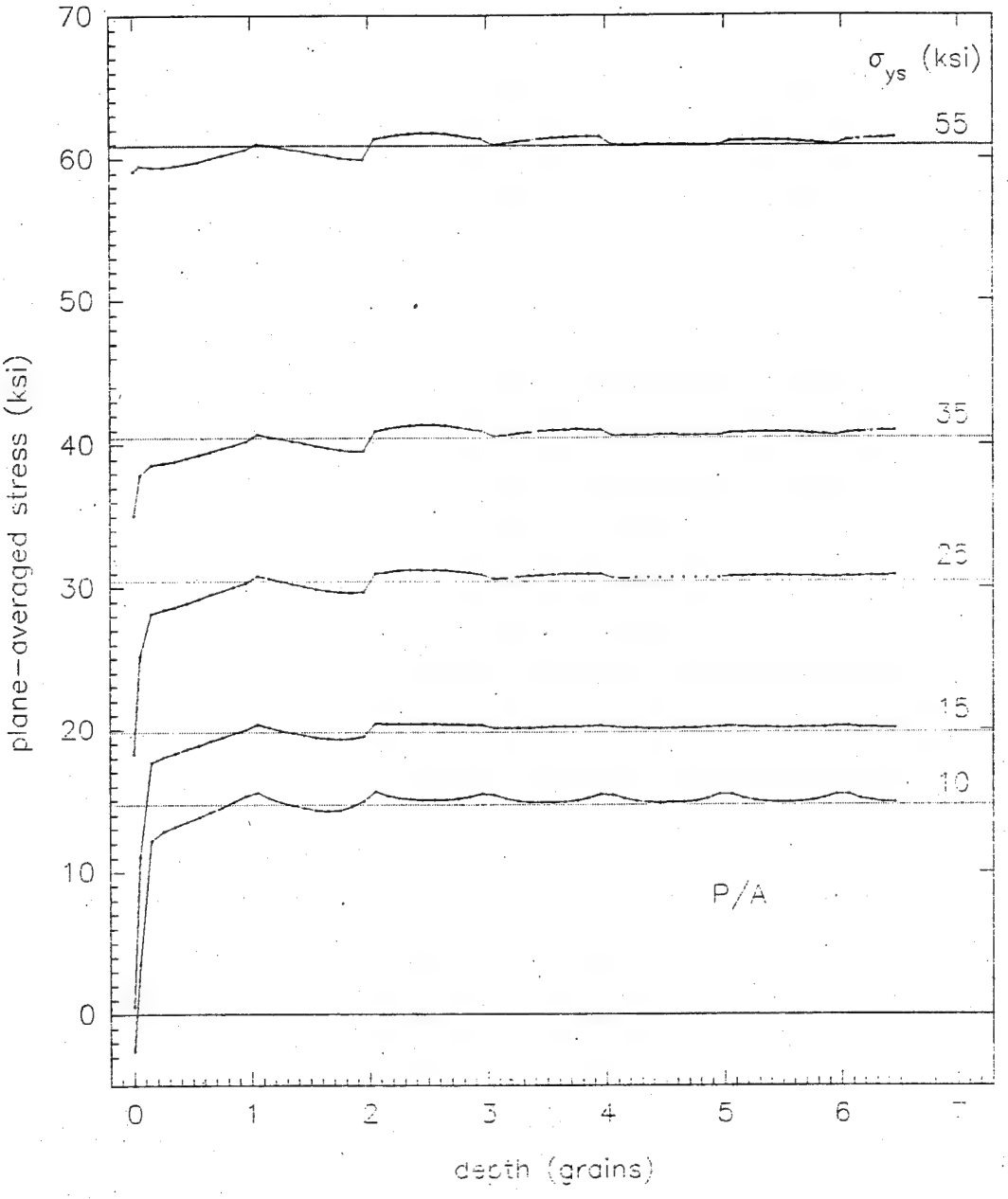

Figure 4.2.2.7-3. Plane-averaged longitudinal stress versus depth in specimens with soft grain yield points of 10, 15, 25, 35, and 55 ksi and a yield point spread of 5 ksi, for a plastic strain in the vicinity of 5%, under load. (f_s = 0.33, E = 30,000 ksi , υ = 0.29, $\sigma_{yh} - \sigma_{ys}$ = 5 ksi, H_s = 0, H_h = 100 ksi.)

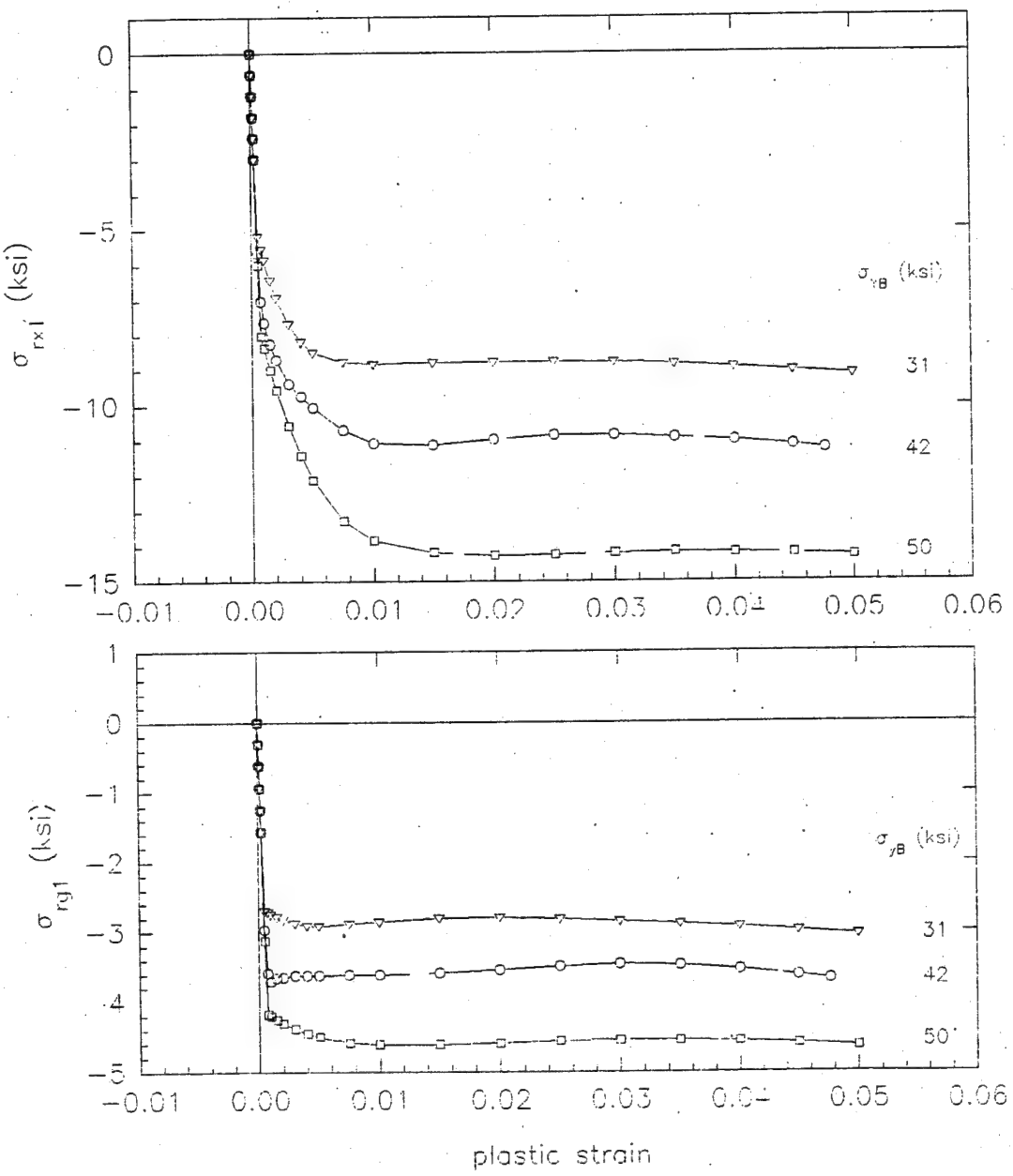

Figure 4.2.2.7-4. The x-ray-averaged residual stress (σ_{rx1}) and the surface-grain-averaged residual stress (σ_{rg1}) versus plastic strain for models with bulk yield points of 31, 42, and 50 ksi and a proportional yield point spread. (f_s = 0.33, E = 30,000 ksi, υ = 0.29, H_s = 0, H_h = 100 ksi.)

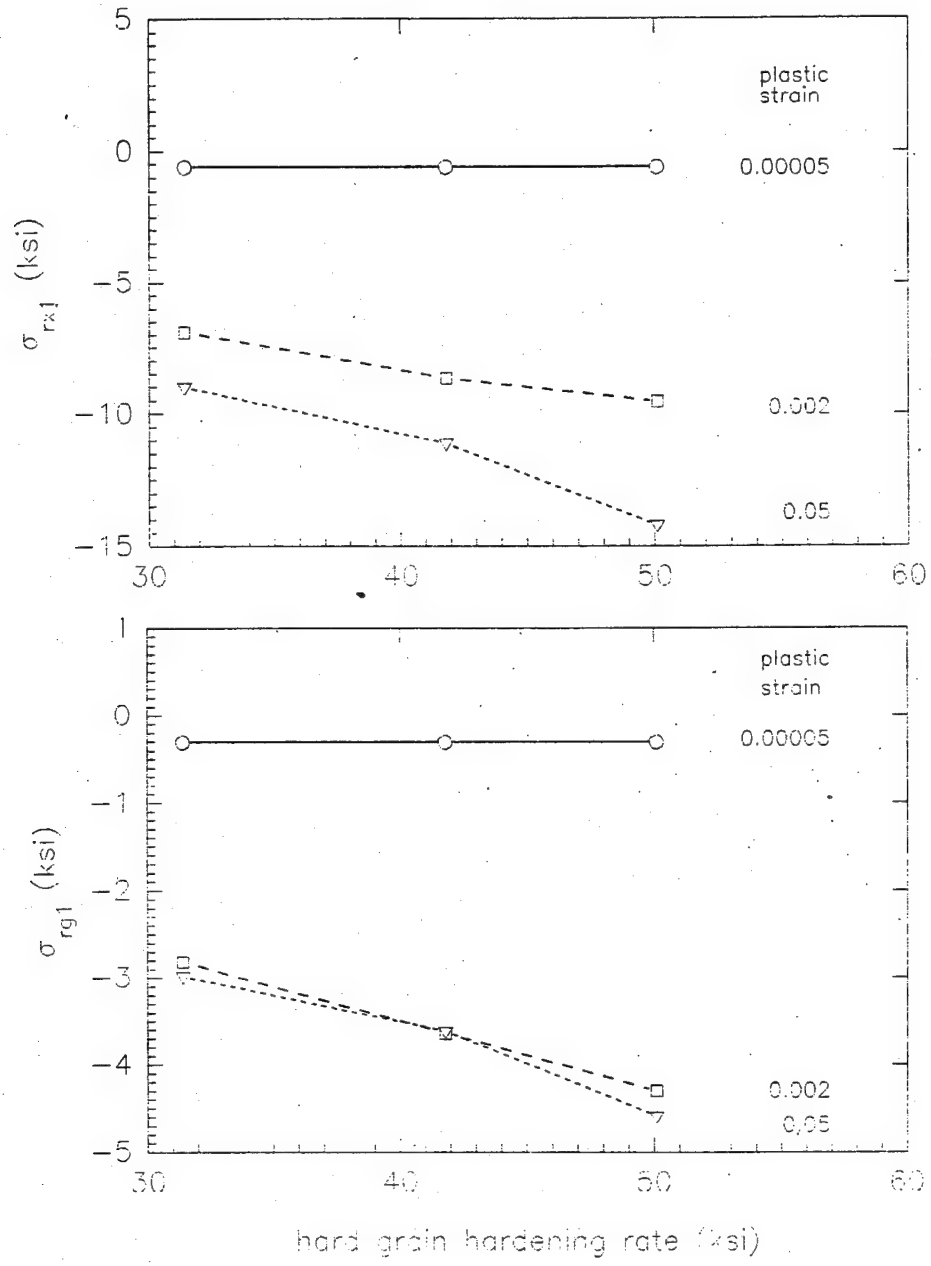

Figure 4.2.2.7-5. The x-ray-averaged residual stress (σ_{rx1}) and the surface-grain-averaged residual stress (σ_{rg1}) versus bulk yield point for plastic strains of 0.00005, 0.002, and 0.05. (f_s = 0.33, E = 30,000 ksi , υ = 0.29, σ_{yh} proportional to σ_{ys}, H_s = 0, H_h = 100 ksi.)

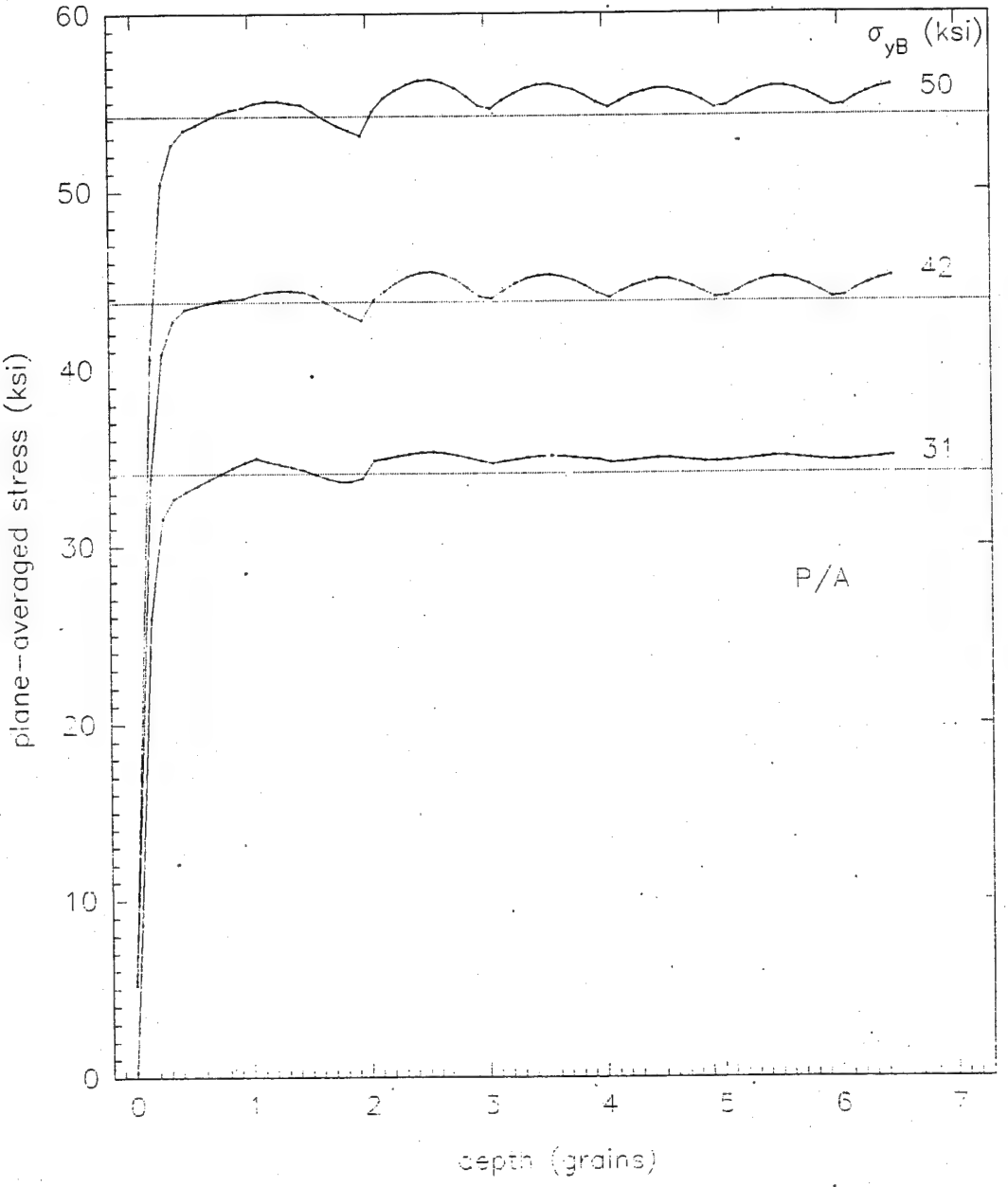

Figure 4.2.2.7-6. Plane-averaged longitudinal stress versus depth in specimens with bulk yield points of 31, 42, and 50 ksi and a proportional yield point spread, for a plastic strain in the vicinity of 5%, under load. (f_s = 0.33, E = 30,000 ksi , υ = 0.29, H_s = 0, H_b = 100 ksi.)

indication of the effect of grain shape, rectangular grains of various aspect ratios were used. The grain aspect ratio (GAR) is defined here as the ratio of the vertical length over the horizontal length. Calculations were performed for aspect ratios from 2/3 to 2 for 33% soft grain concentration and yield point spread of 5 ksi (Table 4.2.2.8-1); for aspects ratios of 1 through 3 for 33% soft grain concentration, 15 ksi yield point spread (Table 4.2.2.8-2); and for aspect ratios from 2 to 0.5 for 25% soft grain concentration and 5 ksi yield spread (Table 4.2.2.8-3). Representing a polycrystalline aggregate of randomly oriented crystals with an ordered array of isotropic soft and hard square grains is an enormous simplification. Using rectangular grains to represent nonequiaxed crystals superimposes yet another enormous simplification. Therefore, these calculations on the effect of grain shape are only to give an indication of trends.

The grain shape has a marked and complex effect on the surface layer effect. The data is best examined graphically. The compressive residual stresses σ_{rxl} and σ_{rgl} are plotted against plastic strain in Figure 4.2.2.8-1 (f_s = 0.33, YPS = 5 ksi), Figure 4.2.2.8-2 (f_s = 0.33, YPS = 15 ksi), and Figure 4.2.2.8-3 (f_s = 0.25, YPS = 5 ksi). The corresponding plots of σ_{rxl} and σ_{rgl} versus GAR are shown in Figures 4.2.2.8-4, 5, and 6. At the onset of plasticity (ϵ_p = 0.00005), the compressive residual stresses σ_{rxl} and σ_{rgl} increase quasi-asymptotically with GAR in all cases, whereas the stress deviation ratio is at a minimum at GAR = 1 for f_s = 0.33 and at GAR = 2/3 for f_s = 0.25. At the bulk yield point (ϵ_p = 0.002), the residual stresses are greatest at GAR = 1 for f_s = 0.33, and at GAR = 2/3 for f_s = 0.25. At 4.5%-5% plastic strain, the x-ray and surface-grain-averaged residual stresses do not follow the same pattern, reflecting the greater weight of the stresses near the free surface in the x-ray-averaged stress. For f_s = 0.33, the magnitude of σ_{rgl} is at a maximum for GAR > 1, whereas that of σ_{rxl} is at a maximum for GAR ≤ 1. For f_s = 0.25, the magnitude of σ_{rgl} is at a maximum at GAR = 1, whereas that of σ_{rxl} is greatest for GAR = 0.5, the smallest value tested. In all cases, the magnitude of σ_{rxl} decreases as the GAR increases, i.e., as the grains become elongated in the direction of the applied load. The effect of grain shape is markedly less for the greater yield spread.

The plane-averaged stress versus depth profiles are shown in Figure 4.2.2.8-7 (f_s = 0.33, YPS = 5 ksi), Figure 4.2.2.8-8 (f_s = 0.33, YPS = 15 ksi), and Figure 4.2.2.8-9 (f_s = 0.25, YPS = 5 ksi). The characteristic stress

decrease in the surface layer becomes more concentrated in the surface grain layer as the GAR increases, the surface layer thickness decreasing from two grains for GAR ≤ 1 to one grain for GAR > 1 (Tables 4.2.2.8-1, 2, and 3). The steep stress drop near the free surface observed for GAR ≤ 1 disappears given a sufficiently high GAR (Figures 4.2.2.8-7, 8, and 9). The stress peaks at the grain boundary planes become most pronounced for GAR < 1, as expected from stress concentration effects, which become larger as the grain becomes elongated perpendicular to the stress. This effect is similar to the stress concentration at the tip of a crack, which increases with crack length [31]. Premature yielding of the specimen due to these stress concentration effects becomes pronounced for GAR ≤ 0.5 with f_s = 0.33 and YPS = 5 ksi (for example, σ_{yB} = 16.6 ksi for GAR = 0.5), which likely biases the surface layer results.

4.2.2.9 Effect of Constraint. The constraints or displacement boundary conditions on the deforming continuum must have a marked effect on the plastic deformation behavior of this continuum if the yield surface is independent of the hydrostatic stress, as is the case for the von Mises yield criterion, used here. The constraint of a grain in an aggregate slab subjected to uniform tension is probably best represented by a state of generalized plane strain if using a 2-D elasto-plasticity because inside the aggregate the grains mutually constrain each other in all directions, but the external boundaries of the slab are free to move. However, the best representation of the surface layer effect in the actual metal with this rudimentary model may be somewhere between plane stress and generalized plane strain. Besides the inherent constraint imposed by compatibility, imposed or external constraints, as in a notch, may be significant. It is therefore useful to establish how sensitive the surface layer effect is to constraint.

In addition to plane stress (PS), the calculations for the basic model were also performed for plane strain (PE), generalized plane strain (GPE), and axisymmetry (AXS). The axisymmetric specimen models an infinitely long round cylinder ("wire") consisting of concentric donought-shaped soft grains embedded in a matrix of hard grains. GPE and AXS are also of interest because non-zero transverse macro stresses which do not arise from external constraints (as for PE) are possible. The calculations were performed for low and high grain yield point spreads (YPS = 5, 15 ksi) , with work hardening of the hard grains (H_h = 100 ksi, H_s = 0 ksi), and no work hardening (H_h = H_s = 0 ksi). The results are summarized in Table 4.2.2.9-1 for YPS = 5 ksi and H_h = 0, Table 4.2.2.9-2 for YPS = 5 ksi and H_h = 100 ksi, Table 4.2.2.9-3 for

Table 4.2.2.8-1. Comparison of models having grain-aspect ratios of 2, 1.5, 1, and 0.667 for a soft grain concentration of 33% and a yield point spread of 5 ksi. For all the models $f_s = 0.33$, $E = 30{,}000$ ksi, $\upsilon = 0.29$, $\sigma_{ys} = 15$ ksi, $\sigma_{yh} = 20$ ksi ($\sigma_{ymix} = 18.33$ ksi), $H_s = 0$, $H_h = 100$ ksi.

GAR		2	1.5	1	0.67
σ_{yB} (ksi)		18.10	18.04	17.90	17.12
σ_{ys}/σ_{yB}		0.83	0.83	0.84	0.88
Ω		0.51	0.37	0.28	0.31
τ (grain)		1	1	2	2
Surface-grain-averaged residual stress, σ_{rg1}					
ϵ_p	0.00005	-0.52	-0.47	-0.31	-0.14
	0.0005	-0.82	-0.99	-0.95	-0.59
	0.002	-0.52	-0.86	-0.90	-0.59
	0.01	-0.49	-0.84	-0.90	-0.71
	0.05	-1.55	-1.72	-1.50	-1.19
X-ray-averaged residual stress, σ_{rx1}					
ϵ_p	0.00005	-0.73	-0.74	-0.60	-0.32
	0.0005	-1.36	-2.06	-2.14	-1.45
	0.002	-0.93	-2.36	-2.58	-1.72
	0.01	-0.45	-2.16	-2.72	-2.33
	0.05	-1.74	-2.47	-3.79	-4.10

Table 4.2.2.8-2. Comparison of models having grain-aspect ratios of 3, 2, and 1, for a soft grain concentration of 33% and a yield point spread of 15 ksi. For all the models $f_s = 0.33$, $E = 30{,}000$ ksi, $\upsilon = 0.29$, $\sigma_{ys} = 15$ ksi, $\sigma_{yh} = 30$ ksi ($\sigma_{ymix} = 25$ ksi), $H_s = 0$, $H_h = 100$ ksi.

Model		SKV02GL	SAM02GL	SAH02GL
GAR		3	2	1
σ_{yB} (ksi)		23.60	23.57	22.45
σ_{ys}/σ_{yB}		0.64	0.64	0.67
Ω		0.62	0.50	0.26
τ (grain)		1	1	2
Surface-grain-averaged stress σ_{rg1}				
ϵ_p	0.00005	-0.52	-0.55	-0.35
	0.0005	-3.06	-3.58	-2.94
	0.002	-2.96	-3.81	-3.14
	0.01	-2.30	-3.41	-3.01
	0.05	-2.59	-3.64	-3.17
X-ray-averaged residual stress, σ_{rx1}				
ϵ_p	0.00005	-0.64	-0.76	-0.64
	0.0005	-4.14	-5.56	-5.54
	0.002	-4.89	-7.53	-7.77
	0.01	-4.74	-8.25	-8.84
	0.05	-2.78	-8.38	-9.07

Table 4.2.2.8-3. Comparison of specimens having grain-aspect ratios of 2, 1.5, 1, 0.667, and 0.5 for a soft grain concentration of 25% and a yield point spread of 5 ksi. For all the specimens f_s = 0.25, E = 30,000 ksi, υ = 0.29, σ_{ys} = 15 ksi, σ_{yh} = 20 ksi (σ_{ymix} = 18.75 ksi), H_s = 0, H_h = 100 ksi.

Model		SDH01HL	SHU01GC	SHS01GC	SHT01GC	SHW01GC
GAR		2	1.5	1	0.67	0.5
σ_{yB} (ksi)		18.41	18.42	18.36	18.28	17.78
σ_{ys}/σ_{yB}		0.81	0.81	0.82	0.82	0.84
Ω		0.66	0.58	0.42	0.35	0.39
τ (grain)		1	1	2	2	2
Average residual stress in surface grain layer, σ_{rg1}						
ϵ_p	0.00005	-0.52	-0.60	-0.55	-0.33	-0.20
	0.0005	-0.76	-0.60	-1.06	-0.99	-0.75
	0.002	-0.46	-0.25	-0.92	-0.95	-0.76
	0.01	-0.36	-0.44	-0.87	-1.02	-0.92
	0.045	-0.98	-1.27	-1.74	-1.64	-1.34
X-ray-averaged residual stress, σ_{rx1}						
ϵ_p	0.00005	-0.65	-0.80	-0.86	-0.61	-0.40
	0.0005	-1.07	-0.77	-1.99	-2.27	-1.81
	0.002	-0.86	-0.28	-2.21	-2.77	-2.23
	0.01	-0.32	-0.40	-1.88	-3.17	-3.12
	0.045	-0.96	-1.24	-2.16	-3.96	-4.28

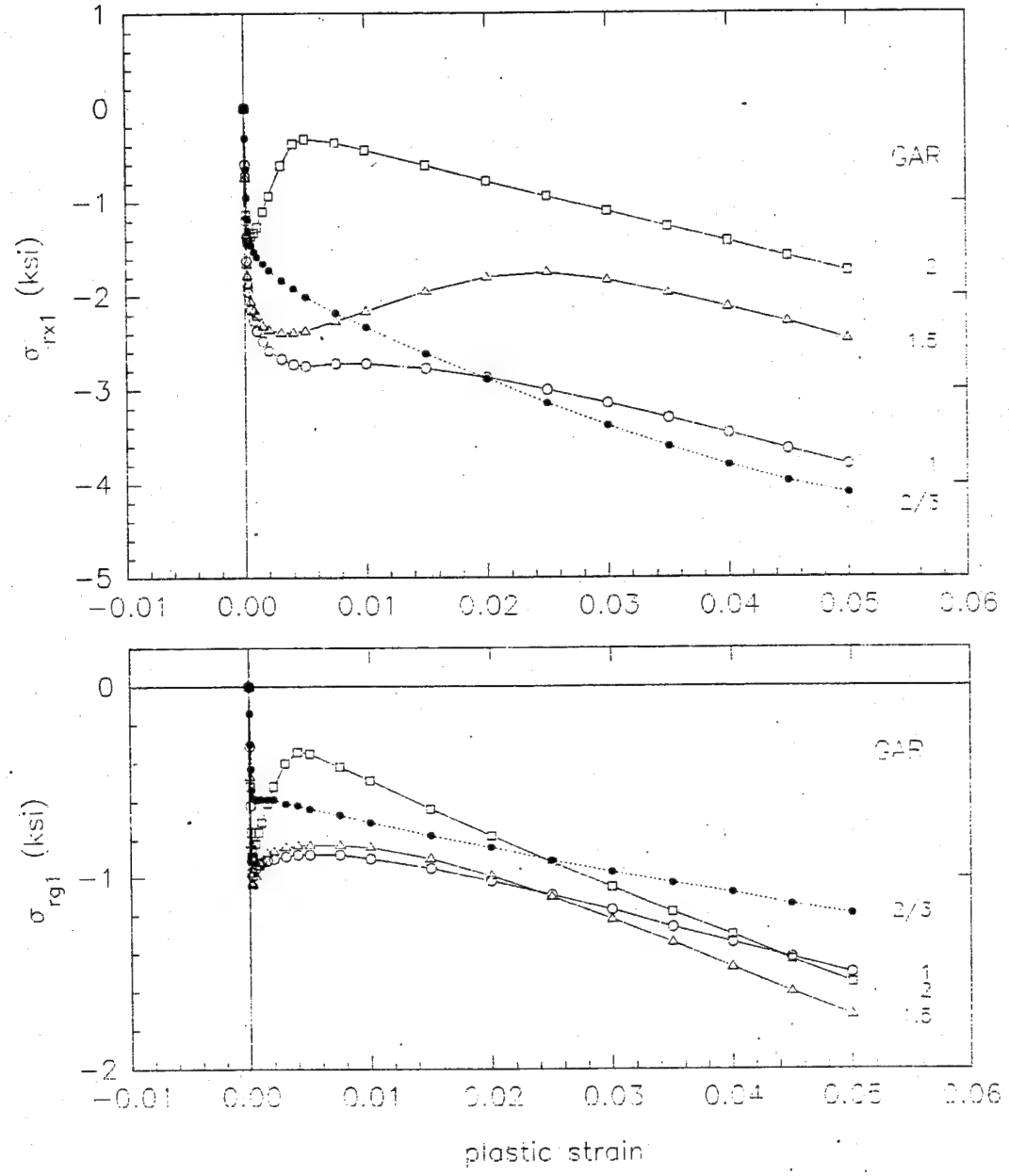

Figure 4.2.2.8-1. The x-ray-averaged residual stress (σ_{rx1}) and the surface-grain-averaged residual stress (σ_{rg1}) versus plastic strain for models with grain aspect ratios (GAR) of 0.667, 1, 1.5, and 2, and a yield point spread of 5 ksi. (f_s = 0.33, E = 30,000 ksi , υ = 0.29, σ_{ys} = 15 ksi, σ_{yh} = 20 ksi, H_s = 0, H_h = 100 ksi.)

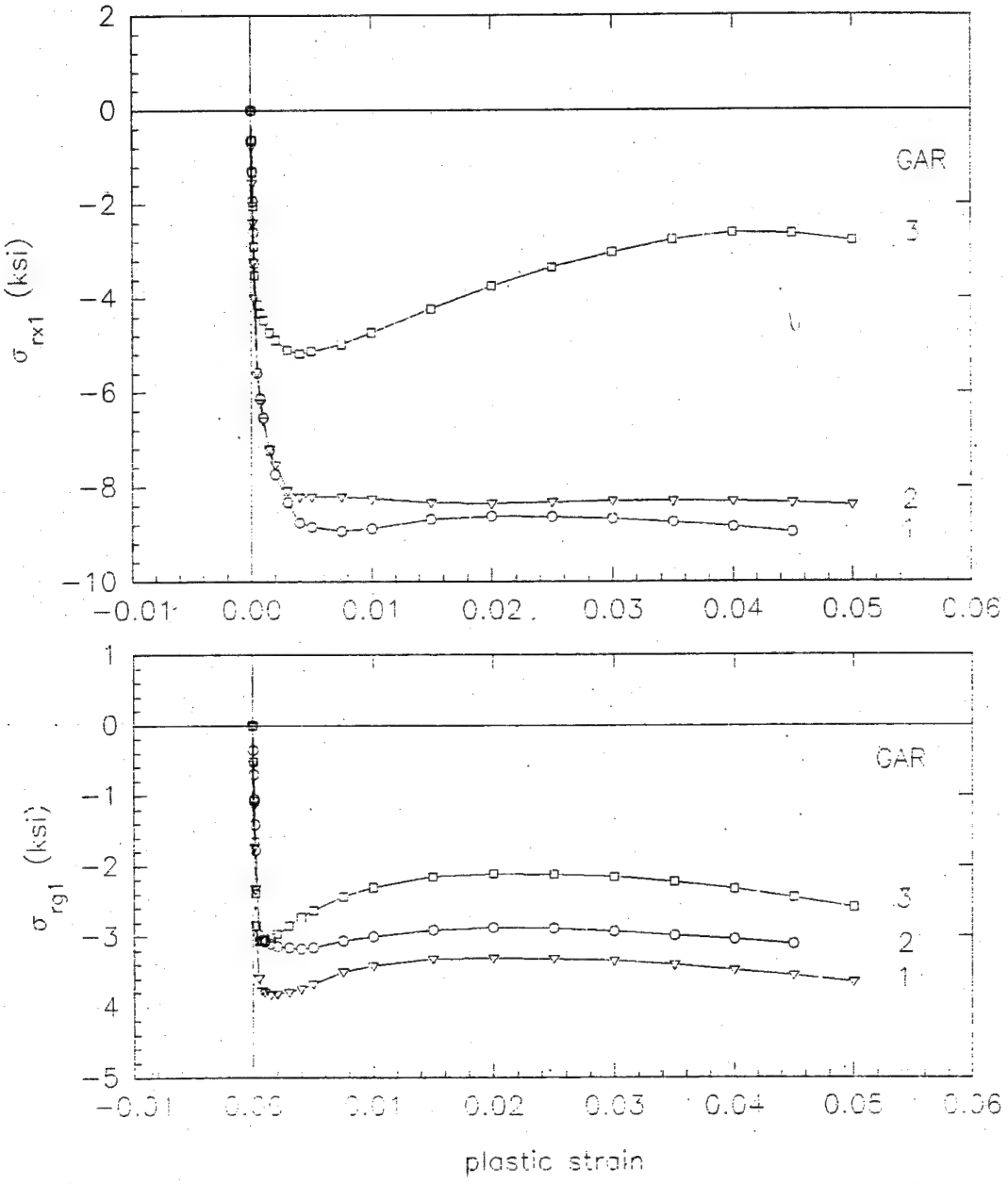

Figure 4.2.2.8-2. The x-ray-averaged residual stress (σ_{rx1}) and the surface-grain-averaged residual stress (σ_{rg1}) versus plastic strain for models with grain aspect ratios (GAR) of 1, 2, and 3, and a yield point spread of 15 ksi. (f_s = 0.33, E = 30,000 ksi , υ = 0.29, σ_{ys} = 15 ksi, σ_{yh} = 30 ksi, H_s = 0, H_h = 100 ksi.)

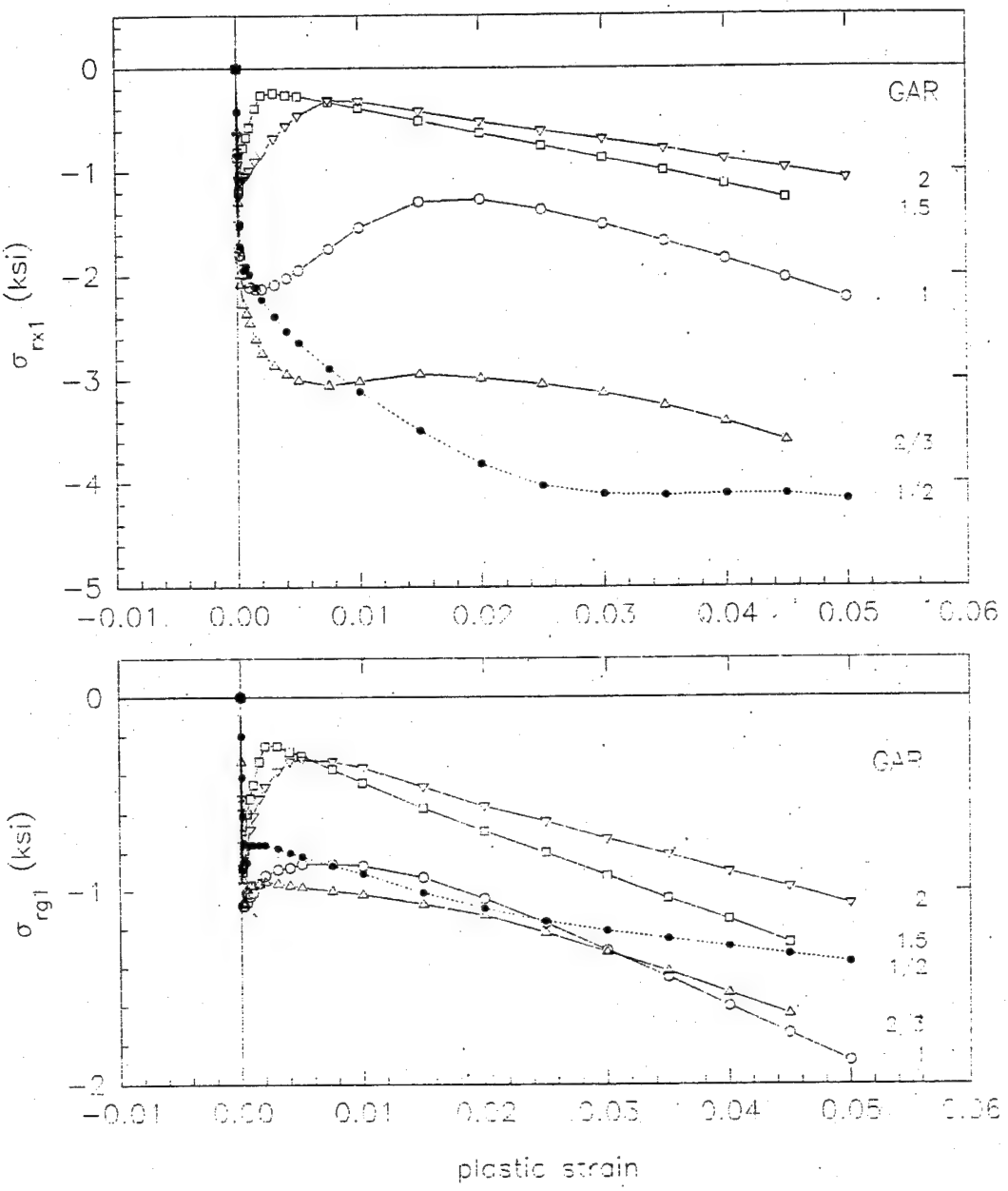

Figure 4.2.2.8-3. The x-ray-averaged residual stress (σ_{rx1}) and the surface-grain-averaged residual stress (σ_{rg1}) versus plastic strain for models with grain aspect ratios (GAR) of 0.5, 2/3, 1, 1.5, and 2, and a soft grain concentration of 25%. (f_s = 0.25, E = 30,000 ksi, υ = 0.29, σ_{ys} = 15 ksi, σ_{yh} = 20 ksi, H_s = 0, H_h = 100 ksi.)

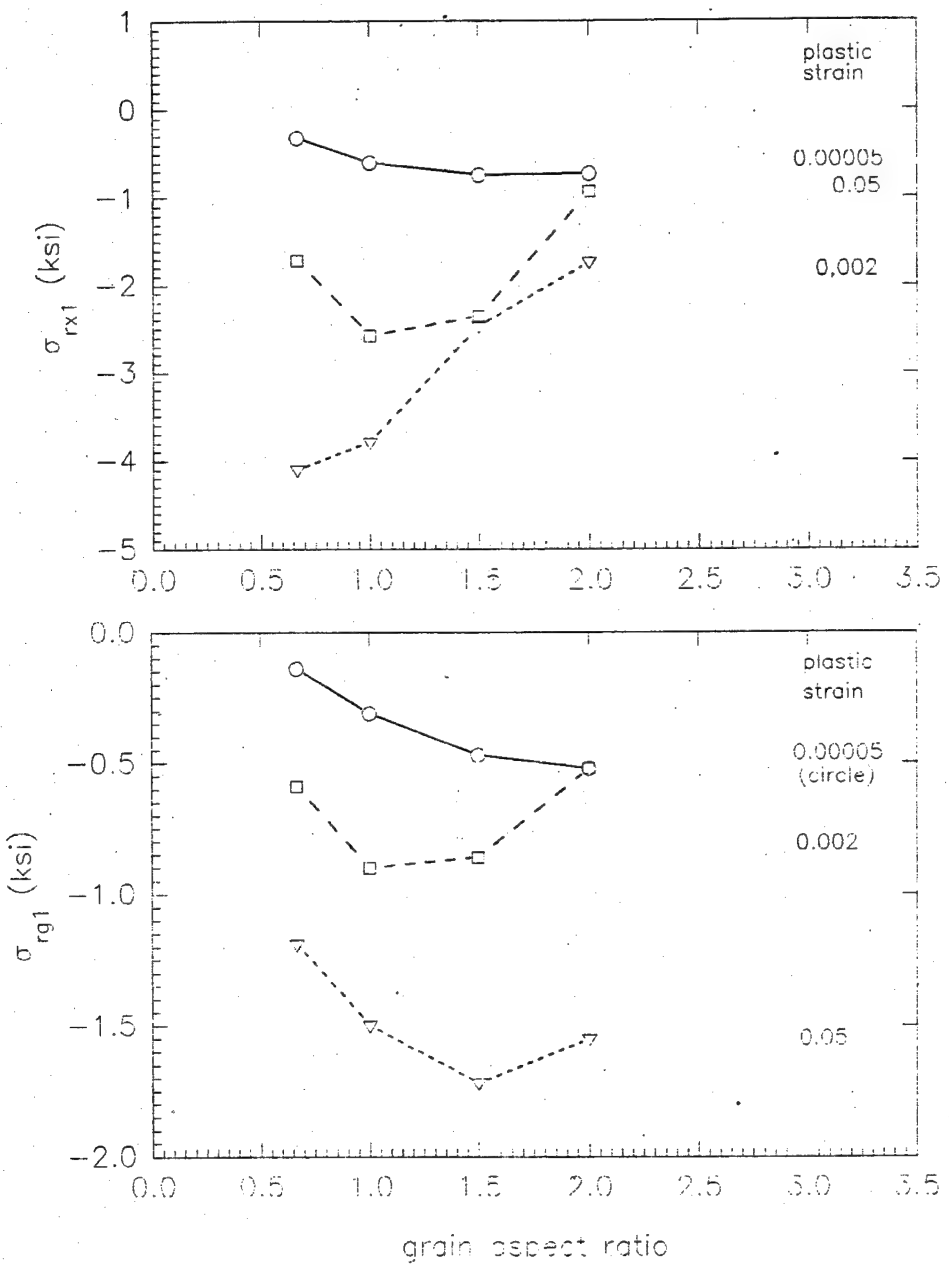

Figure 4.2.2.8-4. The x-ray-averaged residual stress (σ_{rx1}) and the surface-grain-averaged residual stress (σ_{rg1}) versus grain aspect ratio for plastic strains of 0.00005, 0.002, and 0.05. (f_s = 0.33, E = 30,000 ksi , υ = 0.29, σ_{ys} = 15 ksi, σ_{yh} = 20 ksi, H_s = 0, H_h = 100 ksi.)

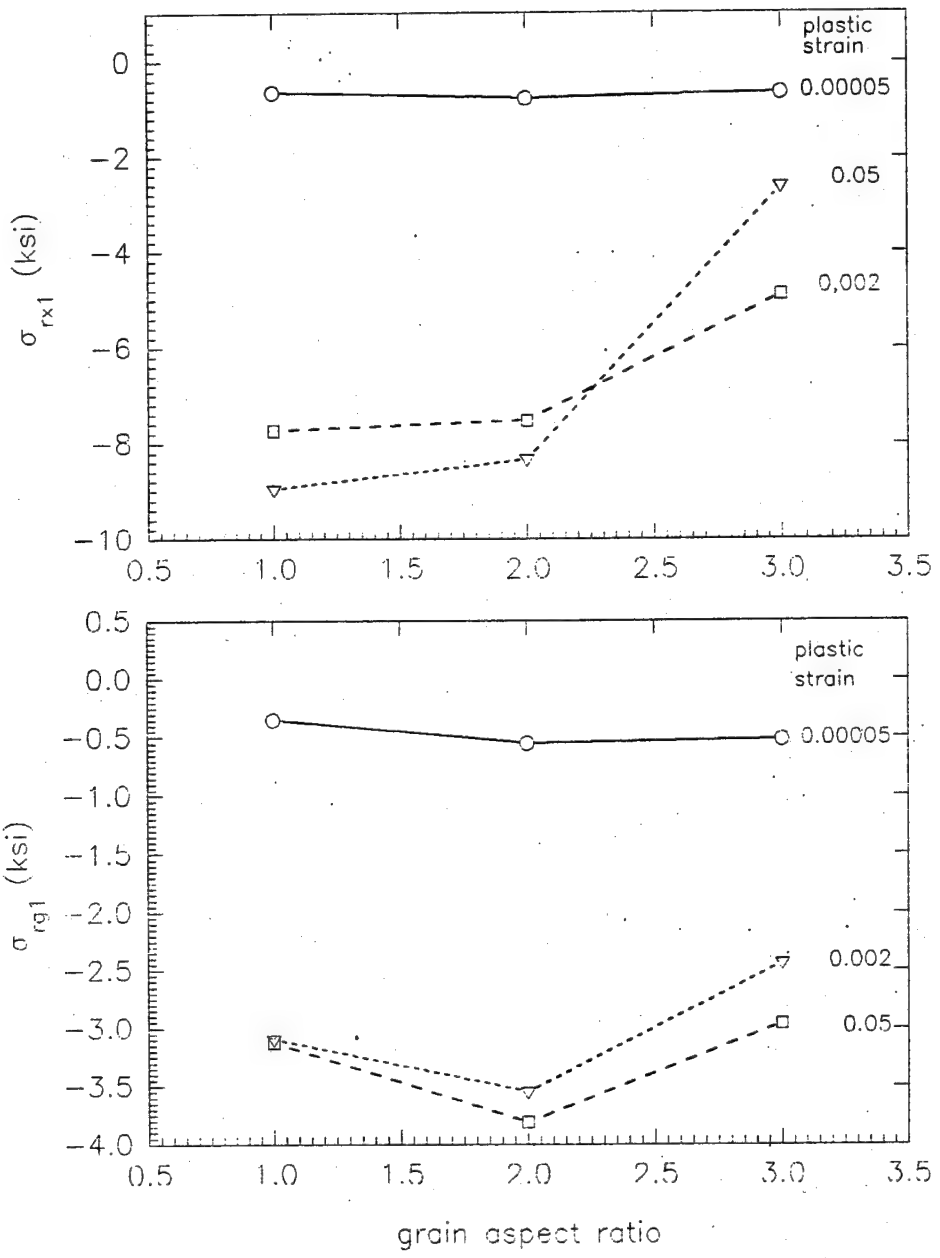

Figure 4.2.2.8-5. The x-ray-averaged residual stress (σ_{rx1}) and the surface-grain-averaged residual stress (σ_{rg1}) versus grain aspect ratio for plastic strains of 0.00005, 0.002, and 0.05 and a yield point spread of 15 ksi. (f_s = 0.33, E = 30,000 ksi, υ = 0.29, σ_{ys} = 15 ksi, σ_{yh} = 30 ksi, H_s = 0, H_h = 100 ksi.)

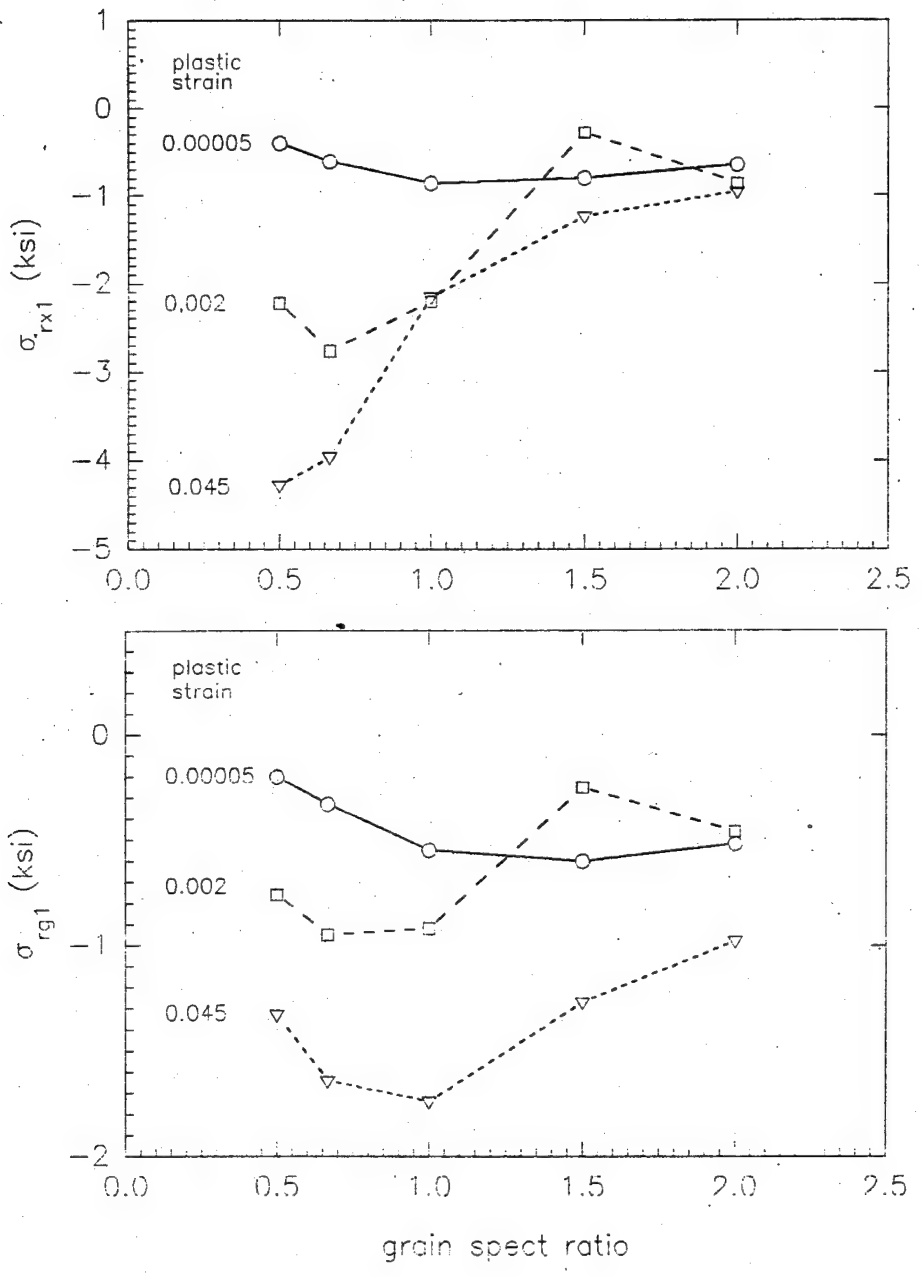

Figure 4.2.2.8-6. The x-ray-averaged residual stress (σ_{rx1}) and the surface-grain-averaged residual stress (σ_{rg1}) versus grain aspect ratio for plastic strains of 0.00005, 0.002, and 0.05 and a soft grain concentration of 25%. (f_s = 0.25, E = 30,000 ksi , υ = 0.29, σ_{ys} = 15 ksi, σ_{yh} = 20 ksi, H_s = 0, H_h = 100 ksi.)

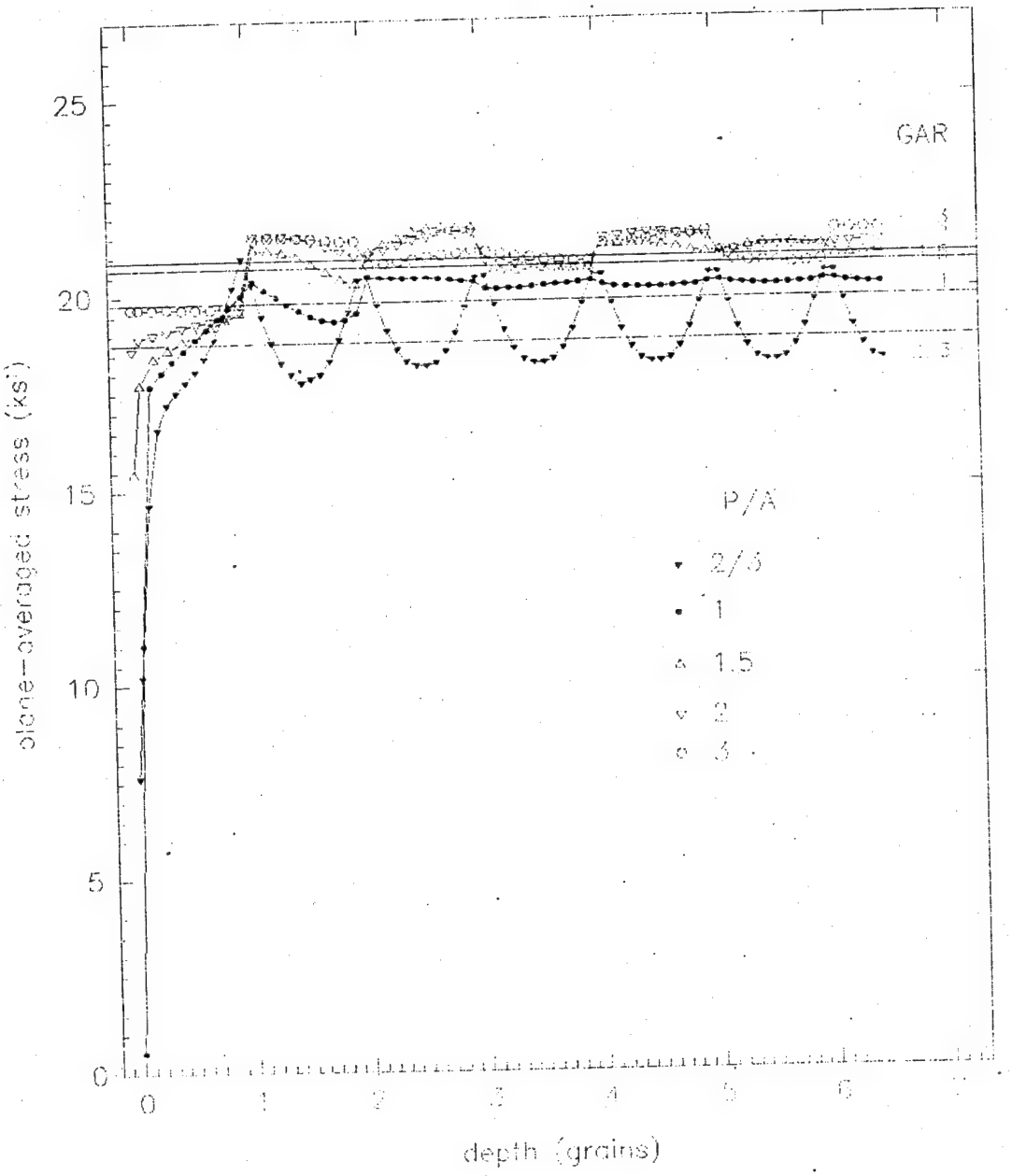

Figure 4.2.2.8-7. Plane-averaged longitudinal stress versus depth in specimens with grain aspect ratios (GAR) of 0.667, 1, 1.5, and 2, and a yield point spread of 5 ksi, for a plastic strain in the vicinity of 5%, under load. (f_s = 0.33, E = 30,000 ksi, υ = 0.29, σ_{ys} = 15 ksi, σ_{yh} = 20 ksi, H_s = 0, H_h = 100 ksi.)

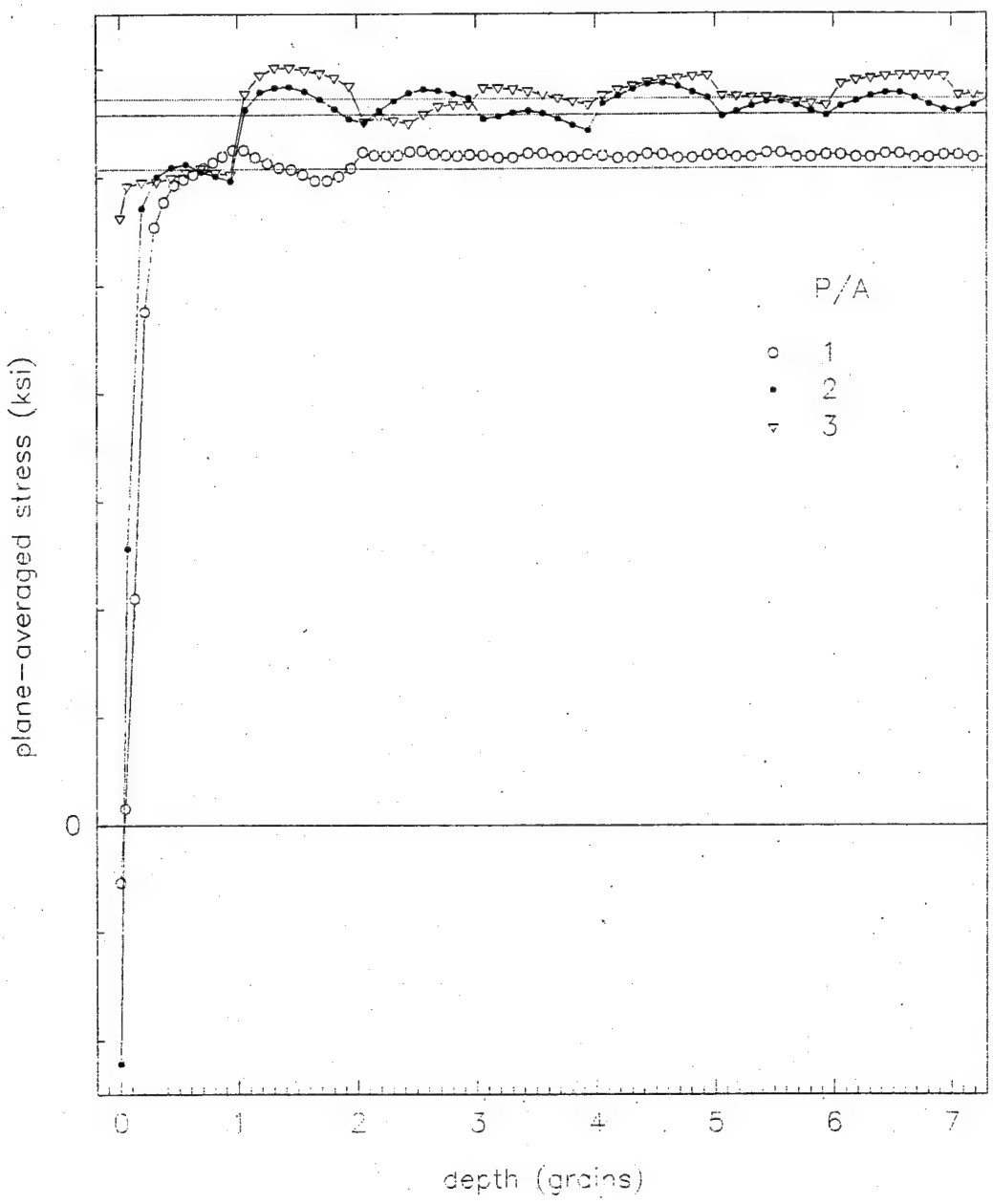

Figure 4.2.2.8-8. Plane-averaged longitudinal stress versus depth in specimens with grain aspect ratios (GAR) of 1, 2, and 3, and a yield point spread of 15 ksi, for a plastic strain in the vicinity of 5%, under load. (f_s = 0.33, E = 30,000 ksi, υ = 0.29, σ_{ys} = 15 ksi, σ_{yh} = 30 ksi, H_s = 0, H_h = 100 ksi.)

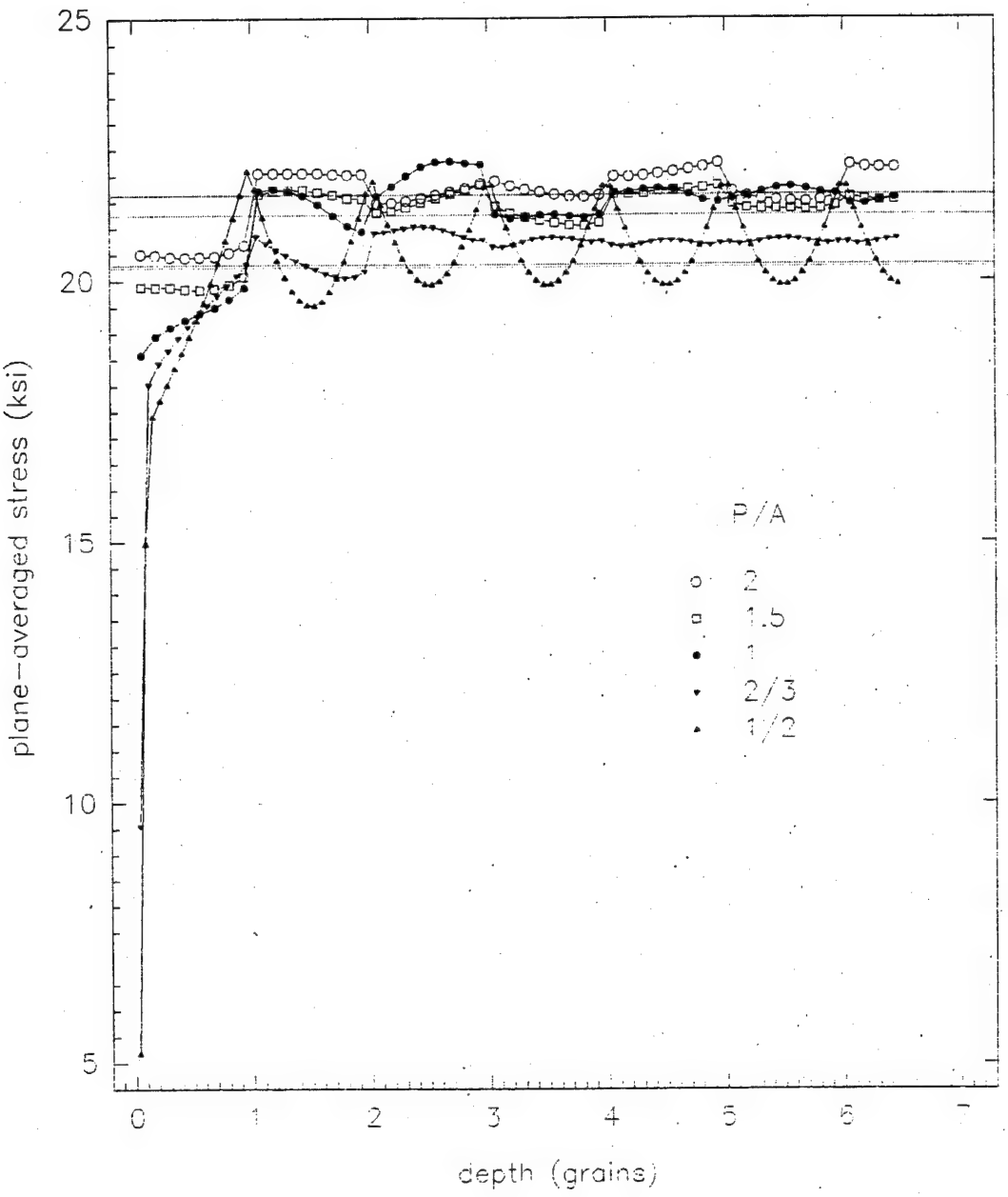

Figure 4.2.2.8-9. Plane-averaged longitudinal stress versus depth in specimens with grain aspect ratios (GAR) of 0.5, 2/3, 1, 1.5, and 2, and a soft grain concentration of 25%, for a plastic strain in the vicinity of 5%, under load. (f_s = 0.25, E = 30,000 ksi , υ = 0.29, σ_{ys} = 15 ksi, σ_{yh} = 20 ksi, H_s = 0, H_h = 100 ksi.)

YPS = 15 ksi and H_h = 0, and Table 4.2.2.9-4 for YPS = 15 ksi and H_h = 100 ksi. The discussion will first focus on the counterparts of the basic model in plane stress, discussed in detail in section 4.2.1, i.e., the models for which YPS = 5 ksi, H_h = 100 ksi, and H_s = 0 ksi.

As for plane stress, the plane-averaged longitudinal stress decreases markedly as the free surface is approached, as shown in Figures 4.2.2.9-1, 3, and 5 for PE, GPE, and AXS, respectively, for a plastic strain in the vicinity of 5%. The corresponding plots for plane stress are shown in Figure 4.2.1-3. The stress peaks at the vertical grain boundaries are much more pronounced than in plane stress because the lateral constraints allow higher stresses to build up at the corners by increasing the stress triaxiality. These stress oscillations are inherent to the array and obscure the surface layer effect. To isolate the effect due to the free surface, the same plots, but with the stresses corrected for the stress variations estimated in the corresponding surface-free model, are shown in Figure 4.2.2.9-2 for PE and Figure 4.2.2.9-4 for GPE. The innermost grain in the half-width model was used to estimate the stress variations in the absence of the free surface. A surface effect spanning up to three grains in PE and two grains in GPE and AXS is clearly evident. The steep stress drop near the free surface observed for plane stress is less pronounced in PE and absent in GPE and AXS.

The x-ray-averaged stress for a penetration depth of one grain is plotted versus the nominal applied stress in Figure 4.2.2.9-6 for PE, Figure 4.2.2.9-7 for GPE, and Figure 4.2.2.9-8 for AXS. The curves follow the same pattern as for plane stress, although the initial deviation of the x-ray stress from the applied stress is not as great as for plane stress, as reflected in the value of stress deviation ratio Ω: 0.27 (PS), 0.73 (PE), 0.72 (GPE), 0,73 (AXS). As noted for plane stress, there is an abrupt change in the x-ray stress at the onset of bulk yielding when the surface hard grains are forced to follow the bulk deformation; the curve becomes smooth again after bulk yielding (ϵ_p = 0.001-0.002). As for plane stress, there are significant x-ray residual stresses after unloading. At the onset of plasticity (ϵ_p = 0.00005), the values in PS and PE are essentially equal (-0.64, -0.63 ksi, resp.), while the values in GPE (-0.42 ksi) and AXS (-0.39 ksi) are approximately two thirds of the value in PS. For a plastic strain of 0.045, the values in PS and PE are again close (-3.66, -3.81 ksi, resp.), while the values in GPE (-1.79 ksi) and AXS (-2.19 ksi) are roughly half the

PS value. The surface-grain-averaged stress, σ_{rgl}, follows the same order as the x-ray stress at the onset of plasticity, but a partially different order at ϵ_p = 0.045, with the magnitude for PE dropping to third largest (Table 4.2.2.9-2). The different order reflects the greater weight given by the x-ray average to the stresses near the free surface compared with the grain-averaged stress, as mentioned previously. Based on the magnitude of the residual stresses and the overall levelling of the x-ray stress versus the applied stress, it is concluded that the x-ray surface layer effect is comparable in plane stress and plane strain, and smaller in GPE and AXS. It is of interest that altough the model with least constraint (PS) yields the greatest SLE, the model with the most constraint (PE) does not lead to the smallest SLE.

The effect of hard grain hardening and yield point spread in combination with constraint will now be considered. Because of the large amount of data, the reader is directed to the tables and graphs for the detailed information. The present discussion will focus on the overall trends. Plots of σ_{xl} and σ_{rgl} versus plastic strain are given in Figures 4.2.2.9-9 (YPS = 5 ksi, H_h = 0), 4.2.2.9-10 (YPS = 5 ksi, H_h = 100 ksi), 4.2.2.9-11 (YPS = 15 ksi, H_h = 0), and 4.2.2.9-12 (YPS = 15 ksi, H_h = 100 ksi). The residual stresses plateau when there is no grain hardening, as expected and discussed previously for plane stress (Section 4.2.2.5). In all cases there is a rapid increase in the residual stresses with plastic strain initially ($\epsilon_p \leq 0.002$), followed by a much more gradual increase (H_h = 100 ksi) or no increase (H_h = 0). With hard grain hardening, the residual stresses increase linearly in all cases, except for plane stress at the larger yield point spread. For the latter case, they tend to level off. The ranking of the magnitudes of the residual as a funtion of constraint at ϵ_p = 0.00005, 0.002, and 0.045 are given in Table 4.2.2.9-5. The overall rankings in terms of the yield point spread and residual stress type are:

YPS	σ_{xl}	σ_{rgl}
5 ksi	PS > AXS > PE > GPE	PS ≥ PE > AXS ≥ GPE
15 ksi	AXS > PS ≈ PE > GPE	PS ≥ PE > AXS ≈ GPE

In particular, the following general order emerges for the residual stresses:

PS ≥ PE > GPE

The ranking for the stress deviation ratio Ω is

$$PS << GPE \approx PE \approx AXS$$

Thus, in all cases, the slope of the x-ray stress versus the applied stress is much smaller in PE than for the other constraints, i.e., the x-ray stress is most depressed in PE. The surface layer depth hovers around two grains, approaching three grains for PE and approaching one grain and being not so well defined for AXS. The overall ranking is

$$PE \geq PS \approx GPE \geq AXS$$

As pointed out earlier, it is of interest that altough the least constraint (PS) yields the greatest SLE, the most constraint (PE) does not lead to the smallest SLE. The explanation for this paradoxical result is likely connected with the fact that the SLE depends on the *difference* in constraint between the surface and bulk grains, rather than the absolute degree of constraint.

In GPE and AXS there is also the possibility of nonzero transverse macrostresses. For both constraints, large compressive residual stresses were obtained in the transverse direction. The results are summarized in Table 4.2.2.9-6 for GPE and Table 4.2.2.9-7 for AXS. The x-ray-averaged and surface grain-averaged transverse stresses (σ_{Trxl} and σ_{Trgl}, resp.), along with the corresponding longitudinal stresses (σ_{rxl} and σ_{rgl}) for comparison, are plotted in Figures 4.2.2.9-13 (GPE: YPS = 5 ksi), 4.2.2.9-14 (GPE: YPS = 15 ksi), 4.2.2.9-15 (AXS: YPS = 5 ksi), and 4.2.2.9-16 (AXS: YPS = 15 ksi). When there is no grain hardening, these transverse compressive residual stresses invariably exceed the corresponding longitudinal stresses, being on the order of 1.5 to twice as large. With hard grain hardening (H_h = 100 ksi), both the longitudinal and transverse compressive residual stresses increase linearly. The slopes are comparable in AXS (Figures 4.2.2.9-15 and 16). In GPE, the residual longitudinal stresses increase faster than the corresponding transverse stresses; they are comparable in magnitude at ϵ_p = 0.05 (Table 4.2.2.9-6). The plane-averaged transverse stress $\langle\sigma_{33}\rangle_{pl}$ versus depth is shown in Figure 4.2.2.9-17 for the basic model under GPE and AXS. The transverse stress profiles are similar to the corresponding longitudinal stress profiles (Figures 4.2.2.9-7 and 4.2.2.9-9), with a surface layer effect of approximately two grains. For a given plastic strain, the value of $\langle\sigma_{33}\rangle_{pl}$ is

the same whether the specimen is loaded or unloaded, indicating the transverse macrostresses arise from differential plastic deformation.

4.2.3 Comparison of Model with Experimental Data

Given the bulk yield point, the proportional limit, Young's modulus and the Poisson ratio for a particular metal, the continuum surface layer effect can be estimated with the model presented in this study. Results are now given for iron, nickel, titanium (Ti-6Al-4V), and aluminum (Al 7475). The iron is of interest because of the substantial experimental data concerning its surface layer effect, including the mechanical onset of the effect. For nickel, Kolb and Macherauch [12] provide data which can be directly compared to the model predictions. The titanium alloy is noteworthy because it exhibits a considerable surface layer effect according to measurements in this study.

4.2.3.1 Onset of the Surface Layer Effect. According to this model, the onset of the x-ray effect occurs when the weakest grains in the surface layer start to yield, and the proportional limit of the specimen is at the yield point of the weakest grains in the surface layer. In other words, the onset of the x-ray effect and the proportional limit coincide. Knowing the yield surface of the individual grains, we can estimate the bulk strength of the aggregate. We can then determine the yield point of the surface relative to the bulk yield point and predict the stress at which departure from linearity should be detectable. Sasaki and Sato [14] experimentally determined that for bcc iron this departure from linearity is at 0.75 of the bulk yield point, and they concluded that the surface layer has a yield stress equal to 0.75 the bulk yield. Calculations will now be performed for comparison with these experimental results.

The yield surface of the crystal can be estimated from its dominant slip system group, assuming that the critical shear stress is independent of the slip plane and that there is no work hardening. Let the dominant slip system group consist of N slip systems and let the nth slip system relative to an arbitrary set of Cartesian axes 1, 2, 3 be specified by the unit vector $m_i^{(n)}$ perpendicular to the slip plane, and by the unit vector $n_i^{(n)}$ in the slip direction. In a crystal in an arbitrary orientation subjected to a uniform stress σ_{ij}, the resolved shear stress on the nth slip system is:

$$\Gamma^{(n)} = \sigma_{ij}\, m_j^{(n)}\, n_i^{(n)}. \qquad (10)$$

Table 4.2.2.9-1. Effect of constraint for a yield point spread of 5 ksi and no grain hardening. For all the models: f_s = 0.33, E = 30,000 ksi, υ = 0.29, σ_{ys} = 15 ksi, σ_{yh} = 20 ksi (σ_{ymix} = 18.33 ksi), $H_s = H_s$ = 0 ksi.

Model		SASZAHG	SEHZ1GG	SFHZ1GG	SXHZIGG
Constraint		PS	PE	GPE	AXS
σ_{yB} (ksi)		17.95	20.27	18.14	18.14
Ω		0.18	0.74	0.71	0.73
τ (gr)		1-2	2-3	2	≈1
surface-grain-averaged stress, σ_{rg1}					
ϵ_p	0.00005	-0.31	-0.38	-0.21	-0.18
	0.0005	-0.94	-0.50	-0.09	-0.37
	0.002	-0.91	-0.39	-0.10	-0.47
	0.01	-0.88	-0.37	-0.10	-0.49
	0.045	-0.81	-0.41	-0.10	-0.49
X-ray-averaged residual stress, σ_{rx1}					
ϵ_p	0.00005	-0.60	-0.76	-0.39	-0.33
	0.0005	-2.15	-1.25	-0.34	-0.59
	0.002	-2.66	-1.15	-0.40	-0.73
	0.01	-3.09	-1.18	-0.41	-0.74
	0.045	-3.01	-1.27	-0.41	-0.74

Table 4.2.2.9-2. Effect of constraint for a yield point spread of 5 ksi and with hard grain hardening . For all the models: f_s = 0.33, E = 30,000 ksi , υ = 0.29, σ_{ys} = 15 ksi, σ_{yh} = 20 ksi (σ_{ymix} = 18.33 ksi), H_h = 100 ksi, H_s = 0.

Model		SAH01HA	SBH01GC	SCH01GC	SXC01GL
Constraint		PS	PE	GPE	AXS
σ_{yB} (ksi)		17.98	20.50	18.27	18.27
H_B (ksi)		41	59	52	52
Ω		0.27	0.73	0.72	0.73
τ (gr)		2	2-3	2	2
Average residual stress in surface grain layer, σ_{rgl}					
ϵ_p	0.00005	-0.35	-0.34	-0.23	-0.22
	0.0005	-1.03	-0.61	-0.17	-0.40
	0.002	-0.94	-0.53	-0.19	-0.53
	0.01	-0.98	-0.50	-0.29	-0.69
	0.045	-1.57	-1.11	-0.75	-1.37
X-ray-averaged residual stress, σ_{rxl}					
ϵ_p	0.00005	-0.64	-0.63	-0.42	-0.39
	0.0005	-2.21	-1.39	-0.45	-0.64
	0.002	-2.58	-1.43	-0.52	-0.83
	0.01	-2.79	-1.92	-0.75	-1.07
	0.045	-3.66	-3.81	-1.79	-2.19

Table 4.2.2.9-3. Effect of constraint for a yield point spread of 15 ksi and no grain hardening. For all the models f_s = 0.33, E = 30,000 ksi , υ = 0.29, σ_{ys} = 15 ksi, σ_{yh} = 30 ksi, $H_h = H_s = 0$.

Model		SDHZ2GG	SBHZ2GG	SCHZ2GG	SXHZ2GG
Constraint		PS	PE	GPE	AXS
σ_{yB} (ksi)		22.18	24.60	23.71	23.79
Ω		0.28	0.73	0.69	0.71
τ (gr)		2	2-3	2	1-2
Average residual stress in surface grain layer, σ_{rg1}					
ϵ_p	0.00005	-0.31	-0.35	-0.22	-0.18
	0.0005	-2.65	-2.19	-1.75	-2.04
	0.002	-2.83	-2.22	-1.49	-2.67
	0.010	-2.63	-2.32	-1.60	-2.81
	0.045	-2.49	-2.35	-1.60	-2.81
X-ray-averaged residual stress, σ_{rx1}					
ϵ_p	0.00005	-0.60	-0.66	-0.41	-0.33
	0.0005	-5.24	-4.48	-3.70	-3.63
	0.002	-7.57	-5.01	-3.80	-4.23
	0.010	-8.43	-5.48	-4.05	-4.39
	0.045	-8.28	-5.63	-4.06	-4.39

Table 4.2.2.9-4. Effect of constraint for a yield point spread of 15 ksi and with hard grain hardening. For all the models $f_s = 0.33$, $E = 30{,}000$ ksi, $\upsilon = 0.29$, $\sigma_{ys} = 15$ ksi, $\sigma_{yh} = 30$ ksi, $H_h = 100$, $H_s = 0$.

Model		SAH02GL	SBH02GL	SCH02GK	SXC02HA
Constraint		PS	PE	GPE	AXS
σ_{yB} (ksi)		21.83	24.77	23.62	23.98
H_B (ksi)		37	68	48	48
Ω		0.27	0.68	0.68	0.69
τ (gr)		2	2	2	1-2
Average residual stress in surface grain layer, σ_{rgl}					
ϵ_p	0.00005	-0.35	-0.36	-0.23	-0.22
	0.0005	-2.94	-2.19	-1.75	-2.31
	0.002	-3.14	-2.26	-1.70	-2.81
	0.010	-3.01	-2.44	-1.75	-3.22
	0.045	-3.17	-3.48	-2.58	-4.08
X-ray-averaged residual stress, σ_{rxl}					
ϵ_p	0.00005	-0.64	-0.68	-0.42	-0.39
	0.0005	-5.54	-4.43	-3.73	-4.00
	0.002	-7.77	-5.14	-3.90	-4.47
	0.010	-8.84	-6.22	-4.51	-5.08
	0.045	-9.07	-9.86	-6.43	-6.56

Table 4.2.2.9-5. Ranking of the surface layer effect as a function of constraint. For all the models $f_s = 0.33$, $E = 30{,}000$ ksi, $\upsilon = 0.29$, $\sigma_{ys} = 15$ ksi.

Criterion		No Hardening (H_h = 0 ksi)	Hardening (H_h = 100 ksi)
YPS = 5 ksi			
Ω		S >>G ≈ A ≈ E	S >>G ≈ E ≈ A
τ (grain)		E > G ≈ S > A	E ≥ S ≈ G ≈ A
Stress drop near surface		S >>E > G ≈ A	S > E >>G ≈A
σ_{rx1} ϵ_p =	0.00005	E ≥ S > G ≈ A	E ≈ S > G ≈ A
	0.002	S > E > A > G	S > E > A ≈ G
	0.045	S >>E > A > G	E ≥ S > A ≈ G
σ_{rg1}	0.00005	E ≥ S > G ≈ A	S ≈ E > G ≈ A
	0.002	S > A ≥ E >>G	S > E > A > G
	0.045	S > A ≥ E >>G	S ≥ A ≥ E > G
YPS = 15 ksi			
Ω		S >>G ≈ A ≈ E	S >>G ≈ E ≈ A
τ (grain)		E ≥ S ≈ G ≥ A	S ≈ E ≈ G ≥ A
Stress drop near surface		S >>E ≈ G > A	S > E > G >>A
σ_{rx1} ϵ_p =	0.00005	E ≈ S > G ≈ A	S > E > G ≈ A
	0.002	S > E > A ≈ G	S > E > A ≈ G
	0.045	S > E > A ≈ G	S ≥ E > A ≈ G
σ_{rg1}	0.00005	E ≥ S > G ≈ A	E ≈ S > G ≈ A
	0.002	S ≈ A > E > G	S ≥ A > E > G
	0.045	A ≥ S ≈ E > G	A ≥ E ≥ S > G

Table 4.2.2.9-6. Transverse residual stresses for generalized plane strain models with yield point spreads of 5 and 15 ksi, with and without hard grain hardening (H_s = 100 or 0 ksi). For all the models: f_s = 0.33, E = 30,000 ksi, υ = 0.29, σ_{ys} = 15 ksi, H_s = 0 ksi.

YPS (ksi)		5		15	
H_h (ksi)		0	100	0	100
Model		SFHZ1GG	SCH01GC	SCHZ2GG	SCH02GK
σ_{yB} (ksi)		18.14	18.27	23.71	23.62
surface-grain-averaged stress, σ_{rgl}					
ϵ_p	0.00005	0.02	0.02	0.02	0.01
	0.0005	-0.15	-0.29	-0.41	-0.42
	0.002	-0.17	-0.29	-1.95	-1.70
	0.01	-0.17	-0.37	-2.33	-2.31
	0.045	-0.17	-0.70	-2.34	-2.56
X-ray-averaged residual stress, σ_{rxl}					
ϵ_p	0.00005	0.03	0.02	0.03	0.02
	0.0005	-0.51	-0.72	-1.25	-1.25
	0.002	-0.65	-0.78	-4.96	-4.86
	0.01	-0.67	-1.02	-6.14	-6.30
	0.045	-0.67	-1.94	-6.14	-7.29

Table 4.2.2.9-7. Transverse residual stresses for axisymmetric models with yield point spreads of 5 and 15 ksi, with and without hard grain hardening (H_s = 100 or 0 ksi). For all the models: f_s = 0.33, E = 30,000 ksi , υ = 0.29, σ_{ys} = 15 ksi, H_s = 0 ksi.

YPS (ksi)		5		15	
H_h (ksi)		0	100	0	100
Model		SXHZ1GG	SXC01GL	SXHZ2GG	SXH02HA
σ_{yB} (ksi)		18.14	18.27	23.79	23.98
surface-grain-averaged stress, σ_{rg1}					
ϵ_p	0.00005	-0.03	-0.05	-0.03	-0.05
	0.0005	-0.73	-0.74	-2.41	-2.52
	0.002	-0.95	-1.00	-5.03	-4.97
	0.01	-0.99	-1.24	-5.26	-5.56
	0.045	-0.99	-2.19	-5.26	-6.53
X-ray-averaged residual stress, σ_{rx1}					
ϵ_p	0.00005	-0.02	-0.05	-0.02	-0.05
	0.0005	-1.03	-1.07	-3.08	-3.29
	0.002	-1.32	-1.41	-7.03	-7.08
	0.01	-1.35	-1.73	-7.25	-7.81
	0.045	-1.35	-3.07	-7.25	-9.26

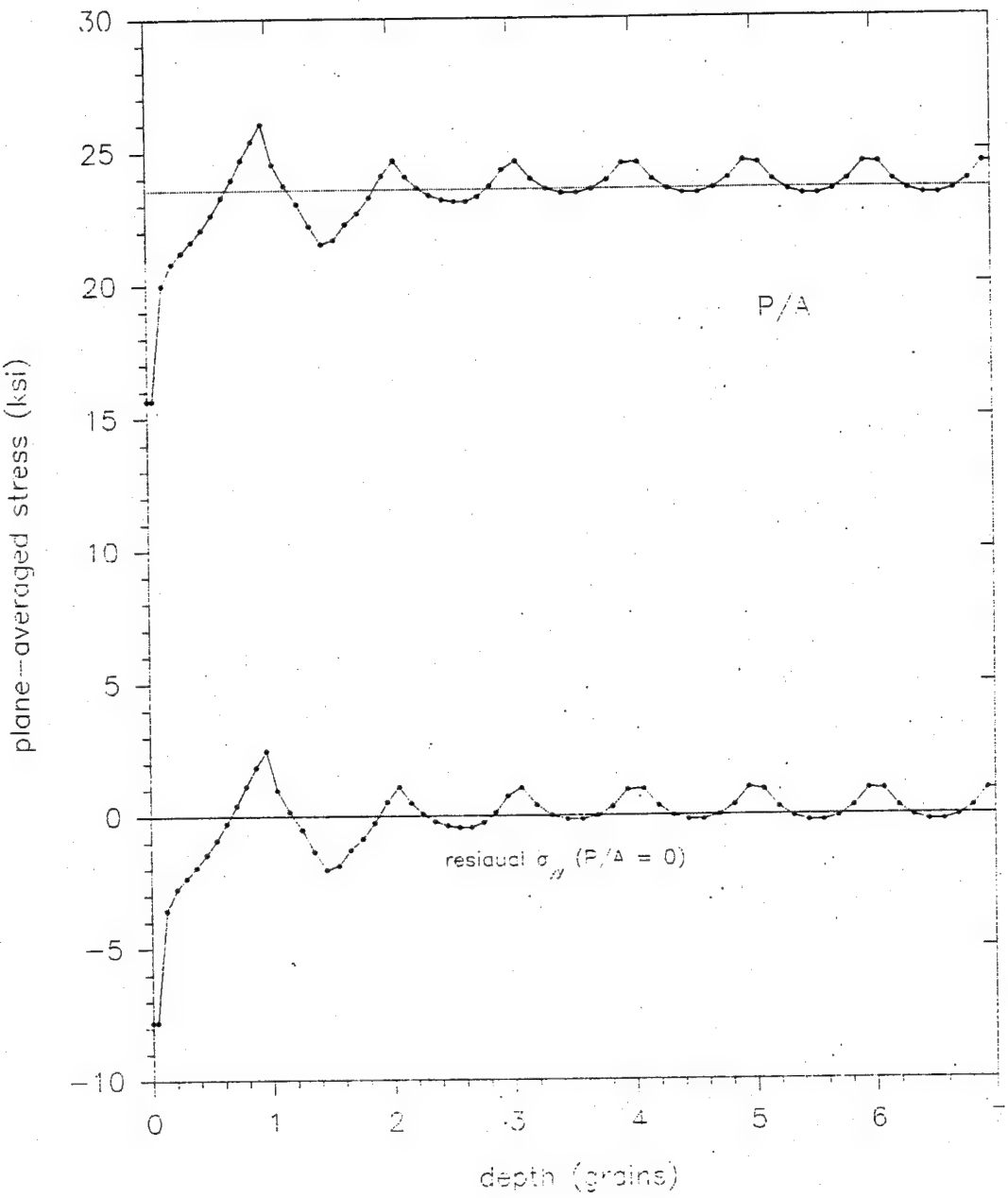

Figure 4.2.2.9-1. Plane-averaged longitudinal stress versus depth for a model under plane strain and a plastic strain in the vicinity of 5%, under load. The yield point spread is 5 ksi, and the hard grain hardening is 100 ksi. (f_s = 0.33, E = 30,000 ksi, υ = 0.29, σ_{ys} = 15 ksi, σ_{yh} = 20 ksi, H_s = 0, H_h = 100 ksi.)

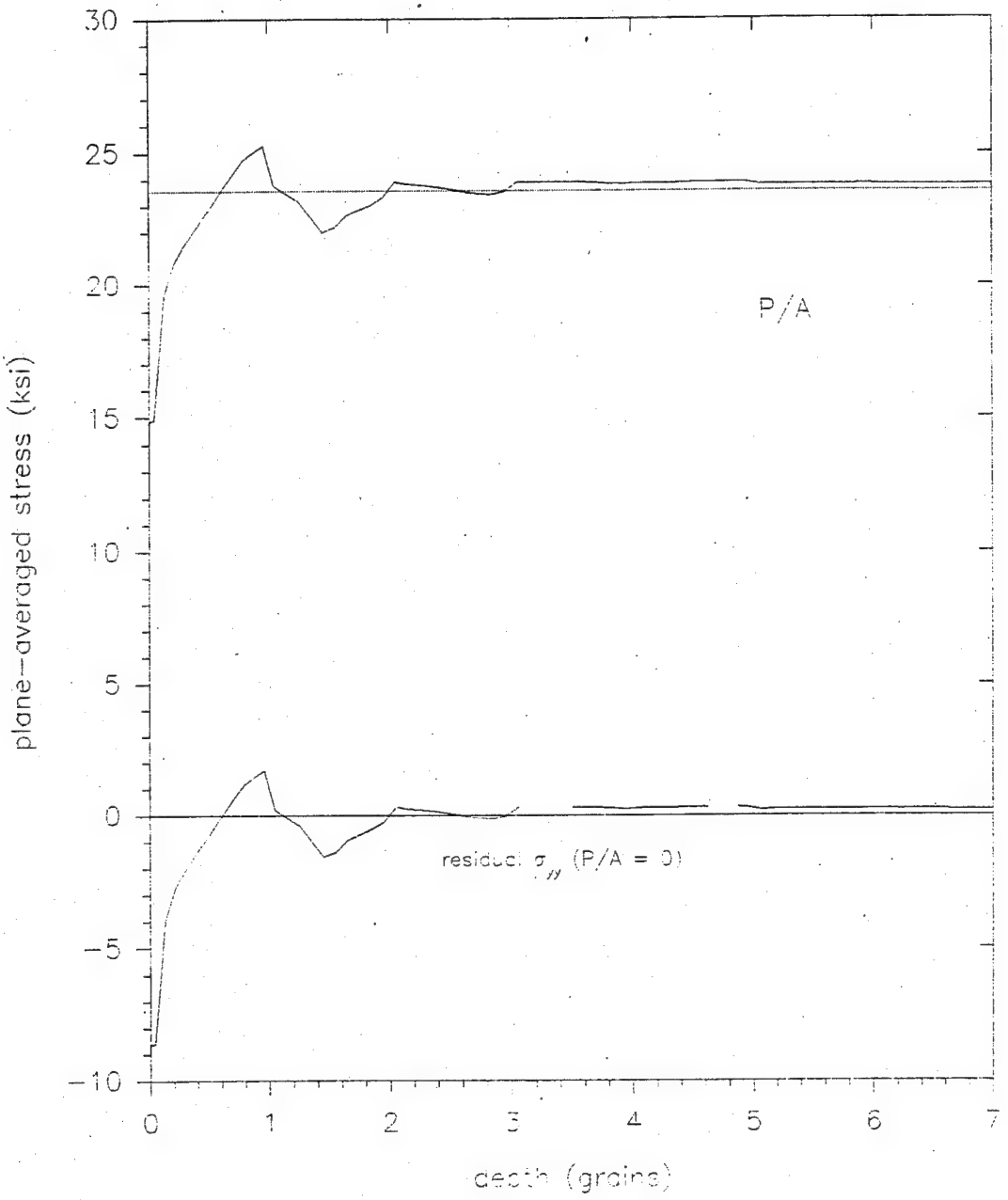

Figure 4.2.2.9-2. Corrected plane-averaged longitudinal stress versus depth for a model under plane strain and a plastic strain in the vicinity of 5%, under load. The uncorrected plot is shown in the previous Figure. (f_s = 0.33, E = 30,000 ksi, υ = 0.29, σ_{ys} = 15 ksi, σ_{yh} = 20 ksi, H_s = 0, H_h = 100 ksi.)

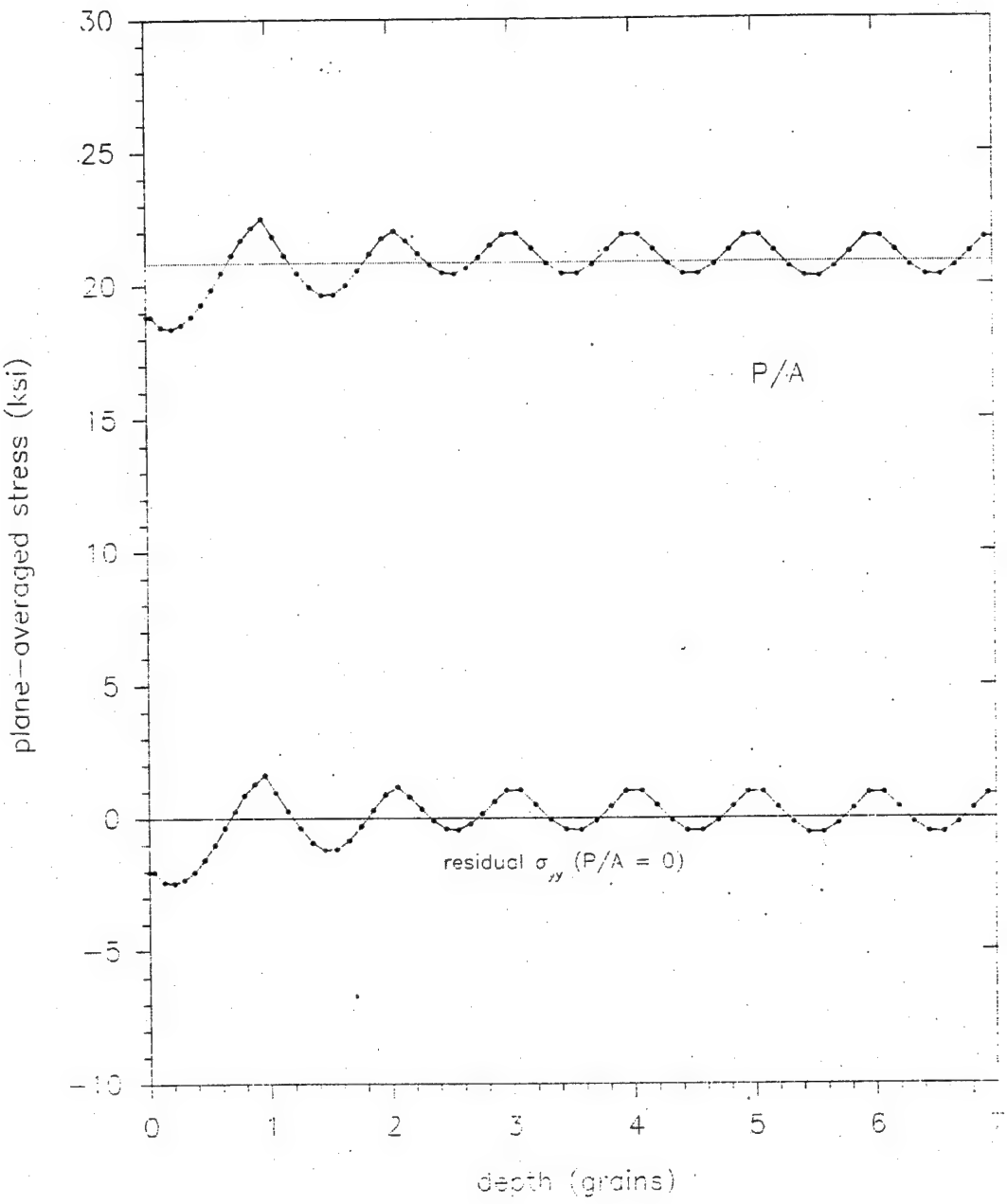

Figure 4.2.2.9-3. Plane-averaged longitudinal stress versus depth for a model under generalized plane strain and a plastic strain in the vicinity of 5%, under load. The yield point spread is 5 ksi, and the hard grain hardening is 100 ksi. (f_s = 0.33, E = 30,000 ksi , υ = 0.29, σ_{ys} = 15 ksi, σ_{yh} = 20 ksi, H_s = 0, H_h = 100 ksi.)

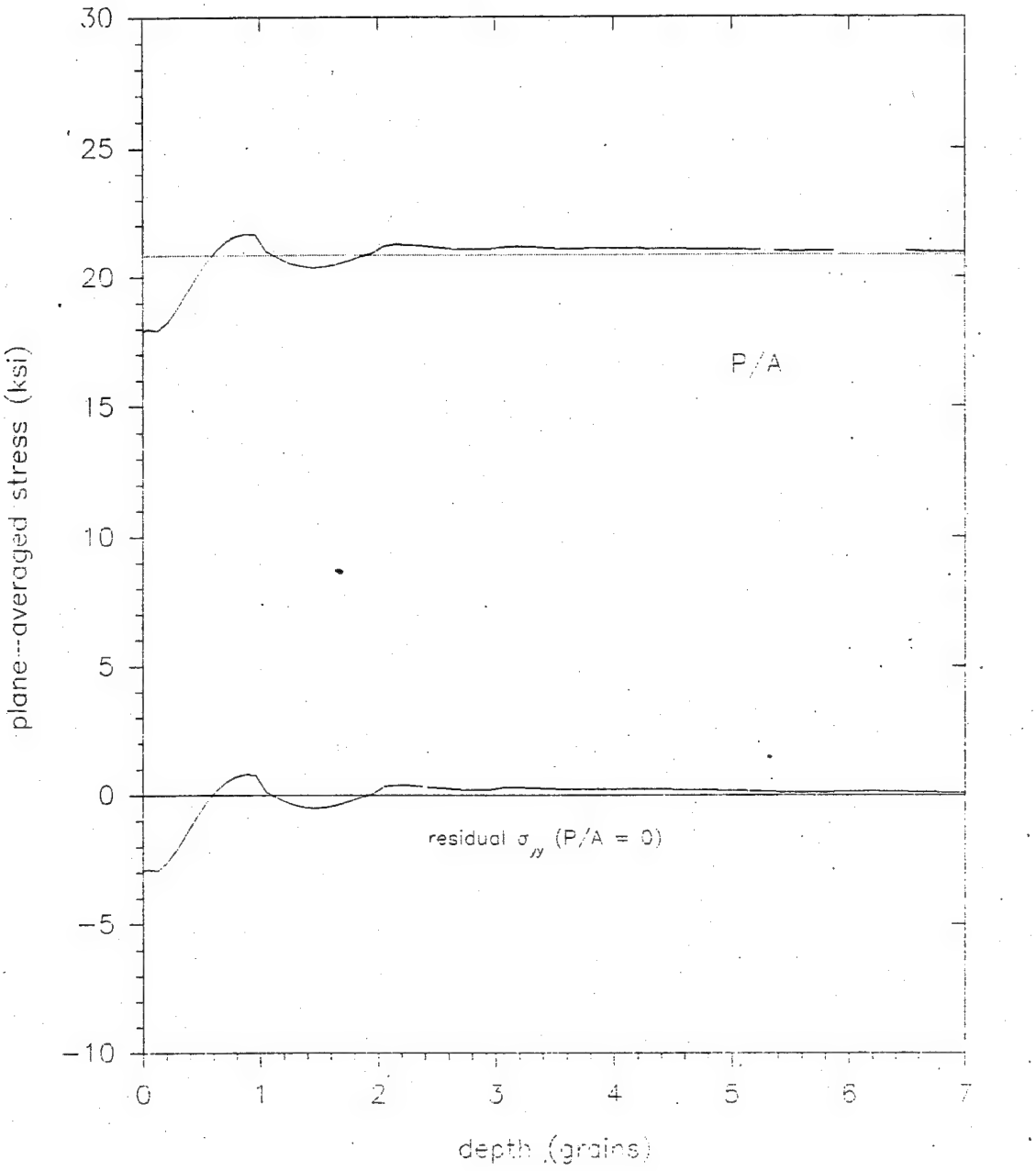

Figure 4.2.2.9-4. Corrected plane-averaged longitudinal stress versus depth for a model under generalized plane strain and a plastic strain in the vicinity of 5%, under load. The uncorrected plot is shown in the previous Figure. (f_s = 0.33, E = 30,000 ksi, υ = 0.29, σ_{ys} = 15 ksi, σ_{yh} = 20 ksi, H_s = 0, H_h = 100 ksi.)

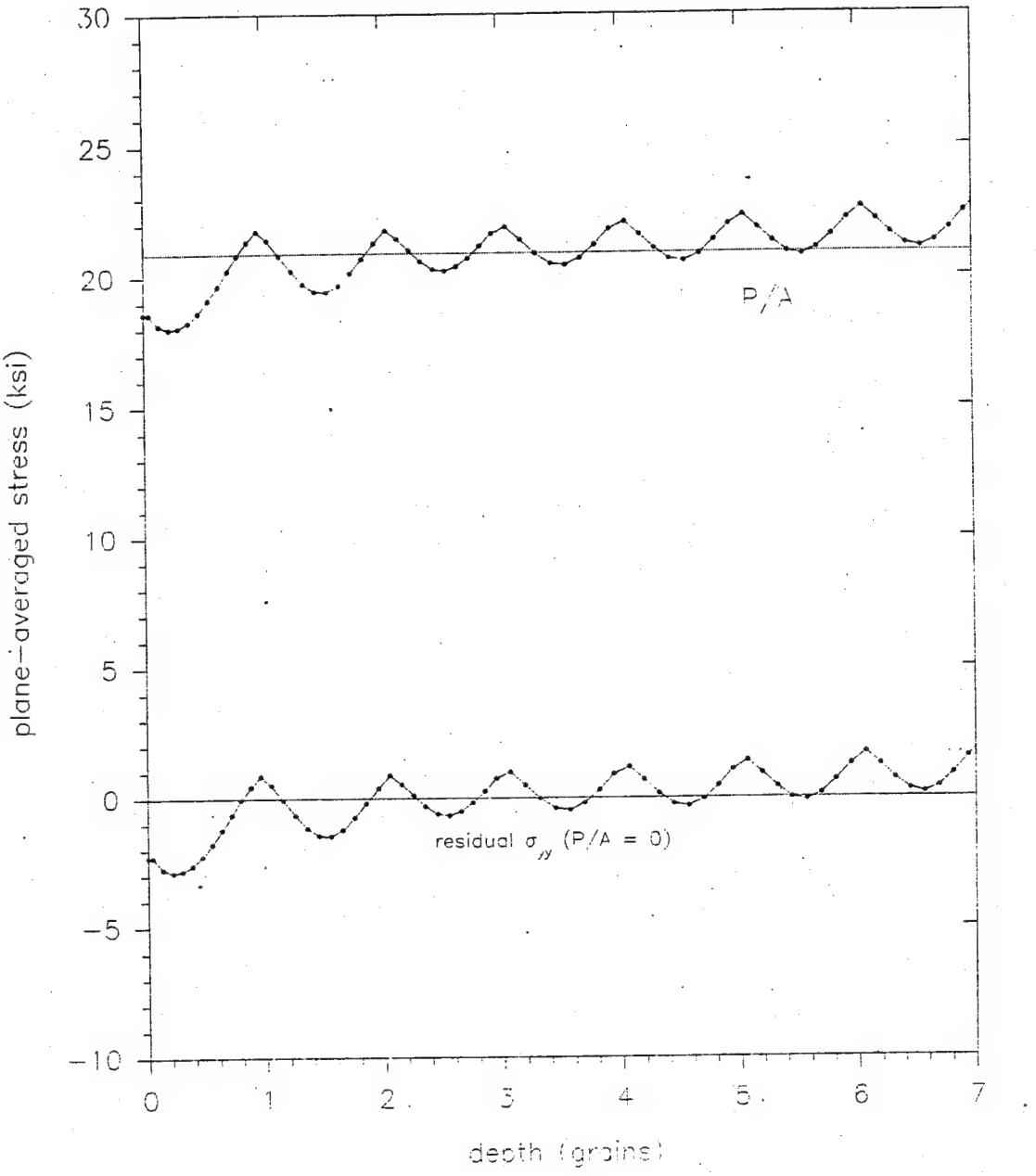

Figure 4.2.2.9-5. Plane-averaged longitudinal stress versus depth for an axisymmetric model, at a plastic strain in the vicinity of 5%, under load. The yield point spread is 5 ksi, and the hard grain hardening is 100 ksi. (f_s = 0.33, E = 30,000 ksi, υ = 0.29, σ_{ys} = 15 ksi, σ_{yh} = 20 ksi, H_s = 0, H_h = 100 ksi.)

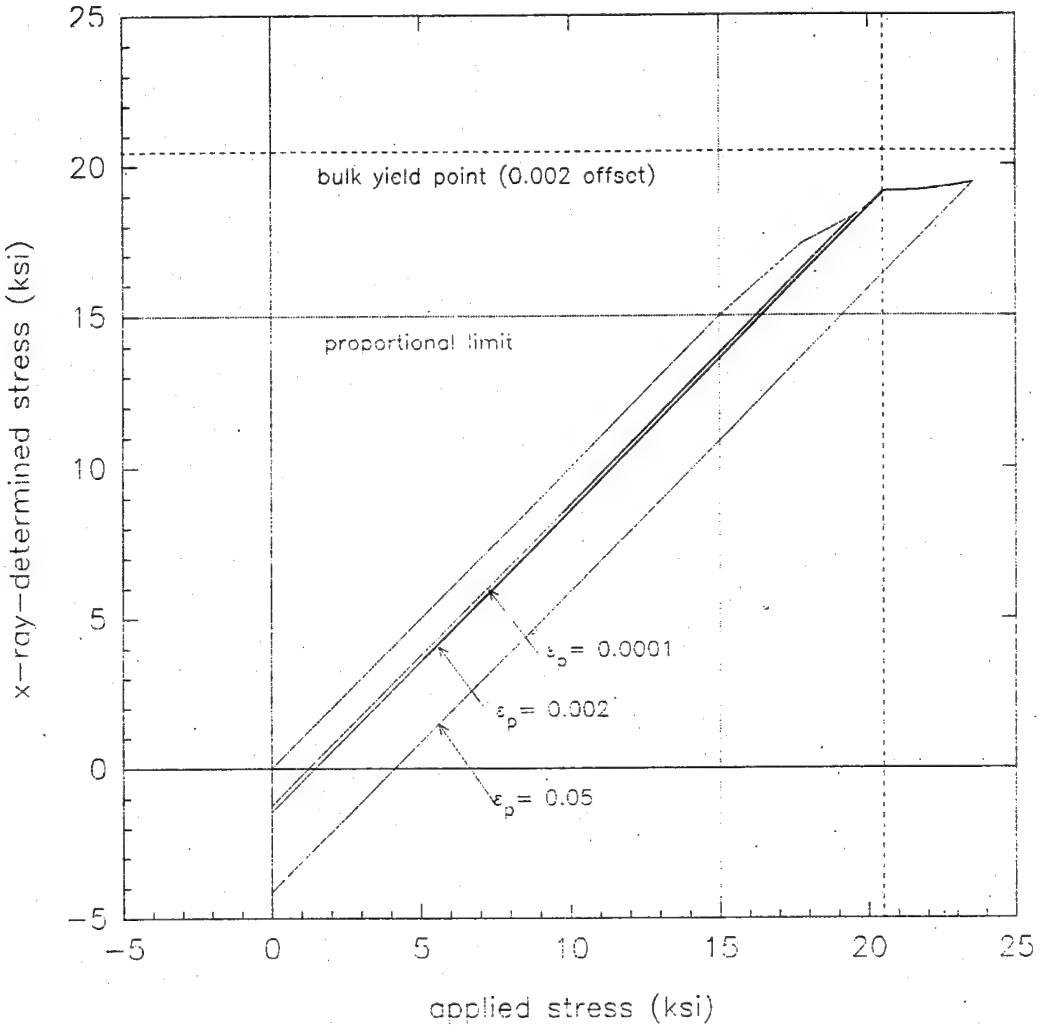

Figure 4.2.2.9-6. X-ray-determined stress versus the nominal applied stress for a model under plane strain. The x-ray effective penetration depth is one grain. (f_s = 0.33, E = 30,000 ksi, υ = 0.29, σ_{ys} = 15 ksi, σ_{yh} = 20 ksi, H_s = 0, H_h = 100 ksi.)

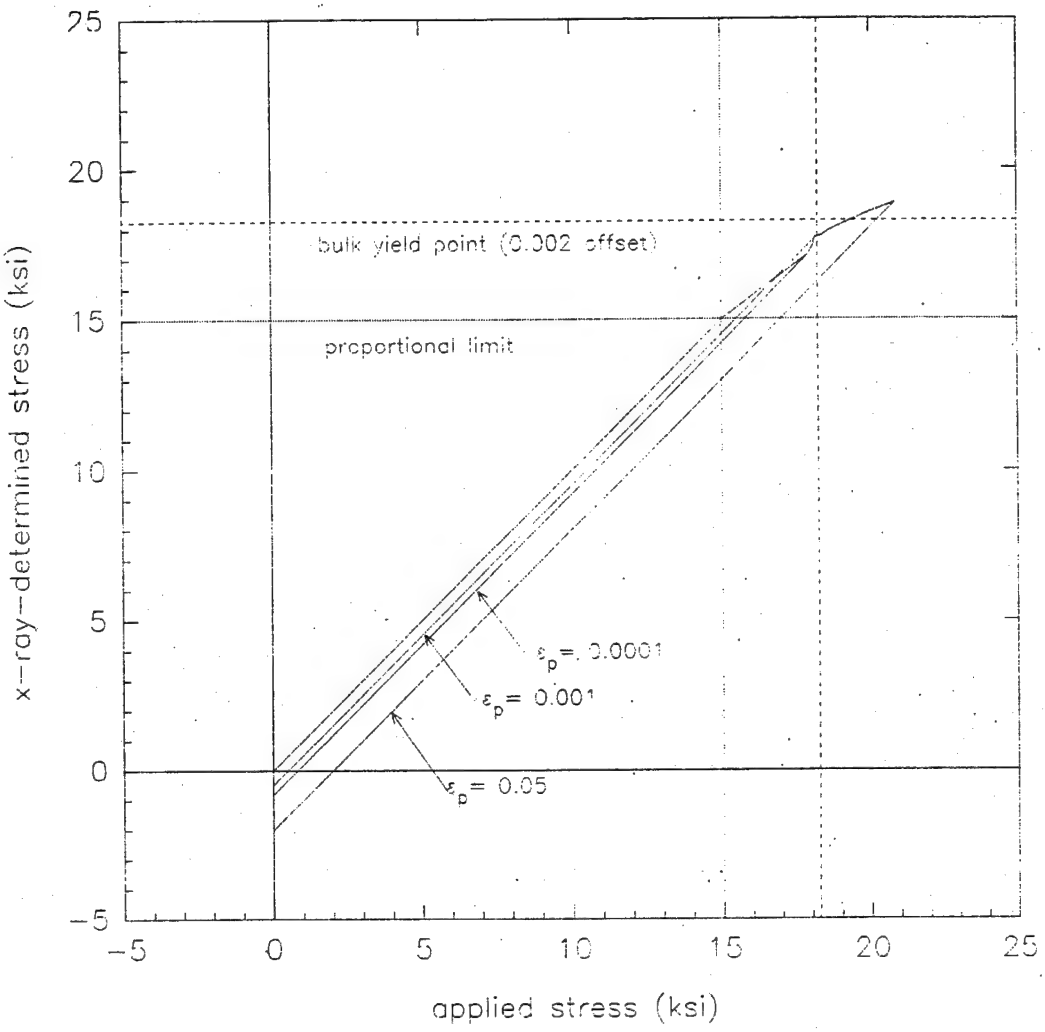

Figure 4.2.2.9-7. X-ray-determined stress versus the nominal applied stress for a model under generalized plane strain. The x-ray effective penetration depth is one grain. (f_s = 0.33, E = 30,000 ksi, υ = 0.29, σ_{ys} = 15 ksi, σ_{yh} = 20 ksi, H_s = 0, H_h = 100 ksi.)

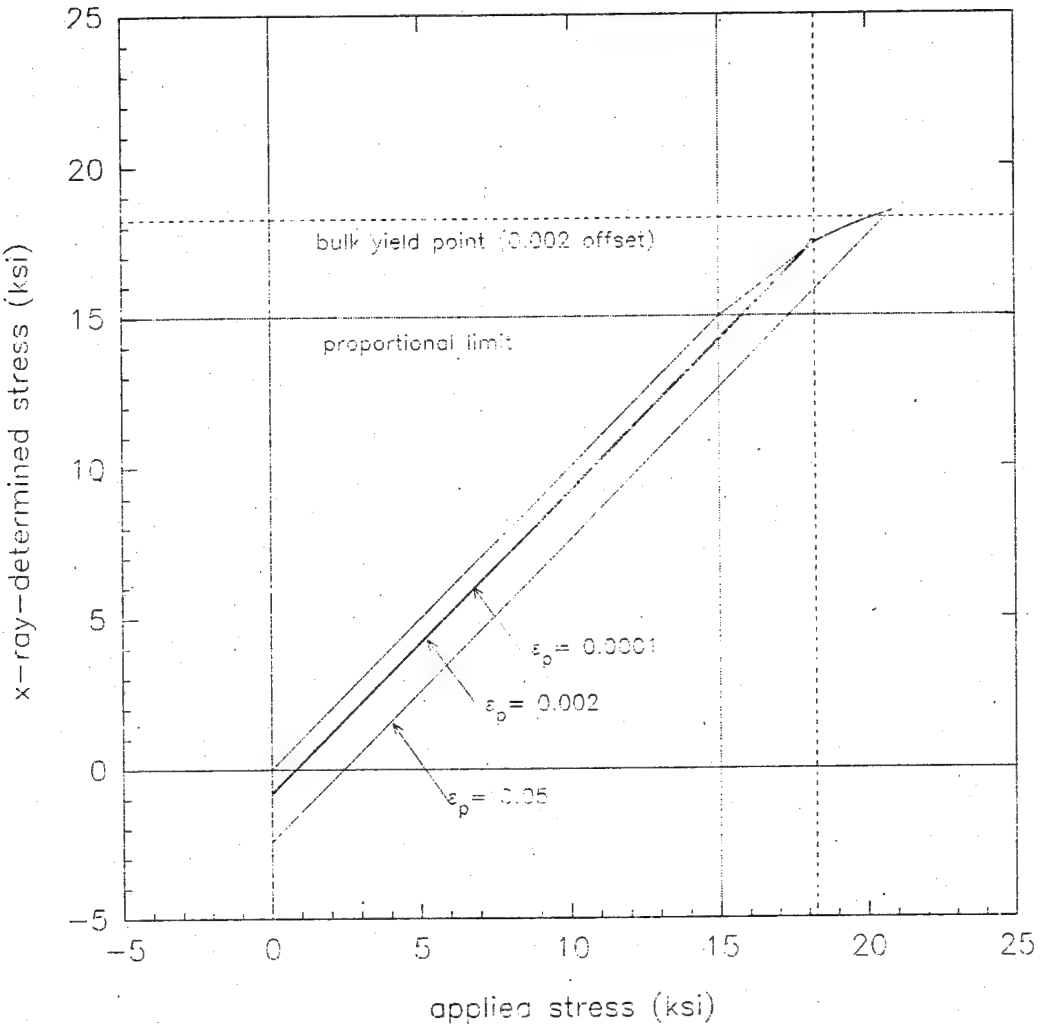

Figure 4.2.2.9-8. X-ray-determined stress versus the nominal applied stress for an axisymmetric model. The x-ray effective penetration depth is one grain. (f_s = 0.33, E = 30,000 ksi, υ = 0.29, σ_{ys} = 15 ksi, σ_{yh} = 20 ksi, H_s = 0, H_h = 100 ksi.)

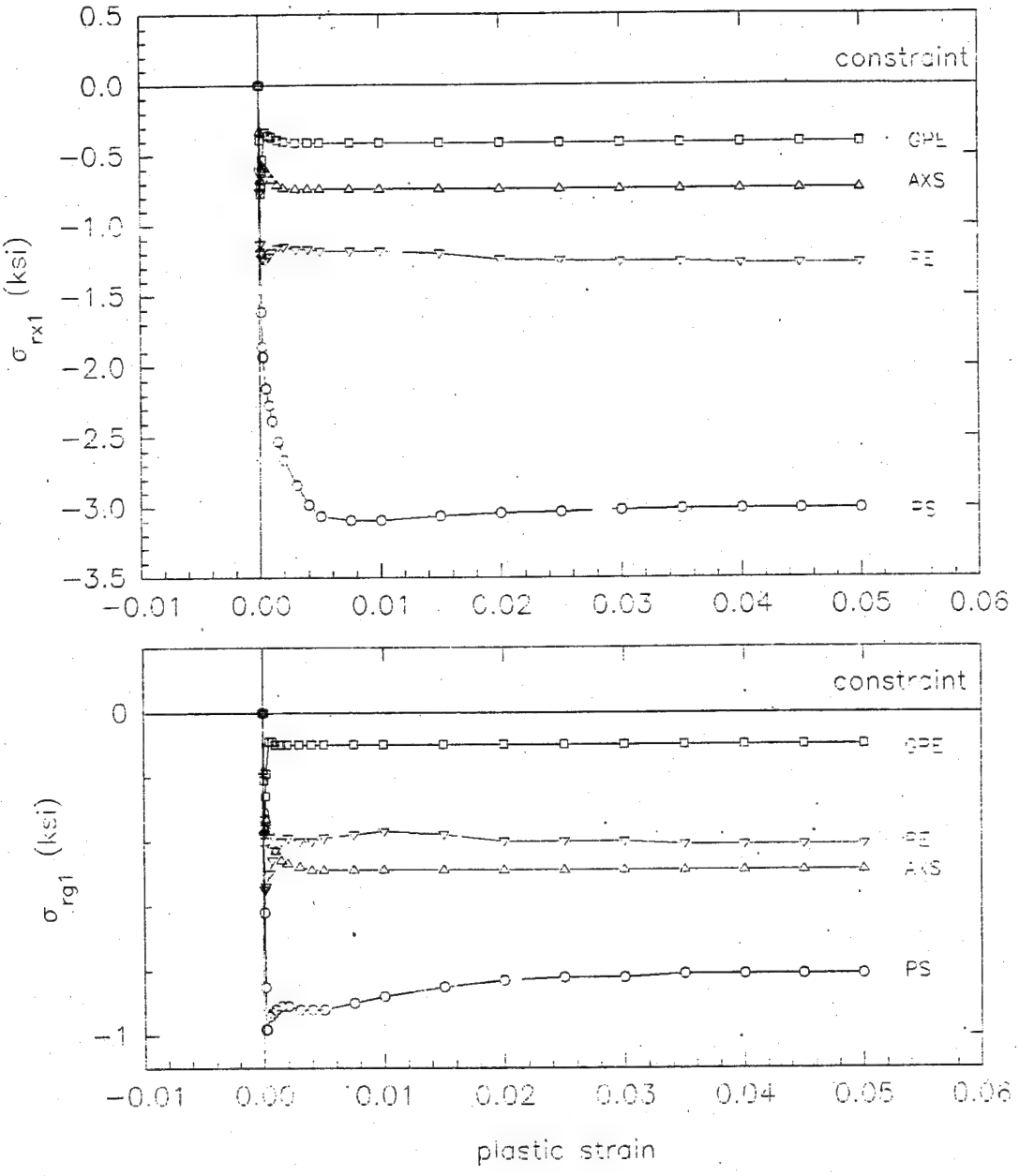

Figure 4.2.2.9-9. The x-ray-averaged residual stress (σ_{rx1}) and the surface-grain-averaged residual stress (σ_{rg1}) versus plastic strain for models under plane stress (PS), plane strain (PE), generalized plane strain (GPE), and axisymmetry (AXS), having a yield point spread of 5 ksi and no grain hardening. (f_s = 0.33, E = 30,000 ksi, υ = 0.29, σ_{ys} = 15 ksi, σ_{yh} = 20 ksi, H_s = H_h = 0 ksi.)

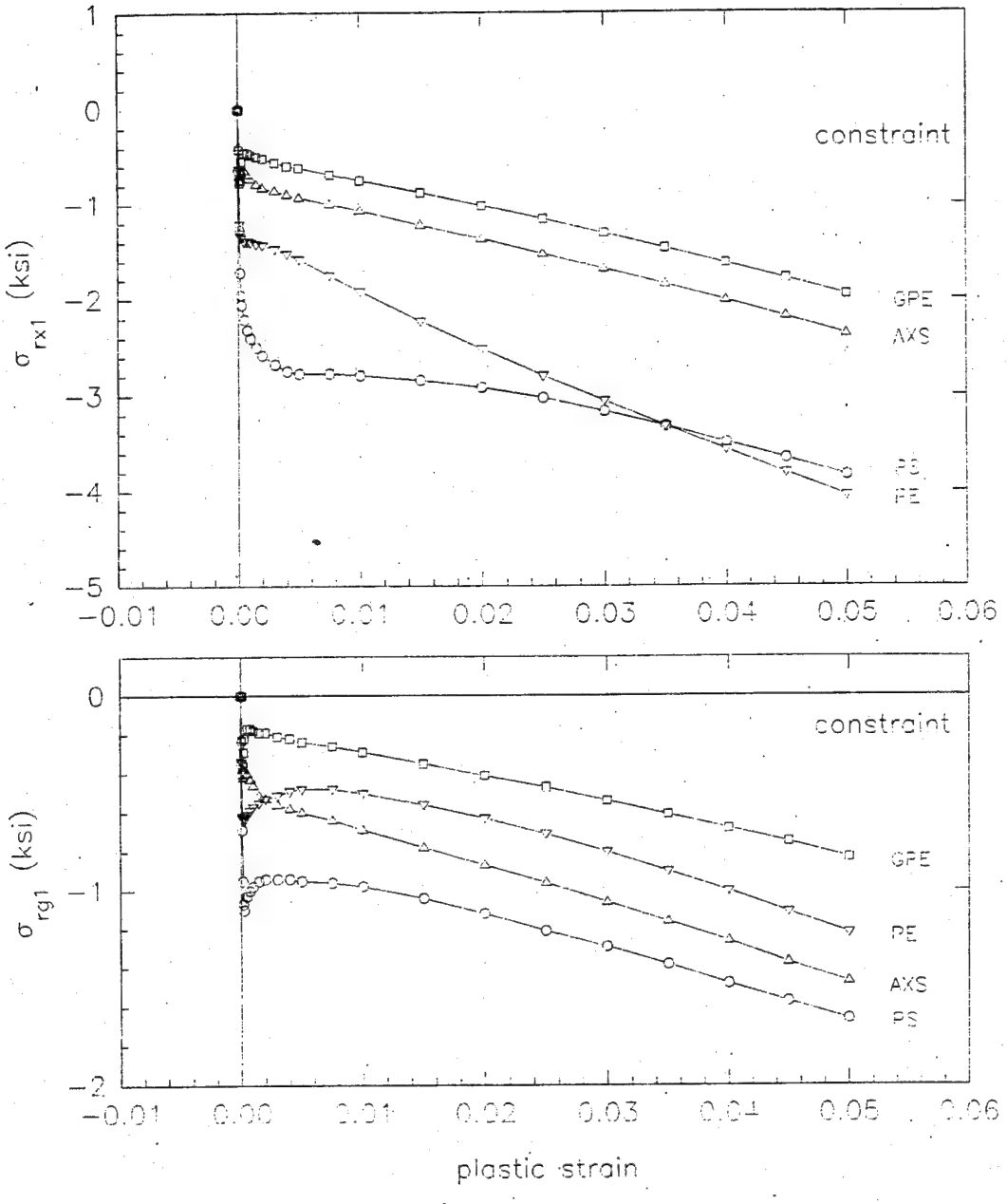

Figure 4.2.2.9-10. The x-ray-averaged residual stress (σ_{rx1}) and the surface-grain-averaged residual stress (σ_{rg1}) versus plastic strain for models under plane stress (PS), plane strain (PE), generalized plane strain (GPE), and axisymmetry (AXS), having a yield point spread of 5 ksi and hard grain hardening of 100 ksi. (f_s = 0.33, E = 30,000 ksi, υ = 0.29, σ_{ys} = 15 ksi, σ_{yh} = 20 ksi, H_s = 0 ksi, H_h = 100 ksi.)

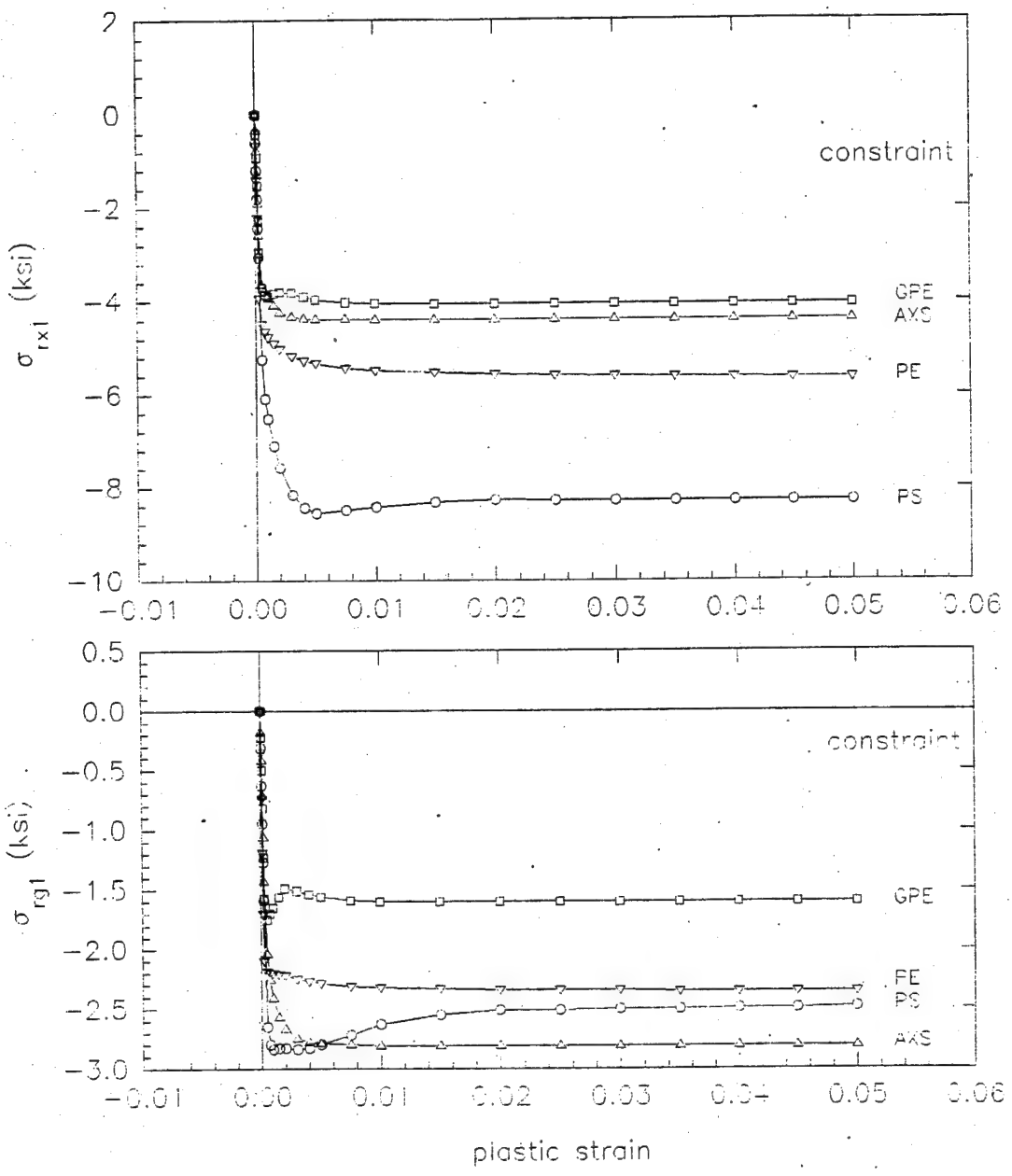

Figure 4.2.2.9-11. The x-ray-averaged residual stress (σ_{rx1}) and the surface-grain-averaged residual stress (σ_{rg1}) versus plastic strain for models under plane stress (PS), plane strain (PE), generalized plane strain (GPE), and axisymmetry (AXS), having a yield point spread of 15 ksi and no grain hardening. (f_s = 0.33, E = 30,000 ksi, υ = 0.29, σ_{ys} = 15 ksi, σ_{yh} = 30 ksi, H_s = H_h = 0 ksi.)

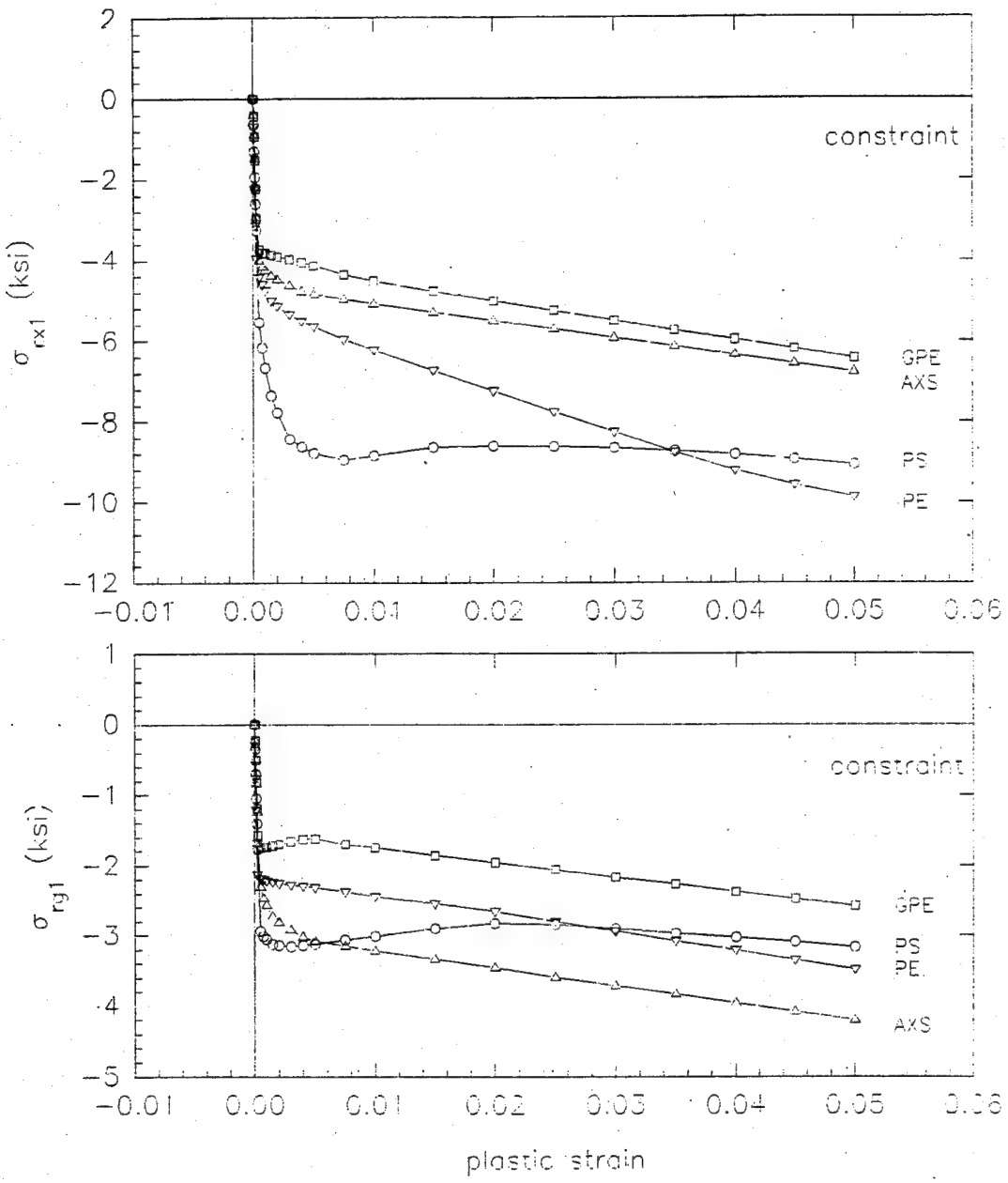

Figure 4.2.2.9-12. The x-ray-averaged residual stress (σ_{rx1}) and the surface-grain-averaged residual stress (σ_{rg1}) versus plastic strain for models under plane stress (PS), plane strain (PE), generalized plane strain (GPE), and axisymmetry (AXS), having a yield point spread of 15 ksi and hard grain hardening of 100 ksi. (f_s = 0.33, E = 30,000 ksi, υ = 0.29, σ_{ys} = 15 ksi, σ_{yh} = 30 ksi, H_s = 0 ksi, H_h = 100 ksi.)

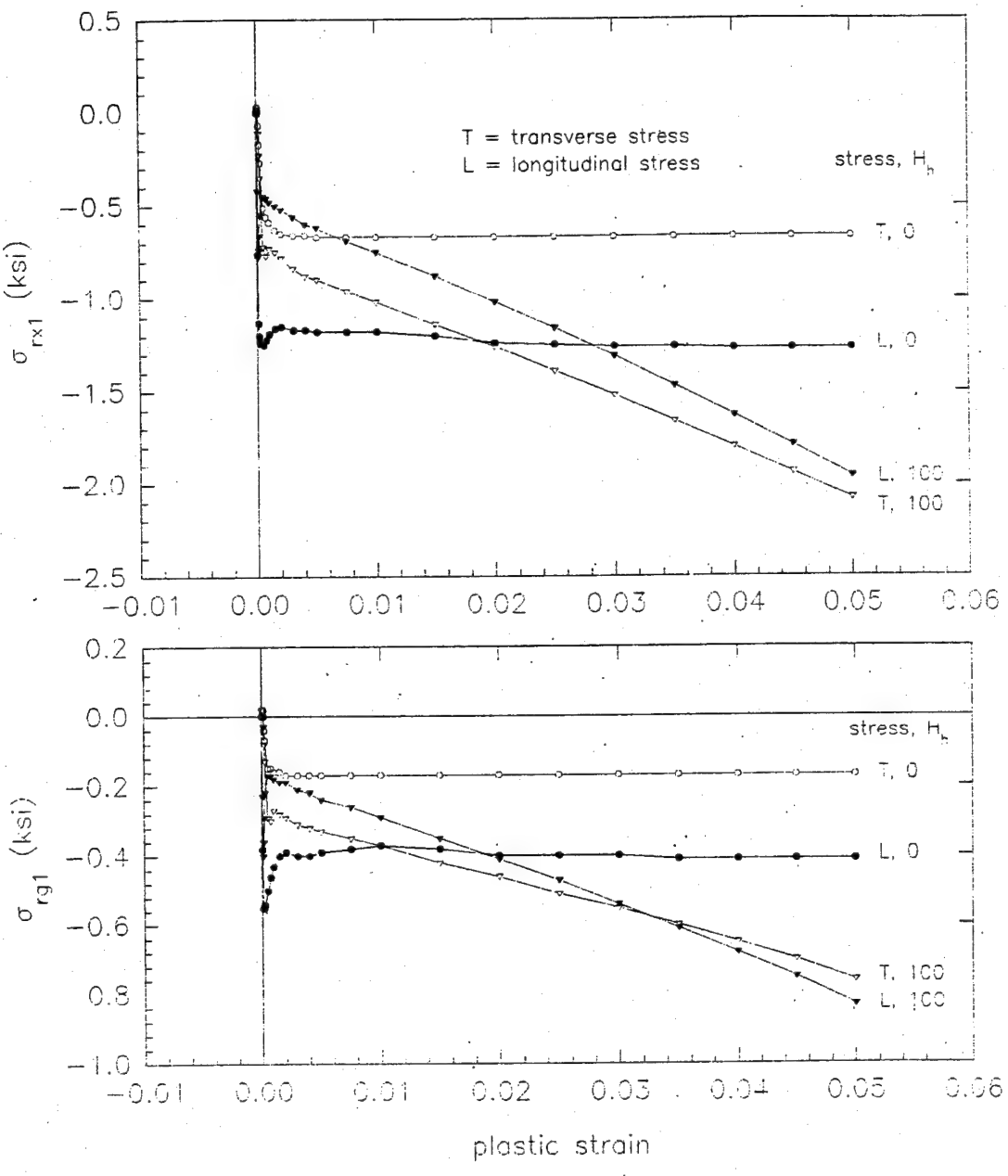

Figure 4.2.2.9-13. The transverse x-ray-averaged residual stress (σ_{Trx1}) and the transverse surface-grain-averaged residual stress (σ_{Trg1}) versus plastic strain for models under generalized plane strain for a yield point spread of 5 ksi, with and without hard grain hardening. The corresponding residual longitudinal stresses are also shown for comparison. (f_s = 0.33, E = 30,000 ksi , υ = 0.29, σ_{ys} = 15 ksi, σ_{yh} = 20 ksi, H_h = 0 or 100 ksi, H_s = 0 ksi.)

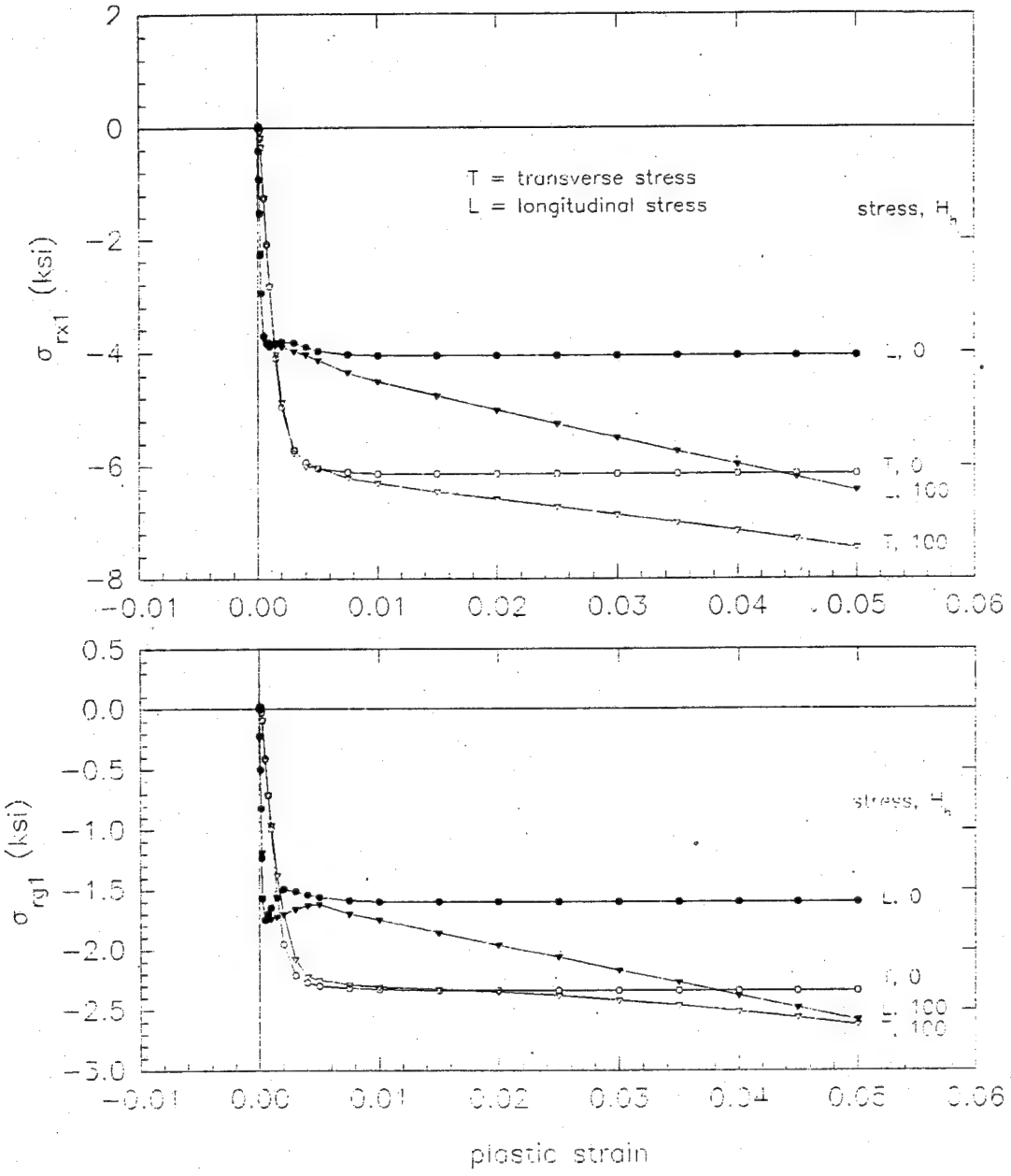

Figure 4.2.2.9-14. The transverse x-ray-averaged residual stress (σ_{Trx1}) and the transverse surface-grain-averaged residual stress (σ_{Trg1}) versus plastic strain for models under generalized plane strain for a yield point spread of 15 ksi, with and without hard grain hardening. The corresponding residual longitudinal stresses are also shown for comparison. (f_s = 0.33, E = 30,000 ksi, υ = 0.29, σ_{ys} = 15 ksi, σ_{yh} = 30 ksi, H_h = 0 or 100 ksi, H_s = 0 ksi.)

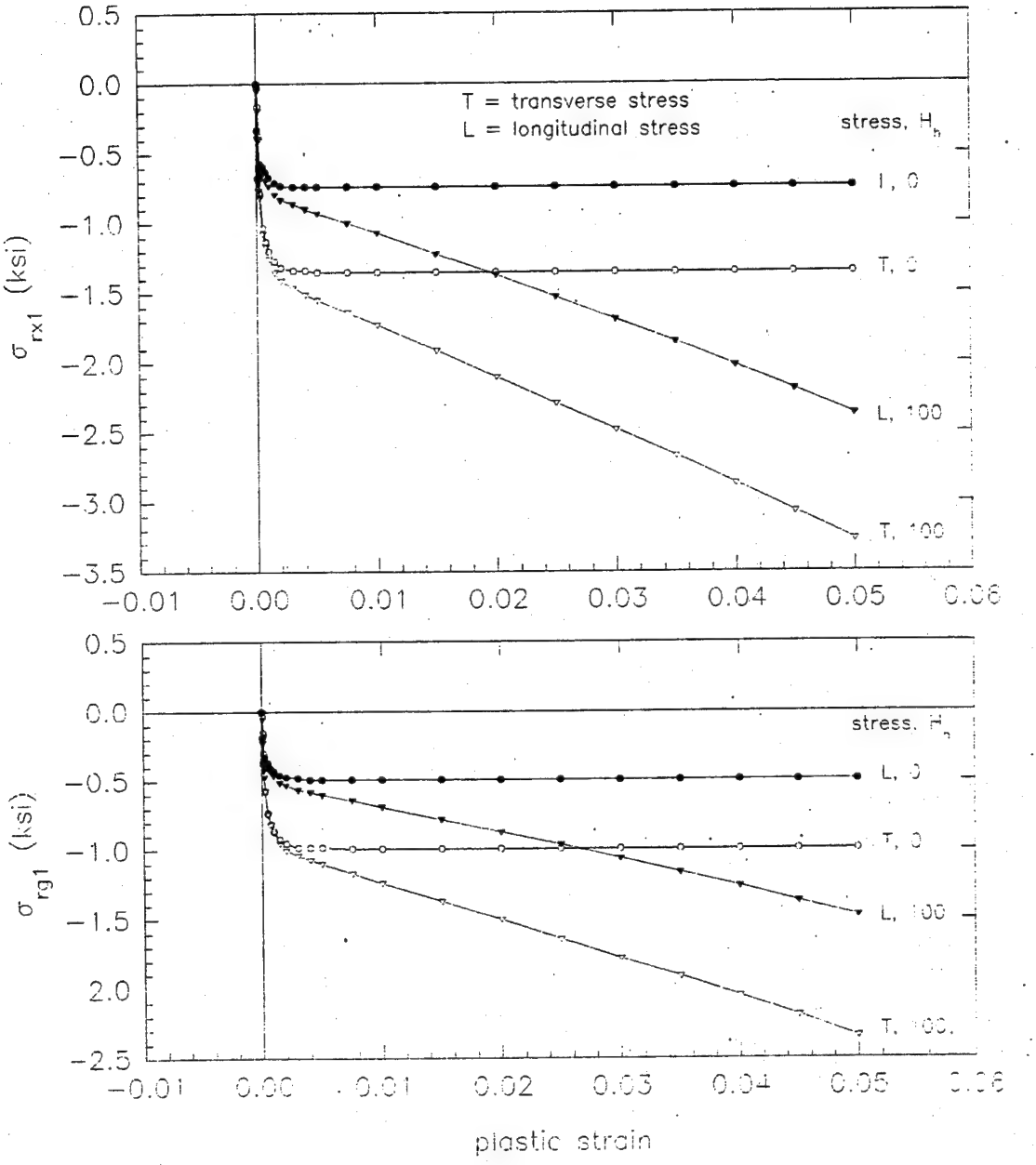

Figure 4.2.2.9-15. The transverse x-ray-averaged residual stress (σ_{Trx1}) and the transverse surface-grain-averaged residual stress (σ_{Trg1}) versus plastic strain for axisymmetric models having a yield point spread of 5 ksi, with and without hard grain hardening. The corresponding residual longitudinal stresses are also shown for comparison. (f_s = 0.33, E = 30,000 ksi, υ = 0.29, σ_{ys} = 15 ksi, σ_{yh} = 20 ksi, H_h = 0 or 100 ksi, H_s = 0 ksi.)

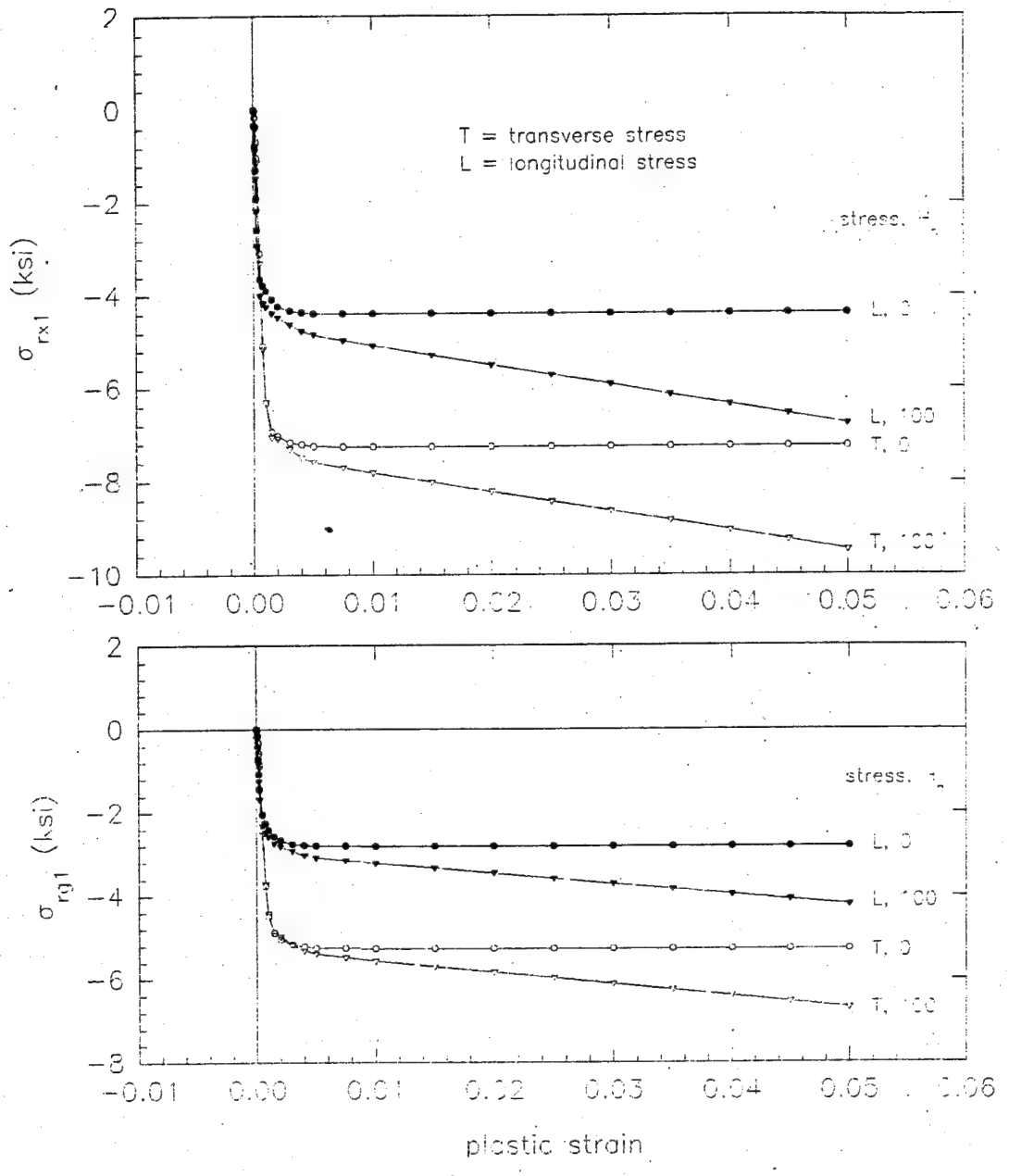

Figure 4.2.2.9-16. The transverse x-ray-averaged residual stress (σ_{Trx1}) and the transverse surface-grain-averaged residual stress (σ_{Trg1}) versus plastic strain for axisymmetric models having a yield point spread of 15 ksi, with and without hard grain hardening. The corresponding residual longitudinal stresses are also shown for comparison. (f_s = 0.33, E = 30,000 ksi, υ = 0.29, σ_{ys} = 15 ksi, σ_{yh} = 30 ksi, H_h = 0 or 100 ksi, H_s = 0 ksi.)

Because the stress tensor is symmetric, this equation may be rewritten in "vector" notation as

$$\Gamma^{(n)} = \sigma_v \, s_v^{(n)}, \quad v = 1, 2, \ldots 6 \qquad (11)$$

where

$$\sigma_1 = \sigma_{11}, \ \sigma_2 = \sigma_{22}, \ \sigma_3 = \sigma_{33},$$
$$\sigma_4 = \sigma_{23} = \sigma_{32}, \ \sigma_5 = \sigma_{13} = \sigma_{31}, \ \sigma_6 = \sigma_{12} = \sigma_{21} \qquad (12a)$$

and

$$s_1 = m_1 n_1, \ s_2 = m_2 n_2, \ s_3 = m_3 n_3,$$
$$s_4 = m_2 n_3 + m_3 n_2, \ s_5 = m_1 n_3 + m_3 n_1, \ s_6 = m_1 n_2 + m_2 n_1 \qquad (12b)$$

omitting the superscript n. The crystal yields if the resolved shear stress exceeds the critical shear stress $\Gamma_{cr}^{(n)}$ for one or more of the slip systems. $\Gamma_{cr}^{(n)}$ is the shear strength on the nth slip system. Taking the shear strength to be the same on all the slip systems, $\Gamma_{cr}^{(n)} = \Gamma_{cr}$, the yield surface of the crystal is then defined by

$$\Gamma^{(n)} > \Gamma_{cr} \qquad n = 1 \text{ or } 2 \ldots \text{ or } N \qquad (13)$$

The normal and shear strengths of the crystal with respect to its principal axes of anisotropy are readily determined. Thus, the normal (tensile) strength, X_1 in the 1 direction is given by the smallest value of

$$X_1 = \Gamma_{cr} \ / \ \sigma_1 s_1^{(n)} \qquad (14)$$

among the n slip systems, and similarly in directions 2 and 3. The shear strengths are given by the smallest value of

$$X_v = \Gamma_{cr} \ / \ s_v^{(n)}, \ v = 4, 5, 6 \qquad (15)$$

for the n slip systems.

The dominant slip system group for bcc iron is defined by <111> {110} and consists of 12 distinct slip systems. They are listed in Table 4.2.3.1-1,

along with the corresponding $s_v^{(m)}$ coefficients and the relative normal and shear strengths of the crystal with respect to its principal axes. The corresponding information for the fcc crystal is given in Table 4.2.3.1-2 for the slip group system <110> {111}, which is dominant in many fcc metals [32]. The relative normal and shear strengths are the same for the fcc and bcc systems.

Now consider a polycrystalline aggregate macroscopically subjected to a uniform uniaxial tensile stress in the longitudinal direction. Its bulk yield point is to be calculated given the crystal yield surface. The bulk yield point will be defined as the applied stress at which all the grains have just yielded. It is assumed that the stress in each grain is uniform and that there is no work hardening up to the bulk yield point. The specimen cross section perpendicular to the applied load, i.e., the transverse cross section, is taken to be large enough that any infinitesimally thin transverse section will contain a representative sampling of grains in all the prescribed orientations, i.e., all transverse slabs are equivalent. The tensile load P sustained by the cross section is

$$P = \sum \sigma_i A_i \tag{16}$$

where σ_i and A_i are the stress and the cross sectional area for the ith grain, and the summation is over the grains in the cross section. The macroscopic or average stress is then

$$\langle\sigma\rangle = P/A = \sum \sigma_i A_i/A = \sum \sigma_i c_i \tag{17}$$

where A is the total slab area, c_i is the surface-area fraction of the ith grain, and the summation is over all the grains in the cross section. At the bulk yield point, $\sigma_{Y\,bulk}$, the grain stress σ_i equals the yield point of the ith grain, and it depends only on the orientation of the grain. This equation may therefore be rewritten in terms of the crystal orientation angles theta and beta (Figure 4.2.3.1-1) as

$$\langle\sigma\rangle = \sigma_{Y\,bulk} = \sum_q \sigma_Y(\theta_q, \beta_q)\,\Delta A(\theta_q, \beta_q)/A \equiv \sum_q \sigma_{Yq}\Delta c_q \tag{18}$$

where the summation is over all the distinct orientation sets q defined by (θ_q, β_q); σ_{yq} and Δc_q are the yield point and total surface-area fraction, respectively, of the grains in the corresponding orientations. (Because all the cross sections are equivalent, the surface-area fraction equals the volume

fraction of a particular grain orientation.) For a continuum of crystal orientations, Δc_q becomes dc given by

$$dc = \alpha(\theta,\beta)d\Omega \tag{19}$$

where $\alpha(\theta,\beta)$ is the distribution density function describing the crystal orientations in the aggregate, and $d\Omega$ is the solid angle differential. The expression for the average stress becomes

$$\begin{aligned}\sigma_{Y\,bulk} &= \int_{unit\ sphere} \sigma_Y(\theta,\beta)\,d\Omega \\ &= \int_{\beta=0}^{2\pi}\int_{\theta=0}^{\pi} \sigma_Y(\theta,\beta)\,\alpha \sin\theta d\theta d\beta\end{aligned} \tag{20}$$

For a random polycrystalline aggregate, all orientations have the same probability, so that $\alpha(\theta,\beta) = k$, a constant. Because

$k = 4\pi$ and

$$\int_{unit\ sphere} \alpha d\Omega = 1 \tag{21}$$

$$\sigma_{Y\,bulk} = \frac{1}{4\pi}\int_{\beta=0}^{2\pi}\int_{\theta=0}^{\pi} \sigma_Y(\theta,\beta)\sin\theta d\theta d\beta \tag{22}$$

The yield stress $\sigma_y(\theta,\beta)$ may be obtained from Eq.(13). A simpler approach will be taken, approximating the yield surface with the Hill - von Mises yield criterion for anisotropic metal specimens [33]. This criterion is given by

$$\begin{aligned}&\frac{\sigma_1^2}{X_1^2}+\frac{\sigma_2^2}{X_2^2}+\frac{\sigma_3^2}{X_3^2} - \sigma_1\sigma_2\left[\frac{1}{X_1^2}+\frac{1}{X_2^2}-\frac{1}{X_3^2}\right] - \sigma_1\sigma_3\left[\frac{1}{X_1^2}+\frac{1}{X_3^2}-\frac{1}{X_2^2}\right] \\ &\quad - \sigma_2\sigma_3\left[\frac{1}{X_2^2}+\frac{1}{X_3^2}-\frac{1}{X_1^2}\right] + \frac{\sigma_4^2}{X_4^2}+\frac{\sigma_5^2}{X_5^2}+\frac{\sigma_6^2}{X_6^2} = 1\end{aligned} \tag{23}$$

where X_i, i = 1, 2, 3, are the tensile strengths and X_i, i = 4, 5, 6, are the shear strengths with respect to the principal directions of the crystal. For cubic symmetry, it reduces to

$$\frac{\sigma_1^2+\sigma_2^2+\sigma_3^2}{X^2} - \frac{(\sigma_1\sigma_2+\sigma_1\sigma_3+\sigma_2\sigma_3)}{X^2} + \frac{\sigma_4^2+\sigma_5^2+\sigma_6^2}{S^2} = 1 \tag{24}$$

because $X_1 = X_2 = X_3 = X$ and $X_4 = X_5 = X_6 = S$. In addition, here X = S, so that

$$\sigma_1^2+\sigma_2^2+\sigma_3^2-(\sigma_1\sigma_2+\sigma_1\sigma_3+\sigma_2\sigma_3)+\sigma_4^2+\sigma_5^2+\sigma_6^2 = X^2 \tag{25}$$

We wish to determine the yield point of an arbitrarily oriented crystal subjected to the uniaxial stress σ_y. By applying the transformation law for the second order Cartesian tensors (Frederick and Chang [34], Chap. 1), the values of the stresses in the principal directions resulting from such a stress are readily shown to be

$$\begin{aligned}
\sigma_1 &= \sigma_{11} = \sigma_y \cos^2(1,y) \\
\sigma_2 &= \sigma_{22} = \sigma_y \cos^2(2,y) \\
\sigma_3 &= \sigma_{33} = \sigma_y \cos^2(3,y) \\
\sigma_6 &= \sigma_{12} = \sigma_y \cos(1,y)\cos(2,y) \\
\sigma_4 &= \sigma_{23} = \sigma_y \cos(2,y)\cos(3,y) \\
\sigma_5 &= \sigma_{13} = \sigma_y \cos(1,y)\cos(3,y)
\end{aligned} \tag{26}$$

Substituting these expressions into Eq. (25) gives

$$\cos^4(1,y) + \cos^4(2,y) + \cos^4(3,y) = X^2/\sigma_y^2 \tag{27}$$

Noting that $\cos(1,y) = \sin\theta\cos\beta$, $\cos(2,y) = \sin\theta\sin\beta$, and $\cos(3,y) = \cos\theta$ (Figure 4.2.3.1-1), the yield point of the crystal in terms of its orientation θ and β is

$$\sigma_y = X[\cos^4\theta + \sin^4\theta\,(\cos^4\beta + \cos^4\beta)]^{-1/2} \tag{28}$$

Substituting this expression in Eq. (22) for the bulk yield point leads to

$$\sigma_{Y\,bulk} = X\int_{\beta=0}^{2\pi}\int_{\theta=0}^{\pi}[\cos^4\theta + \sin^4\theta\,(\cos^4\beta + \sin^4\beta)]^{-1/2}\sin\theta\,d\theta\,d\beta \tag{29}$$

Integration yields

$$\sigma_{Y\,bulk} = 1.331X \tag{30}$$

or

$$X = 0.75\ \sigma_{Y\,bulk} \tag{31}$$

This value is in agreement with the experimental value of Sasaki and Sato [14].

Table 4.2.3.1-1. Stress coefficients $s_v^{(n)}$ and crystal relative strengths X_i/X_1 with respect to the principal axes for bcc cubic crystals based on the slip system group <111> {110}.

Slip Systems			$[1/6]^{½}s_v^{(n)}$					
n	Plane normal	slip dir.	σ_{11} v=1	σ_{22} v=2	σ_{33} v=3	σ_{12} v=6	σ_{23} v=4	σ_{13} v=5
1	1 1 0	1 $\bar{1}$ 1	1	-1	0	0	1	1
2		1 $\bar{1}$ $\bar{1}$	1	-1	0	0	-1	-1
3	1 $\bar{1}$ 0	1 1 1	1	-1	0	0	-1	1
4		1 1 $\bar{1}$	1	-1	0	0	1	-1
5	1 0 1	1 1 $\bar{1}$	1	0	-1	1	1	0
6		1 $\bar{1}$ $\bar{1}$	1	0	-1	-1	-1	0
7	1 0 $\bar{1}$	1 1 1	1	0	1	1	-1	0
8		1 $\bar{1}$ 1	1	0	-1	-1	1	0
9	0 1 1	1 1 $\bar{1}$	0	1	-1	1	0	1
10		$\bar{1}$ 1 $\bar{1}$	0	1	-1	-1	0	-1
11	0 1 $\bar{1}$	1 1 1	0	1	-1	1	0	-1
12		$\bar{1}$ 1 1	0	1	-1	-1	0	1
X_i / X_1			1	1	1	1	1	1

Table 4.2.3.1-2. Stress coefficients $s_v^{(n)}$ and crystal relative strengths X_i/X_1 with respect to the principal axes for fcc cubic crystals based on the slip system group <110> {111}.

Slip Systems			$[1/6]^{½}s_v^{(n)}$					
n	Plane normal	slip dir.	σ_{11} v=1	σ_{22} v=2	σ_{33} v=3	σ_{12} v=6	σ_{23} v=4	σ_{13} v=5
1	1 1 1	$\bar{1}$ 1 0	-1	1	0	0	1	-1
2		$\bar{1}$ 0 1	-1	0	1	-1	1	0
3		0 1 $\bar{1}$	0	1	-1	1	0	-1
4	$\bar{1}$ 1 1	1 1 0	-1	1	0	0	1	1
5		1 0 1	-1	-1	1	1	1	0
6		0 1 1	0	1	-1	-1	0	-1
7	1 $\bar{1}$ 1	1 1 0	1	-1	0	0	1	1
8		0 1 1	0	-1	1	1	0	1
9		$\bar{1}$ 0 1	-1	0	1	1	-1	0
10	1 1 $\bar{1}$	1 0 1	1	0	-1	1	1	0
11		0 1 1	0	1	-1	1	0	1
12		$\bar{1}$ 1 0	-1	1	0	0	-1	1
X_i / X_1			1	1	1	1	1	1

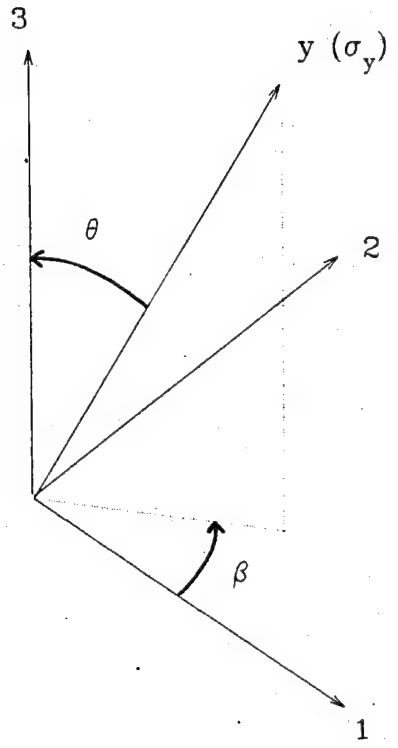

Figure 4.2.3.1-1. Definition of the angles θ and ß to indicate the orientation of the cubic crystal principal axes 1, 2, and 3 relative to the applied uniaxial stress σ_y.

4.2.3.2 Iron and Mild Steel. Greenough [8] studied the surface layer effect in Armco iron (0.02% C) and mild steel (0.1% C) by x-ray diffraction stress measurements. For the Armco iron, plastically extended 11%, he inferred a compressive longitudinal residual stress σ_{xx} of $\leq$ -6.3 ksi and a transverse residual stress σ_{Txx} of -5.7 ksi; for the mild steel (ϵ_p = 6%), he found a transverse residual stress of -6.3 ksi. He used Co K_α radiation for diffraction on the {310} planes of bcc iron at psi angles of 0, 30, 45, and 60° on the mild steel and 0, 45° on the Armco iron, corresponding to average penetration depths of 0.0015 and 0.0022 inch, respectively. Given grain diameters of $\approx$ 0.001 and $\approx$ 0.003 inch in the steel and iron, respectively, this corresponds to average penetration depths of about 1.5 and 0.6 grains, respectively.

In the present calculations, the model with 33% soft grains is used because it seems to model the surface layer effect best, probably because it spreads the soft grains more evenly than the lower concentration models. Greenough did not provide the bulk yield points of the materials he used, but the following tensile stress was required to achieve the respective plastic extension: 43 ksi for 11% in Armco iron and 44 ksi for 6% in mild steel. Because of the low degree of work hardening in these materials, the yield stress can be taken to be approximately equal to 42 ksi. Based on the discussion in the previous section and the results of Sasaki and Sato [14], a reasonable value for the proportional limit is approximately 75% of the bulk yield point. To achieve a bulk yield point in the vicinity of 42 ksi, the grain yield points assigned were Y_s = 32 ksi and Y_h = 51 ksi. The calculations were performed in plane stress, generalized plane strain, and axisymmetry to determine the sensitivity to constraint. Moreover, transverse residual stresses are obtained from generalized plane strain and axisymmetry, in addition to the residual longitudinal stress. The hardening rate of the soft grains was set to zero in all cases. In view of the low degree of work hardening of Armco iron and mild steel, the hardening rate of the hard grains must be low. Values used were 0 and 100 ksi to cover a reasonable range and gage the sensitivity to this parameter.

The x-ray-averaged stress and plastic strain versus loading for penetration depths of 0.5, 1,2, and 5 grains are given for plane stress in Figure 4.2.3.2-1, for generalized plane strain in Figure 4.2.3.2-2, and for axisymmetry in Figure 4.2.3.2-3. In plane stress, the residual stresses are

insensitive to the hard grain hardening rate and level off for $\epsilon_p > 0.01$, e.g., σ_{xx} for one grain penetration depth is -11 ksi for $\epsilon_p \geq 0.01$. In generalized plane strain, σ_{xx} levels off above $\epsilon_p \approx 0.1$ when there is no grain hardening, but it increases linearly with plastic strain for $H_h = 100$ ksi.

The calculated values of σ_{xx} are of the same order of magnitude as the experimental value for iron ($\sigma_{xx} \leq -6.3$ ksi, $\epsilon_p = 0.11$). They range from -16 ksi for plane stress to -4.1 ksi in generalized plane strain for $\epsilon_p = 0.06$, no grain hardening, and a penetration depth of 0.5 grain. The corresponding values for a penetration depth of one grain are -11 ksi and -3.5 ksi, respectively. Closer agreement could be obtained by fine tuning the hardening rates of the grains, noting that σ_{xx} is sensitive to the hardening rate of the soft grains. It is of particular interest that the model predicts correctly the transverse stress which had puzzled Greenough. As observed by him, the transverse and longitudinal residual stresses are comparable in magnitude (Figure 4.2.3.2-4).

Greenough determined the depth of the surface layer in the Armco iron sample to be 2 to 3 grain diameters. This is also in good agreement with the depth of about 2 grains inferred from plots of the plane-averaged longitudinal stress versus depth for $\epsilon_p \geq 0.05$ (Figure 4.2.3.2-5).

4.2.3.3 Results for Nickel. The experimental results of Kolb and Macherauch [12] for nickel will serve as the basis for comparison. These authors observed large residual stresses in the direction of loading by x-ray diffraction measurements on pure nickel (99.8%) subjected to tensile plastic strains of up to 27%. The grain diameter was about 30 um and the yield point of the metal was 14.3 ksi, with a secant work hardening rate of 420 ksi at 6% strain.

The metal was modeled with an array of square grains, 33% soft, such that the yield of the soft grains is 75% of the bulk yield, using the rationale presented earlier. The hardening rate of the soft and hard grains was chosen to approximately achieve the experimental bulk hardening rate and the residual stress at 5% plastic strain. This is necessary because there is no a priori way of assigning the grain hardening rates, except when they are close to zero, such as for iron (cf. previous section). Kolb and Macherauch used copper K_α radiation for diffraction on the Ni {420} and {313} planes and

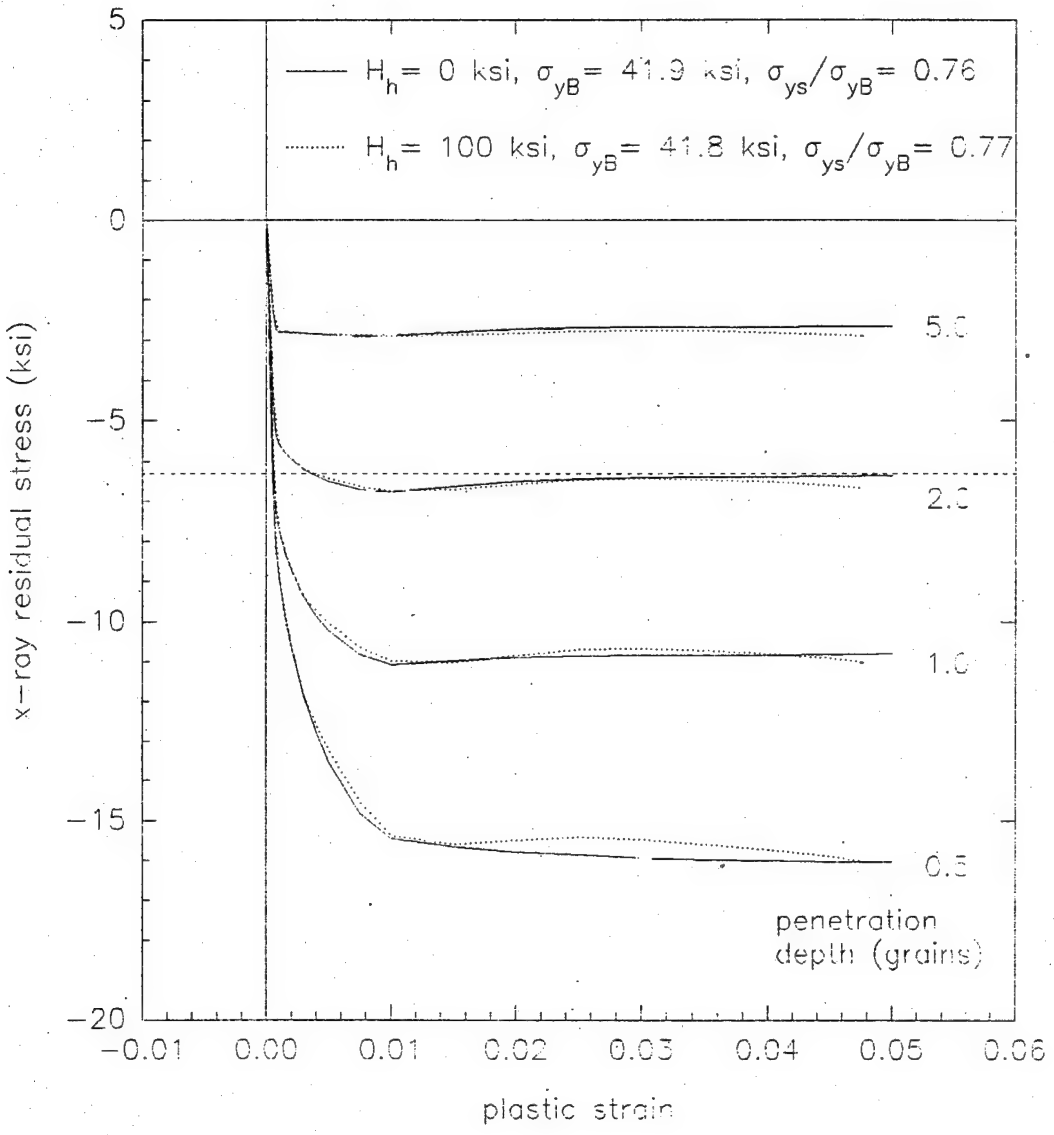

Figure 4.2.3.2-1. Iron and steel modeling - The x-ray-averaged residual longitudinal stress versus plastic strain in plane stress, with and without hard grain hardening, for penetration depths of 0.5, 1, 2, and 5 grains. (f_s = 0.33, E = 30,000 ksi, υ = 0.29, σ_{ys} = 32 ksi, σ_{yh} = 51 ksi, H_s = 0 ksi.)

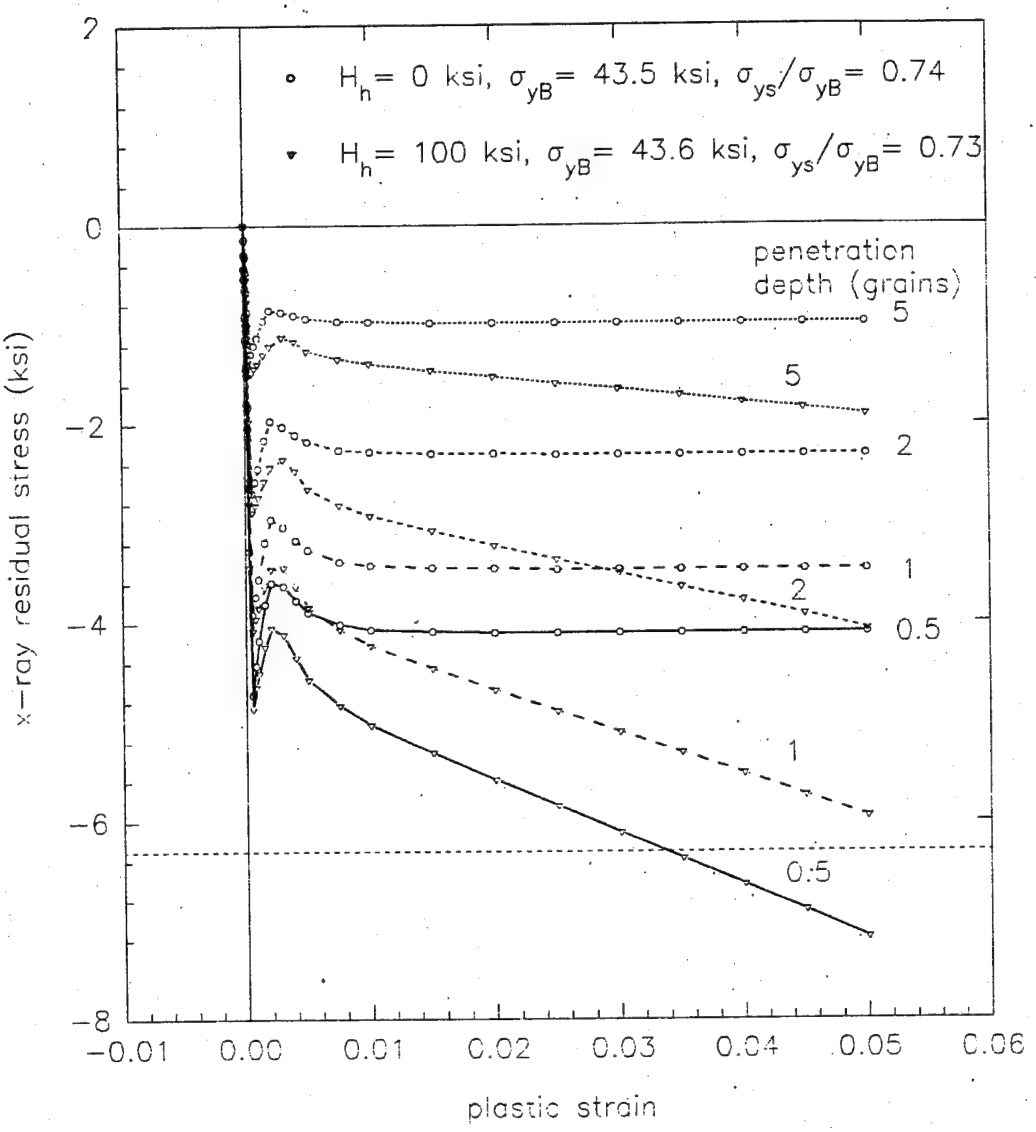

Figure 4.2.3.2-2. Iron and steel modeling - The x-ray-averaged residual longitudinal stress versus plastic strain in generalized plane strain, with and without hard grain hardening, for penetration depths of 0.5, 1, 2, and 5 grains. (f_g = 0.33, E = 30,000 ksi, υ = 0.29, σ_{ys} = 32 ksi, σ_{yh} = 51 ksi, H_s = 0 ksi.)

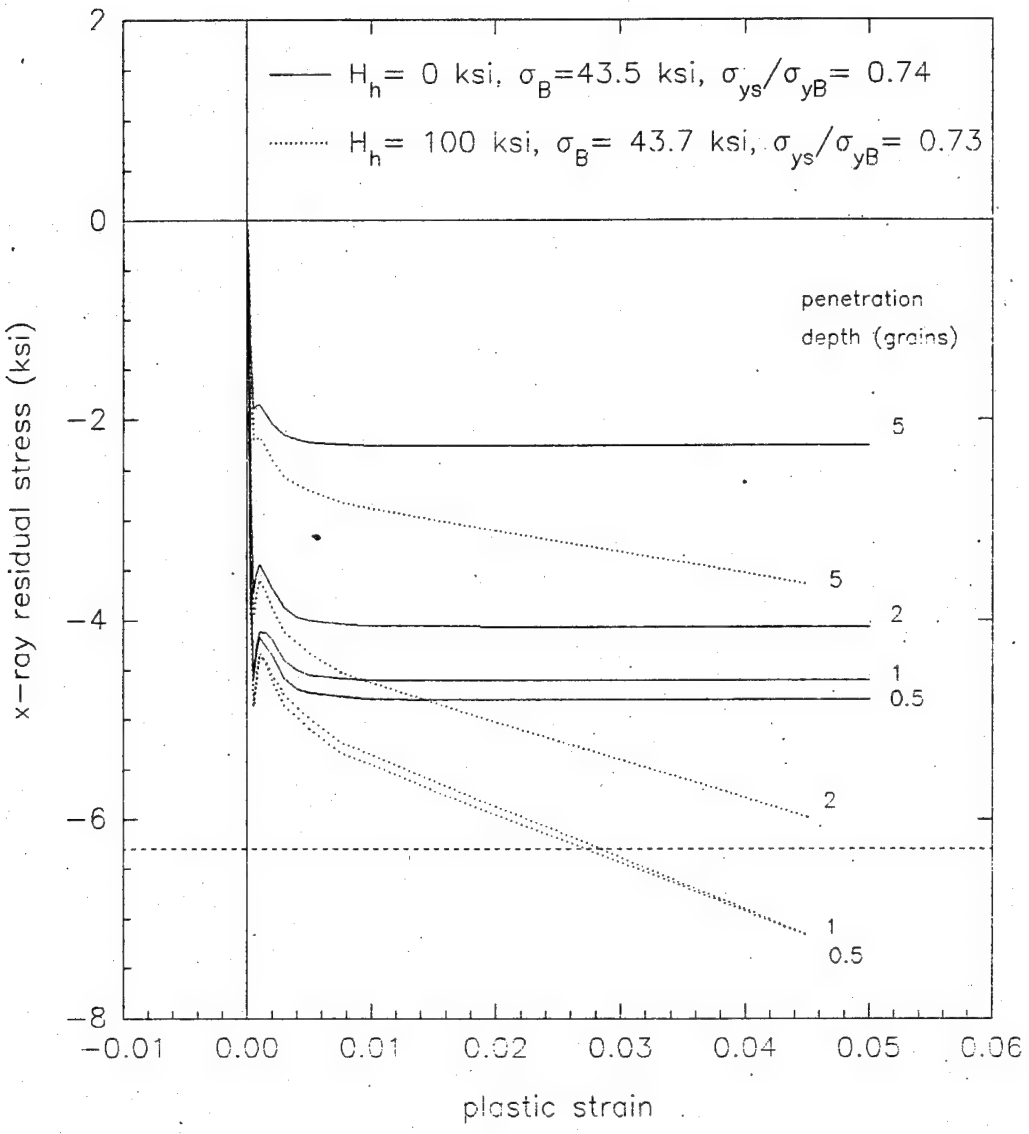

Figure 4.2.3.2-3. Iron and steel modeling - The x-ray-averaged residual longitudinal stress versus plastic strain in axisymmetry with and without hard grain hardening, for penetration depths of 0.5, 1, 2, and 5 grains. (f_s = 0.33, E = 30,000 ksi, υ = 0.29, σ_{ys} = 32 ksi, σ_{yh} = 51 ksi, H_s = 0 ksi.)

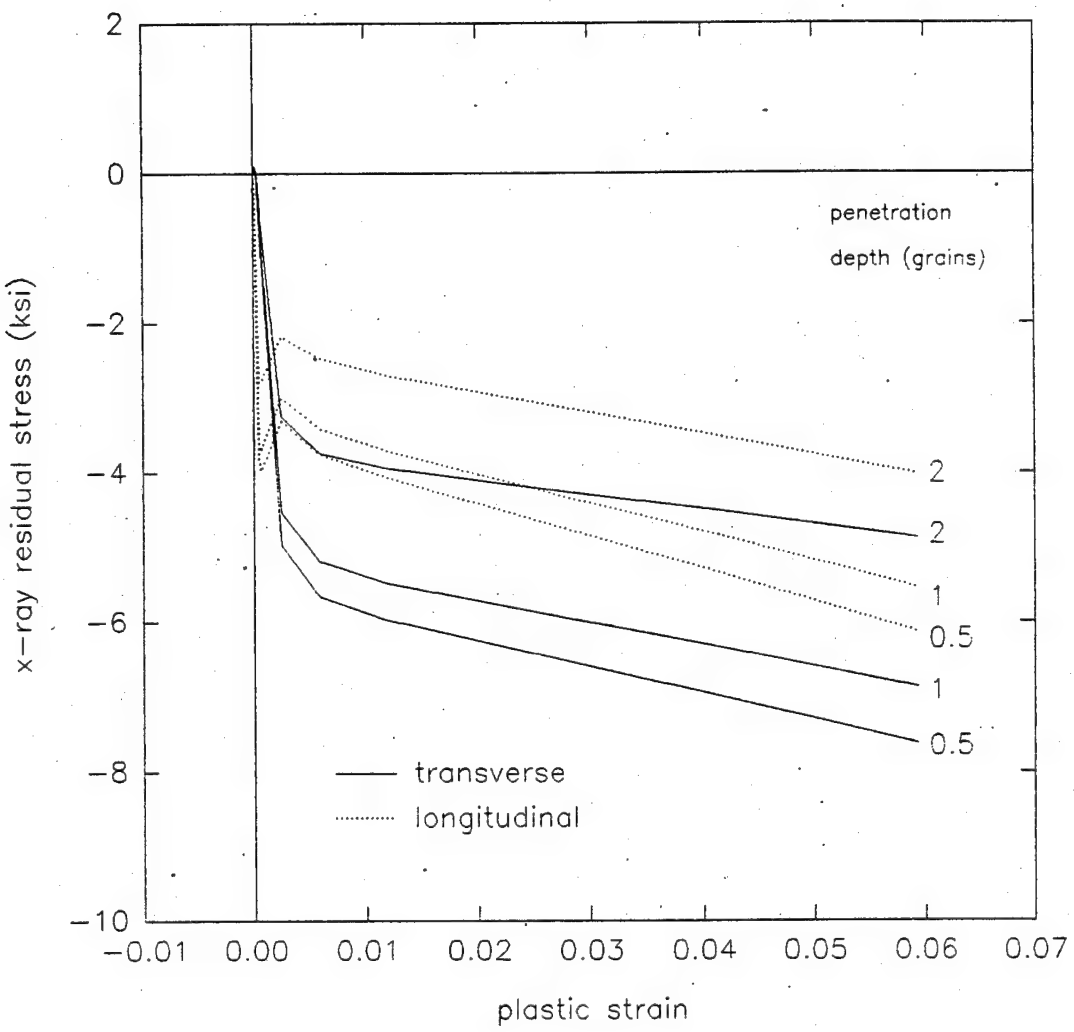

Figure 4.2.3.2-4. Iron and steel modeling - The x-ray-averaged longitudinal and transverse residual stresses versus plastic strain in generalized plane strain, for penetration depths of 0.5, 1, 2, and 5 grains and a hard grain hardening rate of 100 ksi. (f_s = 0.33, E = 30,000 ksi, υ = 0.29, σ_{ys} = 32 ksi, σ_{yh} = 51 ksi, H_s = 0 ksi.)

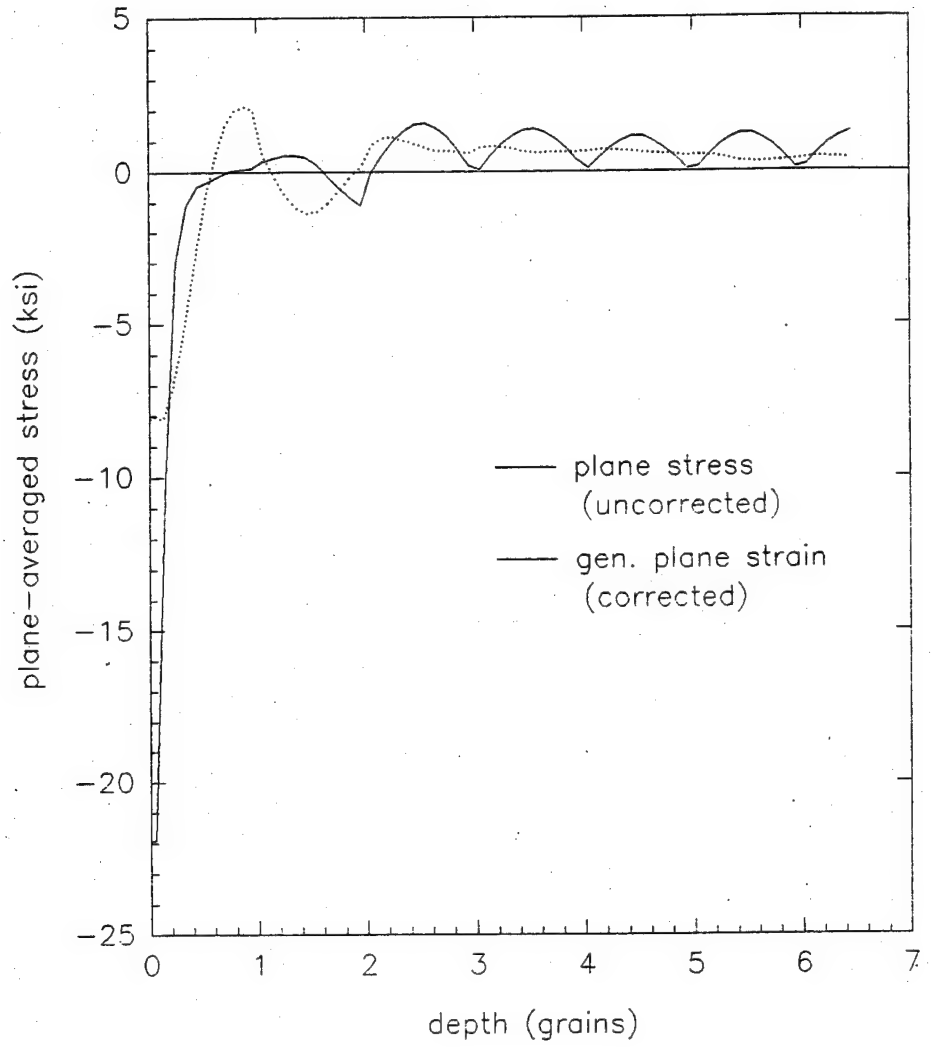

Figure 4.2.3.2-5. Iron and steel modeling - Plane-averaged longitudinal stress versus depth in plane stress and in generalized plane strain, for a plastic strain of 5% and 6%, respectively, under load, and a hard grain hardening rate of 100 ksi. (f_s = 0.33, E = 30,000 ksi, υ = 0.29, σ_{ys} = 32 ksi, σ_{yh} = 51 ksi, H_s = 0, H_h = 100 ksi.)

a maximum psi angle of 51° and 46°, respectively (estimated from graphical data in their paper). Given a mass attenuation coefficient of 48.83 cm^2/g [35] for copper K_α radiation in nickel, the average penetration depth is 1.4 grain diameters, obtained by averaging the penetration depths at 0° (1.7 grains) and 46°, 51° (1.0 grain).

The loading history and calculated x-ray stresses for penetration depths of 0.5, 1, 1.4, 2, and 5 grains are given in Table 4.2.3.3-1 for generalized plane strain. The experimental curves of applied stress and x-ray stress versus strain are compared with the corresponding calculated curves in Figure 4.2.3.3-1. There is excellent agreement for the x-ray stress values under load. The agreement with the x-ray residual stress values is good, but the shape of the curves is different. The calculated values increase approximately linearly, whereas the experimental values tend to increase initially more rapidly and then gradually level off. This levelling-off can easily be incorporated in the model by increasing the soft grain hardening as with plastic strain. It is of interest that the residual stress levels off without soft grain hardening in plane stress (cf. Section 4.2.1). This suggests that the best representation may be between plane stress and generalized plane strain.

4.2.3.4 Titanium Alloy Ti-6Al-4V. The titanium alloy was modeled with the 33% soft grain array in plane stress, using E=17200 ksi, υ=0.35, a yield point of 132 ksi, and a proportional limit of 107 ksi. The value of E and the yield point are from the measured stress-strain curve. The value of the proportional limit is from the x-ray stress versus applied stress curve, being the applied stress at which the x-ray stresses start to level off. Alternatively, the proportional limit from the stress-strain curve could have been used; its value, 115 ksi, is comparable to, but somewhat higher than the value inferred from the x-ray data, as expected. The loading history and the resulting plastic strains and x-ray-averaged stresses are presented in Table 4.2.3.4-1. Because of concentration stress effects at the square grain boundaries, the model bulk yield point is 125 ksi, rather than 132 ksi from the rule of mixtures. Attempts to increase it by increasing the yield point of the hard grains require inordinately large values of the latter, because the array has reached its maximum strength given the soft grain yield point.

The x-ray stress versus applied stress for a penetration depth of one grain (Figure 4.2.3.4-1) is qualitatively similar to that observed for the

Table 4.2.3.3-1. Loading history and x-ray-averaged stresses for nickel in generalized plane strain.

Step No.	Applied Stress (ksi)	Plastic Strain	X-Ray-Averaged Stress (ksi) Penetration Depth (grains) 0.500	1.000	1.400	2.000	5.000
1	11.000	0.0000E+00	11.00	11.00	11.00	11.00	11.00
2	12.418	0.4795E-04	11.99	12.00	12.04	12.10	12.25
3	0.000	0.4796E-04	-0.43	-0.42	-0.38	-0.32	-0.17
4	12.418	0.4795E-04	11.99	12.00	12.04	12.10	12.25
5	13.058	0.7072E-04	12.39	12.42	12.48	12.56	12.80
6	0.000	0.7072E-04	-0.66	-0.64	-0.58	-0.49	-0.25
7	13.058	0.7072E-04	12.39	12.42	12.48	12.56	12.80
8	13.324	0.8236E-04	12.56	12.59	12.66	12.76	13.04
9	0.000	0.8236E-04	-0.76	-0.73	-0.66	-0.56	-0.29
10	13.324	0.8236E-04	12.56	12.59	12.66	12.76	13.04
11	13.611	0.1224E-03	12.84	12.89	12.97	13.07	13.34
12	0.000	0.1224E-03	-0.77	-0.72	-0.64	-0.54	-0.27
13	13.611	0.1224E-03	12.84	12.89	12.97	13.07	13.34
14	13.970	0.4458E-03	13.47	13.51	13.57	13.64	13.82
15	0.000	0.4458E-03	-0.50	-0.46	-0.40	-0.33	-0.15
16	13.970	0.4458E-03	13.47	13.51	13.57	13.64	13.82
17	14.329	0.1206E-02	13.64	13.69	13.77	13.87	14.12
18	0.000	0.1206E-02	-0.69	-0.64	-0.55	-0.46	-0.20
19	14.329	0.1206E-02	13.64	13.69	13.77	13.87	14.12
20	14.704	0.2009E-02	13.84	13.90	14.00	14.13	14.44
21	0.000	0.2009E-02	-0.86	-0.80	-0.70	-0.58	-0.26
22	14.704	0.2009E-02	13.84	13.90	14.00	14.13	14.44
23	16.039	0.4908E-02	14.50	14.62	14.80	15.02	15.58
24	0.000	0.4908E-02	-1.54	-1.42	-1.24	-1.02	-0.46
25	16.039	0.4908E-02	14.50	14.62	14.80	15.02	15.58
26	18.264	0.9835E-02	15.43	15.68	16.00	16.41	17.42
27	0.000	0.9835E-02	-2.84	-2.58	-2.26	-1.86	-0.85
28	18.264	0.9835E-02	15.43	15.68	16.00	16.41	17.42
29	22.714	0.1986E-01	16.95	17.52	18.16	18.97	21.00
30	0.000	0.1986E-01	-5.61	-5.03	-4.39	-3.61	-1.64
31	22.714	0.1987E-01	16.82	17.42	18.08	18.90	20.97
32	29.389	0.3506E-01	18.94	20.01	21.16	22.59	26.24
33	0.000	0.3497E-01	-10.54	-9.32	-8.13	-6.67	-3.05
34	29.389	0.3512E-01	18.08	19.34	20.59	22.15	26.07
35	36.509	0.5133E-01	21.06	22.64	24.30	26.40	31.79
36	0.000	0.5110E-01	-15.64	-13.85	-12.14	-10.02	-4.79

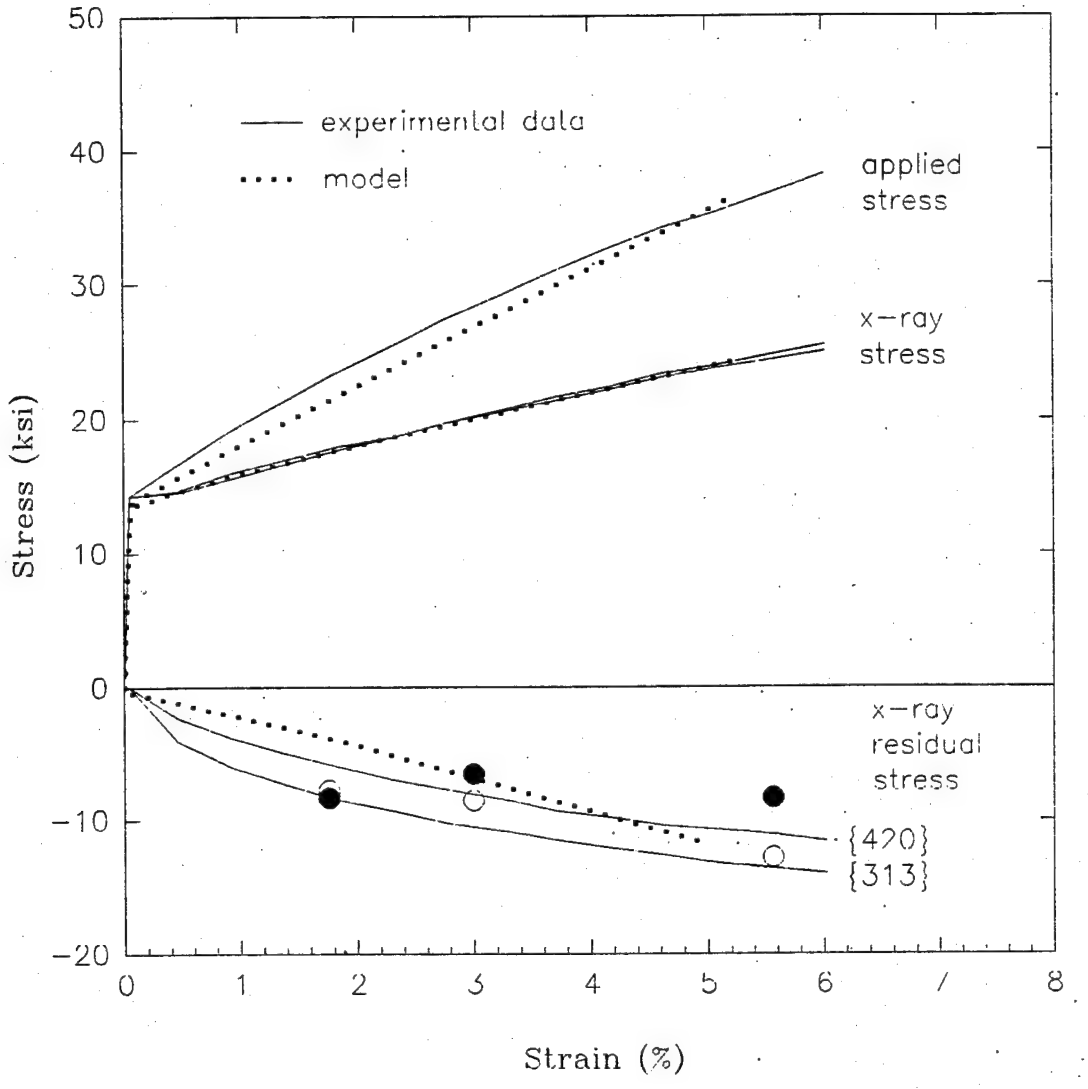

Figure 4.2.3.3-1. Nickel modeling - Comparison of the calculated x-ray stresses in generalized plane strain with the experimental data of Kolb and Macherauch [12]. (f_s = 0.33, E = 30,000 ksi, υ = 0.31, σ_{ys} = 11 ksi, σ_{yh} = 15.5 ksi, H_s = 50, H_h = 850 ksi.)

actual titanium alloy specimen (Figure 4.1-1), as already noted for the basic model (Section 4.2.1). The x-ray penetration depth in our experiments is about one grain and the measured x-ray residual stress values are -20.4 ksi and -45.8 ksi for a plastic strain of 0.44% and 1 - 2%, respectively. This is in fair agreement with the model values of -18 to -24 ksi for a plastic strain in this range. The residual x-ray stress values are fairly sensitive to the penetration depth and to the plastic strain for penetration depths less than 2 grains (Figure 4.2.3.4-2). Beside the aforementioned stress concentration effect, there may be another reason the model seems to predict a lesser effect. Because each x-ray measurement took on the order of one hour, the titanium specimen underwent noticeable creep. For the same reason that the surface layer yields first, it will tend to relax more, thereby leading to greater compressive residual stresses upon unloading.

4.2.3.5 Results for Aluminum . The aluminum alloy specimens used in this study have an ill-defined grain shape and size because they were made from rolled plate stock. It is beyond the capabilities of the model to reproduce this complex situation. Instead, calculations for simple models which can be used as reference points were performed. The usual square grain, 33% soft regular array was used, with E = 10,400 ksi, υ = 0.33. The yield points of the soft and hard grains are 59 and 88 ksi, respectively, such that the yield point by the rule of mixtures Y_{mix} equals the experimental yield point (78.5 ksi, Table 2.1-1) and the ratio Y_s/Y_{mix} = 0.75, consistent with the fcc structure. The hardening rate of the soft grains is zero and that of the hard grains is 500 ksi, so that the tangent hardening rate is approximately equal to that observed (270 ksi from ϵ_p = 0.002 to 0.017).

The loading and x-ray stress histories in plane stress and generalized plane strain are shown in Tables 4.2.3.5-1 and 4.2.3.5-2, respectively. Because the experimental penetration depth is on the order of one grain, the calculated x-ray stress versus the mechanical stress for that penetration depth is shown in Figure 4.2.3.5-1 for both types of constraint. Both curves agree qualitatively with the experimental curves. The generalized plane strain curve appears to be more representative because the deviation of the x-ray stress from the applied stress becomes pronounced substantially above the proportional limit, as observed experimentally (Figure 4.1-2). The calculated longitudinal residual stresses in plane stress and generalized plane strain are, respectively, -10.5 and -4.9 ksi for ϵ_p = 0.003, and -13.3 and -4.41 ksi

Table 4.2.3.4-1. Loading history and x-ray-averaged stresses for Ti-6Al-4V in plane stress.

Step No.	Applied Stress (ksi)	Plastic Strain	X-Ray-Averaged Stress (ksi) Penetration Depth (grains)				
			0.500	1.000	2.000	5.000	6.500
1	107.000	0.0000E+00	107.00	107.00	107.00	107.00	107.00
2	107.520	0.5197E-04	107.14	107.17	107.25	107.38	107.42
3	0.000	0.5170E-04	-0.38	-0.36	-0.27	-0.14	-0.11
4	107.520	0.5197E-04	107.14	107.17	107.25	107.38	107.42
5	108.050	0.1034E-03	107.27	107.33	107.50	107.76	107.83
6	0.000	0.1036E-03	-0.77	-0.72	-0.55	-0.28	-0.22
7	108.050	0.1034E-03	107.27	107.33	107.50	107.76	107.83
8	108.560	0.1556E-03	107.41	107.49	107.75	108.14	108.24
9	0.000	0.1553E-03	-1.16	-1.07	-0.82	-0.42	-0.33
10	108.560	0.1556E-03	107.41	107.49	107.75	108.14	108.24
11	109.580	0.2570E-03	107.66	107.80	108.22	108.87	109.04
12	0.000	0.2571E-03	-1.92	-1.77	-1.36	-0.70	-0.54
13	109.580	0.2570E-03	107.66	107.80	108.22	108.87	109.04
14	111.930	0.4971E-03	108.21	108.49	109.30	110.58	110.89
15	0.000	0.4972E-03	-3.72	-3.44	-2.63	-1.35	-1.04
16	111.930	0.4971E-03	108.21	108.49	109.31	110.58	110.89
17	115.730	0.8962E-03	108.99	109.52	110.99	113.30	113.86
18	0.000	0.8963E-03	-6.74	-6.21	-4.74	-2.43	-1.87
19	115.730	0.8962E-03	108.99	109.52	110.99	113.30	113.86
20	120.890	0.1465E-02	109.83	110.73	113.16	116.93	117.84
21	0.000	0.1465E-02	-11.06	-10.16	-7.73	-3.96	-3.05
22	120.890	0.1465E-02	109.83	110.73	113.16	116.93	117.84
23	129.450	0.3235E-02	110.45	112.53	116.86	123.01	124.47
24	0.000	0.3235E-02	-19.01	-16.92	-12.60	-6.45	-4.98
25	129.450	0.3235E-02	110.45	112.53	116.86	123.01	124.47
26	132.370	0.9139E-02	107.25	111.81	118.26	125.67	127.25
27	0.000	0.9139E-02	-25.12	-20.56	-14.10	-6.70	-5.11
28	132.370	0.9139E-02	107.25	111.81	118.26	125.67	127.25
29	133.370	0.1349E-01	105.62	111.41	118.70	126.54	128.18
30	0.000	0.1349E-01	-27.75	-21.96	-14.67	-6.83	-5.19
31	133.370	0.1349E-01	105.62	111.41	118.70	126.54	128.18
32	134.870	0.2210E-01	102.83	110.43	118.94	127.54	129.30
33	0.000	0.2210E-01	-32.04	-24.44	-15.92	-7.33	-5.57
34	134.870	0.2210E-01	102.83	110.43	118.94	127.54	129.30

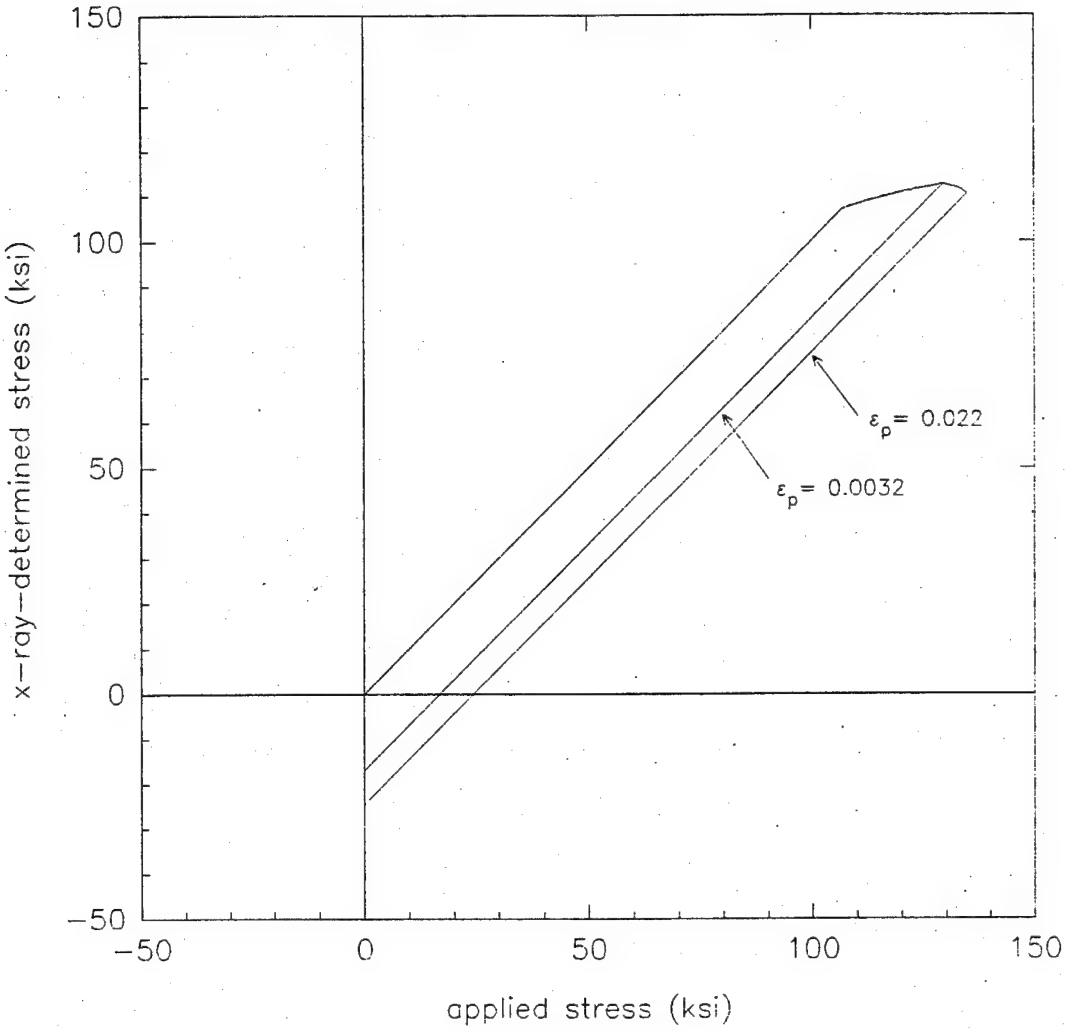

Figure 4.2.3.4-1. Modeling of Ti-6Al-4V - Calculated x-ray stress versus the nominal applied stress for a penetration depth of one grain, in plane stress. (f_s = 0.33, E = 17,200 ksi, υ = 0.35, σ_{ys} = 107 ksi, σ_{yh} = 151 ksi, H_s = 0, H_h = 500 ksi.)

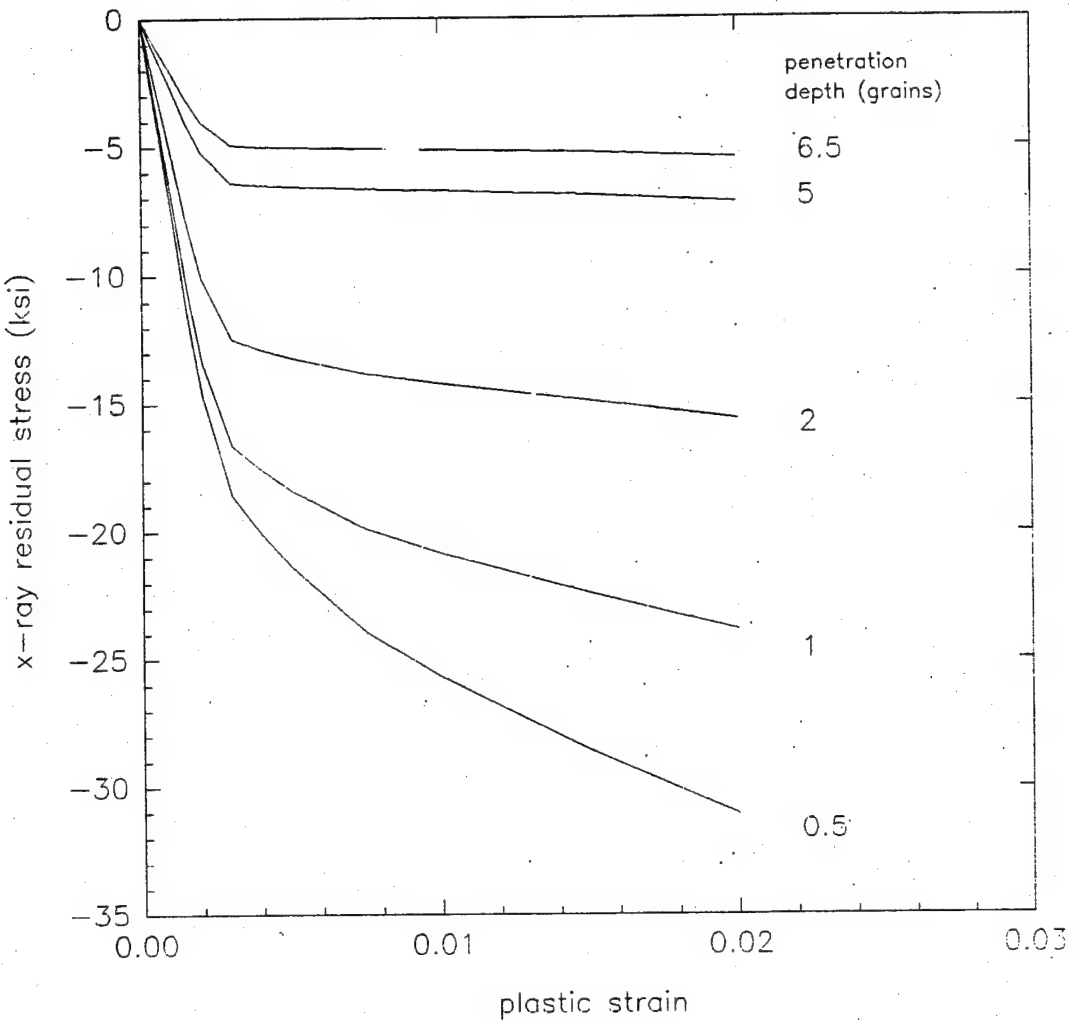

Figure 4.2.3.4-2. Modeling of Ti-6Al-4V - The residual x-ray stress versus plastic strain for penetration depths of 0.5, 1, 2, 5, and 6.5 grains, in plane stress. (f_s = 0.33, E = 17,200 ksi, υ = 0.35, σ_{ys} = 107 ksi, σ_{yh} = 151 ksi, H_s = 0, H_h = 500 ksi.)

for ϵ_p = 0.0075 (Figure 4.2.3.5-2). These values compare with the experimental values of -8.2 ± 1.8 ksi (ϵ_p = 0.003) and -14.1 ± 5.2 ksi (ϵ_p = 0.008). However, because grain elongation will markedly decrease the residual stress, this model probably underestimates the effect. An offsetting factor may be the observed creep near the yield point, which as discussed for the titanium alloy, could considerably increase the surface layer effect.

4.3 SIGNIFICANCE OF THE CONTINUUM SURFACE LAYER EFFECT (CSLE)

The primary motivation for this study was to find an explanation for the anomalous x-ray stress measurements. If the concept presented here is correct, one can expect deviations of the x-ray-determined stress from the nominal applied stresses, as well as significant compressive x-ray residual stresses, when the x-ray penetration depth is of the order of a few grain diameters or less, and the applied stress is in excess of approximately 75% of the bulk yield point. The severity of the deviation and the magnitude of the residual stresses depend on many factors, as discussed in Section 4.2.2., Effects of Various Parameters, and summarized in the Conclusions.

The continuum surface layer effect is, however, not just an x-ray effect. This is demonstrated in the work of Sasaki and Sato [14], in which the deviation from linearity of the stress-strain curve can be related to yielding of the surface layer before yielding of the bulk material. The CSLE may thus play a significant role in metal fatigue, for which it has been shown that crack initiation is often at or near the surface (see for example reference [31], pp. 241-246). The CSLE is relevant whether the problem is approached micromechanically or macroscopically. At the grain or microscopic level, the stress and strain variations are considerably enhanced in the surface layer relative to the bulk, with plastic deformation initially concentrated in the surface soft grains (Section 4.2.1). Under cyclic loading, local plastic deformation will lead to defect and damage accumulation [36], and hence the possibility of failure by fatigue cracks initiated at the surface. This local effect will be enhanced by inclusions and other defects near the surface, and by surface roughness.

Macroscopic models of fatigue may become more accurate if the effective lower yield point of the surface layer is taken into account for both notched and smooth members. Thus, very recently He, Wang, and Nan [37] have reported

Table 4.2.3.5-1. Loading history and x-ray-averaged stresses for the Al 7475-T651 alloy in plane stress.

Step No.	Applied Stress (ksi)	Plastic Strain	X-Ray-Averaged Stress (ksi) Penetration Depth (grains)				
			0.500	1.000	2.000	5.000	6.500
1	59.000	0.0000E+00	59.00	59.00	59.00	59.00	59.00
2	59.326	0.5312E-04	59.09	59.10	59.16	59.23	59.26
3	0.000	0.5311E-04	-0.24	-0.22	-0.17	-0.09	-0.07
4	59.326	0.5312E-04	59.09	59.10	59.16	59.23	59.26
5	59.652	0.1068E-03	59.17	59.21	59.31	59.47	59.52
6	0.000	0.1068E-03	-0.48	-0.45	-0.34	-0.18	-0.14
7	59.652	0.1068E-03	59.17	59.21	59.31	59.47	59.52
8	59.979	0.1608E-03	59.25	59.31	59.47	59.71	59.78
9	0.000	0.1608E-03	-0.73	-0.67	-0.51	-0.26	-0.20
10	59.979	0.1608E-03	59.25	59.31	59.47	59.71	59.78
11	60.630	0.2693E-03	59.41	59.51	59.77	60.18	60.29
12	0.000	0.2692E-03	-1.22	-1.12	-0.86	-0.44	-0.34
13	60.630	0.2693E-03	59.41	59.51	59.77	60.18	60.29
14	62.248	0.5440E-03	59.78	59.97	60.51	61.35	61.56
15	0.000	0.5440E-03	-2.47	-2.28	-1.74	-0.89	-0.69
16	62.248	0.5440E-03	59.78	59.97	60.51	61.36	61.56
17	65.320	0.1086E-02	60.37	60.76	61.84	63.54	63.95
18	0.000	0.1086E-02	-4.95	-4.56	-3.47	-1.78	-1.37
19	65.320	0.1086E-02	60.36	60.76	61.84	63.54	63.95
20	70.100	0.2067E-02	60.93	61.74	63.76	66.85	67.60
21	0.000	0.2067E-02	-9.17	-8.36	-6.33	-3.25	-2.50
22	70.100	0.2067E-02	60.93	61.74	63.77	66.85	67.60
23	70.883	0.2282E-02	60.98	61.89	64.08	67.39	68.19
24	0.000	0.2282E-02	-9.90	-9.00	-6.80	-3.49	-2.69
25	70.883	0.2282E-02	60.99	61.89	64.08	67.39	68.19
26	72.188	0.2743E-02	61.02	62.12	64.61	68.30	69.19
27	0.000	0.2743E-02	-11.17	-10.07	-7.57	-3.88	-3.00
28	72.188	0.2743E-02	61.02	62.12	64.61	68.30	69.19
29	74.798	0.5810E-02	59.93	62.08	65.72	70.34	71.38
30	0.000	0.5810E-02	-14.87	-12.72	-9.07	-4.46	-3.42
31	74.798	0.5810E-02	59.93	62.08	65.72	70.34	71.38
32	78.713	0.2525E-01	54.85	60.42	66.70	73.18	74.52
33	0.000	0.2525E-01	-23.86	-18.30	-12.01	-5.53	-4.19
34	78.713	0.2525E-01	54.85	60.42	66.70	73.18	74.52
35	82.889	0.4944E-01	50.77	59.04	67.45	75.84	77.55
36	0.000	0.4944E-01	-31.11	-23.25	-15.11	-6.93	-5.25

Table 4.2.3.5-2. Loading history and x-ray-averaged stresses for the Al 7475-T651 alloy in generalized plane strain.

Step No.	Applied Stress (ksi)	Plastic Strain	X-Ray-Averaged Stress (ksi) Penetration Depth (grains)				
			0.500	1.000	2.000	5.000	6.500
1	59.000	0.0000E+00	59.00	59.00	59.00	59.00	59.00
2	59.600	0.5450E-04	59.47	59.47	59.50	59.54	59.56
3	0.000	0.5449E-04	-0.13	-0.13	-0.10	-0.06	-0.04
4	59.600	0.5450E-04	59.47	59.47	59.50	59.54	59.56
5	60.200	0.1094E-03	59.93	59.93	59.99	60.09	60.12
6	0.000	0.1094E-03	-0.27	-0.27	-0.21	-0.11	-0.08
7	60.200	0.1094E-03	59.93	59.93	59.99	60.09	60.12
8	60.800	0.1648E-03	60.38	60.39	60.48	60.63	60.67
9	0.000	0.1648E-03	-0.42	-0.41	-0.32	-0.17	-0.13
10	60.800	0.1648E-03	60.38	60.39	60.48	60.63	60.67
11	62.000	0.2772E-03	61.28	61.30	61.45	61.70	61.78
12	0.000	0.2772E-03	-0.72	-0.70	-0.55	-0.29	-0.22
13	62.000	0.2772E-03	61.28	61.30	61.45	61.70	61.78
14	65.000	0.5673E-03	63.41	63.45	63.79	64.38	64.52
15	0.000	0.5673E-03	-1.59	-1.55	-1.21	-0.62	-0.48
16	65.000	0.5673E-03	63.41	63.45	63.79	64.38	64.52
17	70.733	0.1156E-02	67.04	67.17	67.97	69.31	69.64
18	0.000	0.1156E-02	-3.69	-3.56	-2.77	-1.42	-1.10
19	70.733	0.1156E-02	67.04	67.17	67.97	69.31	69.64
20	75.400	0.2179E-02	70.11	70.42	71.65	73.53	73.96
21	0.000	0.2179E-02	-5.29	-4.98	-3.75	-1.87	-1.44
22	75.400	0.2179E-02	70.11	70.42	71.65	73.53	73.96
23	76.198	0.2745E-02	70.90	71.27	72.53	74.38	74.81
24	0.000	0.2744E-02	-5.29	-4.93	-3.67	-1.82	-1.39
25	76.198	0.2745E-02	70.90	71.27	72.53	74.38	74.81
26	77.528	0.5031E-02	72.59	73.13	74.41	76.08	76.44
27	0.000	0.5031E-02	-4.94	-4.40	-3.12	-1.44	-1.09
28	77.528	0.5031E-02	72.59	73.13	74.41	76.08	76.44
29	80.188	0.1540E-01	74.43	74.90	76.39	78.46	78.90
30	0.000	0.1540E-01	-5.76	-5.29	-3.80	-1.73	-1.29
31	80.188	0.1540E-01	74.43	74.90	76.39	78.46	78.90
32	84.178	0.3176E-01	75.38	76.13	78.39	81.54	82.21
33	0.000	0.3176E-01	-8.80	-8.05	-5.78	-2.64	-1.96
34	84.178	0.3176E-01	75.38	76.13	78.39	81.54	82.21
35	88.434	0.4952E-01	76.05	77.18	80.35	84.75	85.69
36	0.000	0.4952E-01	-12.39	-11.25	-8.08	-3.69	-2.75

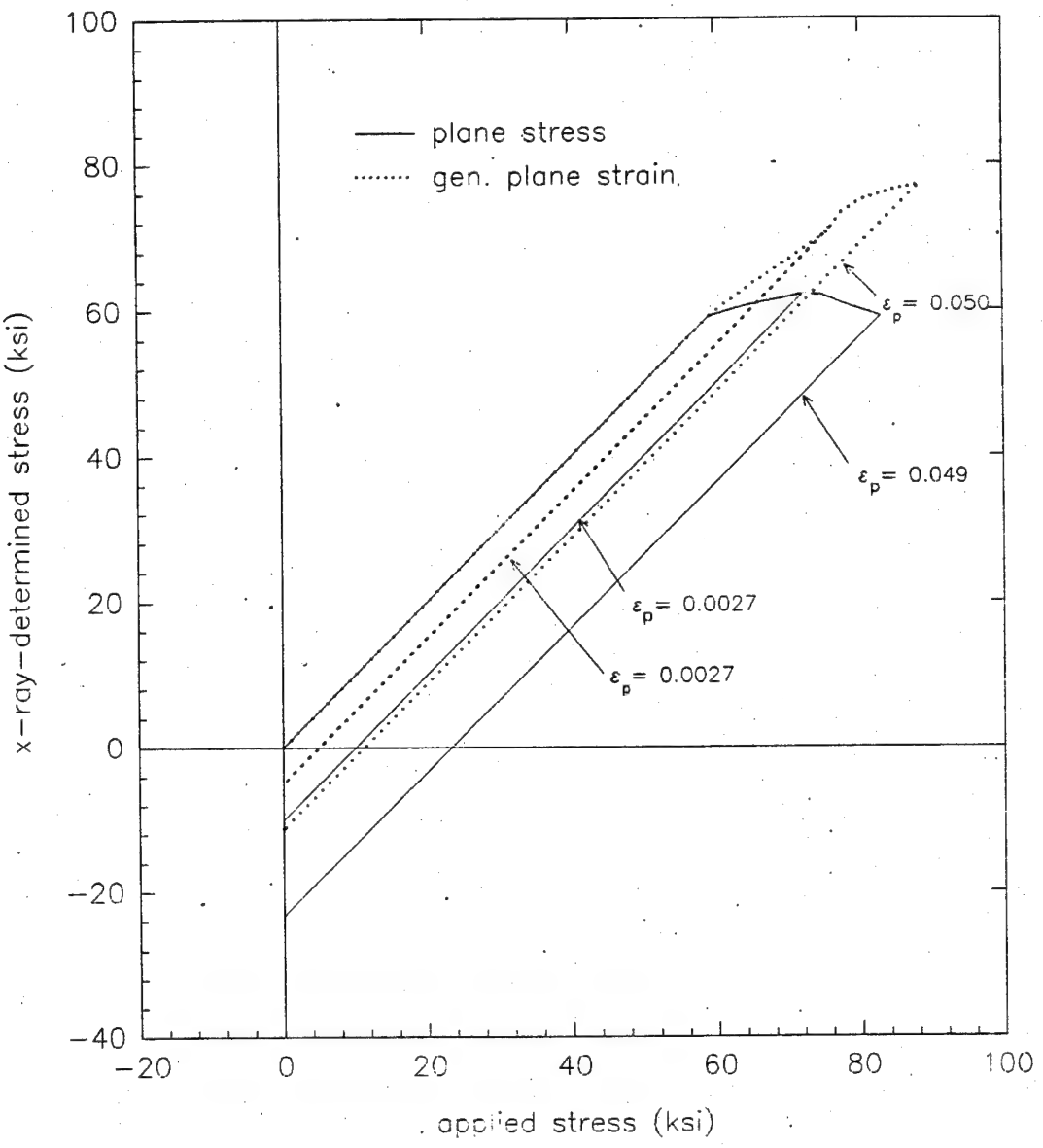

Figure 4.2.3.5-1. Modeling of Aluminum - Calculated x-ray stress versus the nominal applied stress for a penetration depth of one grain, in plane stress and generalized plane strain. (f_s = 0.33, E = 10,400 ksi, υ = 0.33, σ_{ys} = 59 ksi, σ_{yh} = 88 ksi, H_s = 0, H_h = 500 ksi.)

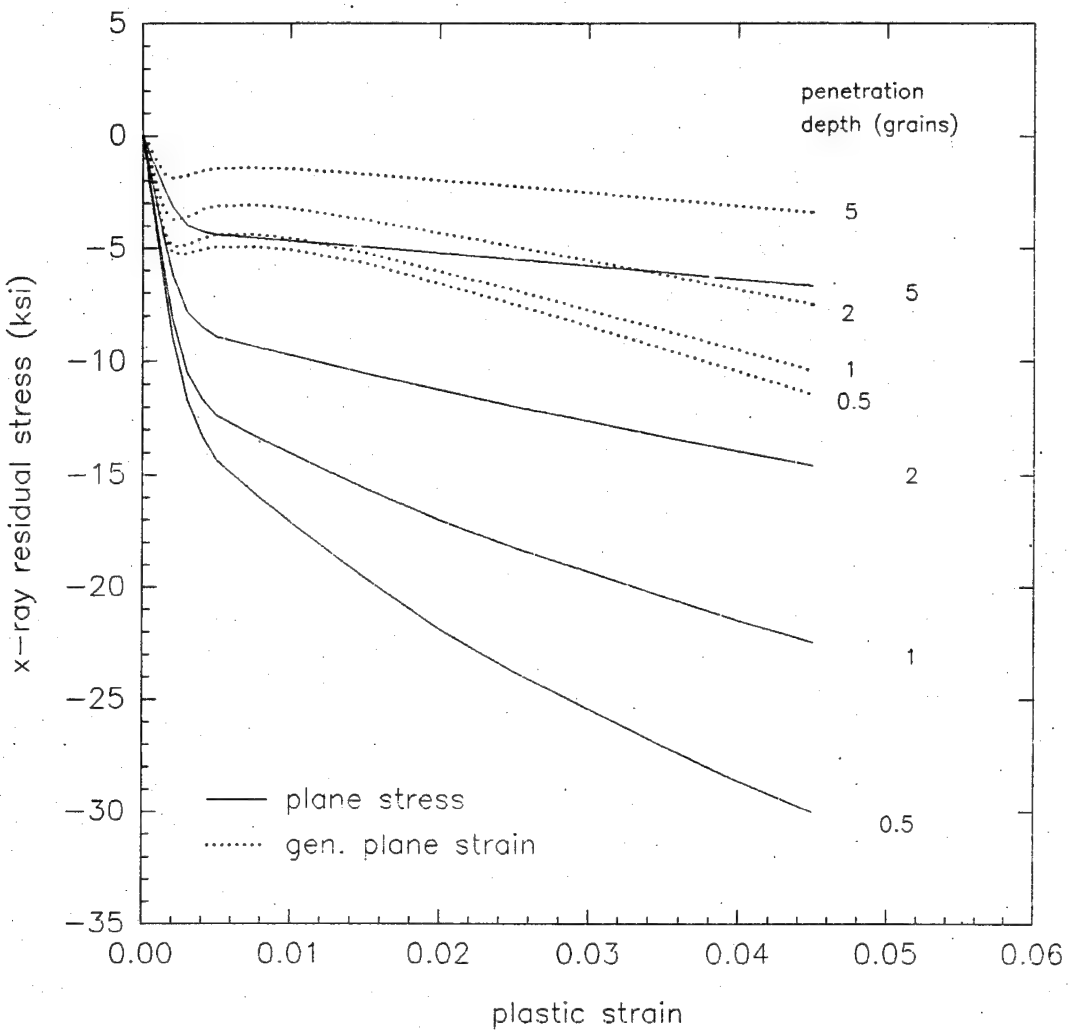

Figure 4.2.3.5-2. Modeling of Aluminum - The residual x-ray stress versus plastic strain for penetration depths of 0.5, 1, 2, and 5 grains, in plane stress and generalized plane strain. (f_s = 0.33, E = 10,400 ksi, υ = 0.33, σ_{ys} = 59 ksi, σ_{yh} = 88 ksi, H_s = 0, H_h = 500 ksi.).

that for a group of four steels with a broad range of strengths, the smooth specimen fatigue limit at the 99.9% survival probability equals the surface yield strength as determined by x-ray diffraction. The authors surmise that when the surface yield strength is reached or exceeded, fatigue damage accumulates under cyclic loading, eventually leading to crack initiation. The well known beneficial effects of inducing compressive residual stresses in the surface layer, such as with shot peening, may in part arise from suppression of the CSLE. The results of this study suggest that prestressing to just below the tensile yield point may be beneficial when there is a large surface layer effect, such as in the Ti-6Al-4V alloy.

In addition, material effects will also contribute, arising from and influencing the CSLE, i.e., the existence of the CSLE induces significant material changes which in turn have an effect on the CSLE. For example, preferential work hardening of the surface layer compared to the bulk material has been demonstrated in Al 2024 alloy specimens subjected to fatigue cycling [38].

5.0 CONCLUSIONS

In uniaxial tension tests performed on uniform cross section specimens of Ti-6AL-4V and aluminum 7475-T651, the stress in the direction of load application determined by x-ray diffraction and the nominal applied stress display the expected linear correspondence up to a maximum stress a little below the bulk yield point. Above this stress, the x-ray stress plateaus. Upon reversing the load, the x-ray stress and applied stress follow each other linearly but with an offset which corresponds to a compressive x-ray stress at zero applied load, i.e., there is a compressive residual stress in the direction of load application. The x-ray diffraction measurements provide average stress values in a surface layer of only a few grain diameters. These results therefore suggest that the surface layer of the metal is yielding at a lower stress than the bulk. Similar results have been reported for other metals, notably iron [8] and nickel [12].

This anomalous behavior is duplicated qualitatively with a continuum model consisting of a 2-D array of isotropic soft square grains embedded in a matrix of isotropic hard grains. Ordered and disordered arrays give similar results. The plastic anisotropy is modeled by the lower yield point of the soft grains, representing crystals or groups of crystals ("domains") in favorable orientations for yielding; the yield point spread between the soft and hard grains represents the degree of grain plastic anisotropy and texture. The Von Mises-Hill yield criterion was used, but similar results are expected with any yield criterion which allows no plastic deformation under a pure hydrostatic stress. The effect is purely mechanical. The greater mutual constraints of the grains in the interior compared with those with a free surface lead to greater hydrostatic stresses in the interior, which inhibit plastic deformation. No material effect, such as a lower yield point or dislocation density for the surface grains, needs to be invoked. The continuum surface layer effect (CSLE) is thus an inherent property of an aggregate of crystals. It may viewed as an extension of the Heyn intergranular stresses to include the effect of a free surface.

The basic model used has a soft grain concentration of 33%, E = 30,000 ksi, υ = 0.29, soft and hard grain yield points of 15 and 20 ksi, respectively, no soft grain hardening, and a hard grain hardening rate of 100

ksi, corresponding to iron or mild steel with a yield point of 18 ksi, a tangent work hardening rate of 39 ksi (1 to 4.5% plastic strain), and partial texturing (≈ 33%). However, the model parameter values were varied over a wide range to determine their effect on the CSLE. The salient features of the surface layer effect are as follows:

(1) The proportional limit and the onset of x-ray stress effect coincide and correspond to the yield point of the soft grains in the surface layer.

(2) The compressive residual stresses increase very rapidly after the onset of plasticity, at ϵ_p = 0.0005 reaching more than 50% of the value at ϵ_p = 0.05 (100 times greater). The magnitude of the residual stresses is sizable

(3) The continuum effect decreases rapidly with depth, becoming negligible for depths exceeding 2-4 grain or "domain" diameters. The thickness of the surface layer hovers around two grains under a wide range of conditions, although it becomes one grain for f_s = 25% or 17% and for a grain aspect ratio greater than one; it approaches three grains in plane strain.

(4) The magnitude of the compressive residual stresses depends only on E at very low plastic strains.

(5) The effect increases with:

- grain plastic anisotropy;
- grain size;
- a decrease in texture;
- E (below the bulk yield point);
- a greater work hardening rate of the hard grains;
- a lower work hardening rate of the soft grains;
- the bulk plastic strain;
- the bulk yield point.

Although this was not shown by calculation, it is expected that the effect is enhanced by time dependent plasticity, i.e., creep.

(6) The effect is insensitive to the bulk value of υ, and, above the bulk yield point, to the bulk value of E.

(7) The CSLE is comparable in plane stress (PS) and plane strain (PE), but significantly less in generalized plane strain (GPE). Thus, the compressive residual stresses in GPE are typically 50% to 65% (and even less for small yield point spread(YPS) and no grain hardening) of those in PS. This paradoxical result is an indication that the CSLE depends on a difference in constraint between the surface and bulk grains, rather than on the degree of lateral constraint.

(8) For plastic strains $\geq$ 1% and constant grain hardening, the residual stresses tend to increase linearly in PE, GPE, and axisymmetry AXS, but level off in PS. Of course, the dependence of the residual stress on plastic strain will also depend on the value of the grain hardening rates with plastic strain.

(9) In GPE and AXS, the model also predicts a transverse compressive residual stress. This stress is comparable in magnitude to or larger than the corresponding longitudinal residual stresses, the difference being greater in the absence of grain hardening.

(10) Grain elongation (i.e., GAR > 1) in the direction of load application decreases the residual stresses, except for very small plastic strains (ϵ_p = 0.00005).

According to this model the surface layer of the polycrystalline aggregate starts to yield when the yield point of the weakest (softest) grains in the surface layer is reached. An estimate of the onset of surface yielding for bcc metals with dominant slip systems <111>{110} and randomly oriented grains, predicts that this onset is at 0.75 of the bulk yield point, in agreement with the experimental value of Sasaki and Sato [14] for steel. The same result is obtained for fcc metals with dominant slip systems <110>{111}.

The model, even though rudimentary, is in good semi-quantitative agreement with the residual stresses reported for iron and nickel. The model not only predicts the compressive longitudinal residual stress, but also the compressive transverse residual stress observed for iron and mild steel. The two residual stresses are of comparable magnitude experimentally and according

to the model. Although reasonable agreement between the experimental and the calculated residual stresses is also obtained for the Ti-6Al-4V and Al 7475-T651 specimens of this study, the model appears to underestimate the residual stresses in both metals. At least part of the discrepancy is probably caused by the creep observed in these metals under the conditions of the measurements. Creep would allow the surface layer which yields first to undergo considerably more plastic deformation than calculated, leading to much greater compressive residual stresses upon unloading. Further work is required to quantify the model for real systems and to assess the importance of material effects acting in conjunction with the continuum effect.

The CSLE may play a significant role in metal fatigue because it has been shown that crack initiation is often at or near the surface. Under cyclic loading, local plastic deformation will lead to damage accumulation and crack initiation in the soft surface grains. This type of mechanism has been suggested recently by He, Wang, and Nan [37] who found that the smooth fatigue limit of steels they tested equals the surface yield strength determined by x-ray diffraction.

6. RECOMMENDATIONS FOR FUTURE WORK

Both the experimental and the theoretical work performed in this study are preliminary efforts. If it should be desired to extend this work, suggestions for future work are:

(1) Refine and expand the finite element calculations:

(a) Include elastic and plastic anisotropic behavior, for a more exact representation of polycrystalline aggregates, in particular of an actual metal, such as iron, for which a substantial surface layer has been observed, and for which considerable mechanical data exists, including single crystal data..

(b) Expand to 3-dimensional models.

(c) Try other yield criteria.

(d) Include creep.

(e) Study the effect of bending and torsion.

(f) Study the effect of cyclic loading.

(g) Consider other specimen shapes, such as notches, which are important practically and theoretically in the study of metal fatigue and stress corrosion cracking.

(h) Develop a more sophisticated model to account for grain shape, preferred orientation, and the presence of more than one phase.

(i) Consider the effect of surface roughness.

(j) Develop a finite element which models crystal physical plasticity processes.

(k) Develop a statistical rationale for the representation of polycrystalline aggregates with arrays of soft square grains in a matrix of hard grains. Optimize soft grain concentration for various crystal orientation distributions, in particular a random distribution.

(2) Test the continuum effect experimentally: For example, the surface layer effect is predicted to increase with grain size and plastic anisotropy.

(3) Further characterize experimentally the nature of the surface layer effect and its variation with the fundamental physical properties of the constituent crystals. Gage the relative importance and coupling of the continuum and material effects. (such work is expected to be difficult and costly if it is to produce definitive results).

(4) Study the time dependence of the surface layer effect.

(5) Study the effect in non-metallic crystalline aggregates.

(6) Examine the implications of the surface layer effect in fatigue and surface treatment.

(7) Approach the problem with a micromechanical self-consistent method (Mura [3], p. 443).

7. REFERENCES

1. Dowling, N. E. and Dunn, D. O., Residual Stress Changes in Fatigue, Volume 1 - Residual Stress Measurements by X-Ray Diffraction in Notched Test Specimens, NADC-88141-60 (Volume I), Air Vehicles and Crew Systems Technology Development, Naval Air Development Center, Warminster, PA 18974-5000, March 1989.

2. Dowling, N. E. and Dunn, D. O., "Direct Stress Measurement by X-Ray Diffraction During Fatigue Testing." ASTM subcommittee E9.01 on Fatigue Research, Reno, Nevada, April 1988.

3. Mura, T., "Micromechanics of Defects in Solids," second edition, Martinus Nijhoff Publishers, Boston, 1987.

4. Bollenrath Von, F., Hauk, V., and Osswald, E., "Ront-genographische Spannungsmessungen bei Uberschreiten der grenze an Zugstaben aus unlegiertem Stahl." Zeitschrift des Vereines deutscher Ingenieure, Vol. 83, pp. 129-132, 1939.

5. Greenough, G. B., Nature, Vol. 166, No. 4221, pp. 509-510, 1950.

6. Smith, S. L. and Wood, W. A., "Internal Stress Created by Plastic Flow in Mild Steel, and Stress-Strain Curves for the Atomic Lattice of Higher Carbon Steels." Proceedings of the Royal Society, Series A, Vol. 182, pp. 404-414, 1944.

7. Greenough, G. B., "Residual Lattice Strains in Plastically Deformed Polycrystalline Metal Aggregates." Proceedings of the Royal Society, Series A, Vol. 197, pp. 556-567, 1949.

8. Greenough, G. B., "Macroscopic Surface Stresses Produced by Plastic Deformation." Journal of the Iron and Steel Institute, Vol. 169, pp. 235-241, 1951.

9. Heyn, E., "Internal Strains in Cold-Wrought Metals, and Some Troubles Caused Thereby." The Journal of he Institute of Metals, Vol. 2, pp. 3-37, 1914.

10. Nakanishi, F., and Sato, Y., "Strength of Surface Layers of Beams Under Bending." Proceedings of the Japan National Congress for Applied Mechanics, 5th, I-36, pp. 169-173, 1955. (Available in English in Selected Papers of F. Nakanishi, Department of Aeronautics, The University of Tokyo, Tokyo, Japan, June 1966).

11. Nakanishi, F. and Hanada, M., "Yield Point of Mild Steel under Sharply Concentrated Stress." Transactions of the Japan Society of Mechanical Engineers, Vol. 19, No. 87 (Nov.), pp. 13-18, 1953 (Available in English in Selected Papers of F. Nakanishi, Dept. of Aeronautics, The University of Tokyo, Tokyo, Japan, June 1966).

12. Kolb, K. and Macherauch, E., "The Flow Stress of Surface Layers of Polycrystalline Nickel and its Influence on the Residual Stresses in Deformed Specimens." Philosophical Magazine, Series 8, Vol. 7, pp. 415-426, 1962. {MRK }{PS Document Body,Document Body}

13. Fleischer, R. L., and Hosford, W. F., Jr., "Easy Glide and Grain Boundary Effects in Polycrystalline Aluminum." Transactions of the Metallurgical Society of AIME, Vol. 221, pp. 244-247, 1961.

14. Sasaki, H. and Sato, Y., "Strength of the Surface Layer of Mild Steel." Journal of Engineering Materials and Technology, Vol. 103, pp. 282-286, 1981.

15. Barrett, C. S., Structure of Metals, 2nd Edition, McGraw-Hill, New York, 1952.

16. Barrett, C. S. and Massalski, T. B., Structure of Metals, Third Revised Edition, Pergamon Press, New York, 1980.

17. Lin, T. H. and Tung, T. K., "The Stress Field Produced by Localized Plastic Slip at a Free Surface." Journal of Applied Mechanics, Vol. 29, pp. 523-532, 1962.

18. Chiu, Y. P., "On the Stress Field and Surface Deformation in a Half Space with a Cuboidal Zone in which Initial Strains are Uniform." Journal of Applied Mechanics, Vol. 45, pp. 302-306, 1978.

19. Seo, K. and Mura, T., "The Elastic Field in a Half Space Due to Ellipsoidal Inclusions with Uniform Dilatational Eigenstrains ." Journal of Applied Mechanics, Vol. 46, pp. 568-572, 1979.

20. RMI Company, "Facts About the Metallography of Titanium." Niles, Ohio.

21. Metals Handbook, 8th Edition, Vol. 8, "Metallography, Structures, and Phase Diagrams," American Society for Metals, Metals Park, Ohio.

22. Noyan, I. C. and Cohen, J. B., Residual Stress - Measurement by Diffraction and Interpretation, Springer-Verlag, New York, 1987.

23. Technology for Energy Corporation, TEC Model 1600 X-Ray Analysis Systems Operation and Maintenance Manual, Knoxville, TN, 1985.

24. Dowling, N. E., Hendricks, R. W., and Ranganathan, K., "X-Ray Residual Stress Measurements in Notched Test Specimens." Appendix A in NADC-88141-60 (Vol. I) by N. E. Dowling and D. O. Dunn, March 1989.

25. James, M. R., "The Use of Oscillation on PSD-Based Instruments for X-Ray Measurement of Residual Stress." Experimental Mechanics, Vol. 27, pp. 164-167, 1987.

26. Chiu, Y. P., "On the Stress Field Due to Initial Strains in a Cuboid Surrounded by an Infinite Elastic Space." Journal of Applied Mechanics, Vol. 44, pp. 587-590, 1977.

27. Owen, D. R. J. and Hinton, E., Finite Elements in Plasticity: Theory and Practice, Pineridge Press Limited, Swansea, U. K., 1980.

28. Chen, W. F. and Han, D. J., "Plasticity for Structural Engineers," Springer-Verlag, New York, 1988.

29. Kocks, U. F., "The Relation Between Polycrystal Deformation and Single Crystal-Deformation." Metallurgical Transactions, Vol. 1, pp. 1121-1143, 1970.

30. Hein, V. L., and Erdogan, F., "Stress Singularities in a Two-Material Wedge." International Journal of Fracture Mechanics, Vol. 7, pp. 317-330, 1971.

31. Ewalds, H. L. and Wanhill, R. J. H., "Fracture Mechanics," Edward Arnold Publishers Ltd, London, 1984.

32. Reed-Hill, R. E., "Physical Metallurgy Principles," 2nd Edition, PWS Engineering, Boston Massachusets, 1973.

33. Hill, R., "The Mathematical Theory of Plasticity," Oxford University Press, 1950.

34. Frederick, D. and Chang, T. S., "Continuum Mechanics," Scientific Publishers, Inc., Cambridge, 1972, Chap. 1.

35. International Tables for Crystallography, Vol. 6, J. A. Ibers and W. C. Hamilton, Editors, Kynoch Press, Birmingham, England, 1974, Section 2.1.

36. Dowling, E. D., "Mechanical Behavior of Materials," Prentice Hall, Englewood Cliffs, New Jersey, 1993, Sections 9.5 and 9.6.

37. He, J., Wang, H., and Nan, J., "Fatigue Strength Evaluation from Surface Yielding Data." Fatigue & Fracture of Engineering Materials & Structures, Vol. 16, pp. 591-596, 1993.

38. Pangborn, R. N., Weissmann, S., and Kramer, I. R., "Determination of Prefracture Fatigue Damage," Report DTNSRDC-80/006, Department of the Navy, Bethesda, Maryland 20084.

SYMBOLS, ABBREVIATIONS, AND TERMINOLOGY

Symbols

$\alpha(\theta,\beta)$	Distribution density function describing the crystal orientations in the polycrystalline aggregate.
$\Gamma^{(n)}$	Resolved shear stress on the nth slip system.
Γ_{cr}	Critical shear stress of slip system.
$\Gamma_{cr}^{(n)}$	Critical shear stress on the nth slip system.
$\Delta A(\theta_q,\beta_q)$	Total cross sectional area of grains belonging to orientation set (θ_q,β_q) normal to the tensile stress.
Δc_q	$\Delta A(\theta_q,\beta_q)/A$
ϵ_p	Bulk plastic strain in the longitudinal direction, i.e., the direction of the applied load.
θ	X-ray diffraction angle.
(θ,β)	Crystal orientation relative to the applied uniaxial stress (see Figure 4.2.3.1-1).
μ	X-ray linear absorption coefficient.
$\sigma(x)$	is the plane-averaged stress component, which is a function of the depth x.
$\langle\sigma\rangle$	Average tensile stress in the polycrystalline aggregate (Sec. 4.2.3.1).
σ_ϕ	Normal stress in direction ϕ.
σ_{app}	Nominal applied stress, P/A. (Also S.)

σ_{dev}	Stress for which the x-ray stress starts to deviate appreciably from the nominal applied stress in a real specimen.
σ_i	Tensile stress in the ith grain of polycrystalline aggregate (Sec. 4.2.3.1).
σ_{pl}	Proportional limit of the specimen.
σ_{rgl}	Average longitudinal residual stress in the surface grains.
σ_{rxl}	X-ray-averaged residual stress in the longitudinal direction for a penetration depth of one grain.
σ_{Trgl}	Average transverse (z-direction) residual stress in the surface grains.
σ_{Trxl}	X-ray-averaged residual stress in the transverse (z-direction) direction for a penetration depth of one grain.
σ_v	Stress tensor components expressed in matrix notation: $\sigma_1 = \sigma_{11}$, $\sigma_2 = \sigma_{22}$, $\sigma_3 = \sigma_{33}$, $\sigma_4 = \sigma_{23} = \sigma_{32}$, $\sigma_5 = \sigma_{13} = \sigma_{31}$, $\sigma_6 = \sigma_{12} = \sigma_{21}$.
$\sigma_{x\text{-}ray}$	is the x-ray-averaged stress component.
σ_{xx}, σ_{yy}, σ_{xy} σ_{11}, σ_{22}, σ_{12}	Stress tensor components ($\sigma_{11} = \sigma_{xx}$, etc.).
σ_y	Uniaxial stress acting on crystal.
$\sigma_{Y\ bulk}$	Bulk yield point of the polycrystalline aggregate (Sec. 4.2.3.1).
$\sigma_Y(\theta\ \beta)$	Yield point of crystal in orientation (θ,β).

σ_{yB}	Bulk yield point of the specimen with 0.002 plastic strain offset, as determined from the finite element calculations.
σ_{yh}	Yield point of the hard grains.
σ_{ymix}	Yield point of the grain array by the rule of mixtures.
σ_{ys}	Yield point of the soft grains.
$<\sigma_{yy}>_{pl}$	Plane-averaged longitudinal stress.
τ	Thickness of surface layer over which the average longitudinal stress pattern appears to be significantly different from that in the bulk.
υ	Poisson ratio.
ϕ	Angle which the plane containing the incident and diffracted s-ray beams make with the sample coordinate system (Figure 2.3-1).
ψ	Angle of the diffracting planes with respect to the specimen surface plane (Figure 2.3-1).
Ω	Initial stress deviation ratio, defined as the initial slope of the x-ray stress versus applied stress (Eq. 4.2.2-1).
A	Cross-sectional area of tensile specimen normal to the applied load.
A_i	Cross sectional area of the ith grain normal to the tensile stress (Sec. 4.2.3.1).
c_i	A_i/A (Sec. 4.2.3.1).

d	Lattice spacing in the strained specimen determined at angles ϕ and ψ.
$d\Omega$	Solid angle differential.
d_0	Lattice spacing of the diffracting planes in the unstrained specimen.
dc	Infinitesimal counterpart of Δc_q.
dI	is the intensity diffracted from an infinitesimally thin layer at depth x below the surface.
E	Young's modulus.
f_c	is the volume fraction of grains that can diffract at the given diffraction angle θ.
f_D	is the fraction of incident energy diffracted per unit volume.
f_h	Hard grain fraction or concentration.
f_s	Soft grain fraction or concentration.
G_p	The fraction of the total x-ray intensity diffracted by the surface layer of thickness x_p (Section 4.2.1).
h	Mesh height.
H_B	Bulk or specimen tangent hardening rate from 0.01 to 0.045 plastic strain.
H_h	Hardening rate for the hard grains.
H_s	Hardening rate for the soft grains.

I_o	is the intensity of the incident beam.
$m_i^{(n)}$	Unit vector perpendicular to the slip plane of the nth slip.
(n)	As superscript, to denote the nth slip system (Section 4.2.3.1).
n_i, i=1, 2, 3	Components of the vector normal to a continuum surface element.
$n_i^{(n)}$	Unit vector in the slip direction of the nth slip.
P	Applied load on tensile specimen.
q (subscript)	To denoted a group or set of grains having the same orientation with respect to the applied load.
S	Shear strength of cubic crystal with respect to the principal directions of the crystal (Section 4.2.3.1).
S	Boundary surface of continuum region (Section 4.2).
S	Nominal applied stress, P/A. (Also σ_{app}.)
$s_v^{(n)}$	Resolved shear stress coefficients: $s_1 = m_1n_1$, $s_2 = m_2n_2$, $s_3 = m_3n_3$, $s_4 = m_2n_3 + m_3n_2$, $s_5 = m_1n_3 + m_3n_1$, $s_6 = m_1n_2 + m_2n_1$. (Section 4.2.3.1.)
u_x, u_y	Displacement vector components in the x and y directions, respectively.
V	Volume of continuum region (Section 4.2).
v	As subscript, to denote tensor vector notation. See σ_v, above, for equivalence with tensor indicial notation.

w	Mesh width.
x, y, z x_i, i=1, 2, 3	Cartesian coordinates.
x_p	The effective penetration depth of the diffracted x-ray beam (Section 4.2.1).
X	Tensile strength of cubic crystal with respect to the principal directions of the crystal.
X_v	Crystal strengths (Section 4.2.3.1).

Abbreviations

AXS	Axisymmetric, axisymmetry
CSLE	Continuum surface layer effect.
el	Element
GAR	Grain aspect ratio, i.e., the ratio of the height (y-dir.) to the width (x-dir.) of the soft grain.
GPE	Generalized plane strain.
gr	grain
L	Linear geometry approximation.
NL	Nonlinear geometry.
PE	Plane strain.
PS	Plane stress.
YPS	Yield point spread between the elastic limit of the hard and soft grains, i.e., $\sigma_{yh} - \sigma_{hs}$.

Terminology and Conventions

The following terminology and conventions apply throughout the text:

The y-direction is the longitudinal or vertical direction of the specimen, and is parallel to the free surface.

The x-direction is normal to the free surface, with x = 0 at the free surface and x > 0 into the specimen. The depth equals x.

The z-direction is the transverse or thickness direction. z = 0 in the plane of symmetry containing the x- and y-axes.

The applied tensile load is always in the y-direction.

The finite element calculations are for models in plane stress, unless otherwise noted.

All the x-ray penetration depths are for 99% of the total diffracted intensity (i.e., $G_p = 0.99$).

"X-ray stress" is short for the x-ray-averaged stress for a penetration depth of one grain corresponding to 0.99 of the diffracted x-ray intensity fraction.

"Stress profile" is short for the profile of the plane-averaged longitudinal stress versus depth.

In comparing residual stresses, the most compressive is termed the largest

APPENDIX

LISTING OF ABAQUS CODE - EXAMPLE

The ABAQUS code for the basic model described in Section 4.2.1 of the main text is given here as a typical example of the code used. This example illustrates load-controlled loading. The code for displacement-controlled loading is similar.

```
*HEADING
MODEL SAS01HD                                07:04:33 WED 22 DEC 1993
STANDARD MODEL, 0.33 SOFT, 100 E/G, W=6.5 G, Ys=15, Yh=20, Hh=100 KSI

    This is the standard model with 33% soft grain concentration,
    E = 30,000 ksi, v = 0.29, soft grain yield point of 15 ksi,
    hard grain yield point of 20 ksi, no soft grain hardening, and
    hard grain hardening of 100 ksi.  Mesh width is 6.5 grains
    (i.e., specimen width is 13 grains), and there are 10 X 10
    elements per grain.  Specimen extends to infinity in the loading
    direction.  Run on ABAQUS 5.2. Default convergence criteria used.

  975 ELEMENTS, 1056 NODES, 2-D, 65 PLANES, 15 EL/COL, 1 REGION(S)
  9.75 GRAINS (1.5 VERT. X 6.5 HORIZ.) TOTAL, 1.5 ON SURFACE
  PLANE STRESS, BILINEAR QUADRILATERAL, 4-NODE ELEMENT, CPS4
  MATERIAL PROPERTY FRACTIONS (PROPERTY #, FRACTION):
     1, 0.667;    2, 0.333;
   (NO PADDING ELEMENTS)
  2 MATERIAL PROPERTIES
```

APPENDIX - Listing of ABAQUS Code (Continued)

```
      E=2.999E7 PSI, V=0.29
      YIELDS (KSI):     20     15
      HARDENING (KSI): 100      0
   LOADING: 36 STEPS, 12 UNLOADINGS                    (ABAQUS 5)
   APPROXIMATE PLASTIC STRAINS (EP):
     0, 0.00005, 0.0001, 0.00015, 0.00025, 0.0005, 0.001, 0.002,
     0.005, 0.01. 0.02, 0.035, 0.051
   INC=333, MIN INC SIZE =6.25E-7
   CONTROLS: DEFAULTS (R=0.005, C=0.010) FOR ALL STEPS
   VALUE OF CONSTANTS USED IN STRAIN-TO-LOAD CALCULATIONS
      E, SPROP, SYIELD, OFFSET STRAIN, H1, H2, N, A:
      30000.00 15.00 17.897 0.00200 17017. 39.9 35.3 3.46338746
   FILE MODULES USED IN GENERATING THIS PROGRAM:
     TITLE:                              SAS01HD TITLE D1
     MESH:                               SAS MESHABQ D1
     ELEMENT PROPERTY ASSIGNMENT:        SAS33 ABQINP D1
     MATERIAL PROPERTY DEFINITIONS:      SI2M1520 CCPROP D1
     LOADING:                            S36LG051 HDSTEP D1
     CONSTANTS FOR LOAD CALCULATIONS:    SAS01GC MODEL D1
   (GENERATED WITH ABQINP, VERSION 5.9)
**DATA CHECK
*PREPRINT, ECHO=NO, HISTORY=NO, MODEL=NO
** BEGIN MESH MODULE SAS **********************
** 975 ELEMENTS, 1056 NODES, 2-D, 65 PLANES, 15 EL/COL, 1 REGION(S)
** 9.75 GRAINS (1.5 VERT. X 6.5 HORIZ.) TOTAL, 1.5 ON SURFACE
** PLANE STRESS, BILINEAR QUADRILATERAL, 4-NODE ELEMENT, CPS4
**
**
** CORNER NODES:    16  1056   CORNER ELEMENTS:    15   975
**                   1  1041                        1   961
**
```

APPENDIX - Listing of ABAQUS Code (Continued)

```
** MESH DIMENSIONS:
**      GRAINS:        WIDTH=6.5, HEIGHT=1.5
**      LENGTH UNITS: WIDTH=6.50, HEIGHT=1.5
**      THICKNESS: 0.153846154 (TO ACHIEVE UNIT CROSS SECTIONAL AREA)
**
** GRAIN SIZE (LENGTH UNITS): WIDTH=1, HEIGHT=1
** GRAIN SIZE REPRESENTATION WITH ELEMENTS (1 REGION(S)):
**     REGION 1: 10 X 10, 100 ELEMENT(S)
**
** NO. OF PLANES (ELEMENTS) AND THEIR WIDTH IN EACH REGION:
**   REGION      NO. OF PLANES     WIDTH, GRAINS     WIDTH, L.U.
**      1              65           0.10000           0.10000
**
*NODE, SYSTEM=R
        1,   0.00000,  0.00000,  0.00000
       16,   0.00000,  1.50000,  0.00000
     1041,   6.50000,  0.00000,  0.00000
     1056,   6.50000,  1.50000,  0.00000
*NGEN, NSET=N1, SYSTEM=R
    1,16,1
*NGEN, NSET=N2, SYSTEM=R
    1041,1056,1
** REGION WIDTH: 65 ELEMENTS, 6.50 LENGTH UNITS
*NFILL, BIAS=1.0,NSET=NREG1
    N1,N2,65,16
*ELEMENT, TYPE=CPS4, ELSET=EFIRST
    1,1,17,18,2
*ELGEN, ELSET=COLALL
    1,15,1,1,65,16,15
** DEFINE SET CONTAINING THE TOP RIGHT CORNER NODE
*NSET, NSET=NTRC
```

APPENDIX - Listing of ABAQUS Code (Continued)

```
    1056,
*NSET, NSET=TOPM1, GENERATE
    16,1040,16
*NSET, NSET=TOP
    1056, TOPM1
*NSET, NSET=EDGER, GENERATE
    1041,1056,1
*NSET, NSET=BOTTOM, GENERATE
    1,1041,16
** FOR DATA COLLECTION ONLY:
*ELSET, ELSET=COLO, GENERATE
    1,15,1
** END MESH MODULE SAS ************************
** BEGIN ELPA MODULE - ELEMENT PROPERTY ASSIGNMENTS -   975 ELEMENTS
** MATERIAL PROPERTY FRACTIONS (PROPERTY #, FRACTION):
**     1, 0.667;    2, 0.333;
**  (NO PADDING ELEMENTS)
**
*ELSET, ELSET=E1
     6,    7,    8,    9,   10,   11,   12,   13,   14,   15,
    21,   22,   23,   24,   25,   26,   27,   28,   29,   30,
    36,   37,   38,   39,   40,   41,   42,   43,   44,   45,
    51,   52,   53,   54,   55,   56,   57,   58,   59,   60,
    66,   67,   68,   69,   70,   71,   72,   73,   74,   75,
    81,   82,   83,   84,   85,   86,   87,   88,   89,   90,
    96,   97,   98,   99,  100,  101,  102,  103,  104,  105,
   111,  112,  113,  114,  115,  116,  117,  118,  119,  120,
   126,  127,  128,  129,  130,  131,  132,  133,  134,  135,
   141,  142,  143,  144,  145,  146,  147,  148,  149,  150,
   151,  152,  153,  154,  155,  156,  157,  158,  159,  160,
   166,  167,  168,  169,  170,  171,  172,  173,  174,  175,
```

APPENDIX - Listing of ABAQUS Code (Continued)

```
181,  182,  183,  184,  185,  186,  187,  188,  189,  190,
196,  197,  198,  199,  200,  201,  202,  203,  204,  205,
211,  212,  213,  214,  215,  216,  217,  218,  219,  220,
226,  227,  228,  229,  230,  231,  232,  233,  234,  235,
241,  242,  243,  244,  245,  246,  247,  248,  249,  250,
256,  257,  258,  259,  260,  261,  262,  263,  264,  265,
271,  272,  273,  274,  275,  276,  277,  278,  279,  280,
286,  287,  288,  289,  290,  291,  292,  293,  294,  295,
306,  307,  308,  309,  310,  311,  312,  313,  314,  315,
321,  322,  323,  324,  325,  326,  327,  328,  329,  330,
336,  337,  338,  339,  340,  341,  342,  343,  344,  345,
351,  352,  353,  354,  355,  356,  357,  358,  359,  360,
366,  367,  368,  369,  370,  371,  372,  373,  374,  375,
381,  382,  383,  384,  385,  386,  387,  388,  389,  390,
396,  397,  398,  399,  400,  401,  402,  403,  404,  405,
411,  412,  413,  414,  415,  416,  417,  418,  419,  420,
426,  427,  428,  429,  430,  431,  432,  433,  434,  435,
441,  442,  443,  444,  445,  446,  447,  448,  449,  450,
451,  452,  453,  454,  455,  456,  457,  458,  459,  460,
466,  467,  468,  469,  470,  471,  472,  473,  474,  475,
481,  482,  483,  484,  485,  486,  487,  488,  489,  490,
496,  497,  498,  499,  500,  501,  502,  503,  504,  505,
511,  512,  513,  514,  515,  516,  517,  518,  519,  520,
526,  527,  528,  529,  530,  531,  532,  533,  534,  535,
541,  542,  543,  544,  545,  546,  547,  548,  549,  550,
556,  557,  558,  559,  560,  561,  562,  563,  564,  565,
571,  572,  573,  574,  575,  576,  577,  578,  579,  580,
586,  587,  588,  589,  590,  591,  592,  593,  594,  595,
606,  607,  608,  609,  610,  611,  612,  613,  614,  615,
621,  622,  623,  624,  625,  626,  627,  628,  629,  630,
636,  637,  638,  639,  640,  641,  642,  643,  644,  645,
```

APPENDIX - Listing of ABAQUS Code (Continued)

```
 651,  652,  653,  654,  655,  656,  657,  658,  659,  660,
 666,  667,  668,  669,  670,  671,  672,  673,  674,  675,
 681,  682,  683,  684,  685,  686,  687,  688,  689,  690,
 696,  697,  698,  699,  700,  701,  702,  703,  704,  705,
 711,  712,  713,  714,  715,  716,  717,  718,  719,  720,
 726,  727,  728,  729,  730,  731,  732,  733,  734,  735,
 741,  742,  743,  744,  745,  746,  747,  748,  749,  750,
 751,  752,  753,  754,  755,  756,  757,  758,  759,  760,
 766,  767,  768,  769,  770,  771,  772,  773,  774,  775,
 781,  782,  783,  784,  785,  786,  787,  788,  789,  790,
 796,  797,  798,  799,  800,  801,  802,  803,  804,  805,
 811,  812,  813,  814,  815,  816,  817,  818,  819,  820,
 826,  827,  828,  829,  830,  831,  832,  833,  834,  835,
 841,  842,  843,  844,  845,  846,  847,  848,  849,  850,
 856,  857,  858,  859,  860,  861,  862,  863,  864,  865,
 871,  872,  873,  874,  875,  876,  877,  878,  879,  880,
 886,  887,  888,  889,  890,  891,  892,  893,  894,  895,
 906,  907,  908,  909,  910,  911,  912,  913,  914,  915,
 921,  922,  923,  924,  925,  926,  927,  928,  929,  930,
 936,  937,  938,  939,  940,  941,  942,  943,  944,  945,
 951,  952,  953,  954,  955,  956,  957,  958,  959,  960,
 966,  967,  968,  969,  970,  971,  972,  973,  974,  975,
*ELSET, ELSET=E2
   1,    2,    3,    4,    5,   16,   17,   18,   19,   20,
  31,   32,   33,   34,   35,   46,   47,   48,   49,   50,
  61,   62,   63,   64,   65,   76,   77,   78,   79,   80,
  91,   92,   93,   94,   95,  106,  107,  108,  109,  110,
 121,  122,  123,  124,  125,  136,  137,  138,  139,  140,
 161,  162,  163,  164,  165,  176,  177,  178,  179,  180,
 191,  192,  193,  194,  195,  206,  207,  208,  209,  210,
 221,  222,  223,  224,  225,  236,  237,  238,  239,  240,
```

APPENDIX - Listing of ABAQUS Code (Continued)

```
   251,  252,  253,  254,  255,  266,  267,  268,  269,  270,
   281,  282,  283,  284,  285,  296,  297,  298,  299,  300,
   301,  302,  303,  304,  305,  316,  317,  318,  319,  320,
   331,  332,  333,  334,  335,  346,  347,  348,  349,  350,
   361,  362,  363,  364,  365,  376,  377,  378,  379,  380,
   391,  392,  393,  394,  395,  406,  407,  408,  409,  410,
   421,  422,  423,  424,  425,  436,  437,  438,  439,  440,
   461,  462,  463,  464,  465,  476,  477,  478,  479,  480,
   491,  492,  493,  494,  495,  506,  507,  508,  509,  510,
   521,  522,  523,  524,  525,  536,  537,  538,  539,  540,
   551,  552,  553,  554,  555,  566,  567,  568,  569,  570,
   581,  582,  583,  584,  585,  596,  597,  598,  599,  600,
   601,  602,  603,  604,  605,  616,  617,  618,  619,  620,
   631,  632,  633,  634,  635,  646,  647,  648,  649,  650,
   661,  662,  663,  664,  665,  676,  677,  678,  679,  680,
   691,  692,  693,  694,  695,  706,  707,  708,  709,  710,
   721,  722,  723,  724,  725,  736,  737,  738,  739,  740,
   761,  762,  763,  764,  765,  776,  777,  778,  779,  780,
   791,  792,  793,  794,  795,  806,  807,  808,  809,  810,
   821,  822,  823,  824,  825,  836,  837,  838,  839,  840,
   851,  852,  853,  854,  855,  866,  867,  868,  869,  870,
   881,  882,  883,  884,  885,  896,  897,  898,  899,  900,
   901,  902,  903,  904,  905,  916,  917,  918,  919,  920,
   931,  932,  933,  934,  935,  946,  947,  948,  949,  950,
   961,  962,  963,  964,  965,
** END ELPA MODULE **********************************
** BEGIN PROP MODULE - CC **********************
** 2 MATERIAL PROPERTIES
**    E=2.999E7 PSI, V=0.29
**    YIELDS (KSI):     20     15
**    HARDENING (KSI): 100      0
```

APPENDIX - Listing of ABAQUS Code (Continued)

```
**
*SOLID SECTION, ELSET=E1, MATERIAL=YIELD1
 0.153846154,
*SOLID SECTION, ELSET=E2, MATERIAL=YIELD2
 0.153846154,
*MATERIAL,NAME=YIELD1
*ELASTIC,TYPE=ISOTROPIC
 2.999E+07, 2.900E-01
*PLASTIC
 20000., 0.
120000., 1.
*MATERIAL,NAME=YIELD2
*ELASTIC,TYPE=ISOTROPIC
 2.999E+07, 2.900E-01
*PLASTIC
15000., 0.
** END PROP MODULE
** BEGIN STEP MODULE - HD - GENERAL ****************************
** LOADING: 36 STEPS, 12 UNLOADINGS                    (ABAQUS 5)
** APPROXIMATE PLASTIC STRAINS (EP):
**   0, 0.00005, 0.0001, 0.00015, 0.00025, 0.0005, 0.001, 0.002,
**   0.005, 0.01. 0.02, 0.035, 0.051
** INC=333, MIN INC SIZE =6.25E-7
** CONTROLS: DEFAULTS (R=0.005, C=0.010) FOR ALL STEPS
**
**
** OUTPUT/PR: ALL ELEMENTS (COLALL), ALL STEPS, CENTROIDAL STRESSES ONLY
**             SURFACE EL.(COLO), NODAL STRESSES
** OUTPUT/FI: ALL ELEMENTS, ALL STRESSES AND STRAINS, 4 STEPS:
**            0.002 AND UNLOAD, 0.05 AND UNLOAD
**
```

APPENDIX - Listing of ABAQUS Code (Continued)

```
** IDENTICAL TO MODULE OD, EXCEPT THAT RELOADING STEP IS INCREMENTED
**    0.475 INSTEAD OF 0.25 TO MAKE LAST INCREMENT SMALLER (0.05
**    INSTEAD OF 0.25) AND THEREFORE EASIER TO CONVERGE. START FOR 0.002
**
** NTRC = NODE, TOP RIGHT CORNER
** PREPARATION: ENTER NTRC NODE NUMBER IN LINE TOPM1, ...
*BOUNDARY
    BOTTOM, YSYMM
    EDGER,  XSYMM
**
*EQUATION
 2
 TOPM1, 2, 1., 1056     , 2, -1.
*STEP, AMPLITUDE=RAMP, INC=5
#1  UNIAXIAL TENSION, LOAD CONTROL
*STATIC, DIRECT
 1., 1., 6.25E-7
*CLOAD
  NTRC, 2, 15000.000
*EL PRINT,ELSET=COLO,   POSITION=NODES,      TOTALS=NO,  FREQUENCY=333
 S
*EL PRINT,ELSET=COLALL ,POSITION=CENTROIDAL, TOTALS=NO,  FREQUENCY=333
 S
*NODE PRINT, NSET=  NTRC, SUMMARY=NO, FREQUENCY=333
   U,CF
** THE FOLLOWING 2 LINES RESERVED FOR CGPE EXTRA NODES
**
**
*END STEP
*STEP, AMPLITUDE=RAMP, INC= 333
#2  UNIAXIAL TENSION
```

APPENDIX - Listing of ABAQUS Code (Continued)

```
*STATIC, DIRECT
 1., 1., 6.25E-7
*CLOAD
  NTRC, 2, 15851.000
*END STEP
*STEP, AMPLITUDE=RAMP, INC= 333
#3  UNIAXIAL TENSION, RELEASE LOAD
*STATIC
 1., 1., 6.25E-7
*CLOAD
  NTRC, 2, 0.000
*END STEP
*STEP, AMPLITUDE=RAMP, INC= 333
#4  UNIAXIAL TENSION
*STATIC, DIRECT
 1., 1., 6.25E-7
*CLOAD
  NTRC, 2, 15851.000
*END STEP
******************
*STEP, AMPLITUDE=RAMP, INC= 333
#5  UNIAXIAL TENSION
*STATIC
 .25, 1., 6.25E-7
*CLOAD
  NTRC, 2, 16702.000
*END STEP
*STEP, AMPLITUDE=RAMP, INC= 333
#6  UNIAXIAL TENSION, RELEASE LOAD
*STATIC
 1., 1., 6.25E-7
```

APPENDIX - Listing of ABAQUS Code (Continued)

```
*CLOAD
  NTRC, 2, 0.000
*END STEP
*STEP, AMPLITUDE=RAMP, INC= 333
#7  UNIAXIAL TENSION
*STATIC
 1., 1., 6.25E-7
*CLOAD
  NTRC, 2, 16702.000
*END STEP
******************
*STEP, AMPLITUDE=RAMP, INC= 333
#8  UNIAXIAL TENSION
*STATIC
 .125, 1., 6.25E-7
*CLOAD
  NTRC, 2, 17458.000
*END STEP
*STEP, AMPLITUDE=RAMP, INC= 333
#9  UNIAXIAL TENSION, RELEASE LOAD
*STATIC
 1., 1., 6.25E-7
*CLOAD
  NTRC, 2, 0.000
*END STEP
*STEP, AMPLITUDE=RAMP, INC= 333
#10 UNIAXIAL TENSION
*STATIC
 1., 1., 6.25E-7
*CLOAD
  NTRC, 2, 17458.000
```

APPENDIX - Listing of ABAQUS Code (Continued)

```
*END STEP
******************
*STEP, AMPLITUDE=RAMP, INC= 333
#11 UNIAXIAL TENSION
*STATIC
 .125, 1., 6.25E-7
*CLOAD
  NTRC, 2, 17663.000
*END STEP
*STEP, AMPLITUDE=RAMP, INC= 333
#12 UNIAXIAL TENSION, RELEASE LOAD
*STATIC
 1., 1., 6.25E-7
*CLOAD
  NTRC, 2, 0.000
*END STEP
*STEP, AMPLITUDE=RAMP, INC= 333
#13 UNIAXIAL TENSION, BACK UP TO FIRST REVERSAL POINT
*STATIC
 1., 1., 6.25E-7
*CLOAD
  NTRC, 2, 17663.000
*END STEP
****************
*STEP, AMPLITUDE=RAMP, INC= 333
#14 UNIAXIAL TENSION
*STATIC
 .125, 1., 6.25E-7
*CLOAD
  NTRC, 2, 17762.000
*END STEP
```

APPENDIX - Listing of ABAQUS Code (Continued)

```
*STEP, AMPLITUDE=RAMP, INC= 333
#15 UNIAXIAL TENSION, RELEASE LOAD
*STATIC
 1., 1., 6.25E-7
*CLOAD
  NTRC, 2, 0.000
*END STEP
*STEP, AMPLITUDE=RAMP, INC= 333
#16 UNIAXIAL TENSION, BACK UP TO FIRST REVERSAL POINT
*STATIC
 1., 1., 6.25E-7
*CLOAD
  NTRC, 2, 17762.000
*END STEP
******************
*STEP, AMPLITUDE=RAMP, INC= 333
#17 UNIAXIAL TENSION
*STATIC
 .125, 1., 6.25E-7
*CLOAD
  NTRC, 2, 17833.000
*END STEP
*STEP, AMPLITUDE=RAMP, INC= 333
#18 UNIAXIAL TENSION, RELEASE LOAD
*STATIC
 1., 1., 6.25E-7
*CLOAD
  NTRC, 2, 0.000
*END STEP
*STEP, AMPLITUDE=RAMP, INC= 333
#19 UNIAXIAL TENSION, BACK UP TO PREVIOUS REVERSAL POINT
```

APPENDIX - Listing of ABAQUS Code (Continued)

```
*STATIC
 1., 1., 6.25E-7
*CLOAD
  NTRC, 2, 17833.000
*END STEP
******************
*STEP, AMPLITUDE=RAMP, INC= 333
#20 UNIAXIAL TENSION
*STATIC
 .125, 1., 6.25E-7
*CLOAD
  NTRC, 2, 17897.000
*NODE FILE,GLOBAL=YES, FREQUENCY=333
U
*EL FILE, FREQUENCY=333
S,E
*END STEP
*STEP, AMPLITUDE=RAMP, INC= 333
#21 UNIAXIAL TENSION, RELEASE LOAD
*STATIC
 1., 1., 6.25E-7
*CLOAD
  NTRC, 2, 0.000
*END STEP
*STEP, AMPLITUDE=RAMP, INC= 333
#22 UNIAXIAL TENSION, BACK UP TO PREVIOUS REVERSAL POINT
*STATIC
 .475, 1., 6.25E-7
*CLOAD
  NTRC, 2, 17897.000
*NODE FILE, FREQUENCY= 0
```

APPENDIX - Listing of ABAQUS Code (Continued)

```
*EL FILE, FREQUENCY= 0
*END STEP
******************
*STEP, AMPLITUDE=RAMP, INC= 333
#23 UNIAXIAL TENSION
*STATIC
 .125, 1., 6.25E-7
*CLOAD
  NTRC, 2, 18017.000
*END STEP
*STEP, AMPLITUDE=RAMP, INC= 333
#24 UNIAXIAL TENSION, RELEASE LOAD
*STATIC
 1., 1., 6.25E-7
*CLOAD
  NTRC, 2, 0.000
*END STEP
*STEP, AMPLITUDE=RAMP, INC= 333
#25 UNIAXIAL TENSION, BACK UP TO PREVIOUS REVERSAL POINT
*STATIC
 .475, 1., 6.25E-7
*CLOAD
  NTRC, 2, 18017.000
*END STEP
******************
*STEP, AMPLITUDE=RAMP, INC= 333
#26 UNIAXIAL TENSION
*STATIC
 .125, 1., 6.25E-7
*CLOAD
  NTRC, 2, 18216.000
```

APPENDIX - Listing of ABAQUS Code (Continued)

```
*END STEP
*STEP, AMPLITUDE=RAMP, INC= 333
#27 UNIAXIAL TENSION, RELEASE LOAD
*STATIC
 1., 1., 6.25E-7
*CLOAD
  NTRC, 2, 0.000
*END STEP
*STEP, AMPLITUDE=RAMP, INC= 333
#28 UNIAXIAL TENSION, BACK UP TO PREVIOUS REVERSAL POINT
*STATIC
 .475, 1., 6.25E-7
*CLOAD
  NTRC, 2, 18216.000
*END STEP
******************
*STEP, AMPLITUDE=RAMP, INC= 333
#29 UNIAXIAL TENSION
*STATIC
 .125, 1., 6.25E-7
*CLOAD
  NTRC, 2, 18615.000
*END STEP
*STEP, AMPLITUDE=RAMP, INC= 333
#30 UNIAXIAL TENSION, RELEASE LOAD
*STATIC
 1., 1., 6.25E-7
*CLOAD
  NTRC, 2, 0.000
*END STEP
*STEP, AMPLITUDE=RAMP, INC= 333
```

APPENDIX - Listing of ABAQUS Code (Continued)

```
#31 UNIAXIAL TENSION, BACK UP TO PREVIOUS REVERSAL POINT
*STATIC
 .475, 1., 6.25E-7
*CLOAD
  NTRC, 2, 18615.000
*END STEP
******************
*STEP, AMPLITUDE=RAMP, INC= 333
#32 UNIAXIAL TENSION
*STATIC
 .125, 1., 6.25E-7
*CLOAD
  NTRC, 2, 19214.000
*END STEP
*STEP, AMPLITUDE=RAMP, INC= 333
#33 UNIAXIAL TENSION, RELEASE LOAD
*STATIC
 1., 1., 6.25E-7
*CLOAD
  NTRC, 2, 0.000
*END STEP
*STEP, AMPLITUDE=RAMP, INC= 333
#34 UNIAXIAL TENSION, BACK UP TO PREVIOUS REVERSAL POINT
*STATIC
 .475, 1., 6.25E-7
*CLOAD
  NTRC, 2, 19214.000
*END STEP
******************
*STEP, AMPLITUDE=RAMP, INC= 333
#35 UNIAXIAL TENSION
```

APPENDIX - Listing of ABAQUS Code (Continued)

```
*STATIC
 .125, 1., 6.25E-7
*CLOAD
  NTRC, 2, 19852.000
*NODE FILE,GLOBAL=YES, FREQUENCY=333
U
*EL FILE, FREQUENCY=333
S,E
*END STEP
*STEP, AMPLITUDE=RAMP, INC= 333
#36 UNIAXIAL TENSION, RELEASE LOAD
*STATIC
 1., 1., 6.25E-7
*CLOAD
  NTRC, 2, 0.000
*END STEP
** VALUE OF CONSTANTS USED IN STRAIN-TO-LOAD CALCULATIONS
**   E, SPROP, SYIELD, OFFSET STRAIN, H1, H2, N, A:
**    30000.00 15.00 17.897 0.00200 17017. 39.9 35.3 3.46338746
** END STEP MODULE
```

DISTRIBUTION LIST

Report No.NAWCADWAR-95033-4.3 Vol. 2

No. of Copies

Office of Naval Research.....1
Attn: A. K. Vasudevan, Code 1216
800 N. Quincy Street
Arlington, VA 22217

Office of Naval Research.....1
Attn: Y. Rajapakse, Code 1132SM
800 N. Quincy Street
Arlington, VA 22217

Director.....1
Naval Research Laboratory
Attn: L. Gause
4555 Overlook Avenue, S.W.
Washington, D.C. 20375-5000

Commander.....1
United States Naval Academy
Attn: Mechanical Engineering Dept.
Annapolis, MD 21402

Commander.....1
U.S. Naval Postgraduate School
Attn: Technical Library
Monterey, CA 93943

Commanding Officer.....1
Wright Laboratory
Attn: FIBEC Dr. G. Sendeckyj
Wright Patterson Air Force Base, OH 45433-6553

Commanding Officer.....1
Picatinny Arsenal
PLASTEC
Attn: Librarian, Code DRDAR-SCM-0, Bldg. 351N
Dover, NJ 07801

Commanding Officer.....1
Advanced Systems Research and Analysis Office ASRAO
Attn: Library, M/S 219-3
Ames Research Center
Moffett Field, CA 94035-1000

Administrator.....1
National Aeronautics and Space Administration
George C. Marshall Space Flight Center
Attn: Technical Library
Huntsville, AL 35812

DISTRIBUTION LIST

Report No.NAWCADWAR-95033-4.3 Vol. 2

No. of Copies

Administrator.....1
National Aeronautics and Space Administration
Lewis Research Center
Attn: Technical Library
21000 Brookpark Road
Cleveland, OH 44153

Boeing Co. Wichita Division.....1
Tech. Library K78-38
P.O. Box 7730
Wichita, KS 67277-7730

General Electric Company.....1
Attn: Technical Library
1 Neumann Way
Cincinnati, OH 45215

General Electric Company.....1
Attn: Technical Library
P.O. Box 8555
Philadelphia, PA 19101

Lockheed Martin/Georgia Company.....1
Attn: Technical Information
Dept. 72-34, Zone 26
Marietta, GA 30063

Lockheed Martin/Missile and Space Company.....1
Attn: Technical Library
1111 Lockheed Way
Sunnyvale, CA 94088

McDonnell-Douglas Aerospace East.....1
Attn: Technical Library
P.O. Box 516
St. Louis, MO 63166

McDonnell-Douglas Aerospace West.....1
Attn: Technical Library
Mail Code 212-10
3855 Lakewood Blvd
Long Beach, CA 90846

Northrop Grumman Corporation.....1
Attn: Technical Library
South Oyster Bay Road
Bethpage, Long Island, NY 11714

DISTRIBUTION LIST

Report No.NAWCADWAR-95033-4.3 Vol. 2

No. of Copies

Northrop Grumman Corporation.....1
Attn: Technical Library
One Northrop Avenue
Hawthorne, CA 90250

Rockwell International/North American Aircraft Division.....1
Attn: Technical Library
P.O. Box 92098
Los Angeles, CA 90009

Sikorsky Aircraft.....1
Attn: Technical Library
North Main Street
Stratford, CT 06601-1381

Naval Air Warfare Center.....7
Aircraft Division Warminster
P.O. Box 5152
Warminster, PA 18974-0591
5 for Code 4.3.3.1.R
2 for Code 7.2.5.5

Defense Technical Information Center.....2
Attn: DTIC-FDAB
Cameron Station BG5
Alexandria, VA 22304-6145

Center for Naval Analysis.....1
4401 Fort Avenue
P.O. Box 16268
Alexandria, VA 22302-0268